Petrology of the Boundary Intrusions and Associated Brecciation in Creighton, Saskatchewan and Flin Flon, Manitoba

A Thesis Submitted to the College of
Graduate and Postdoctoral Studies
In Partial Fulfillment of the Requirements
For the Degree of Master of Science
In the Department of Geological Sciences
University of Saskatchewan
Saskatoon

By

NANCY MICHELLE NORMORE

PERMISSION TO USE

In presenting this thesis in partial fulfilment of the requirements for a Postgraduate degree from the University of Saskatchewan, I agree that the Libraries of this University may make it freely available for inspection. I further agree that permission for copying of this thesis in any manner, in whole or in part, for scholarly purposes may be granted by the professor or professors who supervised my thesis work or, in their absence, by the Head of the Department or the Dean of the College in which my thesis work was done. It is understood that any copying or publication or use of this thesis or parts thereof for financial gain shall not be allowed without my written permission. It is also understood that due recognition shall be given to me and to the University of Saskatchewan in any scholarly use which may be made of any material in my thesis.

Requests for permission to copy or to make other use of material in this thesis in whole or part should be addressed to:

Head of the Department of Geological Sciences
University of Saskatchewan
114 Science Place
Saskatoon, Saskatchewan S7N 5E2
Canada

OR

Dean
College of Graduate Studies and Postdoctoral Studies
University of Saskatchewan
116 Thorvaldson Building, 110 Science Place
Saskatoon, Saskatchewan S7N 5C9
Canada

ABSTRACT

Detailed mapping, petrographical and geochemical data for the Green Street and Louis Lake Boundary Intrusion breccias are presented, as well as petrographical and geochemical data for the Phantom Beach intrusion breccia and the Club Lake intrusion, located in Creighton, Saskatchewan and Flin Flon, Manitoba. The Green Street Boundary intrusion was emplaced in volcanic rocks of the Flin Flon formation as a dyke with the most northerly section containing a largely polymictic, chaotic-textured, matrix-supported intrusion breccia. The margins of the dyke also exhibit evidence of hydraulic brecciation through mosaic or jigsaw textures. The Louis Lake intrusion is a chaotic-textured, matrix-supported breccia and contains no exposed contacts with the Louis formation volcanic host rock, though the presence of large layered blocks indicates the intrusion may have been emplaced as a sill. The Phantom Beach intrusion breccia is also chaotic-textured and ranges from fragment- to matrix-supported. Intrusion morphology and breccia textures suggest possible processes for fragment generation include dyke crack-tip propagation, hydraulic fracturing, mechanical and thermal delamination, and stoping. Fragment populations for all intrusion breccias include mafic to ultramafic intrusives and locally derived volcanics, ranging from angular to rounded to disaggregated, with the intrusive fragments exhibiting greater degrees of rounding and disaggregation. This may suggest the intrusive fragments have had longer residence times or traveled greater distances within the magma than the volcanic xenoliths. Fragment size can reach up to 2 m in diameter with an average diameter typically between 10 – 30 cm. Settling rates of fragments within the magmas, or the magma ascent rate, of the mapped sites are calculated using Stoke's Law (for a Newtonian fluid) and calculations by Shaw (1969) (for a Bingham fluid). Resulting magma ascent velocities range from 0.01 m/hr to 1.84 km/hr for the Green Street intrusion, 0.01 m/hr to 872.16 m/hr for the Louis Lake intrusion, and 1.63 m/yr to 0.33 m/hr for the dominantly clast-supported breccia intruding the Louis Lake breccia.

Petrographical analysis of mafic to ultramafic intrusive fragments within the Green Street intrusion exhibit textures which may suggest different stages of disaggregation and incorporation into the magma matrix. Petrographical comparisons of whole, intact fragments to fragments with irregular boundaries may demonstrate various stages of disaggregation taking place during

emplacement of the intrusion. In addition, comparisons of floating actinolite crysts in the intrusion matrix to known phenocrysts and crystals of actinolite in fragments may further indicate previous disaggregation of intrusive fragments.

Whole rock and trace element geochemistry for the Boundary intrusions and their mafic to ultramafic intrusive fragments show the samples display island arc signatures and are overall calc-alkaline, though select fragment samples from the Phantom Beach area show some tholeiitic tendencies. High field strength element (HFSE) patterns suggest an enriched and complex mantle source for all samples, with the resulting magma possibly affected by magma mixing. HFSE ratios may also indicate contamination by crustal assimilation for the Green Street intrusion. Low mid-ocean ridge basalt (MORB)-normalized TiO_2/Y ratios (<1) suggests that the magma source for the Boundary intrusions was at shallow depths with higher water contents (<50km) where garnet is not a factor in retaining yttrium relative to titanium. Similarities in trace element patterns and higher Zr/TiO_2 ratios suggest fractionation within the sample suite for the Green Street area.

ACKNOWLEDGEMENTS

I would first and foremost like to express my appreciation to the academic help I received from the University of Saskatchewan Department of Geological Sciences, most notably Dr. Kevin Ansdell and Tim Prokopiuk. Dr. Kevin Ansdell kindly provided support and guidance during the writing of this thesis, and the support of the NSERC Discovery grant to Dr. Kevin Ansdell. Thanks to Tim Prokopiuk, for graciously giving his time to help put together an old microscope and show me how to use it, and to go over each and every thin section for which I required help. An extended thanks to Christine McKechnie for offering advice occasionally throughout the entire thesis sampling and writing process, and to Blaine Novakovski for preparing large thin section slides. Additionally, I would like to acknowledge the committee members for their review and comments. Also a great thank you to the Geological Sciences Department Administrators Chantal Strachan-Crossman and Michelle Howe for great conversations and the most enjoyable visits to the office.

I would like to thank UEX Corporation for my employment and the great mentorship during the majority of my thesis.

Finally, I would like to express my appreciation and sincere gratitude to my husband, David Andrew Heasman for his patience and never failing support throughout every stage of my graduate studies.

ABBREVIATIONS USED IN THIS TEXT

Act	Actinolite
AFC	Assimilation-Fractionation-Crystallization
CAB	Calc-Alkaline Basalt
Chl	Chlorite
CL	Club Lake
CSB	Clast-Supported Breccia
EMORB	Enriched Mid-Ocean Ridge Basalt
EPMA	Electron Probe Microanalysis
FF-GC	Flin Flon-Glennie Complex
GS	Green Street
Hbl	Hornblende
HFS(E)	High Field Strength (Elements)
HRE(E)	Heavy Rare Earth (Elements)
IAT	Island Arc Tholeiite
ICP-MS	Inductively Coupled Plasma Mass Spectrometry
ICP-OES	Inductively Coupled Plasma - Optical Emission Spectrometry
km	Kilometer
LIL(E)	Large Io Lithophile (Elements)
LFS(E)	Low Field Strength (Elements)
LL	Louis Lake
LRE(E)	Light Rare Earth (Elements)
LOI	Lost on ignition
m	Meter
MN	Mantle Normalized
MORB	Mid-Ocean Ridge Basalt
MRE(E)	Middle Rare Earth (Elements)
N	Normalized
NMORB	Normal Mid-Ocean Ridge Basalt
Pa s	Pascal second (viscosity as g/cms^{-1})
PB	Phantom Beach
PPL	Plain Polarized Light
Pl	Plagioclase
Qtz	Quartz
SEM	Scanning Electron Microscope
SRC	Saskatchewan Research Council
TAB	Tholeiitic Arc Basalt
THO	Trans-Hudson Orogeny
TS	Thin Section
µm	Micrometer
VAB	Volcanic Arc Basalt
WPB	Within-Plate Basalt
XPL	Cross Polarized Light
XRD	X-Ray Diffraction

TABLE OF CONTENTS

LIST OF TABLES

TABLE OF FIGURES

1.0 INTRODUCTION

1.1 Overview

The Boundary intrusions are located in Creighton, Saskatchewan and Flin Flon, Manitoba, and comprise of three compositionally distinct rock groups, ranging from felsic to ultramafic, and intrude volcanic arc rocks within the Flin Flon domain (Figure 1-1). Breccias have been observed in all the Boundary intrusion types and contain fragments of volcanic or earlier crystallized phases of Boundary intrusion (Syme, 1975). There are observable and measurable properties of breccias, such as fragment-matrix relationships, fragment and matrix similarities or differences, as well as the environment of emplacement, which can be used to make inferences on the intrusion and breccia's processes of formation. No study has been conducted to date which examines the relationships between the brecciated units within the study area, or the relationships of the components within the breccia units themselves. Past studies conducted by Syme (1975), Syme and Forester (1977), O'Hanley and Kyser (1994), and O'Hanley *et al*. (1993) focused on the petrogenesis of the Boundary intrusions using field relationships, thin section studies, major oxide relationships, trace element characteristics, and isotope studies. This proposed study aims to expand on the current knowledge of the Boundary intrusions by focusing on the relationships of select intrusions and their breccia fragments through field relationships, thin sections and geochemical studies.

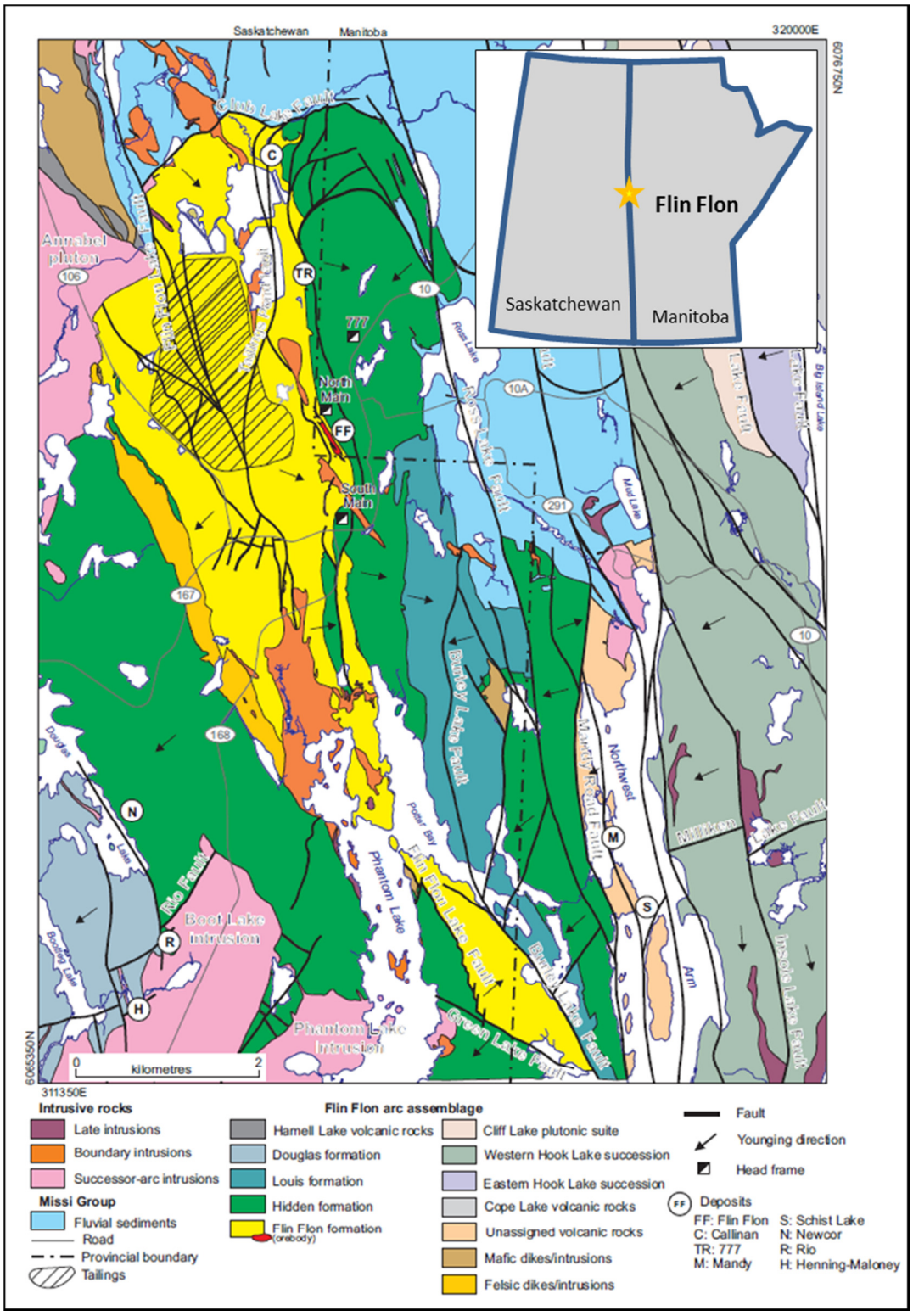

Figure 1-1. Geology of the Flin Flon Area. Taken from Simard *et al.*, 2012.

1.2 Research Objectives

Several episodes of brecciation can be mapped within the Boundary intrusions of the Creighton and Flin Flon area. Considering the limited research existing on the intrusions and the breccias they contain, this study adds new information to the enigmatic igneous bodies. Results and observations help to further constrain the mantle processes and breccia-forming processes which have taken place during the emplacement of the Boundary intrusions.

The objectives of this study were:

1) To examine the lithogeochemical variations between the breccia units and their components to help provide constraints on the petrogenesis of those components. Representative samples were chosen to allow comparison of the petrographical and geochemical characteristics of the intrusions in each of the sample areas. The geochemical results were used to better categorize the geochemical nature of the Boundary intrusions and breccia fragments, and to also develop models which help indicate the mantle processes of formation.

2) To make inferences, using thin section to outcrop scale observation, on the physical/mechanical constraints on the formation of the Boundary intrusion breccias. This included observations that aid in interpretations on fragmentation, fragment transport, and magma ascent.

The present study provides textural and compositional observations made on the Boundary intrusion breccias from three separate sites – Green Street, Louis Lake and Phantom Beach. Club Lake interpretations are limited as no breccias were found in this area.

1.3 Thesis Structure

The contextual information pertinent to the thesis is included in Chapters 1 to 3. Chapter 2 reviews the regional and local geological background for the Boundary intrusion breccias, and

Chapter 3 provides a literature review of breccia types and classification. Methods and analytical techniques are described in Chapter 4, and the thesis results are presented in Chapter 5. Chapter 6 comprises the discussion of the Boundary intrusion breccia petrogenesis with respect to the geochemical and field observation results. The discussion is summarized in Chapter 7, and recommendations for future work on the Boundary intrusion breccias are included in Chapter 8. Appendices A and B include sample lists and geochemistry lab analysis, as well as method summaries and proof of calculations.

2.0 GEOLOGICAL SETTING

2.1 Regional Framework

The study area is located within the Trans Hudson Orogen (THO), a region of widespread tectonothermally reworked Archean and Paleoproterozoic rocks (Figure 2-1A). It is the site of the terminal collision of the Superior Craton with the Rae and Hearne cratons ca. 1.83 – 1.80 Ga, which resulted in the closure of the Pacific-sized Manikewan Ocean (Stauffer, 1984; Ansdell, 2005; Corrigan *et al*., 2009). The THO extends from Nunavut and northern Quebec in Canada, to North and South Dakota in the United States, and may extend as far south as north Arizona. The geological history of the THO is particularly well preserved in the rocks exposed in northern Manitoba and Saskatchewan (Figure 2-1B) (Ansdell, 2005), although outcrops disappear to the south as the Paleoproterozoic rocks are covered by the sedimentary rocks of the Phanerozoic Williston Basin. Overall, two stages can be generalized for the THO based on its tectonomagmatic history (Lucas *et al*., 1996). The first stage involves convergent margin (oceanic) tectonics and magmatism between 1.92 and 1.83 Ga, followed by the consumption of the oceanic basins by the amalgamation of the Sask craton to the Flin Flon-Glennie Complex (FF-GC) by approximately 1.83 Ga. The second stage involves the collision of the Superior craton to the Reindeer Zone ca. 1.83 – 1.80 Ga (Corrigan *et al*., 2009 and references therein). Corrigan *et al*. (2009) further subdivided the THO into four main orogenic events: 1) the Snowbird Orogeny from ca. 1.92 – 1.89 Ga, 2) the Glennie-Flin Flon-Snow Lake Orogeny from ca. 1.88 – 1.865 Ga, 3) the Wathaman Orogeny from ca. 1.865 – 1.845 Ga, and 4) the collision of the Sask craton with the Flin Flon-Glennie Complex (FF-GC) ca. 1.84 – 1.82 Ga. The study area lies within the FF-GC, which consists of the Flin Flon Belt (domain) (includes Amisk Collage and Snow Lake Assemblage), the Hanson Lake Block, and the Glennie Domain (Figure 2.1B). The remnants of these orogenies are preserved in the Manitoba-Saskatchewan section of the THO, within the Hearne Province, the Superior Boundary Zone, and the Reindeer Zone (Ansdell, 2005).

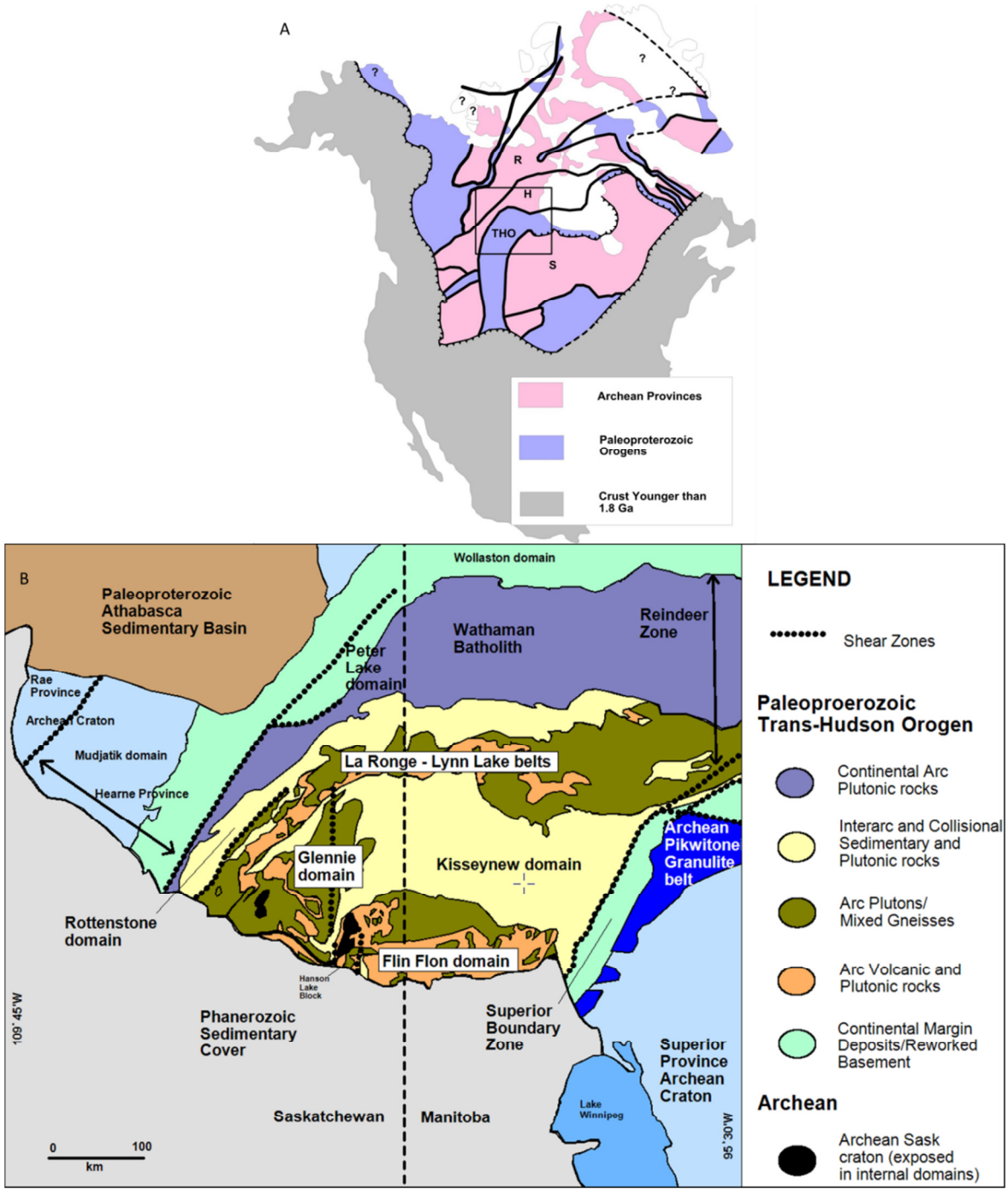

Figure 2-1. North American Craton and Trans Hudson Orogeny. A) Map showing the distribution of Archean and Paleoproterozoic elements within the North American Craton and the location of the THO (modified from Ansdell, 2005). Rectangle outlines location of Figure 2-1B. THO, Trans-Hudson Orogen; S, Superior Craton; H, Hearne Province; R, Rae Province. B) Manitoba-Saskatchewan segment of the Trans-Hudson Orogen. Flin Flon belt (includes the Amisk Collage and Snow Lake assemblage), Hanson Lake Block and Glennie domain comprise the Flin Flon-Glennie Complex (Ashton, 1999). Modified from Ansdell, 2005.

Intraoceanic accretion which resulted in the formation of the FF-GC (Figure 2-1B) occurred from 1.88 – 1.87 Ga and was followed by development of interarc basins and successor arc intrusions from 1.87 – 1.84 Ga (Figure 2-2). The collage collided with the rocks of the La Ronge-Lynn Lake arc rocks and the Hearne craton during the Wathaman Orogeny, and later rifted from them to form the Kisseynew Backarc Basin in the post-accretion period (Figure 2-1B and 2-2F) (Corrigan *et al*., 2009 and references therein). The Kisseynew Domain rocks are metamorphosed marine turbidite sedimentary rocks, initially deposited at ca. 1850 Ma (Ansdell, 2005 and references therein), broadly synchronous with the alluvial-fluvial sediments (Missi Group, ca. 1854 – 1842 Ma) that were deposited adjacent to a highland source in the FF-GC (Ansdell, 2005; Simard *et al*., 2012). As the Sask craton and/or the Superior craton advanced northward underthrusting the FF-GC, the Kisseynew Basin thickened and collapsed (Ansdell *et al*., 1995; Ansdell, 2005). Pre-accretion arc assemblages of the Flin Flon-Glennie Complex were also intruded by calc-alkaline plutons, and by felsic to mafic dykes and sills related to younger magmatic arcs ca. 1.87 – 1.84 Ga, (O'Hanley and Kyser, 1994; Lucas *et al*., 1996; Simard *et al*., 2012), which were coeval with sediment deposition of the Kisseynew Domain and the alluvial-fluvial sediments of the Missi Group. Successor intrusions, such as the Phantom Lake intrusive suite and the Boundary intrusions, cross-cut the Missi Group sediments (Simard *et al*., 2012).

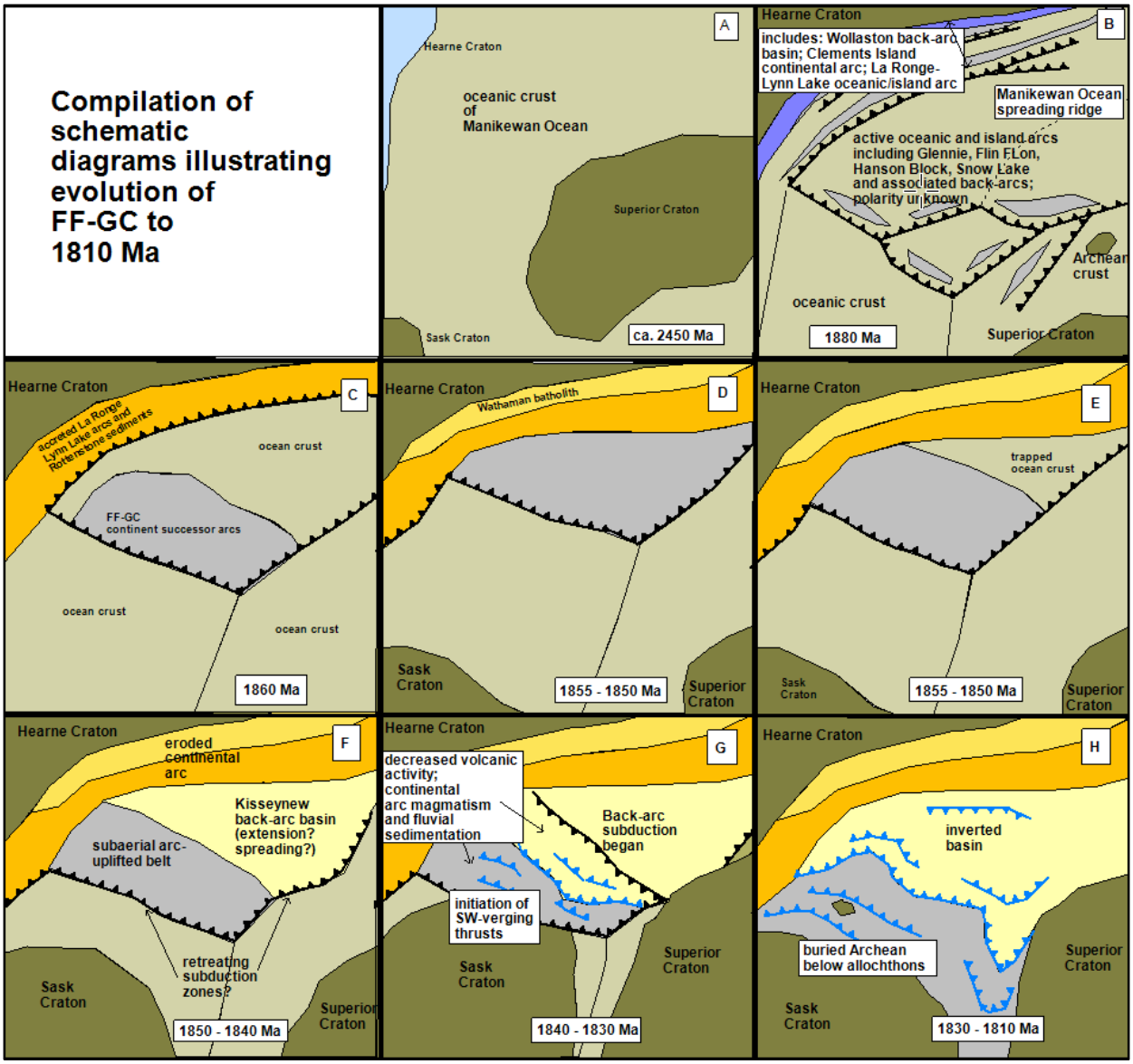

Figure 2-2. Schematic diagram of proposed tectonic evolution involving Flin Flon-Glennie Complex (FF-GC) from ca. 2450 Ma to 1810 Ma. Note that D and E represent alternative histories for the same time period. All units are labeled in diagram. Black triangles = subduction zones; blue triangles = thrust faults. Not to scale. Redrawn and modified after Ansdell *et al*., 1995 and Ansdell, 2005.

The Flin Flon-Glennie Complex comprises a mixture of volcanic, intrusive and sedimentary rocks, and rare Archean Crustal slices (Ansdell, 2005). Geochemical signatures show that there is an evolution in the igneous rocks from primitive tholeiites to more evolved calc-alkaline rocks (Maxeiner *et al*., 1999; Bailes and Galley, 1999). Geochemical signatures also indicate the rocks were generated in juvenile island arc environments, backarc basins, and oceanic plateaus

during the period prior to intraoceanic accretion ca. 1.92 – 1.88 Ga (Lucas *et al*., 1996; *et al*., 2005 and references therein; Simard *et al*., 2012 and references therein). Various syn- and post-volcanic felsic and mafic dykes, which also predate intraoceanic accretion, are found as sills and other types of intrusions cross-cutting other rocks of the arc assemblage (Simard *et al*., 2012). Intrusives which postdate accretion cross-cut older arc rocks of the FF-GC and, as previously mentioned, are synchronous with and crosscutting the Kisseynew and Missi Group sediments.

Figure 2-3 shows the distribution of syn- to post-accretion arc rocks within part of the FF-GC. The term "successor arc rocks" has been used as a collective term for the post-accretion sedimentary and intrusive rocks (Lucas *et al*., 1996). Intrusive rocks intrude as dykes and sills and range from felsic to mafic in composition, and sedimentary rocks comprise continentally derived sandstone and conglomerates, and marine turbidites. Included within the group of successor arc intrusives are the Boundary intrusions and other pre- and post-Missi Group intrusives.

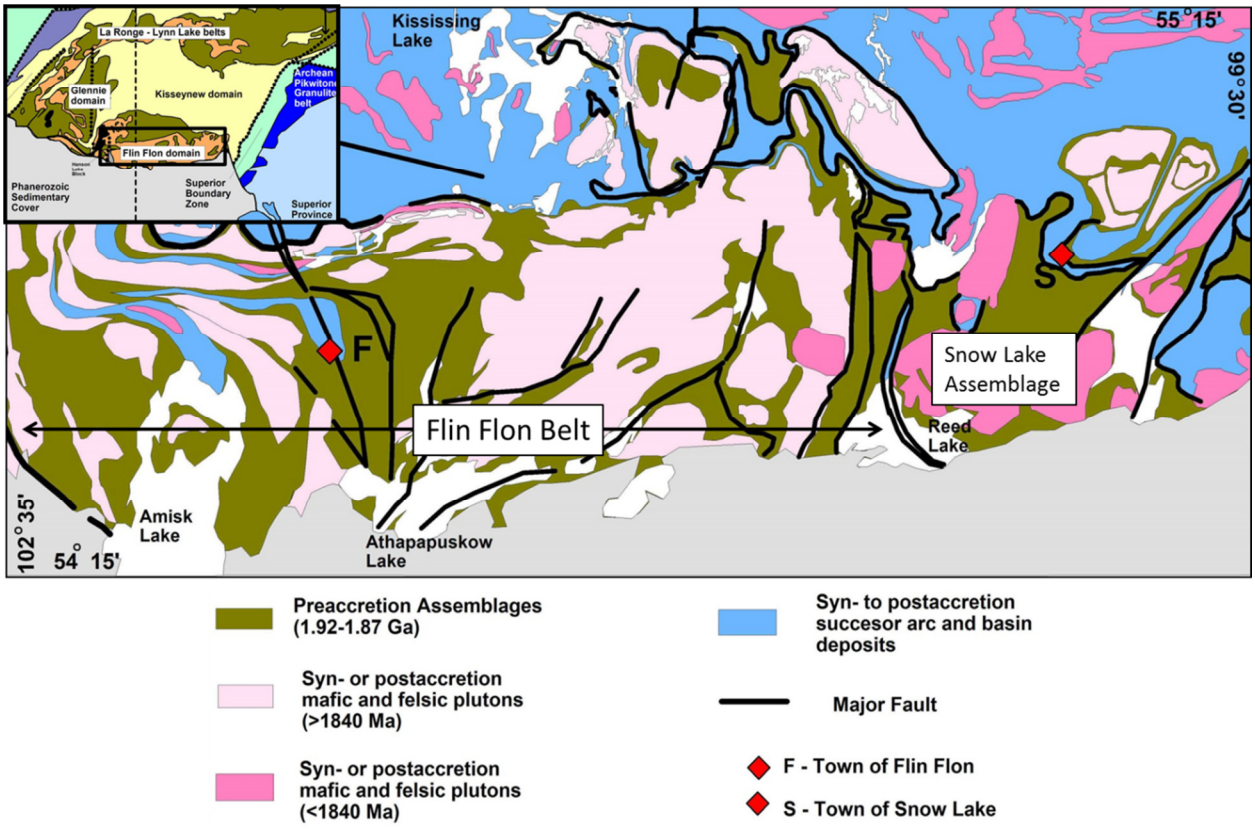

Figure 2-3. Simplified geology of the Flin Flon belt and Snow Lake assemblage. Inset is of Figure 2-1 to show location of Figure 2-3. Modified after Lucas *et al*., 1999 and Lazzorotto *et al*., 2017.

2.2 Local Geology

The Boundary intrusion study area lies within the Flin Flon-Creighton area (Figure 1-1). The geology of this area is comprehensively described by Simard *et al*. (2012) and so only a brief summary will be provided in this thesis. The map area in Figure 1-1 comprises two main groups of rocks: 1) the Flin Flon arc assemblage which consists of >1.88 Ga juvenile oceanic-arc basalt, basaltic andesite, rhyolite, and synvolcanic intrusions (Syme and Bailes, 1993) and 2) <1.88 Ga successor arc calc-alkaline plutons, fluvial-alluvial sedimentary rocks and late intrusions (Bailes and Syme, 1989; Stauffer, 1990; Stern *et al*., 1999). The volcanic rocks of the Flin Flon arc assemblages are overall relatively juvenile and tholeiitic in nature (Syme *et al.*, 1999b; Devine, 2003; Bailey, 2006; Simard and Creaser, 2007; DeWolf *et al*., 2009b; Simard *et al*., 2012). The packages of rocks within the Flin Flon assemblage which are crosscut by the Boundary

intrusions include, from oldest to youngest 1) the Flin Flon formation, 2) the Hidden formation, 3) the Louis formation, and 4) other felsic intrusions of the Flin Flon are assemblage. Only these formations and suites relevant to the Boundary intrusions will be described in the following text.

The Flin Flon formation includes heterolithic and monolithic volcaniclastic rocks, rhyolite flows, domes and associated volcaniclastic rocks, massive to pillowed basalt flows, and flow breccias which are all interpreted as representing successive periods of extension, subsidence and infilling during the subsidence of a volcanic structure (Devine *et al*., 2002; DeWolfe and Gibson, 2006; and Simard *et al*., 2010; Lafrance *et al*., 2016). One of the members of this formation also contains the Flin Flon, Callinan and 777 VMS deposits. The Flin Flon formation is conformably overlain by, intruded by, and in faulted contact with rocks of the Hidden formation. Rocks types of the Hidden formation are predominantly mafic flows, sills and volcaniclastic rocks with lesser basaltic andesite flows, rhyolite flows and felsic volcaniclastic rocks. The formation is interpreted to indicate the onset of hanging wall volcanism atop the Flin Flon formation volcanic center and VMS deposits (DeWolfe, 2008). The Louis formation, conformably overlying the Hidden formation, consists of basaltic flows and mafic volcaniclastic rocks with subordinate rhyolite flows and felsic volcaniclastic rocks, emplaced in fault-controlled basins. Following volcanism, felsic dykes and sills were emplaced within available structures, often coinciding with shear zones interpreted as minor thrust faults that cause repeated sequences of some volcanic rocks.

The 1.84 – 1.87 Ga successor arc rocks consist of alluvial-fluvial sediments and felsic to mafic intrusives that overlie and intrude rocks of the Flin Flon arc assemblage (Lucas *et al*., 1996). Intrusive rocks are medium-K calc-alkaline, diorite-tonalite-granodiorite plutons with lesser high-K gabbro-monzodiorite-granite plutons (Syme, 1988; Whalen, 1992; O'Hanley and Kyser, 1994). Simard *et al*. (2012) divided the intrusives into two groups relative to the deposition of the alluvial-fluvial sediments (termed Missi Group): 1) pre-Missi-Group intrusives, which include the Channing Lake granodiorite suite and the Annabel Pluton, and 2) post-Missi Group intrusives which include, besides the Boundary intrusion suite, the Phantom Lake intrusive suite, the Boot Lake intrusive suite, and other late intrusions which cross-cut the Boundary intrusions and the Phantom Lake intrusion (Simard *et al*., 2012). Trace element geochemistry and isotopic

compositions of these rocks indicate an arc signature and that there was little involvement of older crust in the generation of the magmas (Lucas *et al*., 1996 and references therein).

Peak regional metamorphism in the Flin Flon-Glennie Complex area was reached by ca. 1.815 Ga (Gordon *et al*., 1990) with levels of metamorphism over the entire belt ranging from low grade prehnite-pumpellyite facies to subgreenschist facies (south of Flin Flon, Manitoba) to amphibolite facies to the north (at the boundary with the Kisseynew gneisses) (Lazzarotto *et al*., 2016). Within the central part of the FF-GC, low-grade subgreenschist to greenschist facies metamorphism has affected the volcanic, sedimentary and plutonic rock assemblages.

Seven deformation events are recognized occurring during the convergent margin tectonics and following consumption of oceanic basins that resulted in several shear zones, thrust systems and regional cleavages (Simard et al., 2012; Lafrance *et al*., 2016). The first two events, D1 and D2, took place before the deposition of the Missi Group sediments, during the accretion of the Flin Flon Arc to other terranes to form an accretionary complex. Generally north to northwest and northeast-trending structures typify these events. Post Missi Group deformation (D3-D7) includes west and north directed thrust systems (Simard *et al*., 2012), and other later features coinciding with the collision of the Archean cratons (Sask and Superior) to the Flin Flon-Glennie Complex. The FF-GC comprises a number of tectonostratigraphic assemblages that are fold-repeated and thrust-stacked, and structurally overlie the Sask craton (Pelican Thrust) (Ashton *et al*., 2005). D3-D7 deformation features also include two regional penetrative cleavage events, and late sub-vertical faults with oblique dip-slip displacement. The first penetrative cleavage within the Missi Group sediments contains a north-northwest strike and north-easterly dip, most notable by the flattening of the pebbles. Both cleavage events overprinted some previous foliations (Simard *et al*., 2012).

2.3 Geology of the Boundary Intrusions

The Boundary intrusions were first mapped and briefly described by Stockwell (1946, 1960) of the Geological Survey of Canada as part of a project to map the Flin Flon-Mandy area of Manitoba and Saskatchewan. Stockwell (1946) indicated that the Boundary intrusions ranged

from acidic to ultrabasic in composition and contained "much brecciation both of the country rock and of earlier crystallized phases of the intrusive rock itself" (pg. 2, in Stockwell (1946)). Later work by Byers *et al*. (1965) included mapping and description of the Boundary intrusions in greater detail, outlining their texture, compositions, and placement relationships, however the relative ages were not established. A graduate thesis completed by Syme (1975) is the most detailed study conducted on the petrogenesis of the Boundary intrusions, and much of the detailed geology described below is based on that work. Syme (1975) and Syme and Forester (1977) determined the sequence of intrusions and relative ages in context of the deformational events of the area. The authors also indicated that the combined effects of oxygen and water fugacity in the magma source are a possible mechanism of differentiation leading to MgO-enrichment. Finally, the authors determined that the felsic Boundary intrusions were differentiated from a different magma source than the mafic and ultramafic intrusions, but this was later disputed by O'Hanley *et al*. (1993). O'Hanley *et al*. (1993) focused on using major, trace and rare-earth element data to determine the provenance of the Boundary intrusions and concluded that the group of intrusions did have similar fractionation trends, similar rare earth element and incompatible element patterns, which indicate a similar magma source or are cogenetic. O'Hanley and Kyser (1994) used the lack of an Archean signature in the Rb-Sr and Sm-Nd isotopic systematics, as well as the known age of the Boundary intrusions (1842 ± 3 Ma; Heaman *et al*. (1992)) to bracket the final emplacement of the Flin Flon domain over inferred Archean rocks.

The Boundary intrusions outcrop over an area of approximately 15 x 5 km, centered on the boundary between Saskatchewan and Manitoba in the Creighton-Flin Flon area, and exhibit a general north-northwest trend to their emplacement (Figure 1-1). Syme (1975) suggested that the trend may have been largely controlled by their intrusion within host rocks that have been, and were still being, completely folded and faulted in a northwest orientation. The resulting morphology of the Boundary intrusions is overall irregular, with dyke-like and ellipsoidal shapes most common, and often cross-cut the regional foliation at a shallow angle. Syme (1975) noted that contacts are sharp with little to no metamorphic effects (chilled margins or alteration) observed at the outcrop or hand-sample scale, and dip 65 – 85 degrees east where contacts can be

measured. There is, however, varying degrees of brecciation, shearing and drag folds near some of the intrusive contacts, noted both in the host rocks and Boundary intrusions (Syme, 1975).

Syme (1975) and Syme and Forester (1977) divided the Boundary intrusions into three groups based on modal composition: the olivine-bearing ultramafic rocks, the mafic group rocks, and the felsic group. However, later work by O'Hanley *et al*. (1993) had shown that mafic and ultramafic Boundary intrusion compositions overlap and therefore the subdivision may be inadequate. Nevertheless, field and thin section observations, descriptions and results provided by Syme (1975) are still relevant and will be referenced where appropriate and no other updated information exists. Syme (1975) divided the Boundary intrusion rocks into three groups based on modal compositions:

- The ultramafic Boundary intrusions are olivine-bearing rocks which include ultramafic and gabbroic varieties. The most common and mappable rock units are wehrlite, olivine-gabbro, and serpentinized ultramafic rocks.

- The mafic group rocks include diorites rich in mafic minerals, and some ultramafic or monomineralic rock types which lack olivine. This group constitutes the majority of the Boundary intrusions and shows significant variability in mineralogical and textural characteristics, as well as variability in the alteration and deformation. Porphyritic biotite-augite meladiorite is the most common rock type, with smaller intrusions of hornblende-bearing diorites and lesser pyroxene- and amphibole-rich mafic rocks occurring within the larger mafic variety, or as satellite bodies. Layering is also locally present, typically found at the margins of the intrusions and indicated by layers of felsic to mafic composition. Based on the presence of breccias and several cross-cutting relationships with other Boundary intrusions, this group is considered to be the oldest. Within the mafic group, crosscutting relationships are also shown to be common.

- The felsic group rocks include all feldspar-rich intrusions, which are poor in mafic minerals and are believed to be the youngest according to Syme (1975). However, there is no clear indication of relative age as the evidence of field relationships between the

ultramafic and felsic varieties is currently not available (O'Hanley and Kyser, 1994). The felsic rocks exhibit a wide range of compositions and textures, but are typically characterized by abundant plagioclase. Grainsize ranges from fine- to medium-grained and can be porphyritic. Several dykes and small irregular intrusions contain abundant mafic group fragments.

The Boundary intrusions pre-date regional metamorphism and thus have been affected by greenschist grade metamorphism. Syme (1975) noted that the mafic group, in particular, contain mineral assemblages and textures representative of the greenschist facies. He also observed that the younger, more felsic intrusions have increasingly better preserved igneous textures and phases, and all intrusions are thought to have been affected by late magmatic or deuteric metasomatism.

All Boundary intrusion rocks contain varying degrees of intrusion breccias (Figure 2-4). Breccias within the larger mafic intrusion contain metavolcanic xenoliths derived from rocks of the Flin Flon Belt, as well as fragments of earlier crystallized mafic Boundary intrusions. The younger olivine-bearing and felsic intrusions contain fragments of only the mafic Boundary intrusions (O'Hanley and Kyser, 1994).

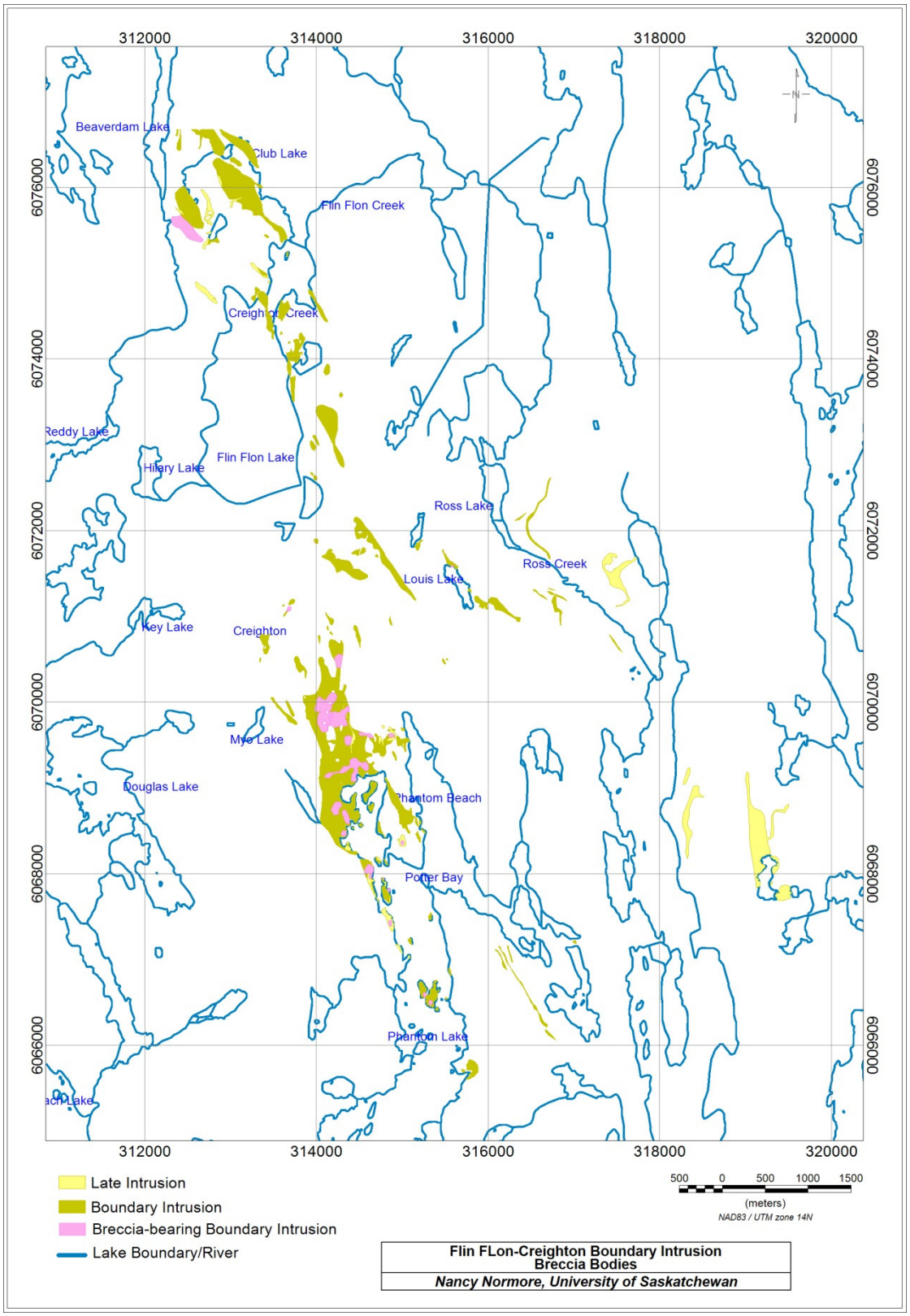

Figure 2-4. Breccia Bodies of the Boundary intrusions. Compiled from Syme (1975) and this study.

3.0 REVIEW OF LITERATURE

3.1 Defining a Breccia

A breccia can be defined as a coarse fragmentite composed of angular to sub-rounded (or rounded) fragments in a usually consolidated matrix (Laznicka, 1988). The components which comprise a breccia can be of any composition and origin and can be aggregated and consolidated in any number of ways (AGI, 2005). Breccias occur in sedimentary, igneous and metamorphic settings and their presence can potentially reveal an abundance of information about the processes of their formation and host environment. Breccias also commonly host several types of ore deposits and are consequently of great economic significance.

It wasn't until the mid-1700's the term breccia was used in French and English literature. The earliest use of the word found (by this author) is in a published (English) document by Emanuel Mendes de Costa, the author of *A Natural History of Fossils*, printed in 1757. Costa notes the term breccia was used by Italians to describe a sort of marble consisting of cemented fragments of different nature. The term was claimed to have been borrowed from the Italian miners of marble and limestone quarries who called it a "broken rock", or breccia (Laznicka, 1988). In the early nineteenth century, the definition of a breccia began to deviate away from its narrow description of broken rock in marbles to include more fragmented rocks types. The term still applied to marbles and limestones but evolved to include volcanic rocks and indicated either rounded (conglomerate) or angular (brecciated) fragments in the matrix. By the later nineteenth century, the extended description of a breccia was generally accepted. Today, breccia is still used to describe rocks with angular fragments, although rounded fragments can be present, and the term encompasses all rock types. Though the extended meaning of breccia appears widely accepted, it is evident that there still exists a lack of consistency in the approach to the description and labeling of breccias.

3.2 Research on Breccias and their Genesis

Breccia research, or research which may include breccias, is abundant in all streams of geology from igneous environments to sedimentary and tectonic settings. For the sake of brevity and relevance, this thesis will focus on breccia research in relation to igneous settings, and in particular, intrusive environments.

Despite the numerous authors that have studied or mentioned breccias at some level, there are a few researchers who are commonly cited for their detailed work on the subject of brecciation in igneous environments. They cover topics surrounding breccias from description and interpretation to their organization (naming and classification) and genesis. Commonly cited authors of breccia description, nomenclature and classification include Fisher (1960), Sillitoe (1985), and Laznicka (1988), although each of them has different approaches to organizing breccia deposits. Other authors such as McPhie *et al*. (1993) and Jébrak (1997) are also frequently referenced, however their work tends to include breccias as part of a broader geological environment or specialize in sub-areas of breccia research, such as statistical analysis of fragment geometry and distribution.

3.3 Description and Organization of Breccias

Due to the abundance and variety of breccias that exists in various geological environments, the need to (consistently) describe, name, and classify them is obviously important. This has been the subject of debate at some level since the creation of the Royal Geological Society of London in the year 1807. For example, Saussure (1796) uses "breccia" to define marbles with angular fragments, and "conglomerate" in a more general sense to include other rocks types containing rounded fragments (p. 45-46). Macculloch (1821), however, noted that previous authors (such as Saussure's (1796) and Kidd (1815)) have distinguished rocks with angular or rounded fragments using the terms "breccia" and "conglomerate", and claimed that "no advantage has arisen from them" as "sharp and rounded fragments can often be united in the same mass" (p. 142). Into the early 1900's, the amount of literature on breccia deposits increased considerably and consequently added to the complexity of the issues associated with the definition and

classification of breccias. Several views were proposed by different authors about the most appropriate way to describe, classify and name brecciated rocks, which often resulted in inconsistency between the various systems. For example, the work of Fisher (1960) and Wright and Bowes (1963) differed in their focus of naming a breccia based on the genesis of the fragments (Fisher) versus naming the breccia based solely on the origins of the matrix (Wright and Bowes). Over thirty years later, Jébrak (1997) pointed out that there was still no consensus among geologists concerning a rigorous approach for breccia description and interpretation. This statement still holds true today. No detailed and thorough work has been produced since work published by Sillitoe (1985) or Laznicka (1988), and their schemes are not used in all streams of geological science.

Each of the authors of breccia description, nomenclature and classification (Fisher (1960), Sillitoe (1985), and Laznicka (1988)) apply a different approach to organizing igneous-related breccia deposits. Work in classifying breccias in volcanic environments began with Fisher in the late 1950's. Fisher (1960) organized volcanic breccias into three categories based on observed mechanisms of brecciation: autoclastic, pyroclastic and epiclastic types. He then approached naming breccias based on the process of fragmentation and did not consider origin of the matrix as a defining factor. He argued the best approach to nomenclature is to consider the first word in the name as denoting the fragment origin of the breccia. The sub-types in Fisher's classification system are as follows: autoclastic breccia types (includes flow breccias), volcanic intrusion breccias (peperites and friction breccias); pyroclastic types (includes vulcanian, pyroclastic flow and hydrovolcanic breccias); and epiclastic types (includes laharic, water-laid volcanic and volcanic talus breccias). Shortly after Fisher's publication, Wright and Bowes (1963) rejected the system and suggested a scheme which instead focused on the matrix of the breccia and thus implied the origin or the deposit. Wright and Bowes also added the terms alloclastic, intrusive, and intrusion breccia in addition to Fisher's system. Wright and Bowes (1963) made the argument that *intrusion breccia* and *intrusive breccia* have different meanings. An intrusion breccia is considered a magma intruding into and incorporating fragmented wall-rock. An intrusive breccia, however, is a magmatic body with (foreign) fragments intruding as a breccia body into the host rock. However, it does not appear that this distinction has been made by many

proceeding authors using these terms as they are commonly used interchangeably (for example, Shao *et al.*, 2008; Nicholl *et al*., 2009; Vry *et al*.,2010; and Olianti and Harris, 2018).

Sillitoe (1985) provided a description and classification for ore-related breccias and organized them according to their genesis in intrusive, volcanic and hydrothermal processes. He also recognized the endless overlap between geological environments and breccia-forming processes, and noted that breccias commonly have a large variety of characteristics and that this is most likely the "norm". Building upon Sillitoe's work, Lawless and White (1990) offered a revised genetic classification system for breccias. Table 3-1 below summarizes the aforementioned authors' work on (ore-related) igneous-related breccias. Sillitoe (1985) and Lawless and White (1990) described breccias in terms of their characteristics of their environment (morphology of breccia deposits, contacts, notable features of fragments and the matrix, for example), their alteration and mineralization (replacement of fragments and previous matrix, associated ore…etc.), and origin (mechanisms for breccia formation).

Table 3-1. Summary of subdivision of (ore-related) breccias outlined by Sillitoe (1985) and Lawless and White (1990).

Breccia Category	Energy Source for Brecciation	Features	Examples
Magmatic-hydrothermal	Magma: hydrothermal fluids from retrograde boiling causing hydraulic fracturing of hostrock	<50% local to common rock flour matrix; angular to subrounded fragments, locally rounded; breccias for within/around single or multiple subvertical pipes	Breccia bodies of porphyry copper deposits
Phreatic, Magmatic-phreatic; Phreatomagmatic	Magma: brecciation is caused by the expansion of steam/gas from a water-dominated fluid heated by magma source; classification depends on varying amounts of magmatic volatiles versus groundwater content and connection to magma source	Rock flour matrix (<50% - 90%); angular to rounded fragments; pipe-like shapes	Diatreme Breccias at the Kelian Gold Mine, Kalimantan, Indonesia[1]; Maar volcano, Ukinrek Maar, Alaska[1]; Cripple Creek diatreme, Colorado[2]
Magmatic (volcanic)	Magma: brecciation is caused by release of pressure of magmatic volatiles (no interaction with groundwater)	Tuff matrix, pumice, cognate lithics; subrounded to rounded fragments	Los Bronces/Rio Blanco, Porphyry copper deposit, Chile[2]; Ashio copper deposit, Japan[2]
Intrusion	Magma: intrusive magma fragments and incorporates wallrock; dykes, sills, and other magmatic intrusion types	Crystalline igneous matrix; angular to rounded clasts	Santa Cruz syenite dykes, Borborema Province, Brazil[3]; Proterozoic minette dyke, Grenville Province, Quebec[4]; Boundary intrusions, Saskatchewan and Manitoba, Canada

[1]Howard, year unknown; [2]Sillitoe, 1985; [3]Ferreira *et al*., 2014; [4]Morin and Corriveau, 1996

A more comprehensive discussion by Laznicka (1988) covered the petrography, genesis and formation processes of all breccia types in several types of geological environments, such as but not limited to, volcanic, hydrothermal, intrusive, sedimentary, tectonic, and impact breccias. In general, he classified a breccia as a rudrock with fragments greater than 2 mm in size and defined it as a typically consolidated fragmentite with angular fragments (but sometimes not). Figure 3-1 illustrates Laznicka's two main criteria for distinguishing between the various types of

fragmentites: fragment shape (angular versus rounded) and size, and the degree of consolidation. Increasing fragment roundness tended to classification as a more sedimentary rock, such as a gravel or conglomerate. This definition is broad and is meant to allow flexibility in applying the name. Rather than devise a naming system and characterize breccias in detail, Laznicka included them as a type of rudrock and goes on to describe in detail the various types of rudrocks (including breccias) and their environments of formation. He notes that empirical organization of breccias is "unsophisticated" and the current practise uses terminology that express a variety of features prominent to the breccia in observation. A few of the examples he provides include friction breccias indicating the generative process, intrusive breccia for emplacement style, and vent breccia for the locale of emplacement (pp. 545 in Laznicka, 1988). The variety of terms used, some which may have analogous meanings (pp. 546), is one obvious reason why classification of these rocks types is difficult to standardize across geological disciplines. In dealing with the subject of breccias, Laznicka considers the observable and measurable properties of breccias of fundamental importance and suggests that genetic factors (and thus classification) are considered secondary, and often dependant on the interpretations of the investigator. In order to reconcile observations with geological theory, it would be ideal to include all possible quantitative parameters, as well as qualitative, in the methods for characterizing breccia bodies.

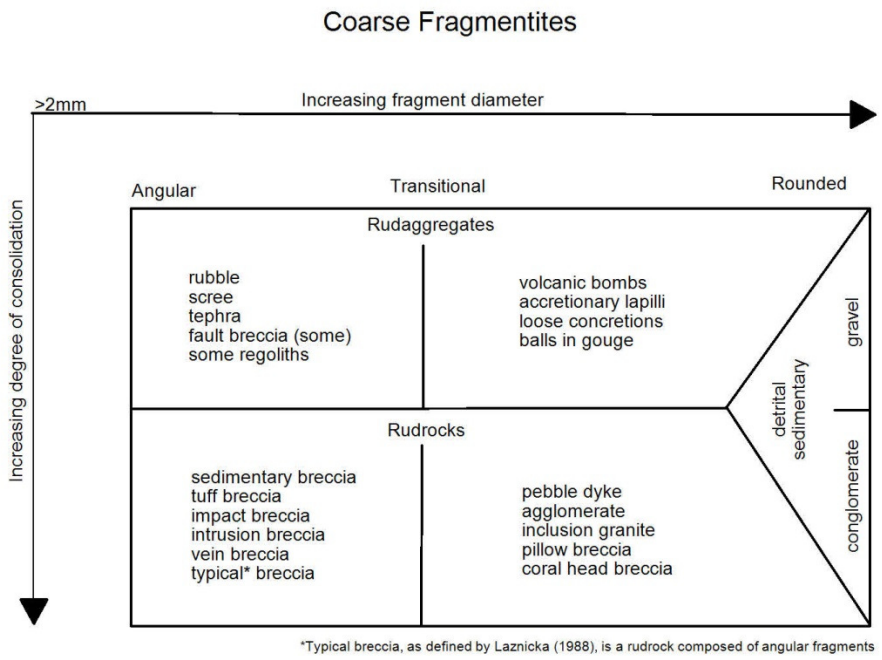

Figure 3-1. Division of rudrocks by Laznicka (1988). Based on degree of consolidation and fragment size and shape.

Work of other authors, such as McPhie *et al*. (1993) and Jébrak (1997), tend to include breccias as part of a broader environment or specialize in sub-areas of breccia research. Jébrak looked into the mechanisms of brecciation in a hydrothermal (ore-bearing) vein system, emphasizing fragment geometry and distribution. McPhie *et al*. (1993) does not focus on breccias in volcanic environments but provides a method to identify and name volcanic deposits which can include breccias within an organizational system similar to Fisher (1960). For breccia deposits, McPhie *et al*. (1993) used terms already common, such as autobreccia, hyaloclastite breccia and pyroclastic breccia, and grouped them under the appropriate volcanic environment.

3.4 Mapping and Describing Breccias

The potential knowledge gained from breccia study necessitates the proper and comprehensive collection of field data. These deposits can reveal an abundance of information on their processes of formation from their fragment-matrix relationships, host-rock lithologies, or from fragments of a distal source incorporated in the breccia, to name a few characteristics. As stated

by Laznicka (1988), in order to reconcile observations with geological theory, it would be ideal to include all possible quantitative parameters, as well as qualitative, in the methods for characterizing breccia bodies.

Collectable information on a breccia body can be divided in to three categories: 1) information pertaining to the breccia body as a whole, 2) information on the breccia fill, and 3) information on the fragments of the breccia. Data is both quantitative and qualitative and considers relationships between the fragments, fill, and between the breccia body and the surrounding environment. Figure 3.2 shows examples of features pertaining to the breccia body (in particular, to intrusion breccias) and relevant fragment features such as patterns of distribution, various fragment shapes and forms, possibilities for contacts with the wallrock, and common textures described in relevant research.

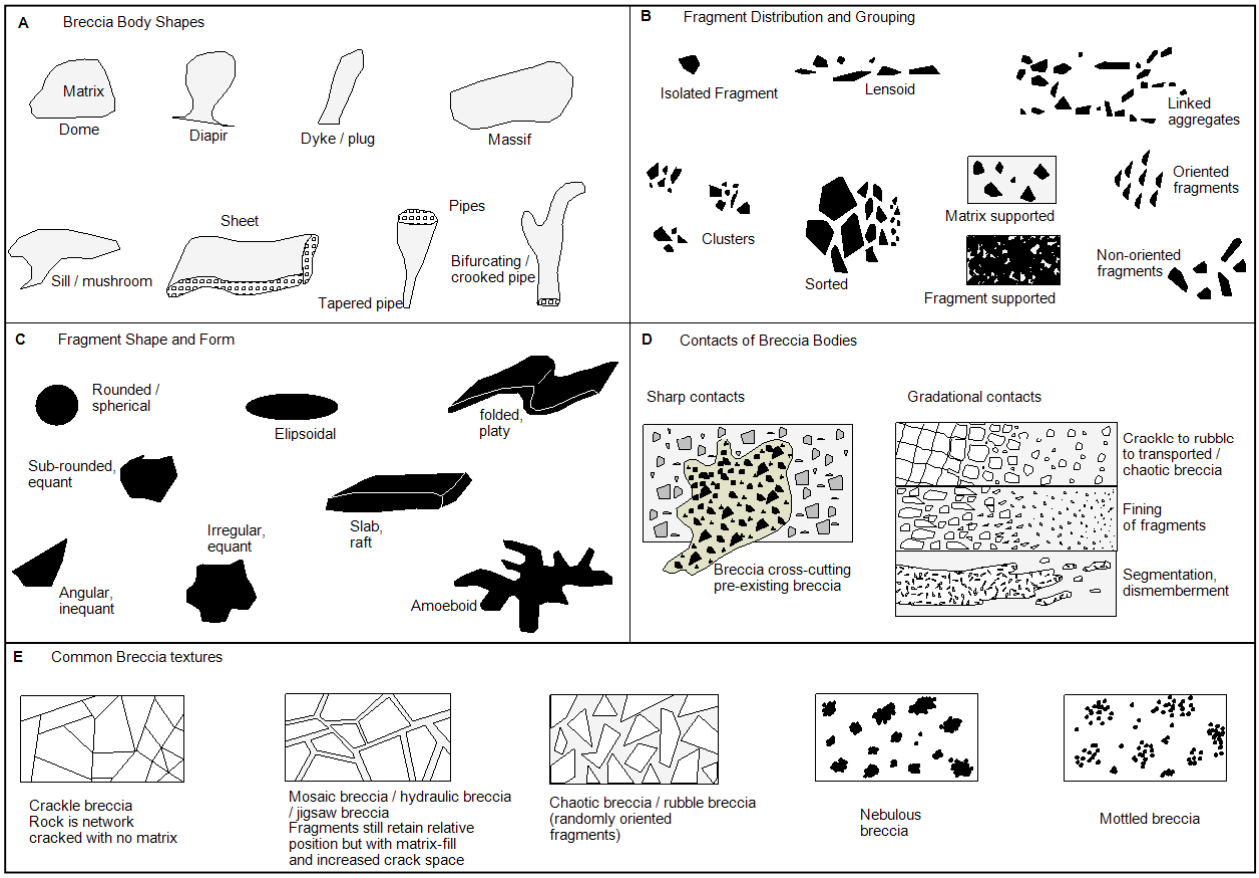

Figure 3-2. Compilation of select breccia body and fragment features with particular relevance to intrusion breccias. Matrix is represented by pale grey-coloured fill. Taken from Laznicka (1988).

When describing the body encompassing the breccia, notable features include the overall shape and morphology of the body, the dimensions, topographical features, occurrence, structural information, contact relationships with adjacent rock units, alteration features, mineralogy of the breccia host, and existing economic mineralization (if present). Within the breccia body, the breccia fill, or matrix, and its estimated volume, as well as composition (from mineralogy or geochemical analysis) and fabric can offer insights into the breccia body formation and alteration history. Depending on the purpose of the breccia study, information collected from the fragments of a breccia can encompass both qualitative and quantitative data. Qualitative data includes descriptions of the various fragment populations (monomictic or polymictic), degree of assimilation or disaggregation within the matrix, contacts with the matrix, overall organization of fragments or groups of fragments, and the composition and fabric of various populations of fragments. Quantitative data includes volume of fragments to matrix, fragments shapes and size, and may include attempts to quantify some qualitative features such as applying a vector to fragment orientation.

3.5 Breccia Formation in Intrusive Settings

Fragments can be generated and incorporated from the initial formation of the magma to the final emplacement of the breccia in a magma plume, associated with the magma transport itself or in relation to syn-magmatic hydrothermally-placed fluids. Transport of fragments can continue along a continuum to volcanic environments and be extruded with magma and volatiles, or new fragments can be created during the extrusive processes. Fragments may be assimilated and contaminate the groundmass to varying degrees depending on various properties of the groundmass, country rock and type of emplacement. Figure 3-3 is a schematic diagram showing a number of end-member breccia environments of formation within igneous-related (and other) environment.

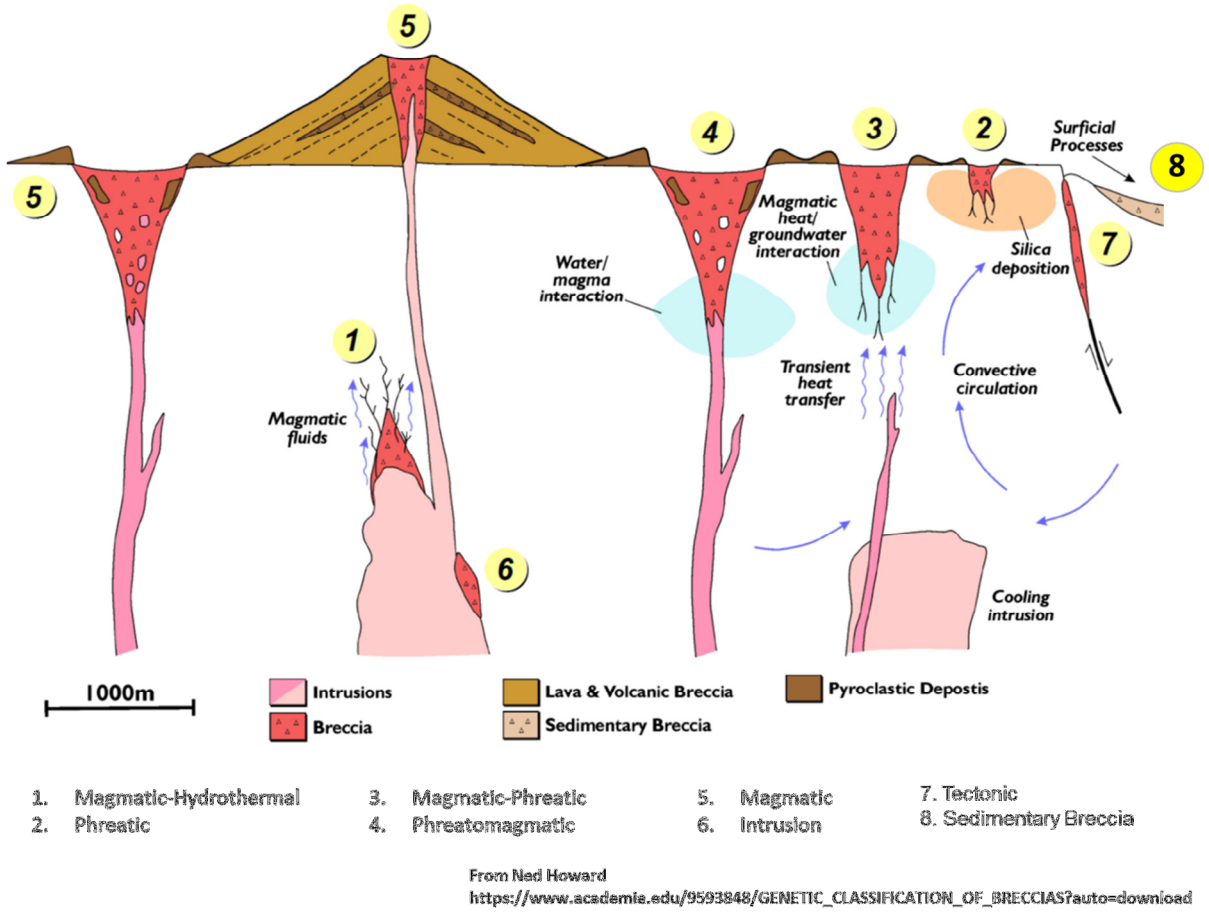

Figure 3-3. Schematic diagram of end-member breccia environments of formation. Taken from Ned Howard, year unknown.

Space is created for a rising magma body through one or more of several emplacement processes, some of which will inevitably create an availability of xenoliths for incorporation (Figure 3-4A). Morin and Corriveau (1996) conducted a study on the fragmentation processes and xenolith transport in a Proterozoic minette dyke in the Grenville Province in Quebec (Canada), and clearly summarized the possible breccia-producing processes that take place during emplacement of a magma body. Depending on the contrasting rheology of the country rocks and characteristics of the magma, a pluton may undergo such fragment generation processes as stoping (Figure 3-4A), dyke propagation and emplacement (Figure 3-4A and B), magmatic fluid exsolution or interaction with groundwaters (Morin and Corriveau, 1996) (Figure 3-4D and F), or fill tectonic voids such as shear zones (Figure 3-4A and E), fold hinges and local

extensional domains in which loose fragments were made available through mechanical disruption (Figure 3-4A and E) (Best and Christiansen, 2001).

In the process of stoping, pressure from the magma intrusion (hydraulic pressure), from exsolved volatiles, and heated groundwater (thermal stress) cause fracturing and subsequently creates fragments which are then incorporated into the magma fluid. The magma dislodges country rock as a way to create space and move upward. As fragments of country rock are created, they are physically incorporated into the magma and may be assimilated to varying degrees (Best and Christiansen, 2001). In order for stoping to be a truly effective process, the country rocks must be denser than the magma and must be brittle, and this therefore necessitates that stoping take place in shallower, cooler crust (Ferreira *et al.*, 2014). Also, the presence of confined water where heating by magma creates greater opposing pressures enhances the likelihood of stoping in the crust (Best and Christiansen, 2001).

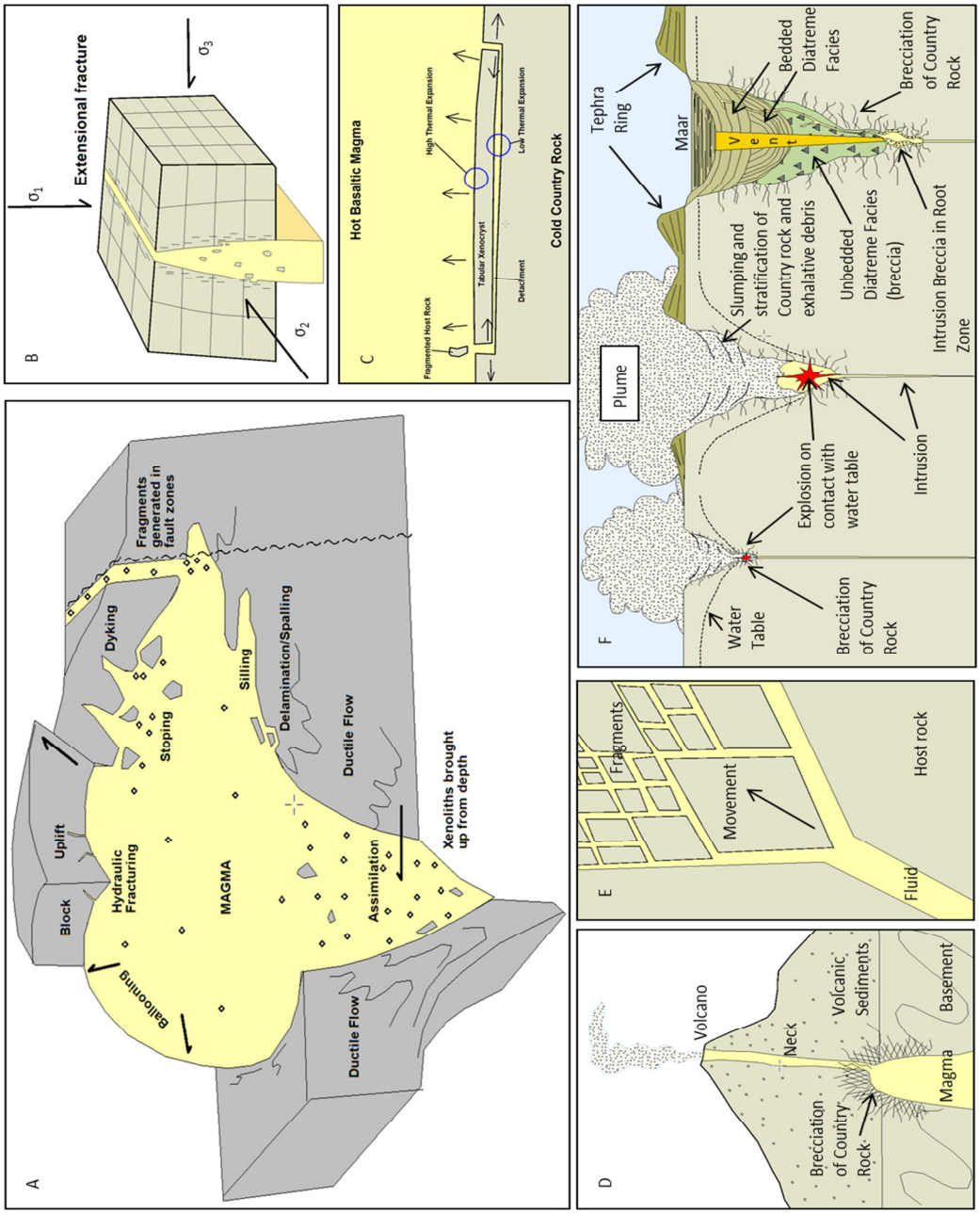

Figure 3-4. Compilation of schematic diagrams illustrating brecciation mechanisms and morphology related to intrusions. See Chapter 3 for description of processes. A) Methods of fragmentation/brecciation associated with general magma emplacement applicable to a variety of scales. Redrawn and modified from Best and Christiansen (2001) and Laznicka (1988). B) Fragmentation (delamination and spalling) during crack-tip propagation of a dyke. Redrawn from Best and Christiansen (2001) and modified after Morin and Corriveau (1996). C) Thermal delamination of tabular fragment. Redrawn from Motoki *et al*. (2009). D) Brecciation associated with porphyry-style deposits. Modified from Earle (2019). E) Brecciation during faulting. Fragment rounding can occur with continued fault movement. Redrawn from Jébrak (1997). F) Brecciation processes and resulting breccia deposits during formation of a diatreme. Modified from Lorenz and Kurszlaukis (2007) and Valentine and White (2012).

Brecciation during magma ascent in dykes can occur through fracturing of the channel wall during magma propagation and emplacement, continuous spalling of the country rock wall during magma movement, or through mechanical and thermal delamination (Ferreira *et al.*, 2014) (Figure 3-4A, B and C). Brittle behaviour (brecciation) occurs in the crust where country rock exhibits low pressure and temperatures and respond to high strain rates by fracturing, breaking apart or losing cohesion. Magma propagation by the crack-tip model (hydraulic fracturing) occurs when the pressure exerted by the magma exceeds the elastic strength of the rock, causing the host rock to split along extensional fractures oriented parallel to σ_1 and perpendicular to σ_3 (Best and Christiansen, 2001). Dyke-parallel fractures are created at the crack-tip (Figure 3-4C), the magma eventually intrudes the fractures and over time the country rock is detached (spalling) (Morin and Corriveau, 1996). In addition to the application of hydraulic pressure to initiate fragmentation, thermal stress is also a significant factor. Temperature differences between the magma and country rock cause thermal expansion at the contact, but less so into the wall of the country rock. This difference in thermal expansion from the inside to the outside of the country rock causes fracturing parallel to the contact plane. Fracturing may continue until the magma can invade the space and cause delamination of the fragmented wallrock (Figure 3-4C) (Motoki *et al*., 2009).

Exsolution of fluids can also occur from a fluid-saturated magma pluton, creating brecciated host rock such as those seen in porphyry deposits (Figure 3-4D). Fluid-oversaturated magmas contain an upward drilling process, which applies hydraulic, and thermoelastic stress fracturing the rock ahead of the magma column. This results in significant brecciation of the wallrock and may also helps create the circular conduit, or pipe shape (Figure 3-4F). Breccia mechanisms capable of creating voids for these upward moving magmas include (from Sillitoe, 1985): 1) upward removal or dissolution of rock material by fluids released from cooling magma (Locke, 1926), 2) release (possibly explosive) of volatiles from magma (Walker, 1928; Emmons, 1938), 3) gravity or collapse of wallrock upon retreat of magma (Hulin, 1948; Perry, 1961), and 4) exsolved volatiles accumulating at the roof of a pluton (Norton and Cathles, 1973). One or all of these processes could be involved in breccia formation. Examples of resulting breccia-laden fluid-oversaturated deposits include kimberlites and other breccia-pipe deposits, which may or may

not extrude to the surface. For those that reach the surface, an explosion crater is formed, adding with it another layer of brecciation.

As magma ascends, it follows the path of least resistance which may be pre-existing structural voids, and consequently incorporates the fragments created through tectonic friction. The main mechanism of brecciation occurs when the stress applied to the rock exceeds the brittle resistance of the country rock. Fractures with fragments can be millimeters to meters wide and many kilometers in length, and fragment shape can be angular to rounded (Jébrak, 1997). Magma infill can pick up and transport fragments, or alternatively solidify them in place, and may or may not affect the fragment shape depending on temperature, composition and time of transport before magma crystallization.

Entrained fragments can be derived from a foreign source or may be genetically related (or cogenetic) to the host intrusion. Streck (2008) pointed out that antecrysts are "cognate crystals that originate from a magma genetically related to the one in which they are found, but are older and did not grow from the liquid in which they are found (Hildreth pers. comm.)". In contrast, xenoliths are not genetically related to the magma in which they are encompassed and are of considerable interest because they are interpreted as being transported from deeper depths. Xenoliths may offer insight to the country rock and processes of ascent relevant to the magma path. Alkaline, silica-undersaturated magmas such as kimberlites and lamproites, for example, can contain xenoliths of eclogite, possibly derived from the mantle or lower crust, plucked from mantle conduit/chamber walls and brought to the surface by rapid ascent (Best and Christiansen, 2001). Using the dimensions of the largest xenolith or antecryst present in a crystallized magma, a maximum ascent rate can be estimated using Stoke's Law modified by Shaw's calculation (See Appendix B). Kimberlite ascent rates, for example, are estimated to be as high as144 km/hr (Peslier and Luhr, 2006; Peslier *et al*., 2008).

4.0 METHODOLOGY

Samples and data were collected from four locations in the Creighton, Saskatchewan and Flin Flon, Manitoba area: Green Street, Louis Lake, Phantom Beach, and Club Lake. Sample sites were largely chosen based on accessibility and the presence of brecciation within the Boundary intrusions as indicated by maps completed by the Manitoba Geological Survey and the Saskatchewan Geological Survey, in collaboration with the Geological Survey of Canada, Laurentian University and Hudson Bay Exploration and Development Company Limited (Simard *et al*., 2010).

Two areas were chosen for detailed outcrop mapping: the intrusion located immediately south of Green Street in Creighton, Saskatchewan, and an outcrop located at the north end of Louis Lake, in Flin Flon, Manitoba. The mapped Green Street Boundary intrusion exposure is approximately 75 m by 65 m, and the Louis Lake outcrop exposure is smaller, covering approximately 10 m by 12 m. Samples were collected from available broken rocks from the main outcrops where their connection to the bedrock was obvious. Samples and the outcrops exhibited similar or the same degree of alteration and the author feels confident that the freshest available samples were obtained. Sample collection included select sampling of rock representing both the matrix and fragments of the intrusions and their breccias. These samples were cut for thin section analysis and analyzed for whole rock and trace element geochemistry.

A total of forty-nine rock samples were collected from the Flin Flon and Creighton areas. Of those, thirty-five were cut for petrographical analysis, and twenty-five samples were chosen for geochemical analysis. Table A1 in Appendix A contains a brief description of each individual section and geochemical sample. Twenty-six thin section chips (26 x 46 mm) were cut from samples using saws in the Department of Geological Sciences at the University of Saskatchewan and sent to Vancouver Petrographics Ltd. in Langley, British Columbia for the

preparation of polished thin sections. Nine large (50 x 75 mm) thin sections were prepared in the Department of Geological Sciences thin section laboratory. All geochemical samples were sent to the Saskatchewan Research Council Geoanalytical Laboratories for analysis. Whole rock analysis was by inductively coupled plasma mass spectrometer (ICPMS) (Perkin Elmer Sciex DRC II ICPMS). Trace element analyses were obtained by using ICPMS fusion (Lithium Metaborate) for trace elements. FeO wt% was tested separately using the HF/H_2SO_4 titration method. Geochemical analysis and method summaries are also included in Appendix A in Table A2.

Rock samples are labeled according to their location (GS for Green Street, LL for Louis Lake, PB for Phantom Beach, and CL for Club Lake) and the order of collection. Rock samples with a letter following the number indicate it is part of a series of samples from the same location. Thin section samples are labeled with the prefix "TS_" to the rock sample from which it was cut. Rocks from which more than one thin section was obtained are numbered and lettered in sequence following a dash in the label, in the same manner as the rock samples. Geochemical samples are identified with the prefix "GC_" and numbered according to preparation sequence.

Density measurements were obtained in-house for a mafic intrusive fragment from the Green Street area, a matrix sample from the Green Street area, and a matrix sample from the Louis Lake sample site. Mass was measured in grams using an analogue scale. Volume of the rock sample was obtained by measuring the amount of water displaced in a container by the sample.

5.0 RESULTS

This study has added detailed geological mapping for two outcrops of the Boundary intrusions: Green Street and Louis Lake (See Figure 5-1). Outcrop observations of the Club Lake and Phantom Beach areas are also included in this section. Petrographical descriptions and major and trace element geochemistry has been completed for all sample sites and are included in the following sections.

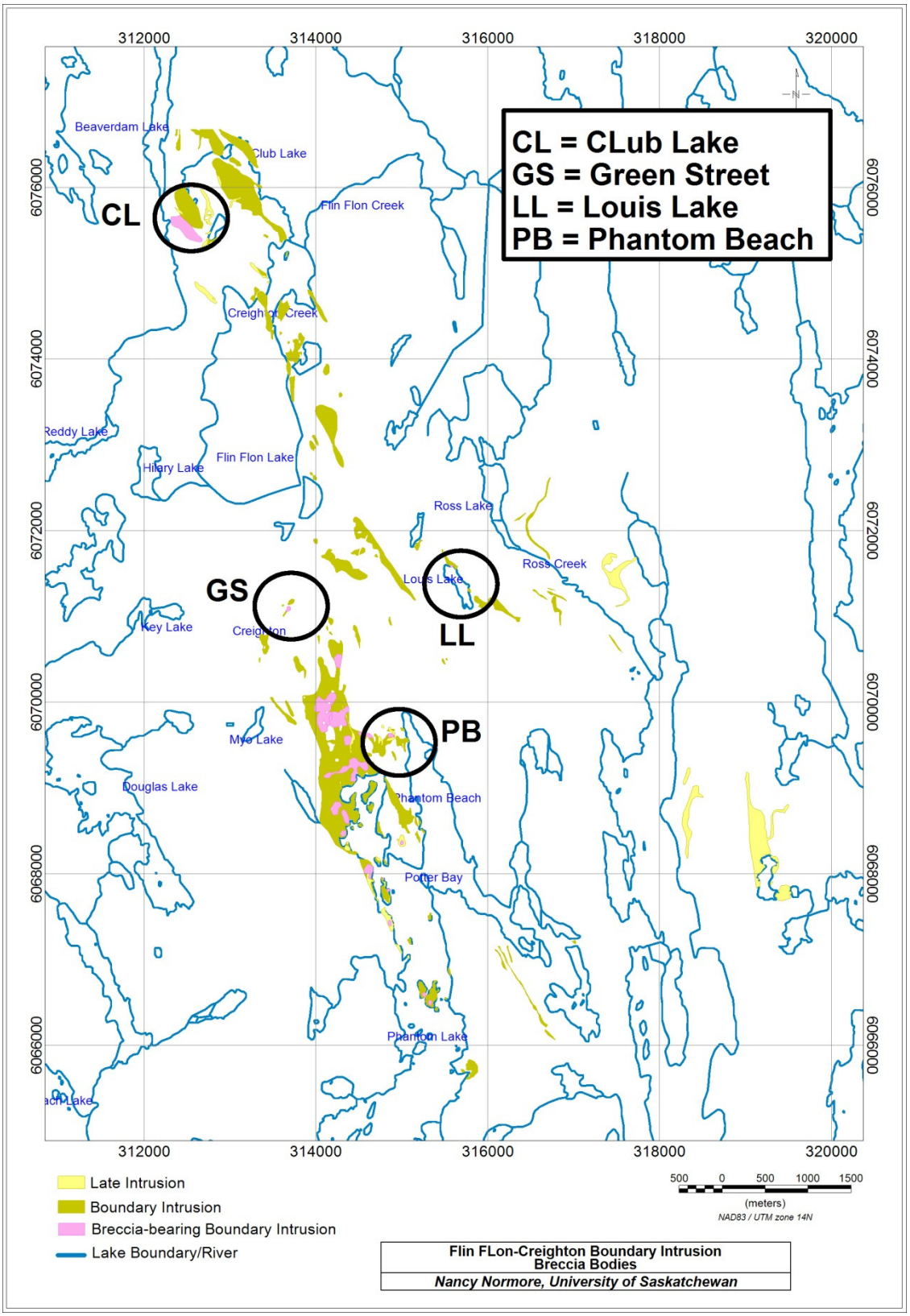

Figure 5-1. Location of breccia outcrops sampled in this study.

5.1 Field Relationships and Petrography

5.1.1 Green Street Intrusion Breccia

The Green Street Boundary intrusion breccia is located at the intersection of Green Street and Five Corners Avenue in Creighton, Saskatchewan, and extends immediately south for approximately 250 m. The Green Street Intrusion occurs as a dyke which trends north-easterly and has dimensions 80 m length by 8 - 17 m width (Figure 5-2). Smaller centimeter scale (≤10-20 cm) dykelets extend from the main intrusion on the northwest side, roughly perpendicular to the trend of the main body. Contacts with the country rock are overall sharp with no obvious evidence of deformation related to intrusion emplacement, or large continuous chilled margin or hydrothermal alteration in the adjacent rocks. An example of intrusion contacts is shown in Figure 5-3 (A and B) and sample GS06 of Figure 5-3D. Evidence of fabric deformation (syn- to) post-deformation at the outcrop scale includes local shearing near and at contacts and within the intrusion (Figure 5-2C), however, there is no preferred orientation to the minerals in the main intrusion. Near and away from the intrusion contact margins, fragments of the country rock are also commonly entrained within the leucocratic diorite intrusion, along with abundant fragments of older Boundary intrusions of gabbro composition. The country rock comprises volcanic rocks from the Blue Lagoon Member of the Flin Flon assemblage and intrusive rocks labeled as "undivided" or "syn-volcanic intrusives" (Simard *et al*., 2010). Exposure of the intrusion is excellent over the majority of the mapped area, with very little lichen on most rock surfaces. Unmapped areas are covered in heavy vegetation that could not be removed.

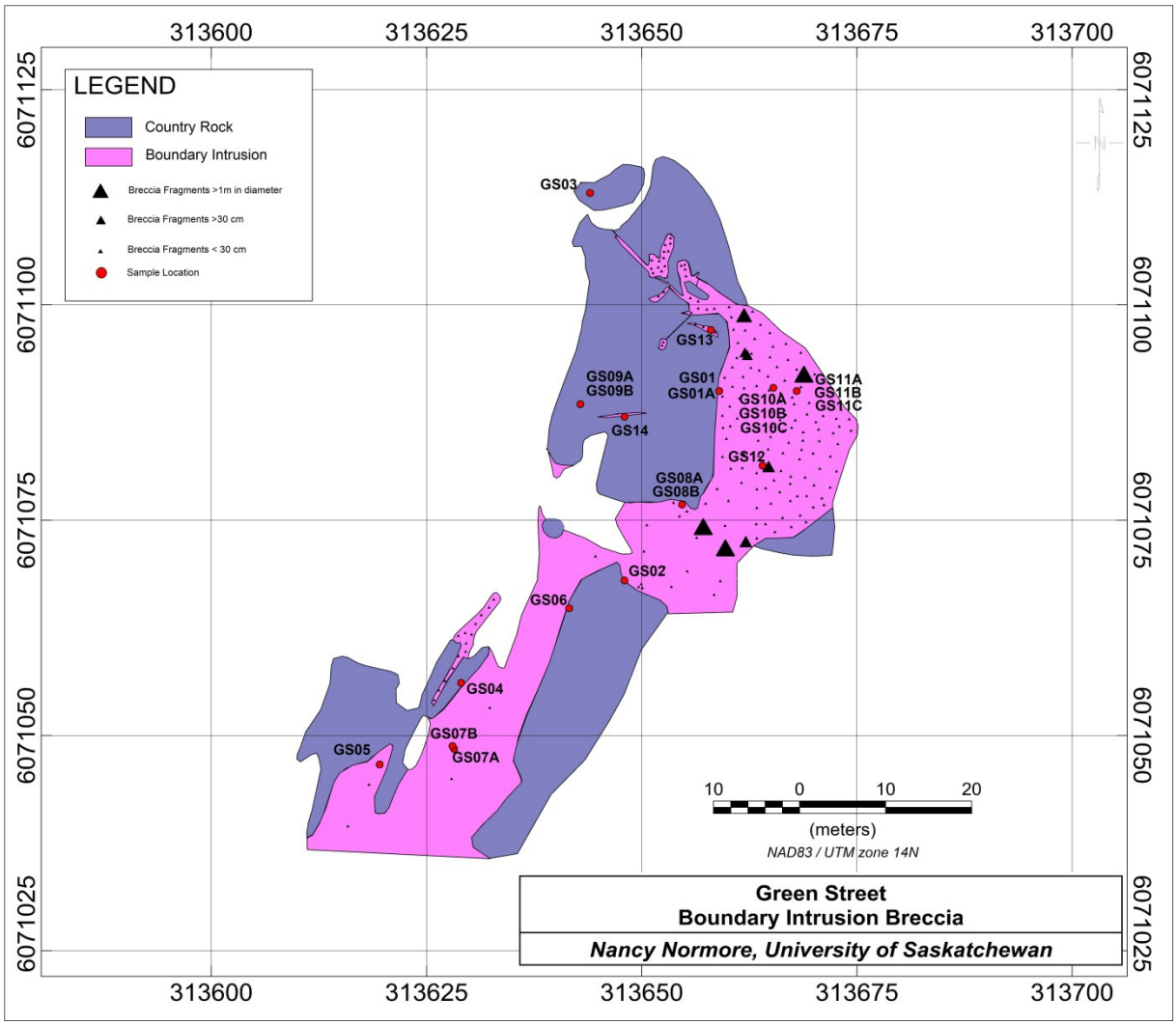

Figure 5-2. Detailed Mapping of the Green Street Boundary intrusion Breccia with sample locations.

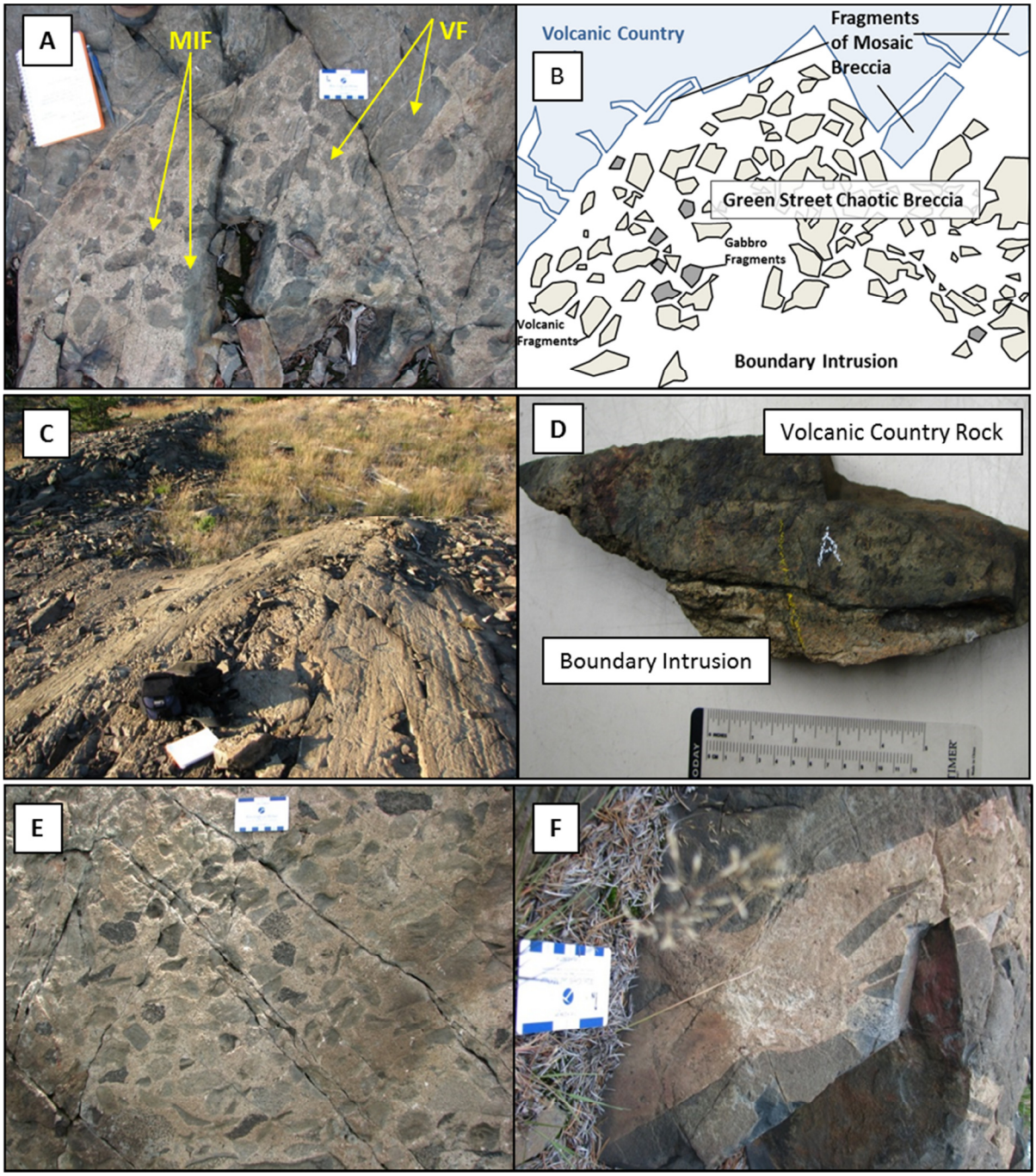

Figure 5-3. Representative images of Green Street sample site. A) Representative example of Green Street Boundary intrusion breccia. Location in area of sample GS08A. Image shows volcanic country rock-Boundary intrusion contact. Arrows with label "MIF" point to mafic intrusive fragments (gabbro); arrows with label "VF" are volcanic country rock fragments. B) Diagrammatic representation of image A. C) Green Street post-deformation in outcrop. Shearing of country rock and Boundary intrusion rocks. Located to west of GS04. D) Hand sample (GS06) of Boundary intrusion-volcanic country rock contact. E) and F) Further examples of chaotic breccia (in area of GS12 and GS08A) and hydraulic brecciation (in area of sample GS03) in the Green Street intrusion breccia.

The main cluster of fragments within the polymictic intrusion breccia is located in the most north-easterly 25 m of the mapped Green Street dyke, and spans the entire width of that section (Figure 5-2). Relative fragment density is indicated by the distribution of black triangle symbols, and fragment size is grouped into three categories, as indicated in the legend. Fragment population decreases southwestward beyond the "kink" in the dyke, most likely a step in the structure the dyke has intruded. Beyond the step, fragments in the body are infrequent to rare and are mostly restricted to the contact margins, with the exception of one dykelet to the west of sample GS04 (Figure 5-2). Larger fragments up to 1.8 m in diameter are comparatively few compared to fragments up to 10 - 15 cm in diameter (typically average a few centimeters to 10 cm) and are located mostly towards the edges of the main fragment cluster. From observation in plan-view, it appears that larger fragments in the area of sample GS08A and B (in the area of the step of the dyke) may be somewhat of a barrier to smaller fragments potentially reaching the rest of the intrusion.

The Green Street breccia is a polymictic, matrix-supported breccia with both mosaic (hydraulic) and chaotic (randomly oriented) patterns of fragment arrangement (Figure 5-3A and B). The majority of the Green Street breccia is chaotic patterned with the exception of a very weak alignment of polymictic fragments and mosaic patterned brecciation near contact margins. Mosaic breccias are found near margins of the intrusion where country rock has been incorporated, but fragments have not traveled any significant distance from the source. The breccia fragment population is made up of various compositions of volcanic rock and mafic intrusive fragments, and intrusive fragments comprise up to 15 - 20% of the fragment population. The space between chaotically arranged fragments in the Green Street intrusion matrix in the most densely populated area (Figure 5-2) ranges from 0 – 6 cm, the matrix area ranges from 39 – 42% surface area, and there are approximately 170 to 200 fragments per square meter. In the southern half of the intrusion where fragments are rare, fragment density ranges from 0 – 1 fragment per square meter and matrix area is near or equal to 100%. Some fragments can blend with the matrix colour or may be assimilated (melted) into the matrix. It can therefore be difficult to be sure of the exact number or types of fragments present.

Maps of the Green Street intrusion by Simard *et al*. (2010) label it simply as Boundary intrusion, and label an intrusion immediately to the north (within 25 – 100 m), which appears to be a continuation of the Green Street intrusion shown here, as hornblende melomonzodiorite, melatonalite and/or meta-quartz-diorite. Analysis of a fragment-free thin section of the intrusion indicates crystalline hornblende-bearing quartz diorite composition. Petrographic analysis shows dominant plagioclase with 15 – 20% quartz, 10 – 20% mafic minerals (actinolite and hornblende), and accessory minerals which include chlorite, calcite, epidote, rutile, sulphides and oxides (Figure 5-4). Anorthite values suggest albite, but variations in extinction angles in the twinning vary greater than four degrees resulting in few reliable measurements. The feldspar is considerably altered through sericitization and epidotization. Plagioclase occurs as subhedral to euhedral tabular grains with quartz and some actinolite or other amphiboles growing interstitially or as phenocrysts. Quartz occasionally exhibits undulose extinction. Crystals of all types can reach up to 2 mm in diameter, but are commonly less. Subhedral to anhedral, pale green to medium green actinolite may be altered phenocrysts to the plagioclase and quartz matrix (Figure 5-4C - F), but also as possible altered xenocrysts or antecrysts. Some actinolite crystals can be up to 5 mm in diameter, but are commonly less than 3 mm. Quartz grain-size is typically less than 1 mm. All minerals present show no preferred orientation.

The typical matrix of the Green Street intrusion contains two main types of amphibole crystals (sample GS07B, Figures 5-4A - J): 1) regular, anhedral to subrounded to round, floating crystals of actinolite ranging from 1 – 3 mm in diameter (images A - F); and 2) anhedral to euhedral, bladed and rhombohedral hornblende (and/or actinolite) typically 1 – 2 mm in length, but can reach 4 – 5 mm (images G - J). Type 1 grains may have intergrowth of several smaller actinolite crystals (images C and D) or may be one single crystal (images E and F). The actinolite can be partially altered to chlorite and exhibit a mottled texture (images E and F), or grains can be relatively unaltered and closer to subhedral in shape with no other intergrowths present. Actinolite grains of Type 1 are often rimmed with smaller actinolite or hornblende crystal growth and/or chlorite (images C - F). The floating actinolite crystals found in the matrix of the fragment-free section of the Boundary intrusion are similar to the grains of the gabbro fragments of the breccia (images C - F). Type 2 crystals may also be rimmed with chlorite or smaller

grains of actinolite, although the rim is thinner in width. The rhombohedral amphibole is assumed to be cross-section of the bladed grains.

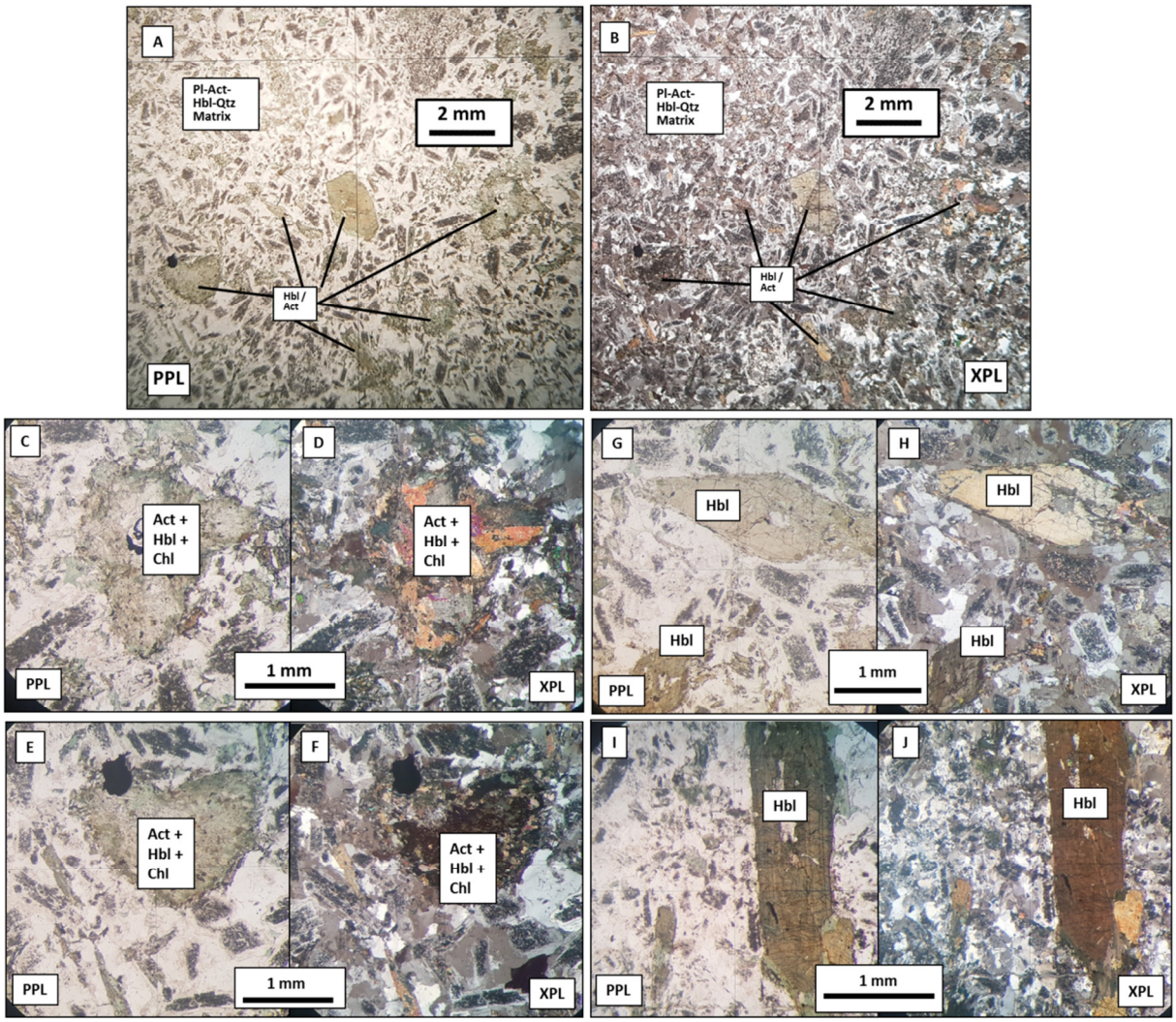

Figure 5-4. Sample TS_GS07B. A) and B) Plain Polarized Light (PPL) and Cross Polarized Light (XPL) of sample GS07B. Sample is representative of fragment-free Boundary intrusion matrix. C) – J) Examples from thin section showing two main types of amphibole crystals in the Green Street Boundary intrusion matrix. Each image shows crystals in PPL and XPL. C) and D) Intergrowth of several amphibole crystals (actinolite ± hornblende) in single grain with finer-grained chlorite ± amphibole (hornblende) rim. E) and F) Singular amphibole crystal partially altered to chlorite. G) and H) Euhedral rhombohedral hornblende. I) and J) Singular bladed euhedral hornblende. Act = Actinolite; Hbl - hornblende.

Mafic intrusive xenoliths are gabbro to plagioclase-bearing ultramafic in composition and considered to be earlier versions of the mafic Boundary intrusions incorporated from depth. The

bulk of these fragments are also typically less than 10 - 15 cm, but some can reach boulder size up to 1.8 m (Figures 5-5A and B). Gabbro xenoliths are usually rounded to subrounded and may exhibit varying degrees of disaggregation into the intrusion matrix, resulting in a nebulous or mottled breccia texture (Figure 3-2E). Figure 5-5C to G and J compare a whole fragment and a partially disaggregated fragment in field photos and thin section. The actinolite grains of the fragments are altered pyroxenes, most likely augite. The whole fragments (C and D) are in sharp contact with the matrix, however, where disaggregation may take place, individual amphibole grains appear separated from the fragment where boundaries were once shared with adjacent crystal grains (E, F and J). Plagioclase crystals between disaggregated amphibole grains show an alignment with the grain boundaries (Image J), but it is unclear if this is indicative of any process taking place during possible disaggregation. Mafic fragments could also be plagioclase-bearing ultramafic rocks, depending on how much plagioclase was originally in the fragment before incorporation into the intrusion.

Volcanic fragments range from leucocratic to melanocratic and are predominantly less than 10 - 15 cm in diameter, but occasionally can be larger (Figure 5-3A, B, E and F). Clasts are rounded to angular in shape. Where fragments occur in the mosaic breccia and have not travelled far from their source, fragments are very angular (Figures 5-3A, B and F). However, angular fragments are also found throughout the intrusion breccia. Partial melting with the intrusion matrix occurs locally. Overall, the intrusion matrix adjacent to the volcanic fragments shows no obvious chilled margins from field observations. However, some thin section samples do exhibit a subtle change in grain-size of the matrix at the margins of volcanic fragments or at the country rock contact. GS13-01 (Figure 5-5H) shows a decreased grainsize of plagioclase and quartz minerals within 2 – 3 mm of the volcanic fragment, and an approximately 1 mm quartz-rich margin is noted at the volcanic country rock-intrusion contact within the dykelet of thin section sample GS14-01 (Figure 5-5I).

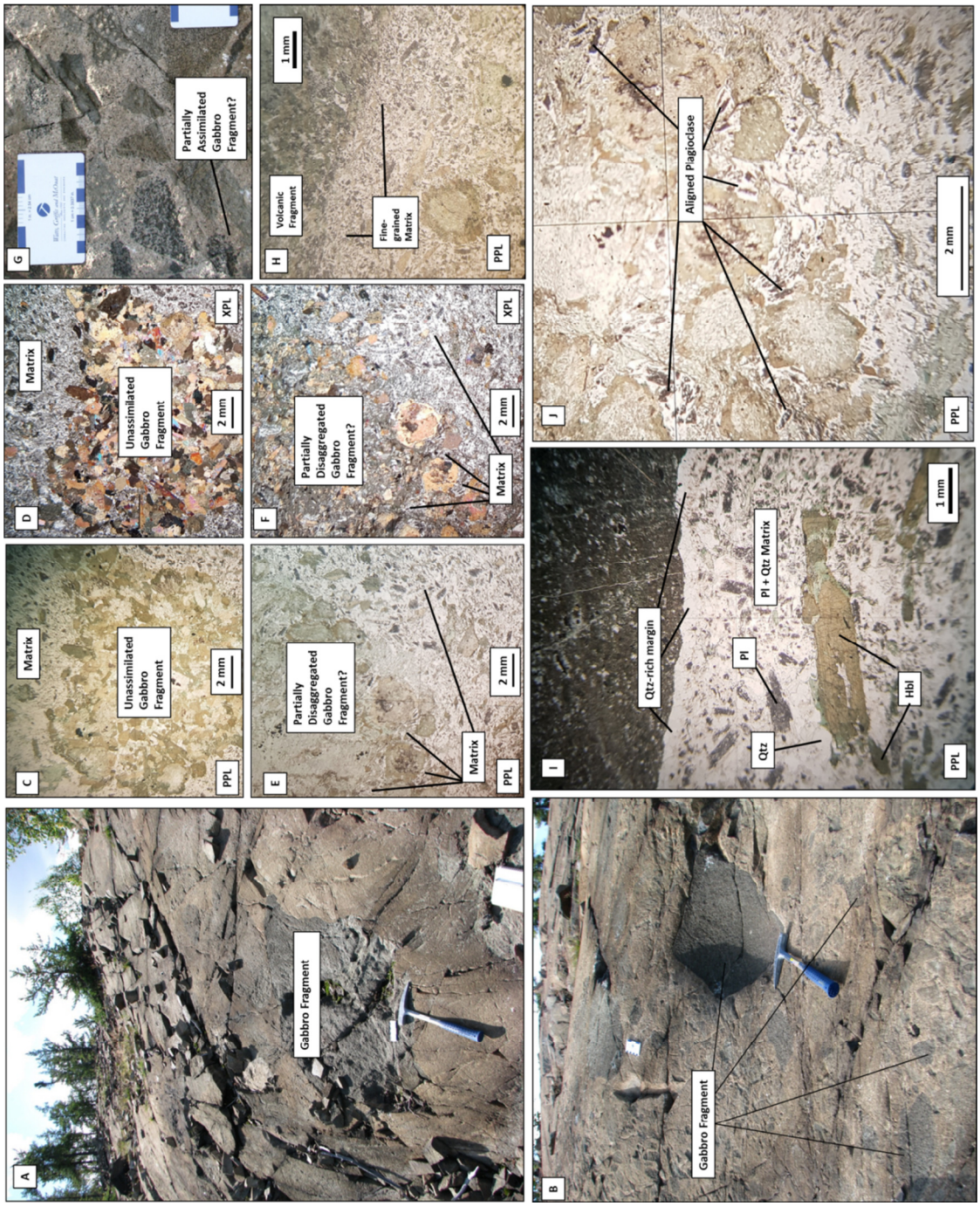

Figure 5-5. Field and thin sections photos of the Green Street area. A) and B) Examples of gabbro xenoliths in the Green Street Boundary intrusion from the north extension of the intrusion breccia. C) – G) Textures of whole fragment (C and D) in sample TS_GS01A-02B, and partially disaggregated fragment (E and F) in plain polarized light (PPL) and cross polarized light (XPL) of sample TS_GS10C-01, and in outcrop (G). H) Chilled margin in thin section of sample TS_GS13-01 in plain polarized light (PPL). I) Quartz-rich margin at Boundary intrusion dykelets-country rock contact in sample GS14-01. J) Close-up of sample TS_GS10C-01 (Image E and F). Qtz = Quartz; Pl = Plagioclase; Act = Actinolite; PPL = Plain Polarized Light; XPL = Cross Polarized Light.

5.1.2 Louis Lake Intrusion Breccia

The Louis Lake intrusion breccia is located at the north end of Louis Lake in Flin Flon, Manitoba (Figure 5-1). The exposed mapped area of the Louis Lake intrusion is irregularly-shaped and covers an area of approximately 13 x 10 m (Figure 5-6). Exposure is excellent with little to no lichen-cover, however, the rock surface is variably oxidized. Shearing is most evident on the west side of the outcrop (Figure 5-7) and the ductile fabric suggests compression post-deposition of the intrusion. Subtle ductile compression features such as grain alignment and more obvious brittle features such as veining can be noted locally in the outcrop. Samples were also collected from breccia-free intrusions to the southeast of the mapped area (Figure 5-8).

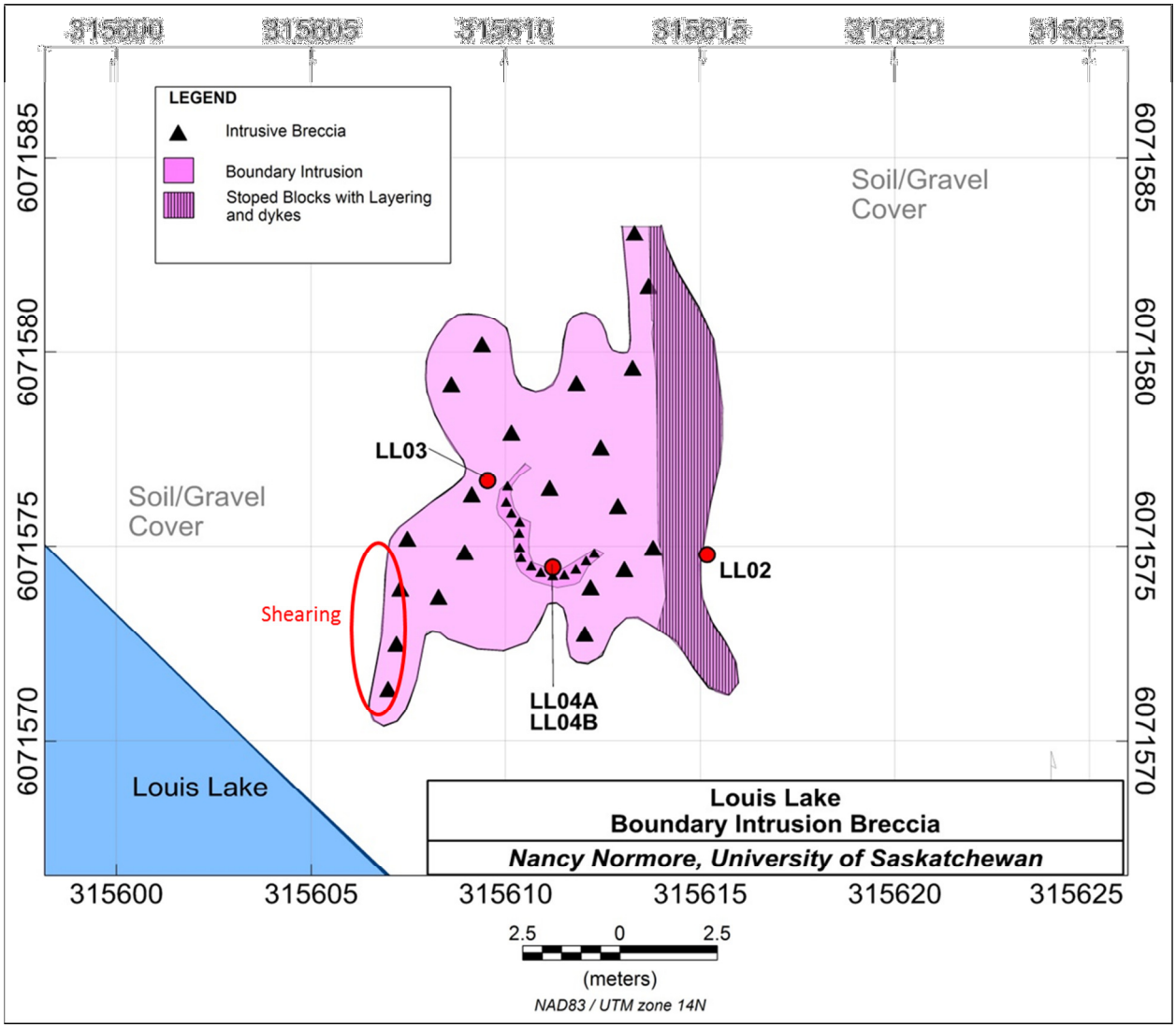

Figure 5-6. Detailed mapping of the Louis Lake intrusion breccia with sample locations.

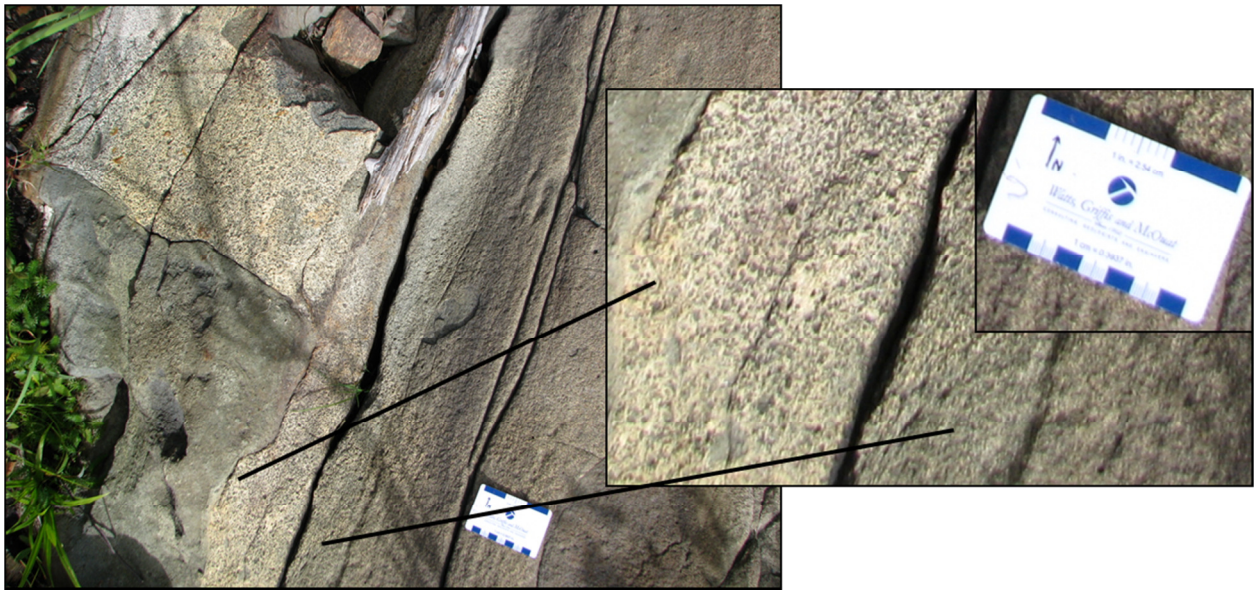

Figure 5-7. West side of Louis Lake outcrop. Images show alignment of fabric due to compression (See "shearing" in Figure 5-6).

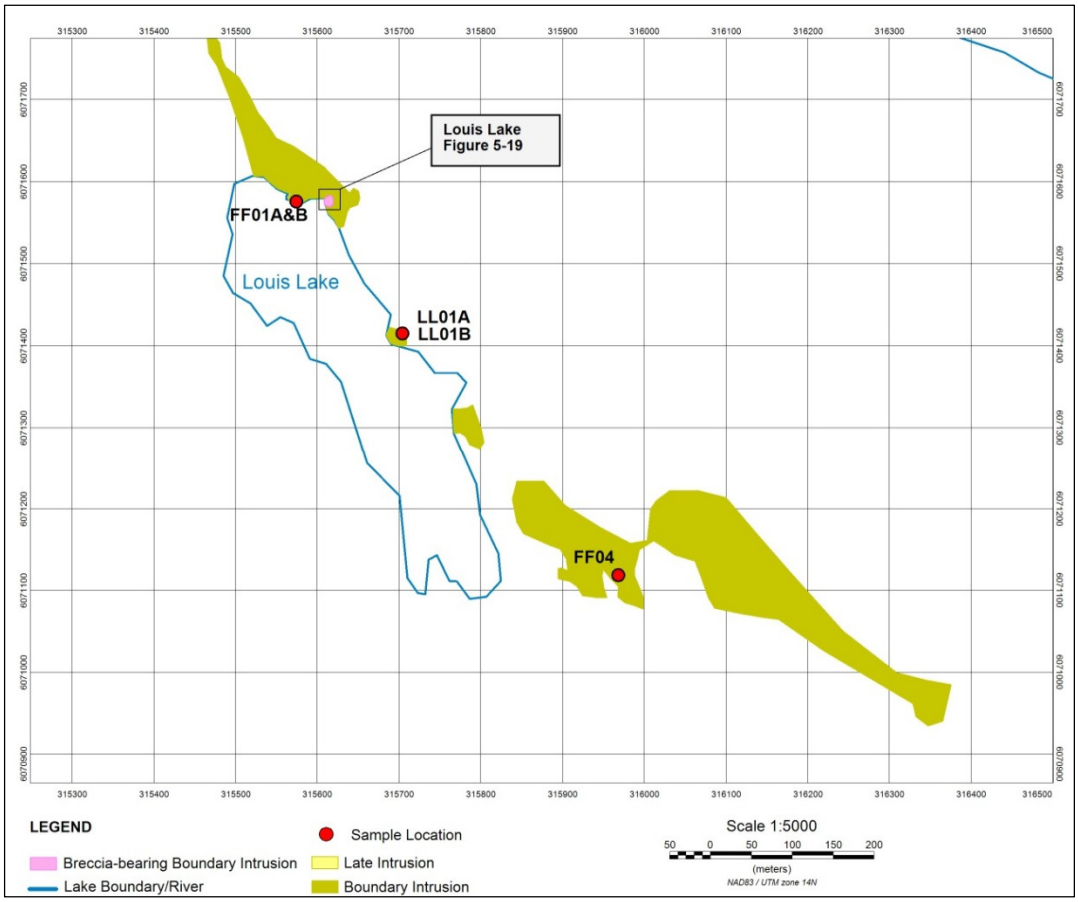

Figure 5-8. Sample locations to west and southeast of Louis Lake mapped outcrop.

The Louis Lake breccia is polymictic and comprises leuco- to melanocratic volcanic and intrusive fragments within a mesocratic to melanocratic intrusive groundmass. The intrusion is heavily laden with volcanic (country rock?) fragments, fragments of earlier crystallized melanocratic Boundary intrusion, and possible stoped blocks of earlier crystalized Boundary intrusion. For the sake of brevity, the possible stoped blocks will herein be referred to as simply stoped blocks. There are three distinct types of breccia patterns within the outcrop, which includes the dominant matrix-supported chaotic intrusion breccia (Figure 5-9A - A1), a mosaic breccia including stoped blocks as fragments (Figure 5-9C - C1), a narrow (partially) clast-supported chaotic intrusion breccia cross-cutting the main intrusion breccia at a shallow angle (Figure 5-9B - B1). The texture of the narrow intrusion breccia varies from fragment-supported to matrix-supported, and this feature, as well as the average fragment size, distinguishes this breccia from the host intrusion breccia. For simplicity and distinction, this breccia will be referred to the fragment- or clast-supported breccia. The fragment-supported breccia intrudes the host rock at a gentle angle, dipping approximately 8 degrees to the south, and is located roughly in the center of the outcrop (Figure 5-6). Within the dominant matrix-supported intrusive breccia, fragments occur throughout the entire outcrop. On average, fragment density ranges from 1 to 15 fragments per square meter, and fragment surface area ranges from 0% - 49% (51 – 100% matrix surface area). Volcanic and mafic intrusive fragments are common (not including the stoped blocks) and mafic fragments may comprise 15% to 50% of the fragment population. Textures are not always clear as factors such as weathering or partial melting in some areas obscure boundaries. Within the clast-supported breccia and the stoped block mosaic breccia, fragment surface area is estimated at greater than 80%, comprising both volcanic and mafic intrusive fragments. Mafic intrusive fragments comprise 50 – 60% of the population.

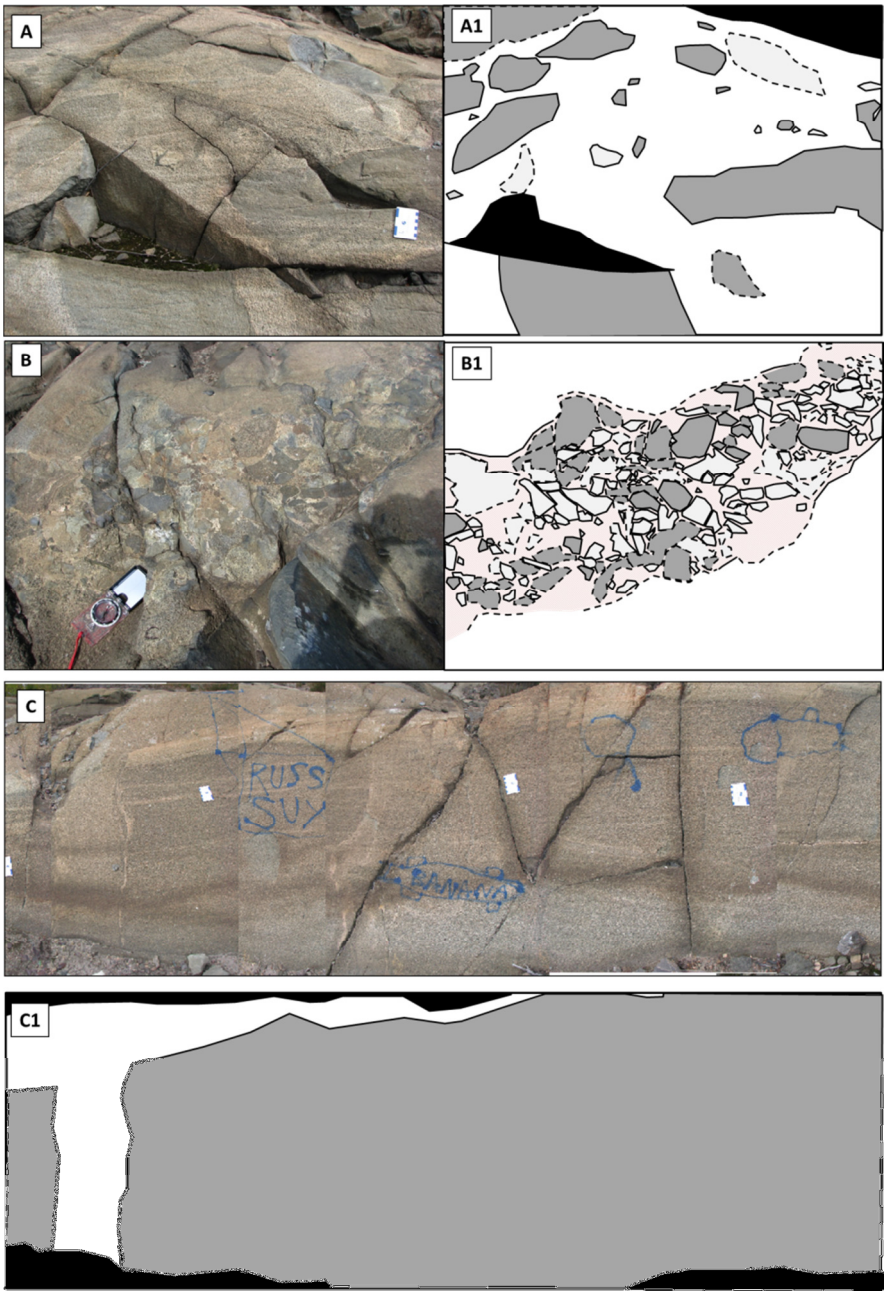

Figure 5-9. Breccia types hosted within the mapped Louis Lake Boundary intrusion. A) and A1) Matrix-supported chaotic intrusion breccia image (left) and diagrammatic representation (right) (SW portion of mapped area). B) and B1) mosaic breccia including stoped blocks as fragments (in area of sample LL02); C) and C1) Clast-supported chaotic breccia (in area of sample LL04A). Legend: Solid line indicates clear and obvious fragment-matrix boundary; dashed line indicates fragment-matrix boundary is unclear and uncertain; White = Boundary intrusion matrix; Pale pink = Clast-supported breccia matrix; Light grey = Volcanic Fragments; Dark grey = Gabbroic or previous Boundary intrusion fragments; Black = gravel or otherwise not part of the intrusion.

Mineral assemblages of the breccia matrix (intrusion) are plagioclase and amphibole (actinolite and hornblende) dominant with abundances of each from 40 – 50%. Interstitial quartz is present from 3 – 5%, and accessory minerals include chlorite, sericite, epidote, biotite, and oxide minerals (Figure 5-10). The presence of primary hornblende and significant actinolite as secondary metamorphic replacement of primary pyroxenes (or olivine or hornblende?) suggests this sample is gabbro composition. The plagioclase is strongly altered to sericite and/or epidote resulting in no reliable estimation of anorthite percent. Plagioclase are tabular and subhedral to euhedral with interstitial quartz, and other accessory minerals. Crystal grainsize is typically less than 1 mm in length. Relict textures are evident in some actinolite crystals, most likely an indication of the replacement of the primary pyroxene (Figure 5-11). Oxides and/or sulphides exist as fine-grained inclusions within the larger primary mafic minerals. There is no observed preferred orientation to the fabric in the thin section, however there is local minor undulose extinction of some quartz grains. Mineral assemblages indicate greenschist facies metamorphism.

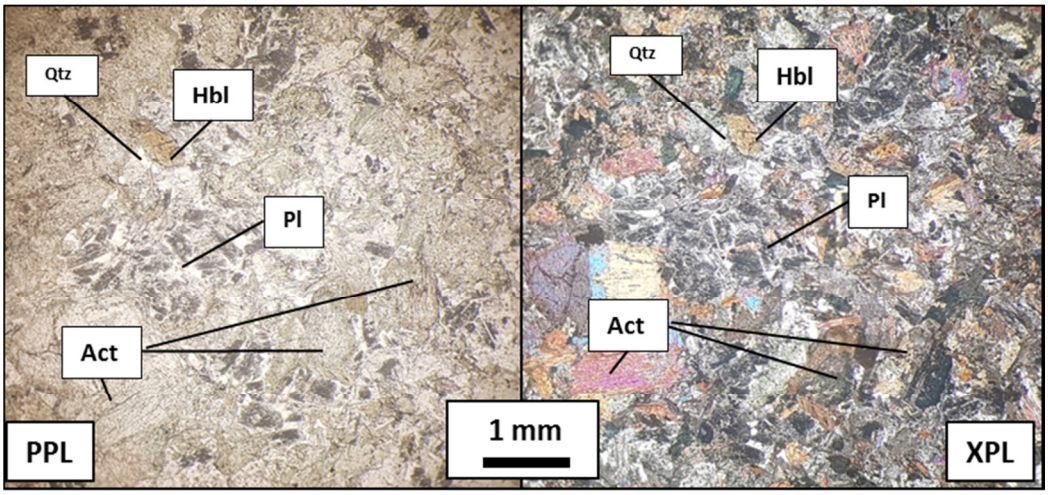

Figure 5-10. Sample TS_LL03A-01. Thin section showing matrix of Louis Lake Boundary intrusion in plain polarized light (PPL) and cross polarized light (XPL). Act = Actinolite; Hbl = hornblende; Pl = Plagioclase; Qtz = Quartz.

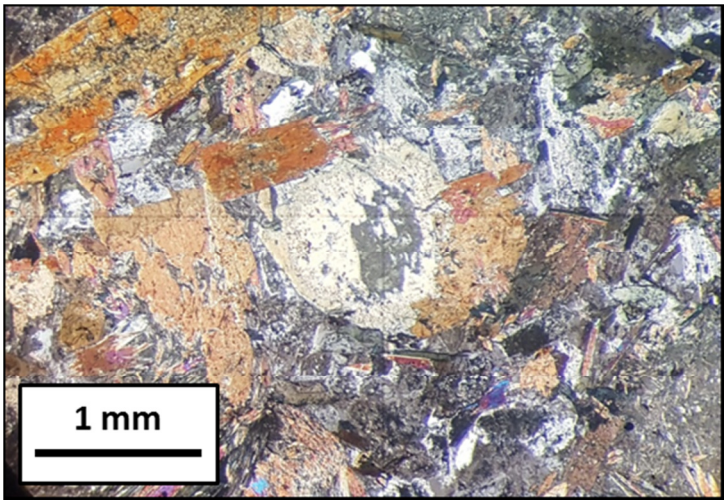

Figure 5-11. Sample TS_LL03A-01. Cross polarized light showing relict textures indicating actinolite replacement of former pyroxene mineral. Shown by variation in birefringence in center of grain.

Fragments of the randomly oriented, matrix-supported breccia comprise leucocratic to mesocratic volcanic rocks and meso- to melanocratic coarse-grained gabbro (Figure 5-12A). Volcanic clasts are most likely country rock of the Louis formation and gabbro clasts are thought to represent earlier Boundary intrusions entrained at depth. Fragment size for both rock types is typically greater than 15 cm (average of 30 cm is estimated), and up to (but less commonly) 2 m in diameter. Smaller fragments are present disseminated between larger fragments or clustered locally in parts of the outcrop but make up considerably less of the surface area compared to the larger fragments. Shapes are subangular to rounded, and in some cases, volcanic fragments appear to be partially melted into the matrix (Figure 5-12, B). Unlike the Green Street breccia, gabbro fragments do not appear to be disaggregated and incorporated into the matrix as fragment contacts with the Louis Lake intrusion matrix appear comparatively clear and definable overall.

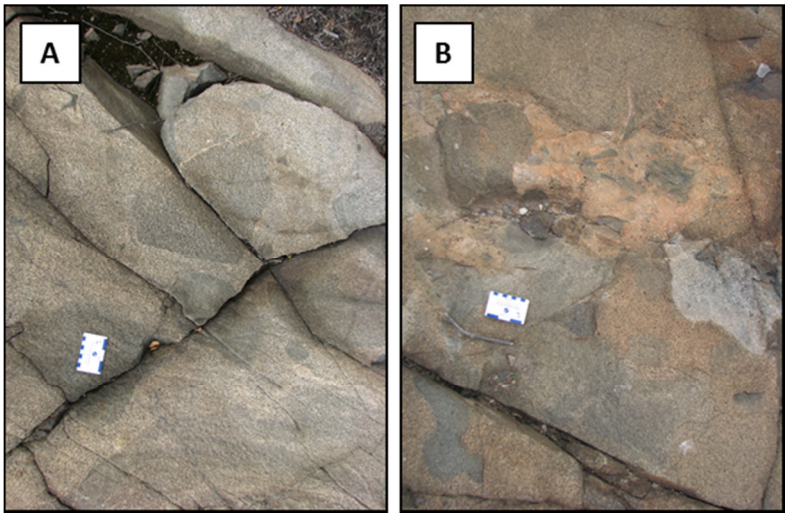

Figure 5-12. Fragments included within the Louis Lake matrix-supported breccia. A) Gabbro fragments. Located on west of outcrop. B) Partial melting and mixing of volcanic fragments. Located south of clast-supported breccia.

Mafic intrusive fragments have been collected for analysis where possible. Due to the outcrop's smoothness and lack of loose rock, only one thin section sample was obtained for both mafic intrusive fragments and volcanic fragments in the main intrusion. Petrographic analysis of a gabbro fragment reveals an amphibole-dominant gabbro with 45 – 50% actinolite including minor tremolite, 15 – 25% interstitial plagioclase, 15 – 20% hornblende, 5 – 7% interstitial quartz, and accessory minerals including sericite, epidote, carbonate, oxides and sulphides (Figure 5-13A). Actinolite grains are up to up to 4 mm in diameter and grain shape is subrounded to rounded. The actinolite exhibits intergrowth texture of several actinolite crystals and tends to be rimmed with darker green finer-grained actinolite, brown hornblende and sometimes chlorite. Relict textures indicating actinolite replacement of a primary pyroxene (?) are also present (Figure 5-13B). The hornblende rim present can extend between the larger actinolite grains and appear interstitial. Plagioclase is anhedral to subhedral and typically 0.5 mm in length or less. The feldspar is strongly altered with a grainy grey center, a mixture of epidote and/or sericite. No anorthite content can be obtained due to the level of alteration and lack of definable twinning. The largest quartz grains are 0.5 mm in diameter, and most grains are 0.25 mm or less. A few quartz grains were noted to exhibit undulose extinction. Oxides and sulphides are mostly found as inclusions in actinolite grains.

The volcanic fragment's groundmass is actinolite and hornblende dominant, ranging from 70 – 80%, intermingled with 10 – 15% plagioclase (Figure 5-13C and D). Grain-shape of the plagioclase and actinolite are anhedral and bladed, respectively, and grainsize is fine-grained, typically 500 µm or less for both minerals. The fragment is overall porphyritic. Within the actinolite groundmass, larger actinolite grains can reach up to 2 mm in diameter but are more commonly less than 1 mm and make up 30 – 40% of the fragment area. Grains are rounded to subrounded and can be a single actinolite crystal or glomerocryst. Actinolite replaced primary pyroxene (?) (+ olivine?) as a result of greenschist grade metamorphism. Other minor and accessory minerals include chlorite, possibly epidote, oxides and sulphides.

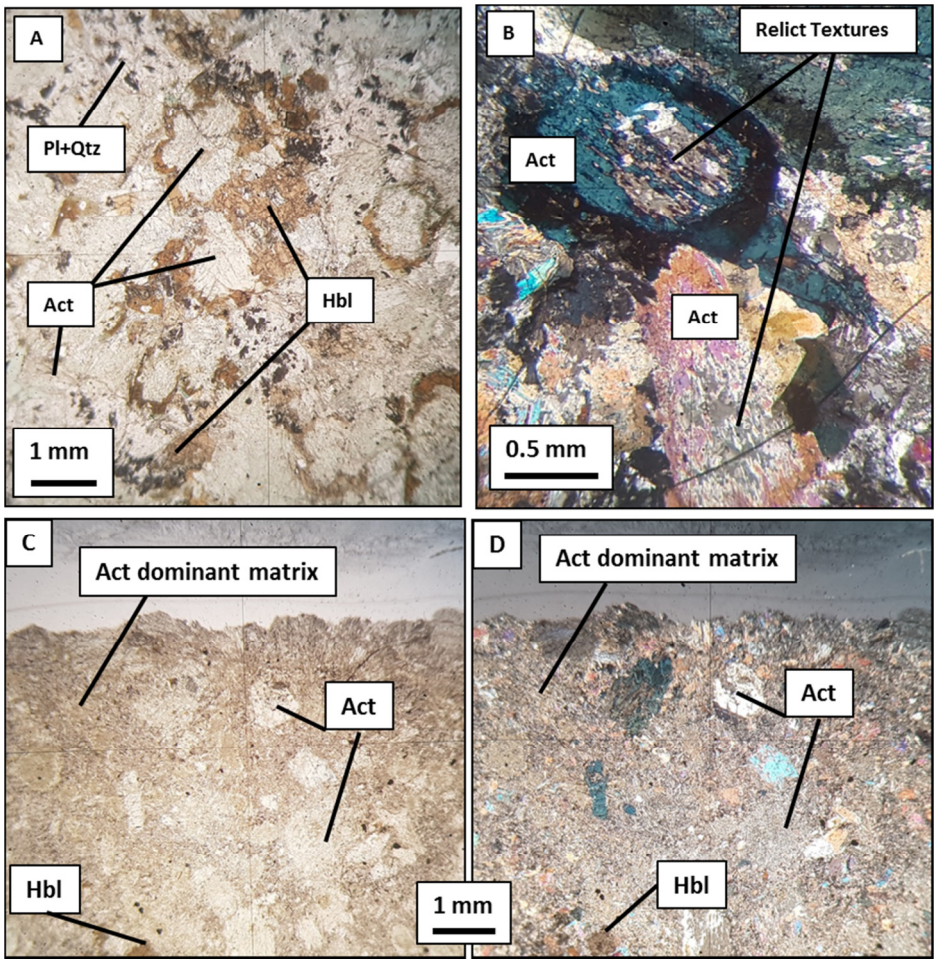

Figure 5-13. Sample TS_LL03A-01. Image A: Plain polarized light of gabbro fragment mineralogy. Image B: Cross polarized light focused on two actinolite grains showing relict textures. Image C and D: Plain polarized light and cross polarized light of a volcanic fragment in the Louis Lake breccia. Matrix is amphibole dominant with lesser plagioclase. Act = Actinolite; Hbl = Hornblende; Pl = Plagioclase; Qtz = Quartz.

The stoped block (Figure 5-9C) is approximately 10 m in length and contains cross-cutting dykelets where the block may have been broken during stoping. The stoped blocks can be considered part of a mosaic breccia as its overall shape of the block has been preserved despite the dykelets separating some pieces (Figure 5-9 C and C1, and Figure 14A). Contacts with the matrix are sharp and the block appears angular in shape, though not all edges are visible. The bulk composition of the block is the similar to the matrix, however, the block exhibits a layering of a more mafic melanocratic layer and a more mesocratic plagioclase-rich layer. The presence of the layered stoped blocks suggests a sill setting, which provided a chamber for crystal grains settling and separation (creating distinct mineral layers), and then doming and stoping of crystalized layered intrusions.

The petrographic sample in Figure 5-14, images B - E shows the melanocratic versus mesocratic layering of a sample representing the stoped blocks of the mosaic breccia. Both layers contain the same mineralogy, but at different abundances as shown in Table 5-1. It is clear that the mesocratic layer is richer in plagioclase compared to the melanocratic layer, and the melanocratic layer contains more actinolite and hornblende. Quartz, chlorite and accessory minerals (which can include oxides, sulphides, epidote and sericite) are observed to have similar abundances.

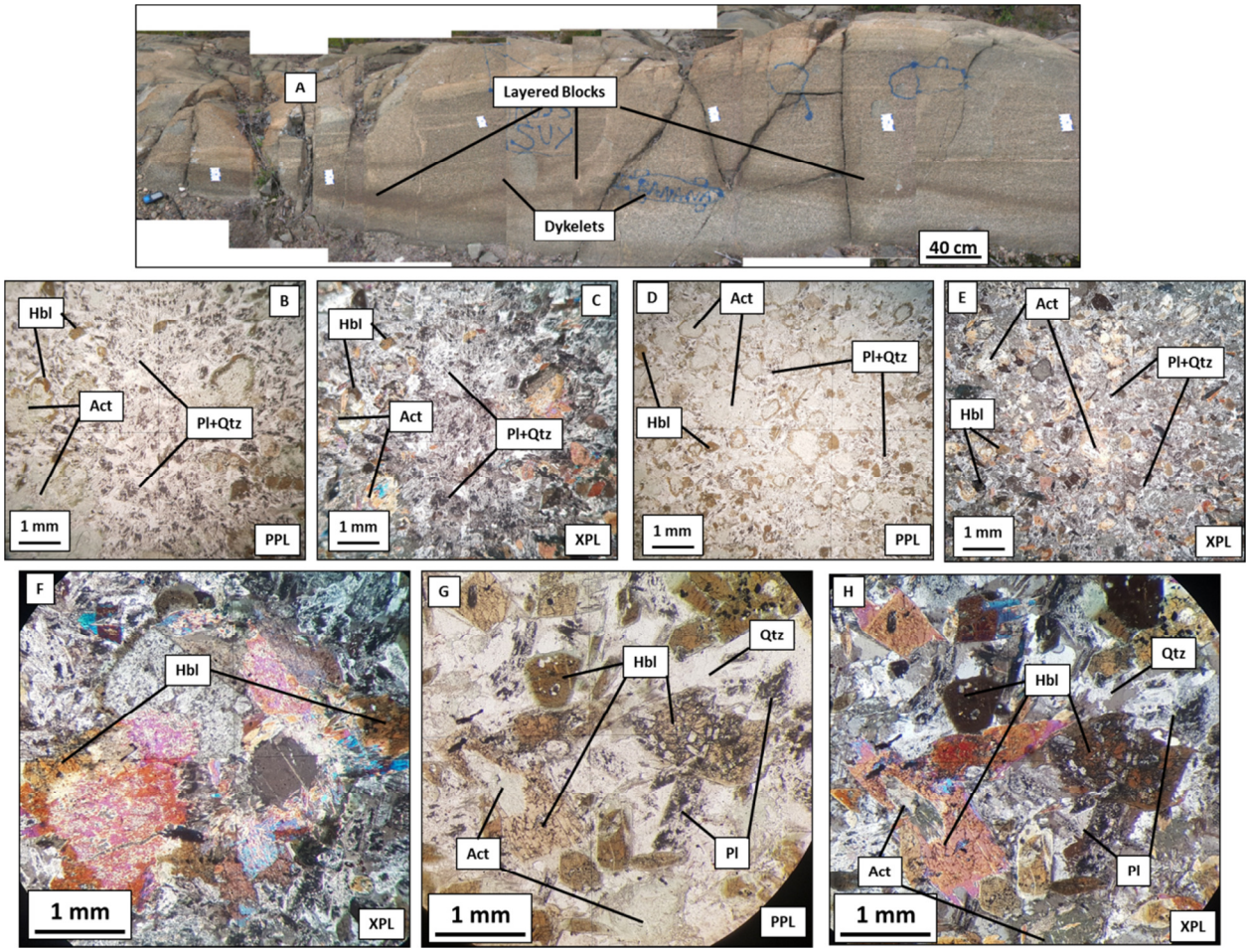

Figure 5-14. Outcrop and petrographic images of the stoped blocks and their layering in the mosaic breccia of the Louis Lake intrusion breccia. A) outcrop of stoped blocks (LL02). B) to E) Plain and cross polarized views of mesocratic and melanocratic layering within the stoped block (TS_LL02-02 and TS_LL02-01, respectively). F) Actinolite glomerocryst with hornblende rim (TS_LL02-01). G) and H) Plain and cross polarized views of inclusions in hornblende (TS_LL02-01). Act = Actinolite; Hbl = Hornblende; Pl = Plagioclase; Qtz = Quartz; PPL = plain polarized light; XPL = cross polarized light.

Table 5-1. Comparison of mesocratic layer and melanocratic layer mineral abundances in stoped blocks of mosaic breccia.

Mineral	Mesocratic Layer TS_LL02-02	Melanocratic Layer TS_LL02-01	Relationship
Actinolite	20 – 25%	30 – 40%	Greenschist facies-altered primary crystals/xenocryst
Plagioclase	40 – 50%	20 – 25%	Groundmass
Quartz	5 - 10%	7 – 10%	Interstitial in groundmass
Hornblende	10 – 15%	15 – 20%	Rim to actinolite grains; in groundmass
Chlorite	≤ 3%	3 – 5%	Alteration of mafic minerals
Oxides & Sulphides	Accessory	Accessory	Disseminated in groundmass or as inclusions

Subhedral to euhedral plagioclase comprise the groundmass and is up to 1 mm in length in both layers of the stoped block (Figure 5-14A - E). In the mesocratic layer, however, plagioclase is typically less than or equal to 0.5 mm, whereas in the melanocratic layer they are on average between 0.5 – 1 mm in length. Epidote and sericite alteration are common throughout the thin section. Actinolite grains are rounded to subrounded and measure up to 4 – 5 mm in diameter in both layers, but are most commonly found to be less than 3 mm. Most have an intergrowth texture of several actinolite crystals, as best seen in cross polar view (Figure 5-14F) and are rimmed by or in contact with brown-coloured hornblende. Both the hornblende and actinolite contain inclusions: actinolite and hornblende grains typically have minor amounts of small (100 µm) scattered or disseminated oxides and/or sulphides (Figure 5-14G and H); and also contain euhedral grey and dusty black crystals (≥ 100 µm) which have grey or third order birefringence colours, possibly sericite-altered plagioclase or apatite (?). Quartz is interstitial within the plagioclase groundmass, is less than 1 mm in diameter and occasionally exhibit undulose extinction.

The clast-supported intrusion breccia is a separate intrusion from the encompassing Boundary intrusion (Figure 5-6). The matrix is similar to the encompassing Boundary intrusion

composition but is overall slightly more leucocratic. The breccia comprises clasts of volcanic country rock and earlier Boundary intrusion gabbro (Figure 5-15A). Fragment size is typically less than 10 cm, shapes are rounded to angular, and fragments are overall randomly oriented. Parts of the breccia are difficult to differentiate between fragment and matrix due to melting or disaggregation of fragments and mixing into the matrix, or due to numerous small fragments or xenocrysts caught in the matrix (Figure 5-15B).

Petrographic analysis shows the crystalline matrix consists of 50 – 60% plagioclase, 25% actinolite, hornblende, ± tremolite, 10 – 15% quartz, approximately 5% chlorite, and 3 – 5% oxides and sulphides (Figure 5-15C - D). The plagioclase is euhedral to subhedral and typically less than or equal to 1 mm in length. No fresh plagioclase crystals are present and consequently lacks twinning as all are significantly sericitized or have undergone epidotization. The amphiboles are considered xenocrysts or antecrysts and two main types are present: 1) glomerocrysts, and 2) euhedral bladed/rhombohedral crystals (depending on the cut of the section). This is similar to that seen in the groundmass of the Green Street Boundary intrusion. The glomerocrysts are rounded to subrounded and range from 1 – 3 mm in diameter. They are commonly rimmed with hornblende and/or actinolite. Accessory oxides and sulphides are very fine-grained and typically occur as inclusions in larger minerals.

The clast-supported breccia contains mafic intrusive fragments that are gabbro composition and similar to the intrusive fragments included within the larger intrusive breccia, and to those found in the Green Street breccia. The existing plagioclase, however, is distinctly different from the groundmass of other Boundary intrusions in that the plagioclase is considerably less altered and twinning is present (Figure 5-15E to F). Anorthite content was measured for several grains and the average percentage was found to be An_{60}. Plagioclase occupies 40 – 50% of the total minerals, is euhedral and is less than 1 mm in length. Actinolite and hornblende (± tremolite) comprise approximately 35 - 40% and occur as subrounded to rounded glomerocrysts or anhedral to euhedral bladed crystals. Hornblende commonly partially or completely rims actinolite glomerocrysts. Glomerocrysts can reach up to 4 mm in diameter, while bladed amphiboles are typically less than 1 mm in length. Chlorite content is 5 – 7% and largely replaces hornblende. Approximately 3 – 5% calcite is found interstitial to the plagioclase.

Sulphides and oxides are minor and are very fine-grained and disseminated in some amphibole grains.

Volcanic fragments in the clast-supported breccia are very fine-grained and vitrophyric in texture (Figure 5-15G). Grainsize is typically less than 100 µm. Actinolite and hornblende grains are common within the phyric ground mass and can reach up to 1 mm or more in length, but overall the entire fragment appears equigranular. Percentages on actinolite and plagioclase are difficult to discern due to the fine-grained nature. The grains within the fragment show a preferred orientation, aligned with the fine-grained layers noted when viewing the entire fragment (Figure 5-15H).

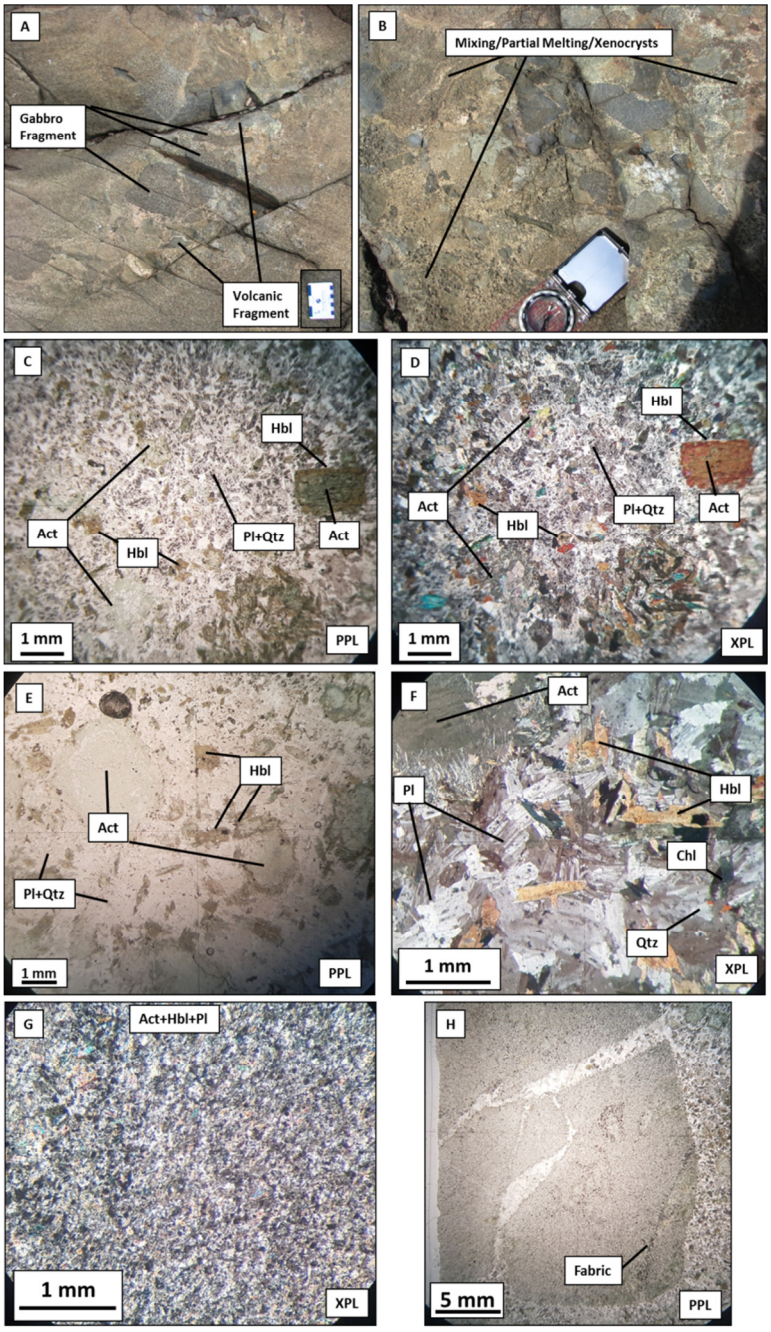

Figure 5-15. Outcrop and thin section photos showing features of the clast-supported breccia from TS_LL04A-03. Image A and B show fragment types and fragment incorporation into the breccia matrix (intrusion). Images C and D are plain and cross polarized light images of the representative matrix of the breccia. Images E and F include examples of a gabbro fragment in the breccia in plain and cross polarized light. Images G and H represent the matrix and the fabric of the volcanic fragment in the breccia. Act = Actinolite; Chl = Chlorite; Hbl = Hornblende; Pl = Plagioclase; Qtz = Quartz; PPL = plain polarized light; XPL = cross polarized light.

5.1.3 Phantom Beach Intrusion Breccia

Phantom Beach sample site is located east of the largest Boundary intrusion in the Creighton and Flin Flon area, immediately west of Potter Bay (Figures 5-1 and 5-16). Mapping completed by Syme (1975) displays breccia bodies within the intrusion and the younger late Boundary intrusions, however, breccias within the mafic Boundary intrusion were not successfully located. Breccias within the late intrusions were easily found and sampled for petrographic and geochemical analysis (both matrix and mafic intrusive fragments) to compare with the results of fragments and matrices in other areas. Samples were also obtained from the mafic Boundary intrusion cut by the late intrusion for comparison to the breccia fragments. The Phantom Beach sample site was not mapped due to time constraints.

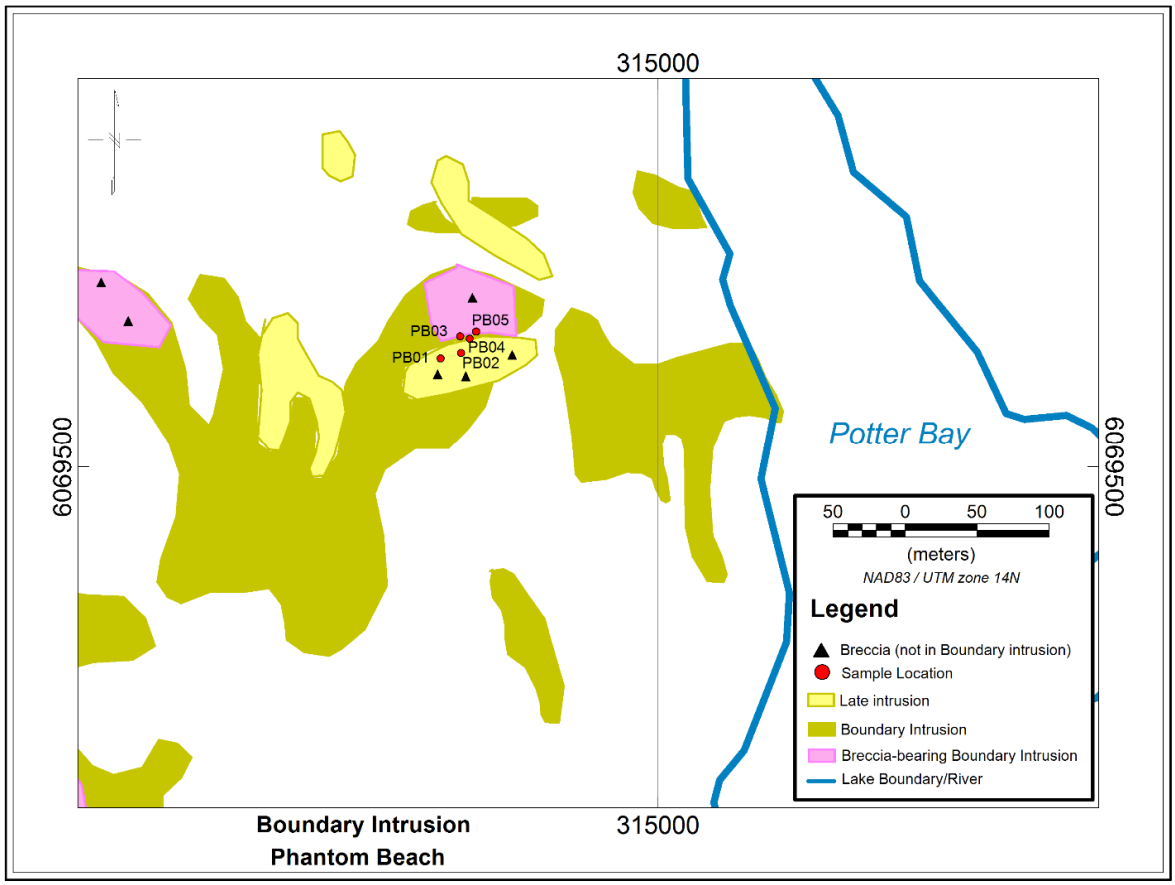

Figure 5-16. Breccia bodies within the Boundary intrusions of the Phantom Beach sample site. Breccia locations based on mapping by Syme (1975).

Mafic Boundary intrusion rock types in the map area include mostly hornblende melamonzodiorite, melatonalite, and mela-quartz diorite. Less voluminous rock compositions comprise various meladiorites, pyroxenites and/or hornblendites (Simard *et al*., 2010). Petrographic analysis (described below) of the sample area (Figure 5-17A) representing the mafic intrusion indicates a medium-grained hornblendite. The outcrop shows no obvious deformational fabric and is cross-cut by an east-west trending tonalite intrusion containing multiple mafic intrusive and intermediate to mafic volcanic fragments (Figure 5-17B and C). The contact between the hornblendite and the tonalite is sharp and shows no evidence of chilled margins (Figure 5-17B and D). No assimilated fragments were found in the breccia. This latter feature may be due to the difference in composition and/or temperature between the fragment and breccia (intrusion) matrix, as lower temperature magmas do not have the ability to quickly melt and assimilate higher temperature-forming crystals that exist in the mafic intrusive fragments.

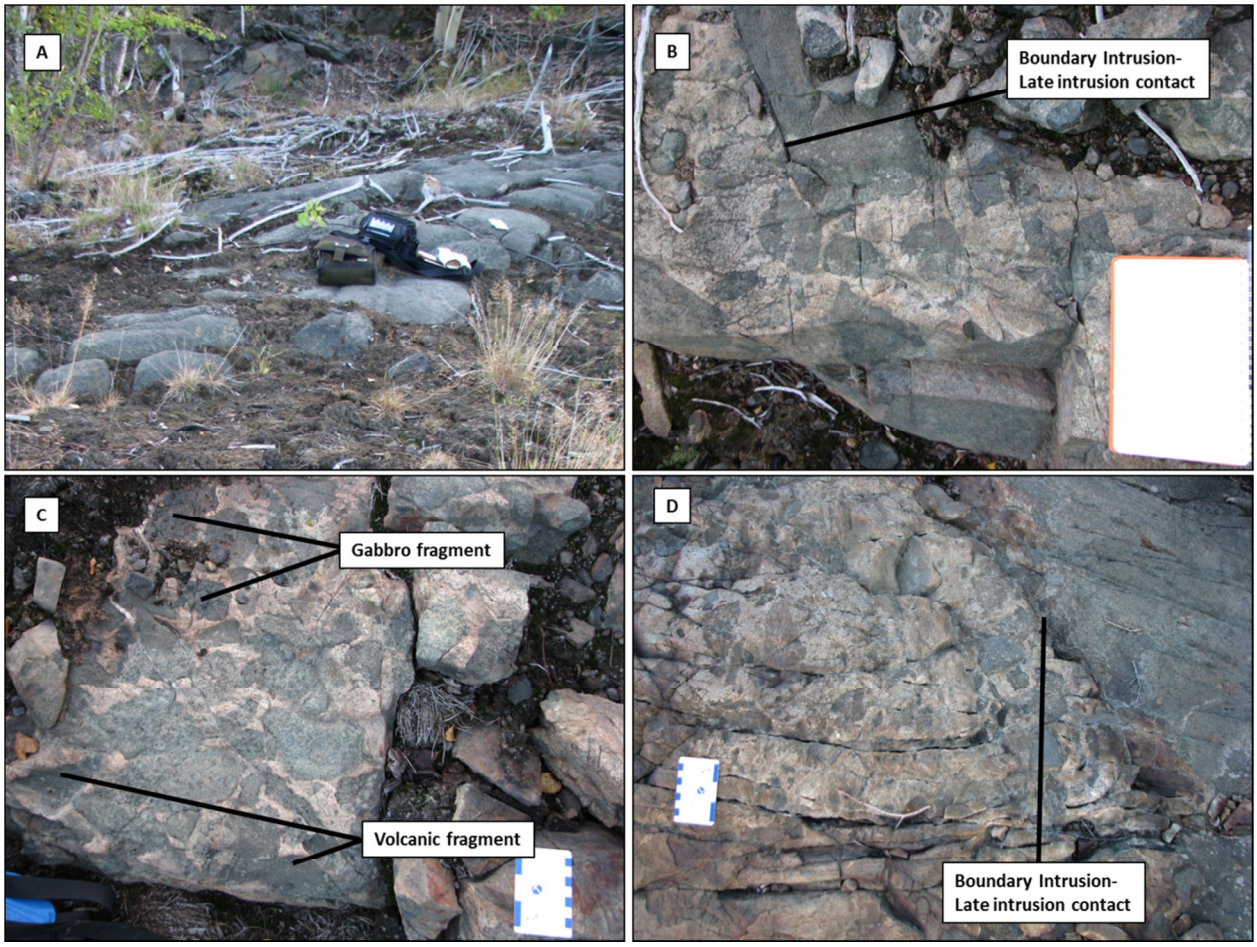

Figure 5-17. Outcrop photos of hornblendite Boundary intrusion and late tonalite intrusion breccia. A) Hornblende diorite Boundary intrusion (PB03). B) Matrix-supported late intrusion breccia in contact with diorite Boundary intrusion (near PB01). C) Fragment- to matrix-supported late intrusion breccia containing volcanic and Boundary intrusion fragments (near PB01). D) Matrix-supported breccia in late intrusion in contact with hornblendite intrusion (north of PB02).

The breccia within the late intrusion is polymictic and varies from a matrix-supported to fragment supported breccia with a chaotic pattern (Figure 5-17B to D). Fragment rock types are volcanic and earlier mafic intrusions, and the mafic intrusion fragments appear to dominate the population (50% to near 100% in certain parts of the intrusion). Fragments are typically rounded to angular in shape. Matrix area ranges from 10 – 50% and fragment density varies from 47 fragments to 75 fragments per square meter. Exposure to weathering of the fragment-matrix boundaries may have caused parts of the intrusion breccia to exhibit a pitted texture or the

impression the matrix has been “carved out” around hornblendite fragments (Figure 5-18). Examples of fragment assimilation into the matrix were not observed in the outcrop.

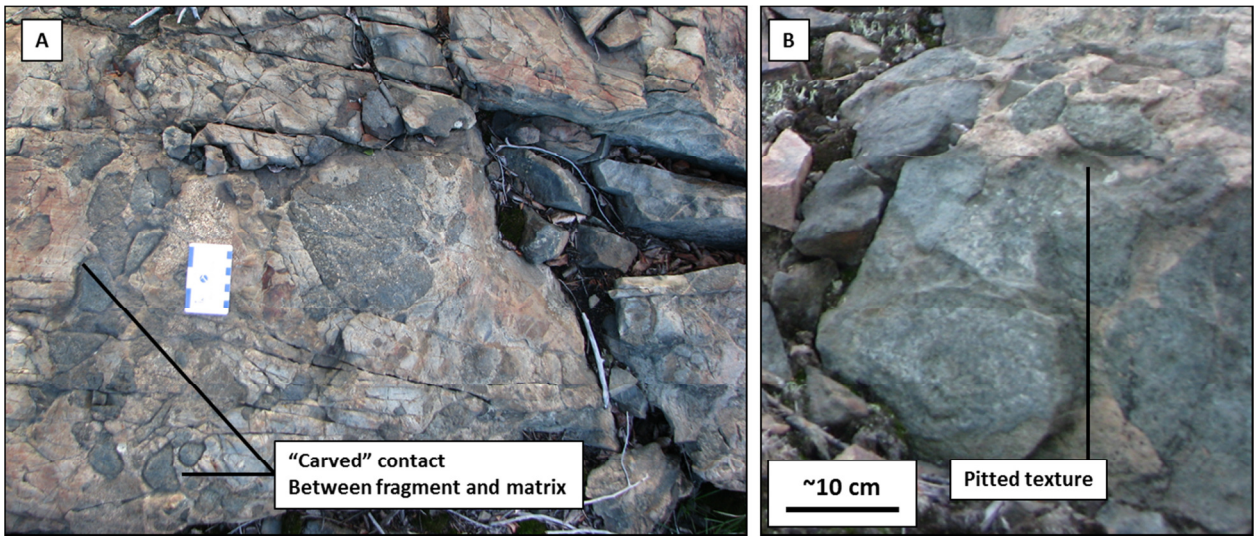

Figure 5-18. Images displaying carved contact around mafic intrusive fragments (Image A, near PB02) and pitted texture (Image B, near PB01) in breccia of the late intrusion.

In the medium-grained hornblendite Boundary intrusion (PB03), amphiboles are the dominant mineral and display replacement and alteration by biotite and chlorite (Figure 5-19A and B). Pale brown hornblende comprises 30 - 45%, and green actinolite/tremolite comprises 15 – 20% of the sample. Biotite is observed replacing hornblende. Displayed in Figure 5-19C, a larger altered (oxidation and chlorite) hornblende is partially replaced by biotite. Colourless actinolite, tremolite or sericite (?) comprise approximately 20 -25% of the mineralogy and are largely interstitial or included within the less altered hornblende and actinolite. They are also found to be surrounded by oxidized hornblende and actinolite (Figure 5-19D). Biotite, chlorite and apatite occur as minor minerals, ranging from 3 – 10%, and accessory minerals include quartz and opaques. The sample (Image E) shows little evidence of deformation with the exception of the biotite which exhibits a wavy form, undulose extinction along the bends (inset), and has inclined extinction.

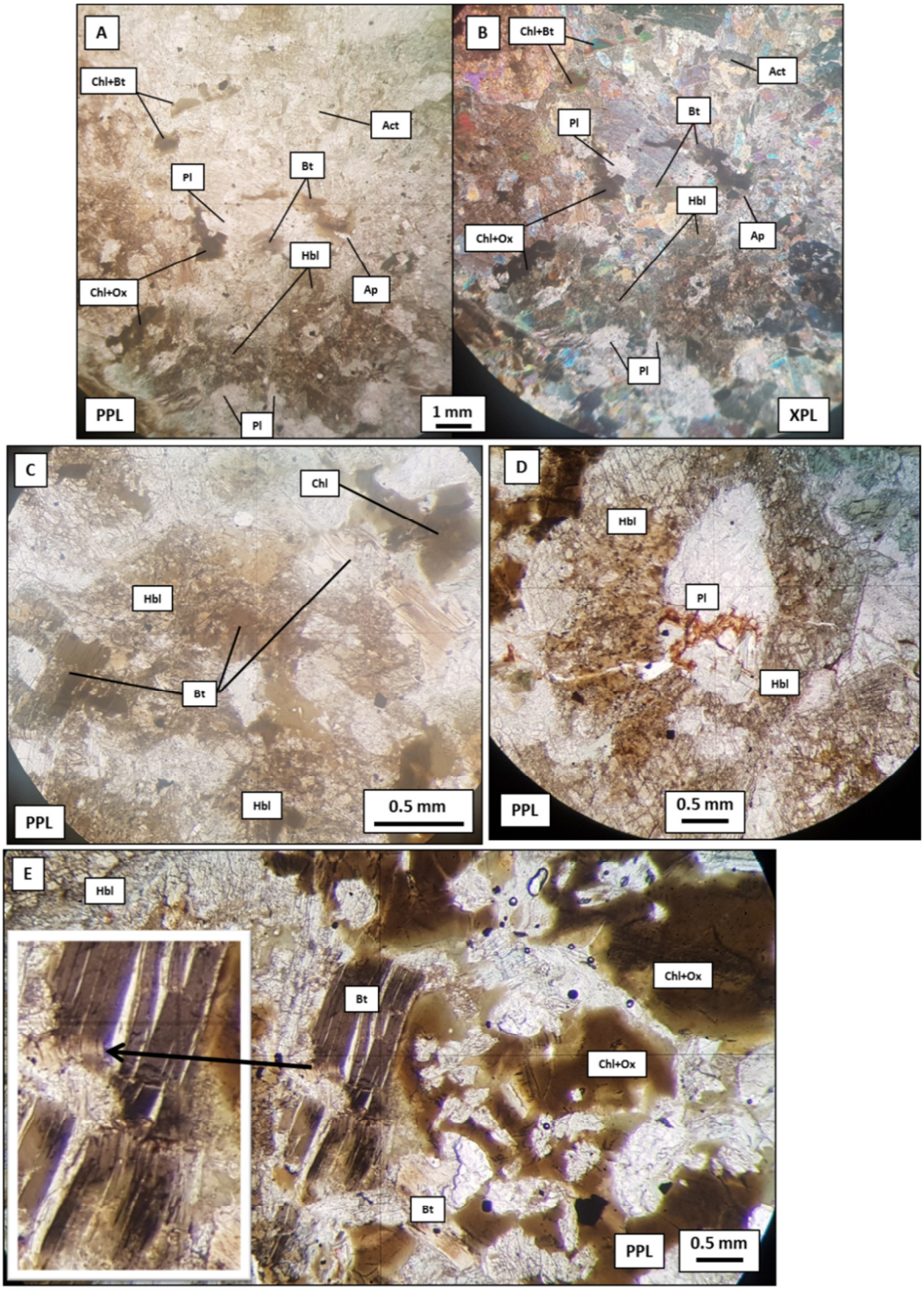

Figure 5-19. Plain polarized light (PPL) and cross polarized light (XPL) (Image B only) of hornblendite intrusion (sample TS_PB03-01). A) and B) Representation of typical mineralogy in PPL and XPL. C) Biotite replacement of hornblende showing inclined extinction and deformation of biotite. D) Hornblende with feldspar inclusion. E) Deformation of biotite (north-south polarizers are vertical and visible on inset). Act = Actinolite; Ap = Apatite; Bt = biotite; Chl = Chlorite; Hbl = Hornblende; Ox = Oxide; Pl = Plagioclase; Qtz = Quartz.

The late intrusion contains a significant amount of quartz, essentially equal to the amount of feldspar present at approximately 20 – 25% (Figure 5-20A and B). The quartz and feldspar occur interstitially and average a few hundred micrometers in diameter. Twinning cannot be found in the feldspar due to strong sericitization. Hornblende and (now) actinolite occur as phenocrysts and altered primary igneous minerals, respectively, vary from anhedral to euhedral, and are up to 2 mm in length. Since there were no obvious or common outcrop examples of disaggregation or assimilation of fragments into the matrix, it is difficult to distinguish if some of the grains could be floating disaggregated fragment crysts (xenocrysts or antecrysts). Opaque minerals are fine-grained and disseminated throughout the section, mostly as inclusions in the mafic minerals.

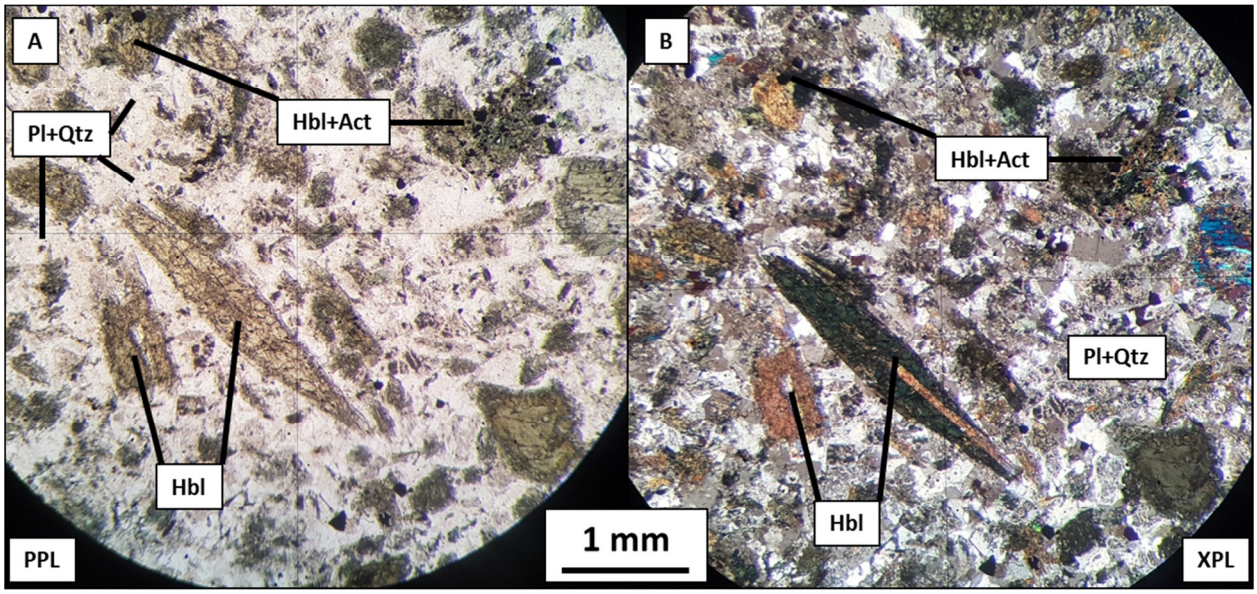

Figure 5-20. TS_PB01-02. Images representative of late intrusion matrix. Act = Actinolite; Hbl = Hornblende; Pl = Plagioclase; Qtz = Quartz.

Mafic intrusive fragments entrained within the tonalite contain trace amounts of feldspar and no quartz, and are dominated by actinolite, hornblende ± tremolite (Figure 5-21A and F). Though the fragments are overall identical in mineralogy, their textures vary from crystalline fine- to medium-grained, and are roughly equigranular to inequigranular. All fragments contain actinolite and/or hornblende which are subrounded to euhedral, and form an interlocking homogenous matrix, with the exception of one smaller rounded fragment which contains bladed

and rounded hornblende and actinolite grains partially disaggregated within the tonalite matrix (Figure 5-21C and D). Glomerocrysts are present in all fragments to varying degrees and sizes (Figure 5-22A and B). Mineralogy of the fragments is very similar to the Boundary intrusion to which the breccia cross-cuts (PB03-01), but contains no biotite or other accessory minerals such as apatite, quartz, and contains considerably less opaque minerals. Alteration of actinolite or hornblende to sericite (?) or iron-oxidation is trace to none (3% or less) and localized to micrometer-sized spaces or inclusions, small fractures or the edges of the fragments.

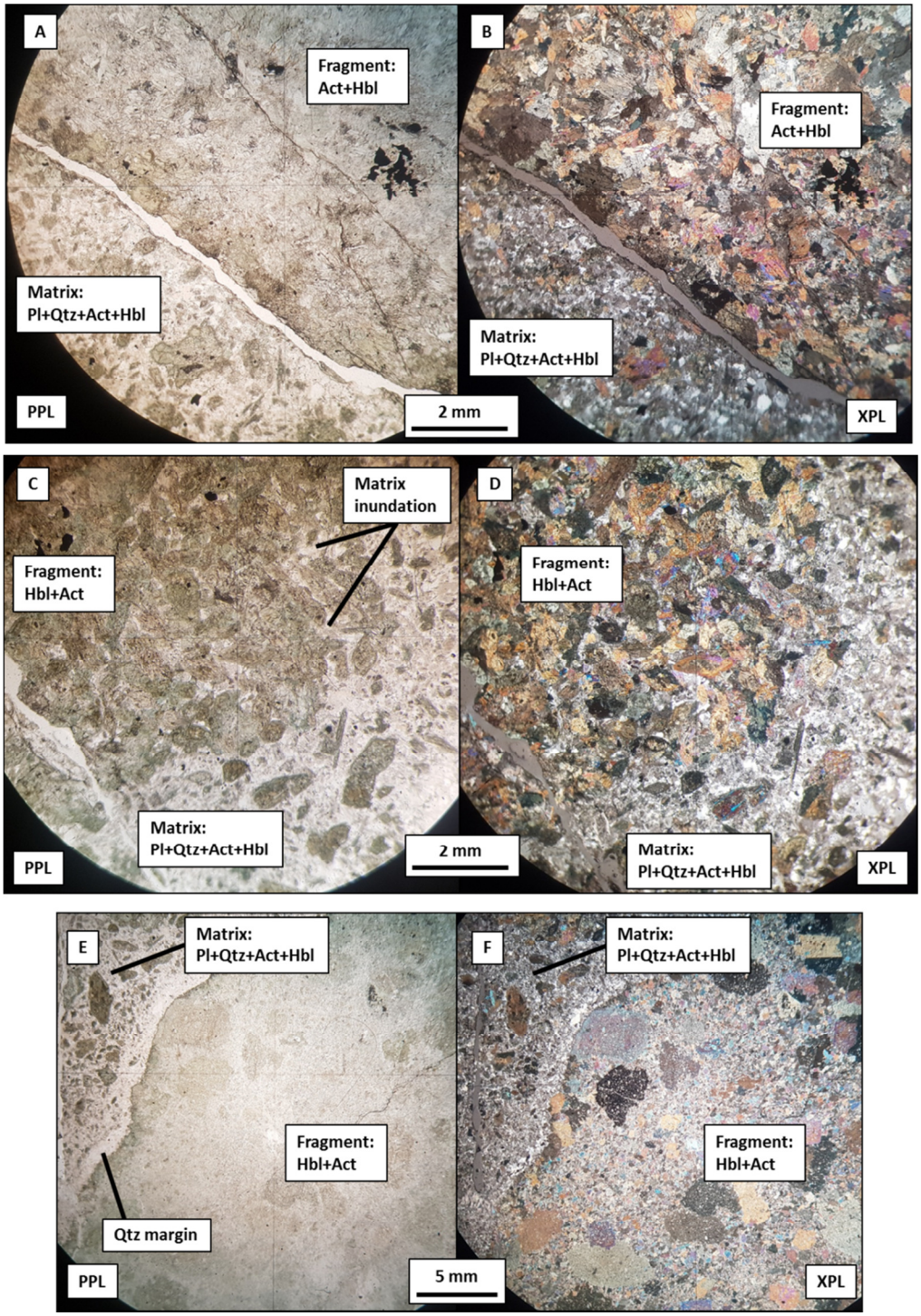

Figure 5-21. TS_PB01-02. Plain and cross polarized views of various mafic intrusive fragments in tonalite breccia matrix. A) and B) Fine- to medium-grained, moderately equigranular hornblendite. C) and D) partially assimilated hornblendite. Plagioclase and quartz matrix inundate between grain boundaries; its effect decreasing towards the center of the grain. E) and F) Porphyritic amphibole fragment. Fragment is rimmed by quartz-rich margin. Act = Actinolite; Hbl = Hornblende; Pl = Plagioclase; Qtz = Quartz.

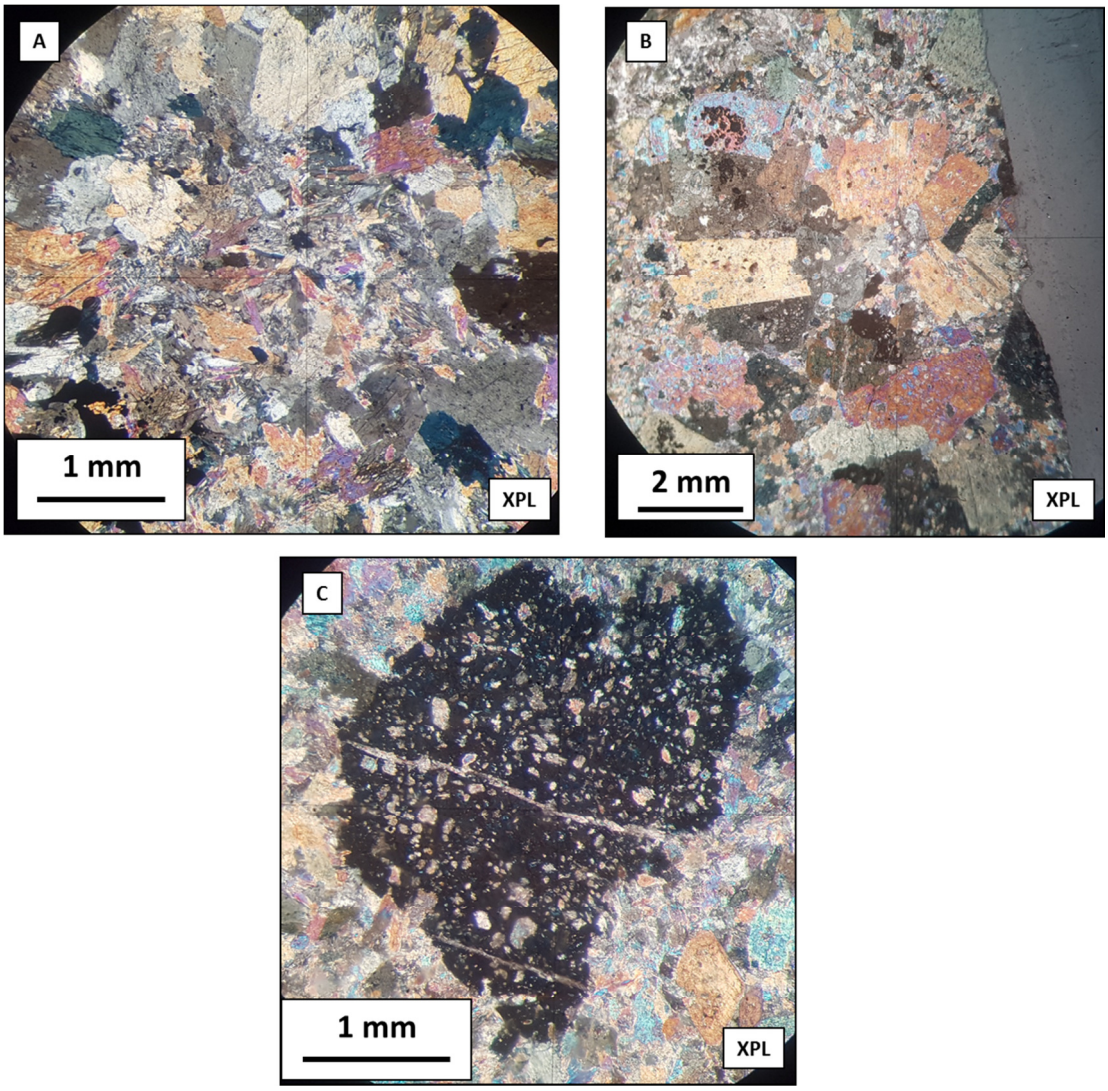

Figure 5-22. TS_PB01-02. Cross polarized view of glomerocrysts in hornblendite fragments (Images A and B) and inclusions in actinolite-hornblende crystal grain (Image C).

5.1.4 Club Lake Intrusion

Boundary intrusions found to the northwest end of the map area (Figure 5-1 and Figure 5-23) are named the Club Lake intrusions for this study. Syme (1975) had indicated a sizable intrusion breccia (approximately 500 x 130 m) (Figure 5-23, pink polygon), however, only breccias associated with narrow dykes were located around the perimeter of the non-breccia bearing intrusion (see location for sample CL02, Figure 5-23). Geochemical and petrographic samples

were collected for analysis from the main intrusion (CL01 and CL01A, Figure 5-23) and smaller Boundary dykes intruding the Missi Group sedimentary rocks (CL02 and CL02A-C, Figure 5-23). No samples could be obtained of xenoliths in dykes. These sample locations were chosen to compare these rock types to fragments and matrix samples of Green Street, Louis Lake, and Phantom Beach areas. Due to time constraints, the area was not mapped in detail.

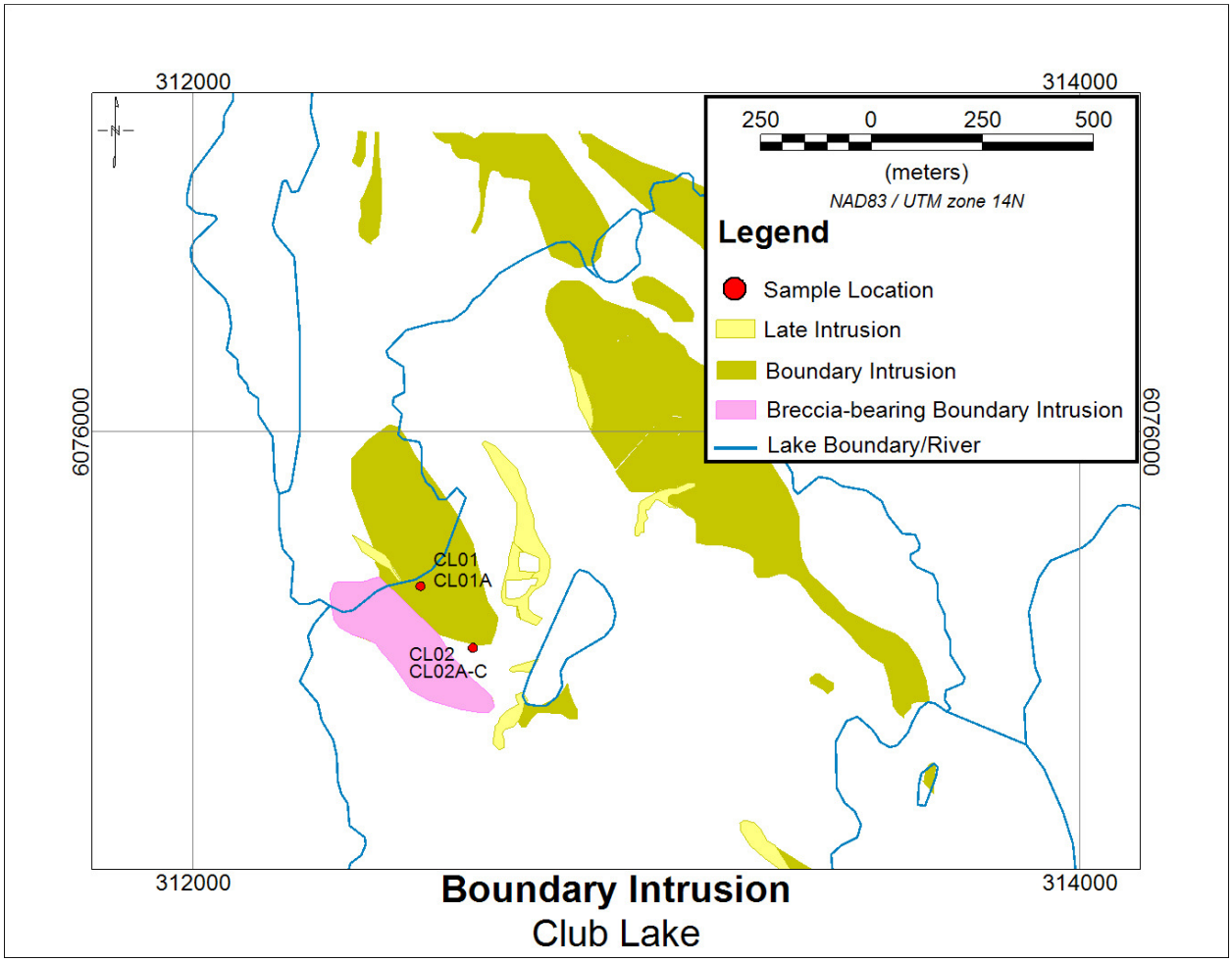

Figure 5-23. Map showing sample locations, Boundary intrusion and intrusion breccias in the Club Lake area. Based on work by Syme (1975).

The Club lake Boundary intrusions intrude rocks of the Missi Group. Simard *et al.* (2010) indicate the intrusion rock type in the sample areas as porphyritic gabbro and melagabbro. Other intrusions in the Club Lake area shown in Figure 5-23 include hornblende melamonzodiorite, melatonalite, melaquartz diorite, and biotite-augite meladiorite. Field observations reveal sample

CL01 (Figure 5-24A) corresponds to rock type as indicated by Simard *et al.* (2010) for that area, whereas the dyke in samples of the CL02 series (Figure 5-24B) is of the melaquartz diorite composition. CL02 samples are more leucocratic and quartz-rich, and contain less amphibole in comparison to the CL01 samples. Rocks in both locations are coarse-grained and exhibit a deformational fabric, which is weak in the gabbro, but moderate in the dykes. Lineations trend east and southeasterly, but no plunge could be obtained. Volcanic and earlier mafic intrusive fragments are present in the dykes, and are up to 50 cm in diameter, but typically 5 cm or less. Grain-shape is subrounded to subangular, and some fragments have been deformed and aligned with the rock fabric (Image B, inset). None of the fragments could be sampled.

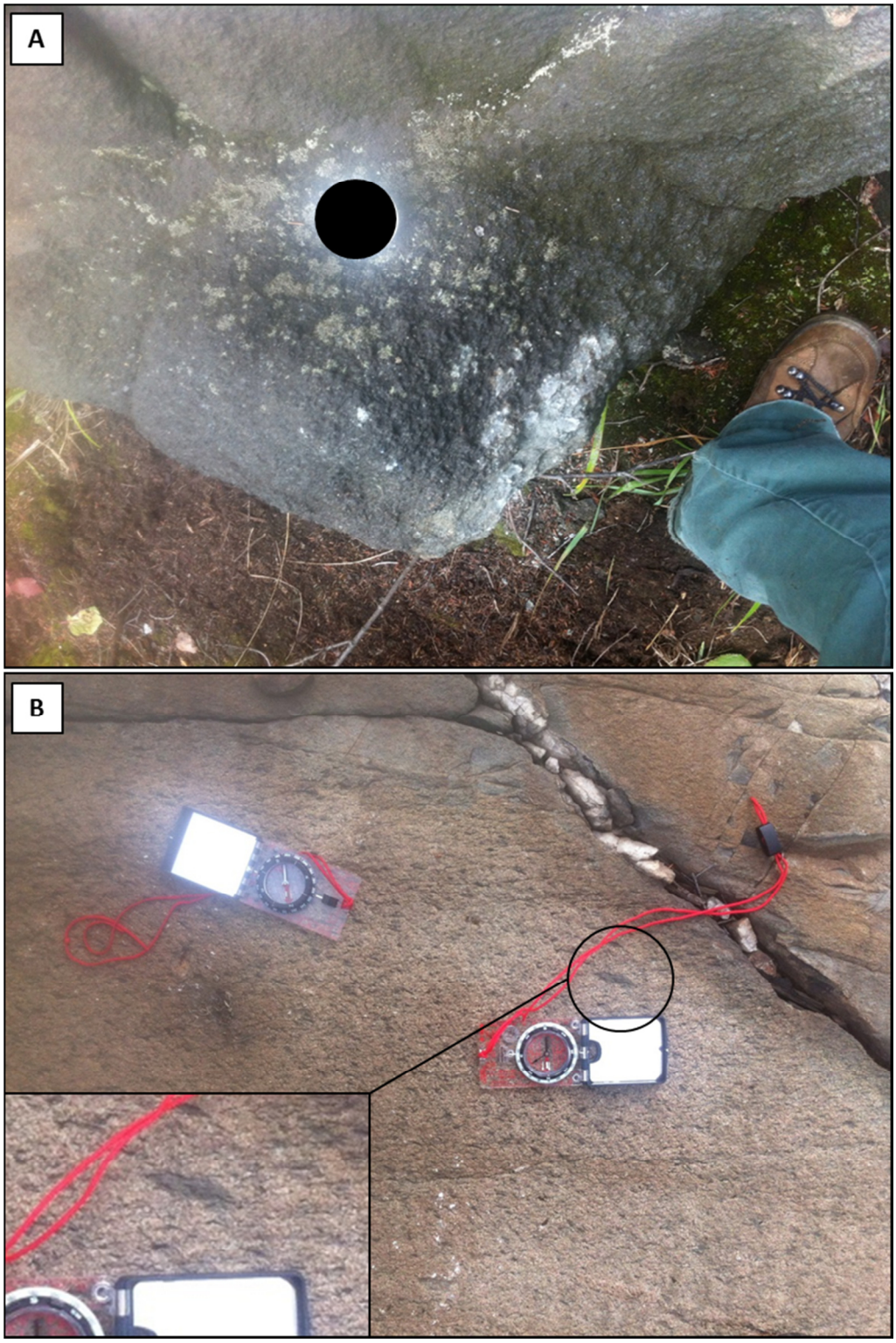

Figure 5-24. Outcrop photos for Club Lake sample site. A) Outcrop image of gabbro sample location CL01. B) Outcrop image of leucocratic Boundary intrusion dyke (CL02 area) with small fragments visible (upper right corner, to left and right of quartz vein). Some fragments are oriented with the fabric (noted above lower compass).

Petrographic analysis of the gabbro gives the following mineral abundances: 65 – 80% actinolite/tremolite, 10 – 15% biotite, 5 – 7% quartz, 5 – 10% plagioclase, less than 5% chlorite, and trace (≤3%) to rare oxides and sulphides (Figure 5-25A and B). In PPL, tremolite and actinolite occur as mainly colourless to very pale green glomerocrysts or single crystals with a darker actinolite rim, which are rounded to subrounded, anhedral to subhedral, and up to 6 mm in diameter. Biotite is pale brown, occurs interstitially and replacing actinolite. A weak fabric is also visible through the distribution of the biotite in Figure 5-25C and D. Plagioclase and quartz occur interstitially to the actinolite/tremolite and are typically less than 1 mm in length or diameter. The plagioclase displays little alteration and twinning is visible and sharp. However, some larger plagioclase grains (up to 2 mm) exhibit a dusty texture and little to no twinning. Minor chlorite is also found replacing actinolite in some grains. Oxides and sulphides are fine-grained and disseminated in actinolite, biotite and within the interstitial minerals.

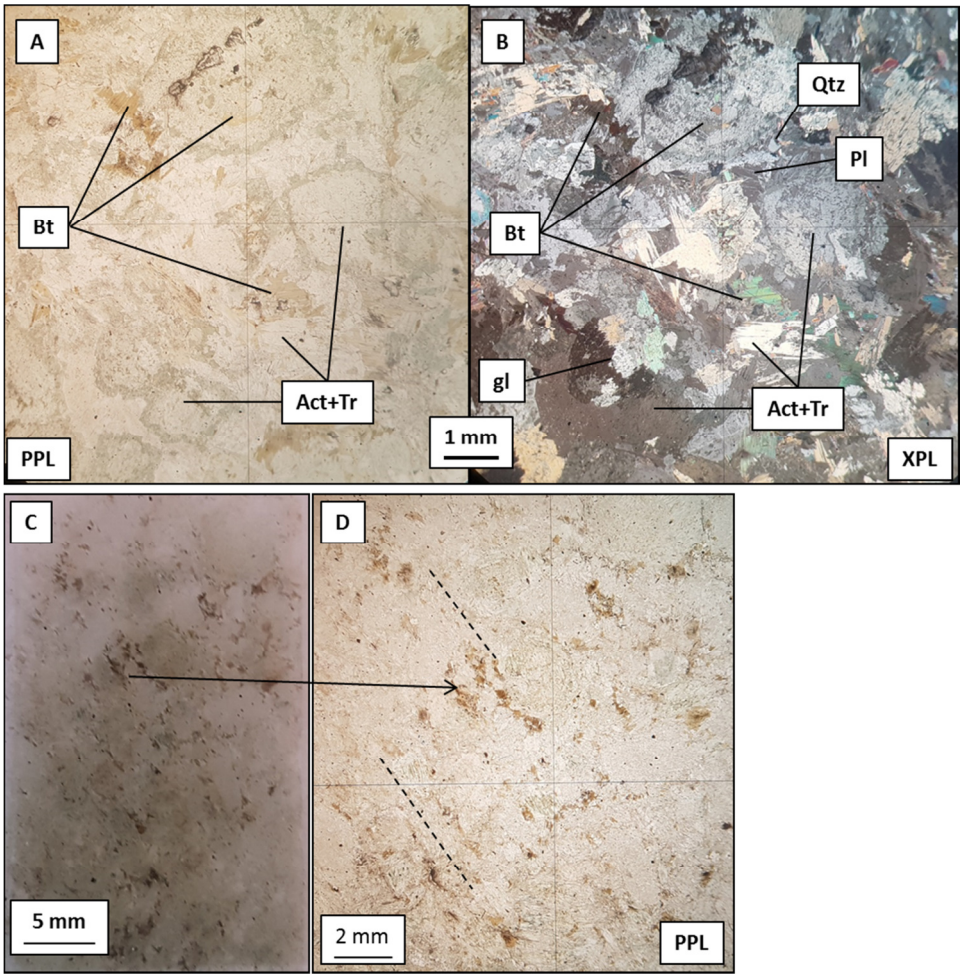

Figure 5-25. Thin section sample (CL01) representing gabbro Boundary intrusion of Club Lake area. Image A and B show the thin section in plain and cross polarized light. Glomerocrysts of actinolite are identifiable in cross polarized light. Image C and D are a photograph of the section (not on a microscope) and a view in plain polarized light, respectively. These photos outline weak fabric (dashed line). Act = Actinolite; Bt = biotite; Pl = Plagioclase; Qtz = Quartz; Tr = Tremolite; PPL = plain polarized light; XPL = cross polarized light.

Leucocratic dykes are plagioclase dominant with significant quartz and moderate amounts of biotite and chlorite (Figure 5-26A and B). The crystal grains are elongated and pinched, and there is an overall consistent orientation to the fabric. Feldspar comprises 50 – 60% of the section and has been largely overprinted by fine-grained sericite and epidote alteration, although some grains in the thin section show very faint remnants of albite twinning (Figure 5-26C). Grainsize is commonly between 0.5 – 1 mm in length and grains are overall euhedral. Quartz makes up 20 – 25% of the rock and is typically less than 0.5 mm in diameter. Many quartz grains exhibit undulose extinction. Discontinuous wavy lenses of biotite and chlorite,

comprising 10 – 20% of the sample, clearly show the foliated texture of the sample (Figure 5-26D). Accessory minerals (2 – 3%) include oxides and sulphides found disseminated between grain boundaries or as inclusions in minerals, most often associated with the biotite-chlorite lenses. Trace subordinate calcite is also present interstitially. Accessory fine-grained sericite and epidote replace feldspars.

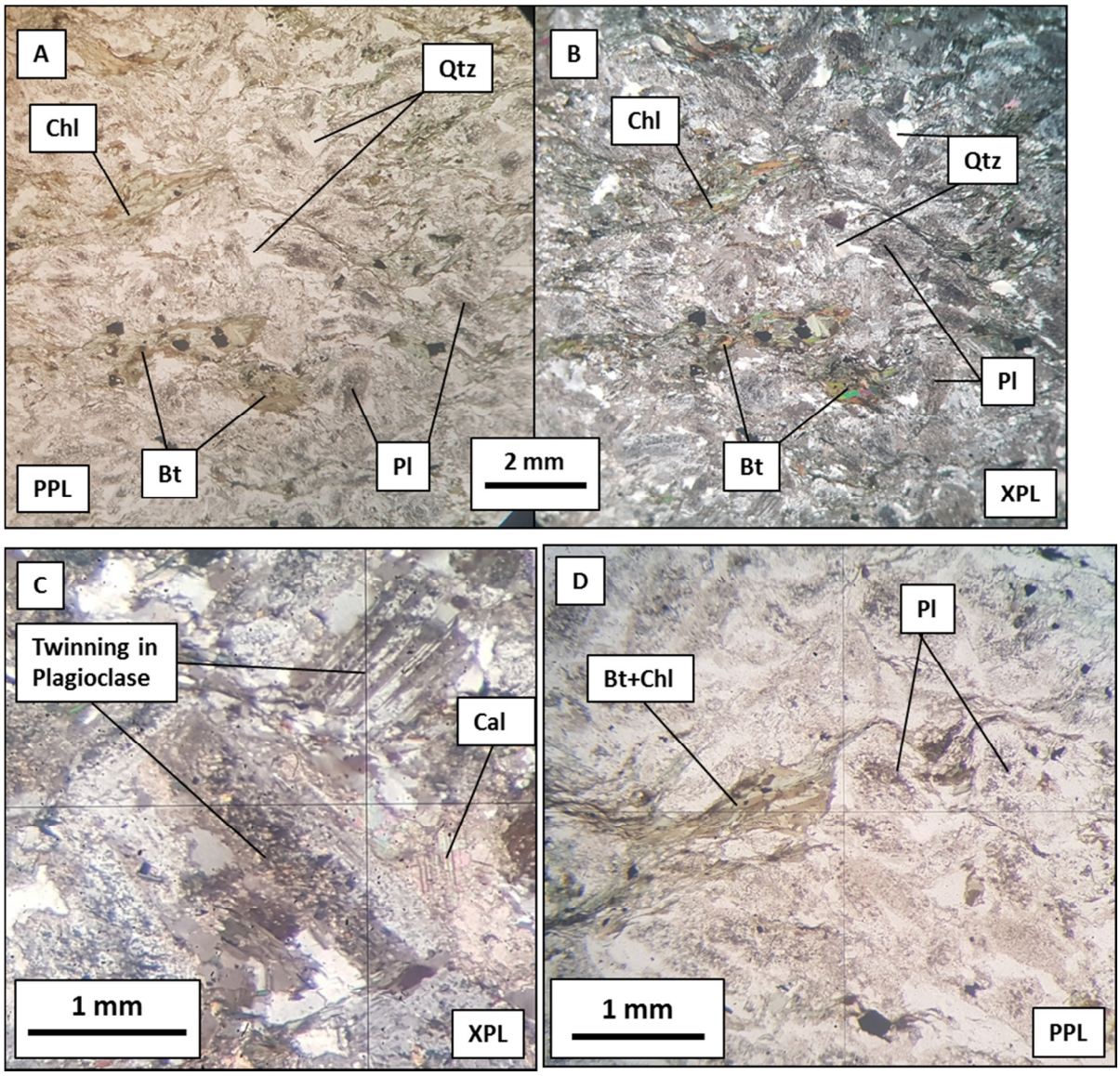

Figure 5-26. Petrographic images of TS_CL02-02. Images show representative matrix (images A and B), altered feldspars and remnant twinning (image C), and foliated fabric (image D). Bt = biotite; Cal = Calcite; Pl = Plagioclase; Qtz = Quartz; PPL = plain polarized light; XPL = cross polarized light.

Table 5-2 below summarizes all the samples of this study and the primary breccia components (matrix or fragment), includes a brief sample description, and the rock names as determined by the Simard *et al*. (2010) and through petrographic analysis in this study.

Table 5-2. Sample list and description for Boundary intrusions breccias.

Area	Sample ID	F/M/MF/I	Sample Description	Rock Type	
				MGS (2010)	Petrography (this study)
GS	TS_GS07A-01	M	Matrix; fragment-free area	Hornblende melamonzodiorite, melatonalite, mela-quartz-diorite	Hornblende-bearing quartz (leuco)diorite - tonalite
	TS_GS08A-01	M	Matrix; fragment-free area		
	TS_GS10C-01	M	Matrix; near fragments		
	TS_GS12-02	M	Matrix; next to fragment GS12-01		
	TS_GS14-01	M	Dykelet off main intrusion		
	TS_GS10C-02	F	Mafic intrusive fragment	NA	Gabbro to plagioclase-bearing ultramafic
	TS_GS12-01	F	Mafic intrusive fragment		
LL	TS_LL01A-01	I	Homogeneous coarse-grained melanocratic intrusion	Biotite-augite meladiorite; hornblende meladiorite	Gabbro
	TS_LL02-01	F	Meso-melanocratic layer in stoped block of Louis Lake Boundary intrusion		Augite hornblende meladiorite
	TS_LL02-02	F	Mesocratic layer in stoped block of Louis Lake Boundary intrusion		Hornblende- & augite leucodiorite
	TS_LL03A	M	Mesocratic Louis Lake Boundary intrusion; breccia matrix	NA	Augite hornblende melagabbro
	TS_LL03A-01	F	Mafic intrusive fragment	NA	Melatonalite -Quartz Melagabbro
	TS_LL04-01	MF	Subhorizontal clast-supported breccia; matrix and fragment mix	NA	Augite hornblende leucodiorite
	TS_LL04A-03	F	Mafic intrusive fragment in clast-supported breccia	NA	Gabbronorite - Hornblende gabbro
	TS_FF04	M	Matrix; no brecciation	Hornblende meladiorite	No thin section taken
PB	TS_PB01-01	F	Mafic intrusive fragment	NA	Hornblendite
	TS_PB02-01	F	Mafic intrusive fragment	NA	
	TS_PB02-02	M	Leuco- to mesocratic matrix	Tonalite	Tonalite - melatonalite
	TS_PB03-01	I	Mafic Boundary intrusion		Hornblendite
	TS_PB04-01	M (+F?)	Leuco- to mesocratic intrusion; possible mixing with fragments	Tonalite	Tonalite - Melatonalite
CL	TS_CL01-01	I	Very coarse-grained melanocratic intrusion	Porphyritic gabbro, melagabbro	Plagioclase-bearing gabbro
	TS_CL02-01	M	Homogeneous leucocratic dyke	Tonalite	Tonalite - melatonalite
	TS_CL02B-01	I	Medium- to coarse-grained leucocratic intrusion; near contact with Missi Group sediments		

Note: Includes rock names as listed by the Simard *et al*., (2010) and this study. F = Fragment; M = Matrix; I = Intrusion with no brecciation; NA = Not available.

5.2 Geochemical Results

5.2.1 Sample Selection

Samples were selected to represent the components of brecciation in the Green Street, Louis Lake and Phantom Beach areas (Figures 5-2, 5-6, 5-16), and the intrusion and related dykes in the Club Lake area (Figure 5-23). Loose boulders were readily available in Green Street area and Phantom Beach, and were chosen to allow for sampling of the breccia mafic intrusive fragments and the breccia matrix, or host intrusion. The Louis Lake outcrop contained few accessible boulders and no mafic intrusive fragments could be obtained that were not weathered, with the exception of the mesocratic layer in the stoped block of Boundary intrusion. Rocks of non-brecciated intrusions were also sampled in the Louis Lake area to compare with the matrix and fragments in sampled breccias (Figure 5-8). Caution was taken during the sample preparation process to ensure the freshest sample could be obtained for analysis. A rocksaw was used to cut away weathered surfaces, and to separate the fragment from matrix in brecciated samples.

Twenty-five samples were analyzed for major and trace element data. A list of thin section samples, as well as geochemical results, are listed in Tables A1 and A2 (respectively) in Appendix A. In order to help distinguish groups of samples in the following presented geochemical graphs, samples are represented as follows:

- Samples are coloured according to their sample area. Green Street (GS) samples are green; Louis Lake (LL and FF) samples are yellow; Club Lake (CL) samples are pink; and Phantom Beach (PB) samples are blue.

- Samples representing the intrusion breccia matrix, or intrusion, are represented by circles.

- Fragments are symbolized by triangles; and fragment-matrix mixes are denoted by squares.

5.2.2 Element Mobility

Initial analysis of the geochemical results involved testing for effects of element mobility due to local alteration or regional metamorphism. Rocks in the Flin Flon area, including the Boundary intrusions, have been affected by greenschist metamorphism; and felsic and/or quartz ± carbonate ± epidote veins are common throughout the area, suggesting local effects from hydrothermal alteration. All elements from the major and trace element dataset with values above the detection limit for that oxide or element analysis have been correlated to zirconium (Zr), a high field strength element (HFSE) considered to remain unchanged in content through weathering and metamorphic processes (Cann, 1970). Figure 5-27 (Graphs A - F) provide the Zr binary plots for select major and trace elements. Major oxides Na_2O and CaO do not show the degree of scatter as seen in the binary plot of Zr with K_2O. Thin section analysis reveals much of the original rock crystallinity and fabric, and significant amounts of hornblende have been preserved following regional greenschist metamorphic alteration. The sample distribution of Al_2O_3 (not shown here) coincides with the trend displayed by Na_2O and most likely reflects the presence of Na_2O in plagioclase albite, a product of greenschist metamorphism. The correlation shown by the scatter plots presented here suggests that, besides mobilization of K and other similar ionic potential LFSE during greenschist grade metamorphism, minimal processes have affected HFSE concentrations and that many of the original compositions can be reflected by the elements outside of the low field strength (LFS) group. Loss on Ignition (LOI) values for the Boundary intrusions ranges from 1.6% to 4.3% with most Green Street matrix samples having the lowest values (1.6 – 2.2%). Increased LOI% may likely represent increased content of hydrous minerals in the rock, such as micas and amphiboles, and to a lesser extent, carbonate minerals.

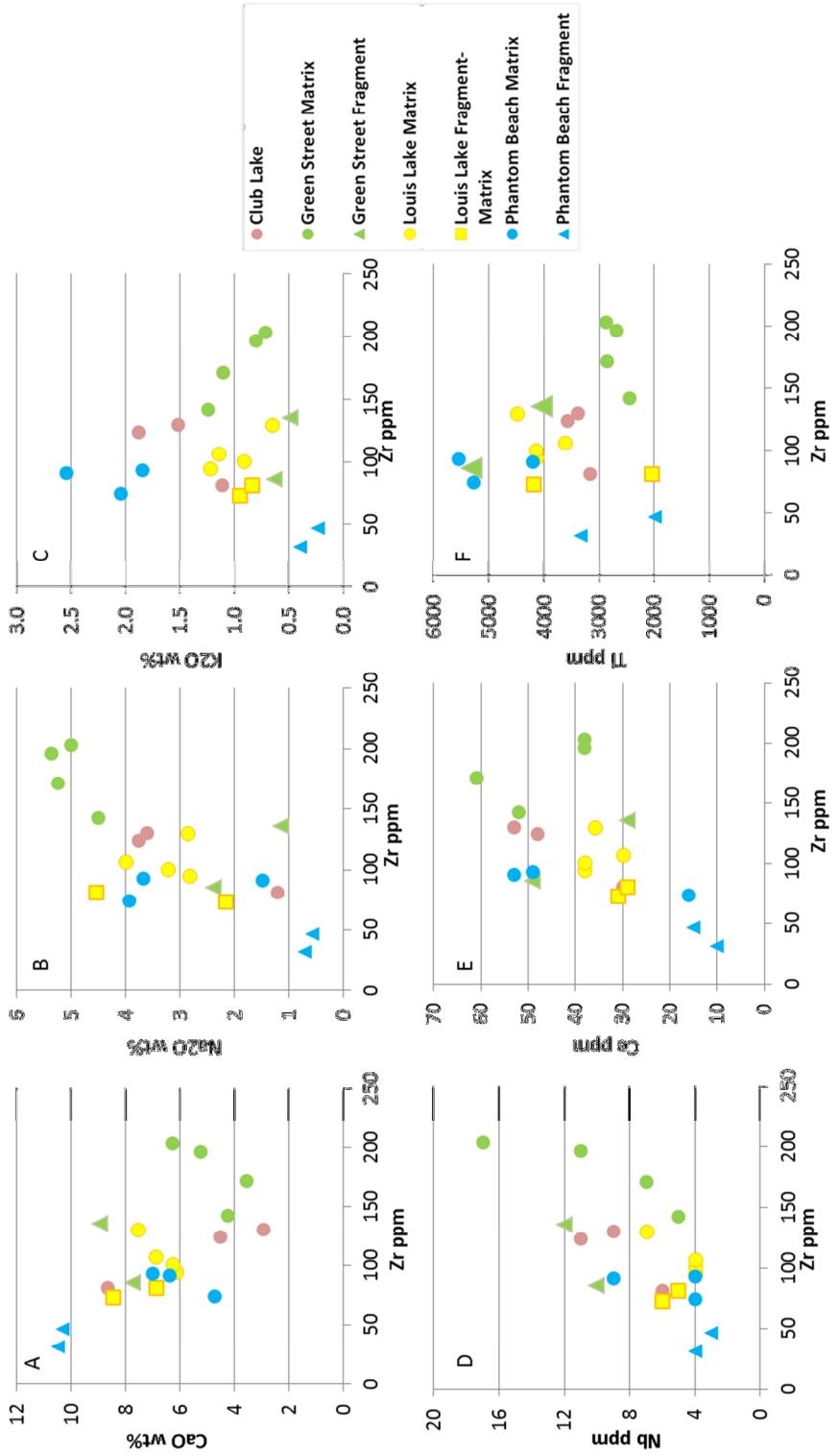

Figure 5-27. Binary plots with HFSE Zr on x-axis used to detect element mobility for the Boundary intrusion samples. Graphs A-D: Binary plots for select major oxides. Graph E-H: Binary plots for select trace elements. Legend for all diagrams displayed on right.

5.2.3 Geochemical Classification

Rock samples have been geochemically classified using volcanic classification by Pearce (1996), modified from the Winchester and Floyd (1978) diagram (Figure 5-28). Most samples are basaltic to andesitic in composition, with the exception of some of the Green Street samples, which show to be more alkaline. All Green Street breccia matrix samples are leucocratic quartz-diorite to tonalite, and mafic intrusive fragments are melanocratic and, according to petrographic analysis, gabbro (or hornblendite) in composition (see Table 5-2).

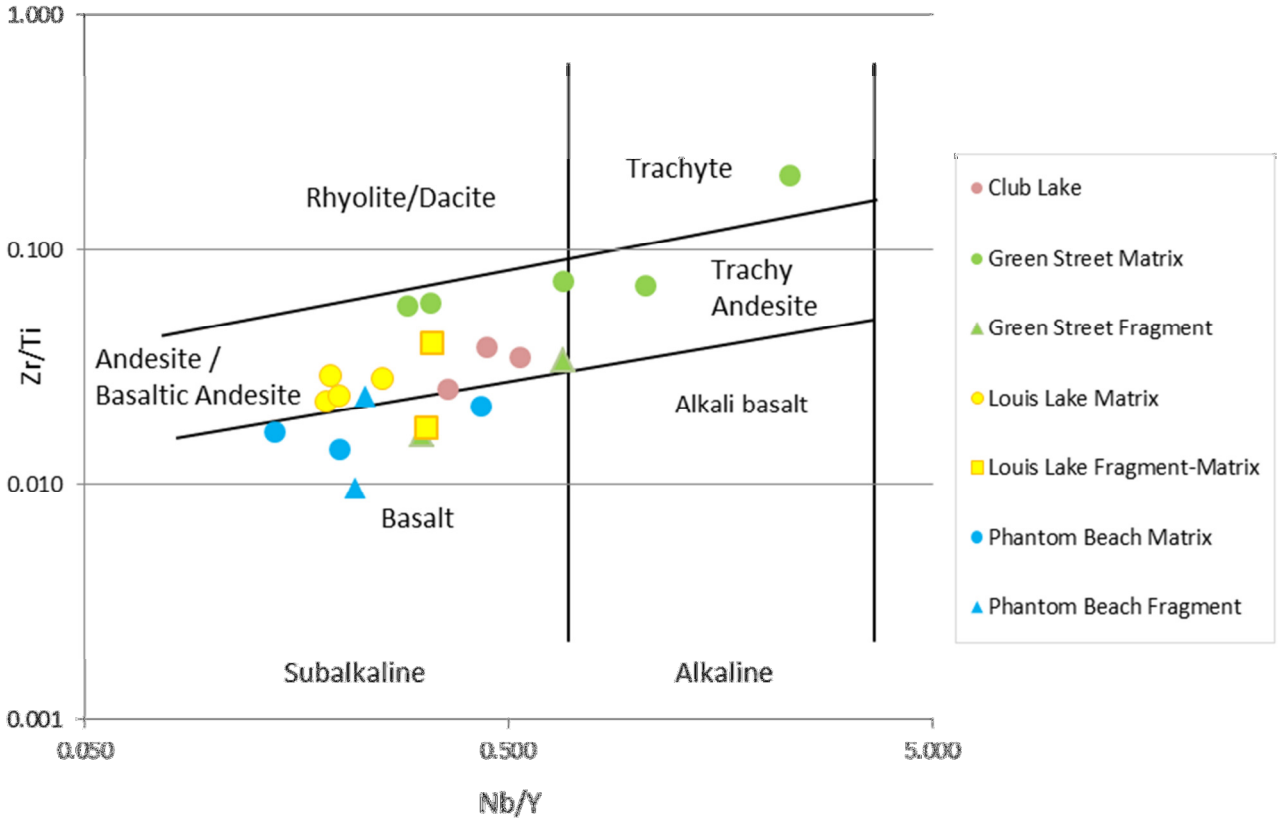

Figure 5-28. Geochemical classification of Flin Flon samples using the volcanic discrimination diagram by Pearce (1996) (modified).

Bivariate plots (Figure 5-29A and B) of the less mobile elements can help distinguish between tholeiitic and calc-alkaline rocks and suggests that most (or all) samples in this study are calc-alkaline in nature. The Zr-Y scatter plot subalkaline basalt classification scheme from Ross and Bédard (2009) shows that Boundary intrusion samples exhibit characteristics typical of calc-

alkaline to transition sequences, with three samples plotting in the tholeiite field. However, the La-Yb scatter plot, also by Ross and Bédard (2009), shows all samples in the calc-alkaline field. When major oxides are used for classification, the Jensen cation plot (Jensen, 1976) (Figure 5-29C) shows a gradation from calc-alkaline to high Mg tholeiitic basalts, with the melanocratic gabbro plotting in the komatiite field. This overall agrees more closely with the Zr-Y plot. Diagram D (Figure 5-29) indicates that the bulk of samples lie within the volcanic arc basalt field, but three anomalies lie near or within the E-MORB/within plate transition field. These three samples are fragments of the Phantom Beach and Green Street breccia, all of which are amphibole (hornblende and actinolite) dominant with minor to no plagioclase or quartz.

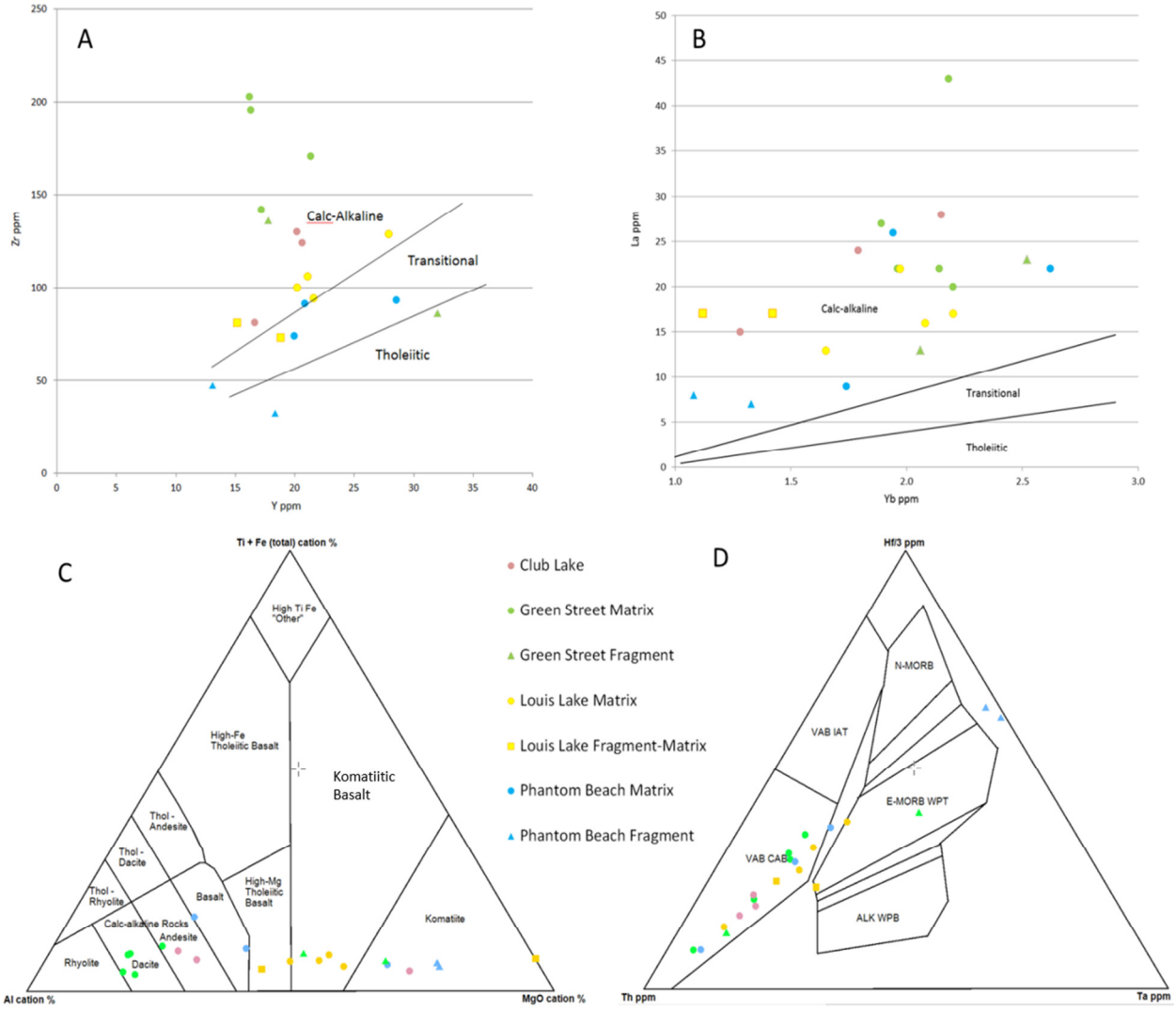

Figure 5-29. Geochemical (tholeiitic to calc-alkaline (Ross and Bédard, 2009) and tectonic classification of the Flin Flon Boundary intrusion samples. Graph A) Zr ppm vs Y ppm. Graph B) La ppm vs Yb ppm. Diagram C) Jensen cation plot (1976) for classification of sub-alkaline rocks. Diagram D) Tectonic discrimination ternary plot (Wood, 1980). Alk WPB = alkali within plate basalt; E-MORB WPT = enriched mid-ocean ridge basalt within plate transition; N-MORB = normal mid-ocean ridge within plate transition; Trans Alk WPB E-MORB WPT = transitional alkali within plate basalt enriched mid-ocean ridge within plate transition; VAB CAB = volcanic arc basalt calc-alkaline basalt; VAB IAT = volcanic arc basalt island arc transition.

5.2.4 Major Element Oxide Trends

Whole rock major element analyses illustrate the relationship between oxides with respect to SiO_2 and MgO between the breccia fragments and matrix, and intrusions without brecciation

(Figure 5-30). MgO values for the dataset vary over a slightly large range (16.4 wt%) than SiO_2 (16.6 wt%).

Resulting trends of Harker diagrams are meant to represent a liquid line of descent (or fractionation) for related suite of igneous rock samples. However useful, it is important to keep in mind the limitations of determining the processes causing variation of oxide proportions inherent in the (Harker) diagrams. In the case where rocks are porphyritic, curves may not exactly correlate to the liquid line of decent (Wilcox, 1979). Due to how the oxides are presented, as a portion of a total sum of oxides, change in the concentration of one oxide will therefore subsequently cause a change in the proportion of another. A false correlation can subsequently arise due to an existing correlation between two other oxides. Also, the higher concentrations of SiO_2 and MgO to the remaining oxides can also cause a false negative correlation due to the constant sum effect. Pearce (1968) describes the limitations for the bivariate diagrams, but demonstrates that they are applicable in illustrating genetic relationships where there is a fundamental relationship between rocks of varying compositions.

Broadly linear relationships exist between the plotted oxides in Figure 5-30, with the least linear correlation occurring between K_2O and TiO_2 for both MgO and SiO_2. The diagram shows oxide plots for Al_2O_3, CaO and TiO_2 for both SiO_2 and MgO. Al_2O_3, K_2O, Na_2O, and SiO_2 all show a negative correlation with MgO, and the alkalis conversely show a positive correlation with SiO_2. MgO appears to show a slightly better correlation with other oxides compared to SiO_2. The scatter and consequently low correlation of both K_2O can be explained by the mobility of potassium in basaltic rocks during greenschist grade metamorphism (Pearce, 1976).

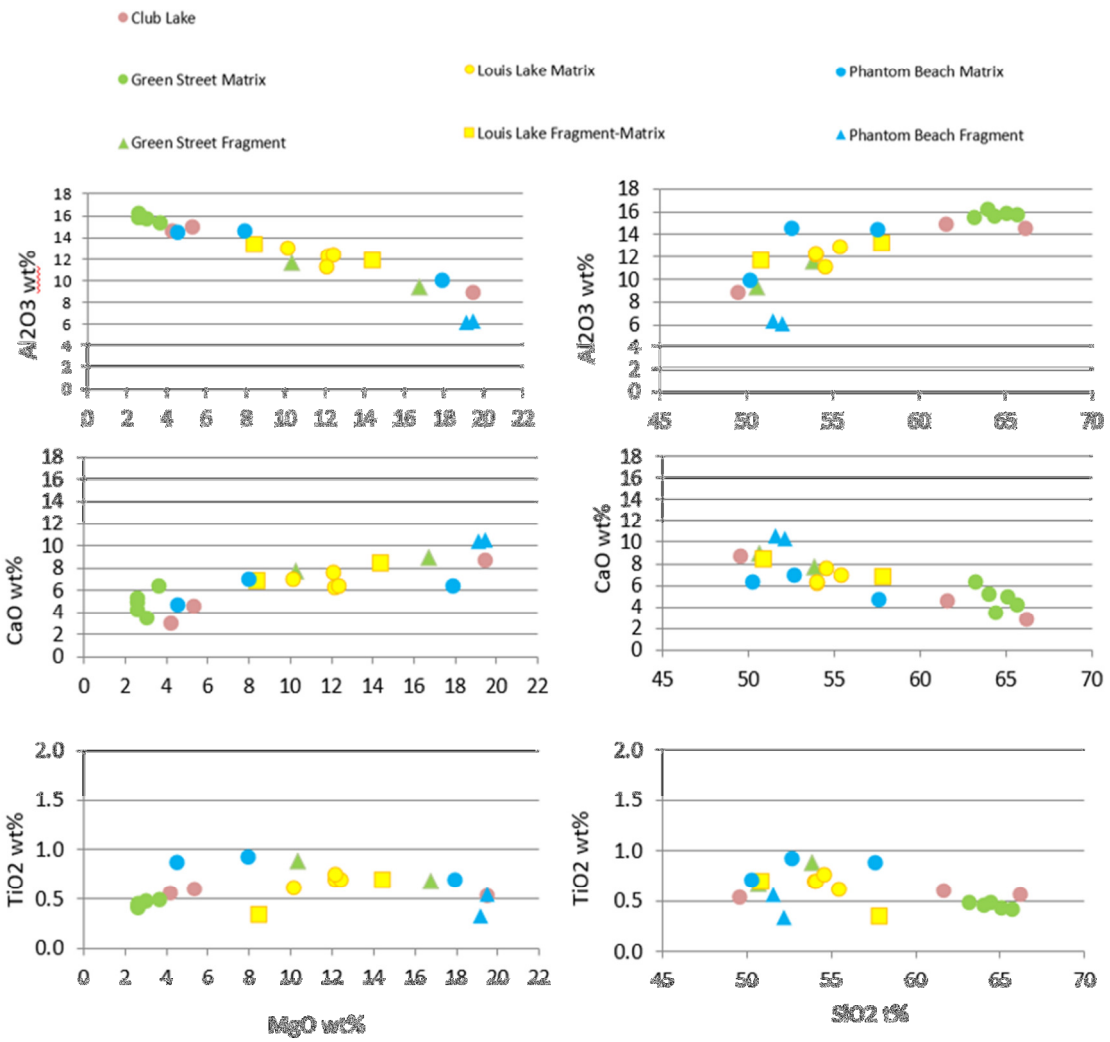

Figure 5-30. Harker diagrams with SiO_2 and MgO on x-axis for the Boundary intrusion dataset.

Magnesium numbers have been calculated for the presented dataset (Table A3, Appendix A) and ratios range from 55.2 to 83.5. The samples with the lowest Mg number are leucocratic matrix samples, while the highest Mg numbers (most primitive) include the most meso- to melanocratic samples with the least amount of plagioclase. The bivariate plot of Mg number versus SiO_2 shows the range of Mg numbers with respect to averaged representative Mg # - SiO_2 values for common rock types. The dataset ranges between the averages lherzolite and granodiorite rock types (Figure 5-31).

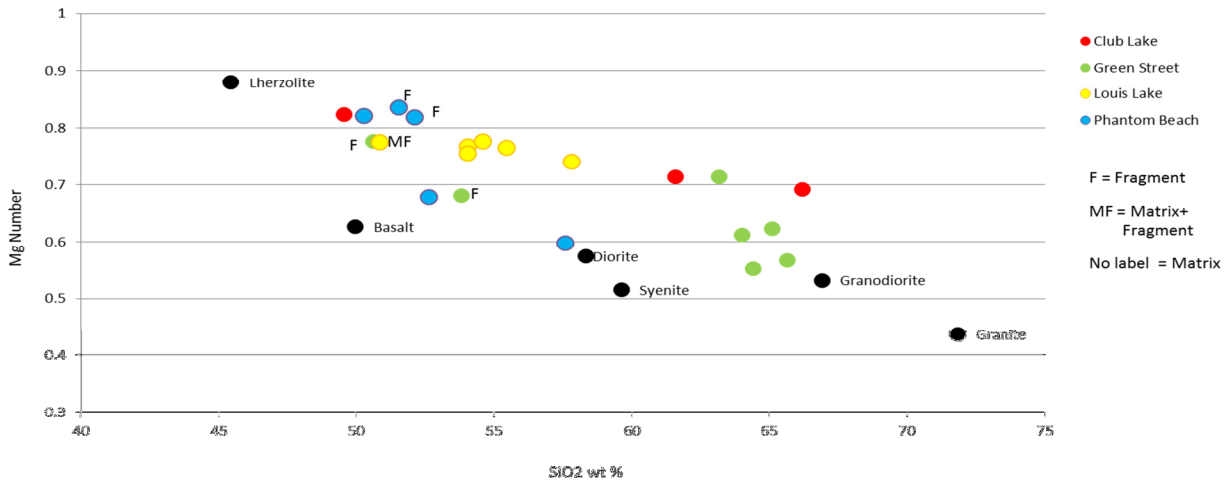

Figure 5-31. SiO_2 wt% plotted against Mg number for Boundary intrusion samples. Graph includes common rocks types for comparison (values for common rock types from LeMaitre (1976)).

5.2.5 Trace Element Characteristics

The majority of Boundary intrusion samples have negative Nb anomalies with respect to Th and Ce and depleted Ti and Y concentrations relative to N-MORB, typical of volcanic arc settings (Table 5-3 and Figure 5-32). Samples which exhibit positive or near unity Nb anomalies include gabbro to ultramafic Green Street fragments, matrices near the fragments, and Phantom Beach hornblendite fragments. Negative Nb anomalies are typically interpreted as potentially representing a magma source that has been affected by dehydration of a subducting slab, leading to the fractionation of Th and Ce from Nb by preferential separation of the former elements into fluids relative to the latter elements (Pearce, 1996). Trace element patterns are most similar to the island arc volcanic and transitional basalts described by Pearce (1996). The samples are light rare earth element (LREE) and large ion lithophile (LIL) element enriched with middle to heavy rare earth element (HREE) and high field strength (HFS) element abundances near or below MORB values. Co and Ni values are anomalous in samples with a greater content of mafic minerals (hornblende- and actinolite-rich) (Figure 5-32).

Table 5-3. Niobium anomalies for Boundary intrusion samples.

Sample ID	Nb Anomaly Value	Sample ID	Nb Anomaly Value
GC_CL01	0.29	GC_LL01A	0.12
GC_CL02	0.31	GC_LL02-01	0.37
GC_CL02B	0.24	GC_LL02-02	0.31
GC_GS07A	0.08	GC_LL03A	0.35
GC_GS08A	0.16	GC_LL04A	0.29
GC_GS10C-01	0.85	GC_PB01	7.28
GC_GS10C-02	0.25	GC_PB02-01	2.23
GC_GS12-01	0.89	GC_PB02-02	0.47
GC_GS12-02	0.59	GC_PB03	0.18
GC_GS14	0.39	GC_PB04	0.17
GC_FF04	0.2		

Note: Values less than 1 are considered negative anomalies. Nb anomaly with respect to Th and Ce.

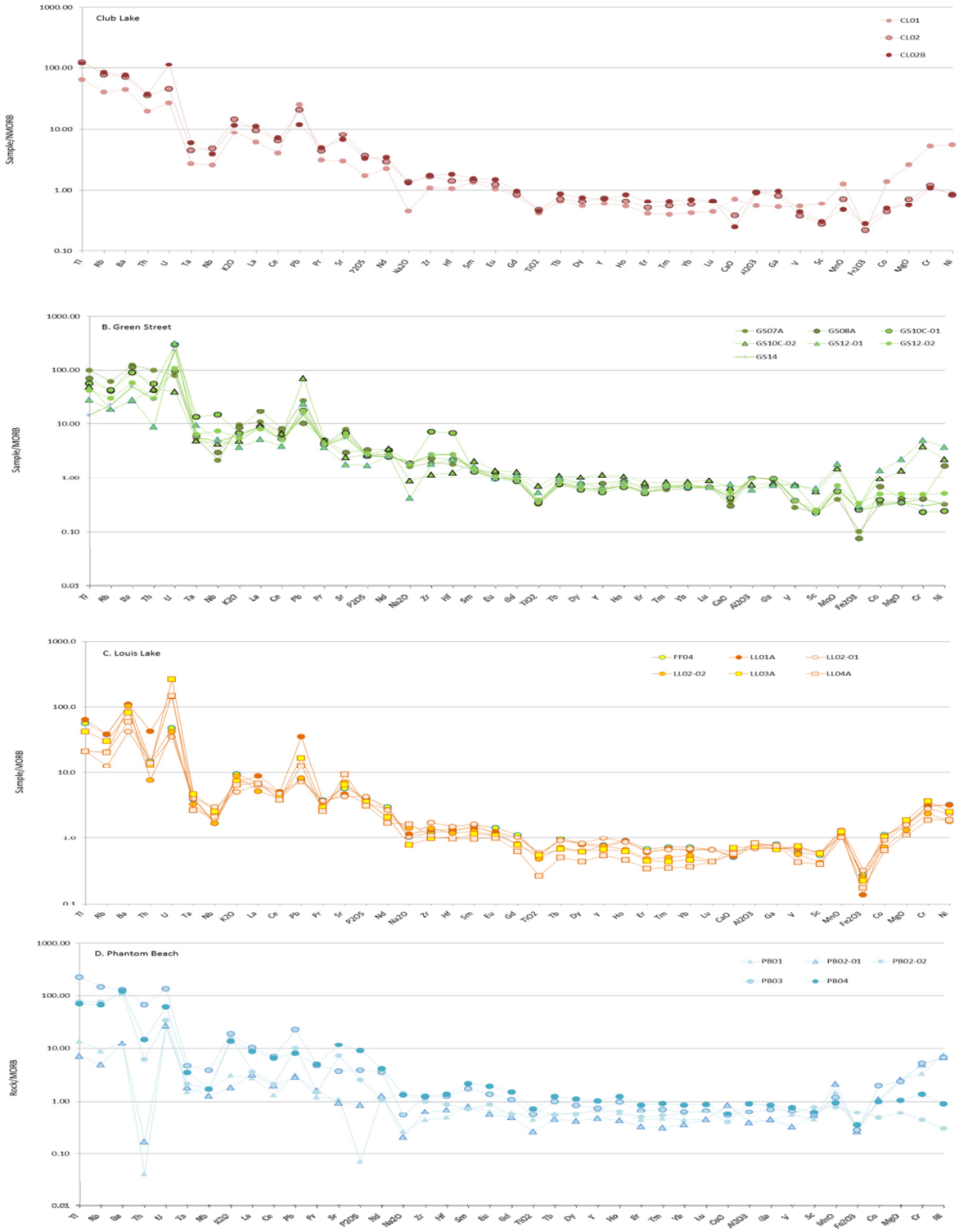

Figure 5-32. Trace element diagrams for Boundary intrusion samples (this study) arranged in order of compatibility in spinel lherzolite mantle. Normalization values for MORB from Sun and McDonough, 1989.

Rare earth element patterns (Figure 5-33A to D) are similar in shape and abundances for most Boundary intrusion samples, with the exception of Phantom Beach. The majority of samples have enriched LREE, MREEs slightly above or near 10x chondrite values, and HREE typically (but not always) below 10x chondrite values. All Phantom Beach fragments and one host intrusion sample (PB04) show LREEs closer to 10x chondrite values, middle and heavy REEs near or below 10x chondrite values, and overall displaying a flatter pattern. All samples are LREE enriched (Figures 5-33 and 5-34A) with LREE abundances greater than HREE, an indication of fractionation of mafic minerals (hornblende, pyroxene, olivine) forming the residua and leaving less compatible elements in the melt. Light and heavy REE fractionation is shown in Figure 5-34B and C, and the trends are broadly linear. LREE distribution in Figure 5-34B exhibits a positively sloping pattern overall and within most sample suites except for the Louis Lake sample set. HREE distribution for all samples range between 1.0 to 2.0 (averaging 1.5), suggesting little to no fractionation within the HREE (Figure 5-34C).

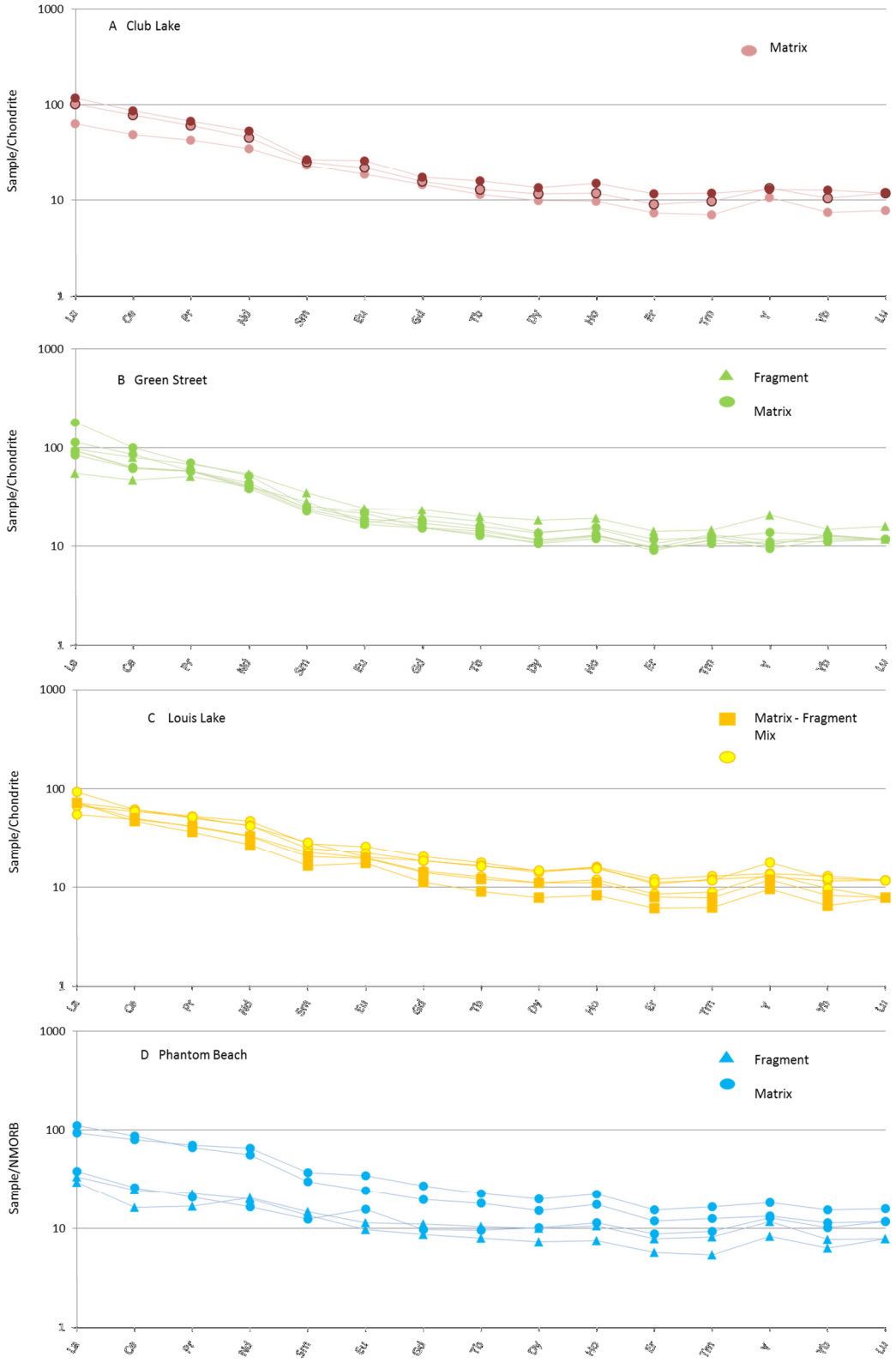

Figure 5-33. Rare earth element diagrams for Boundary intrusion breccia samples. Chondrite values from Sun and McDonough, 1989.

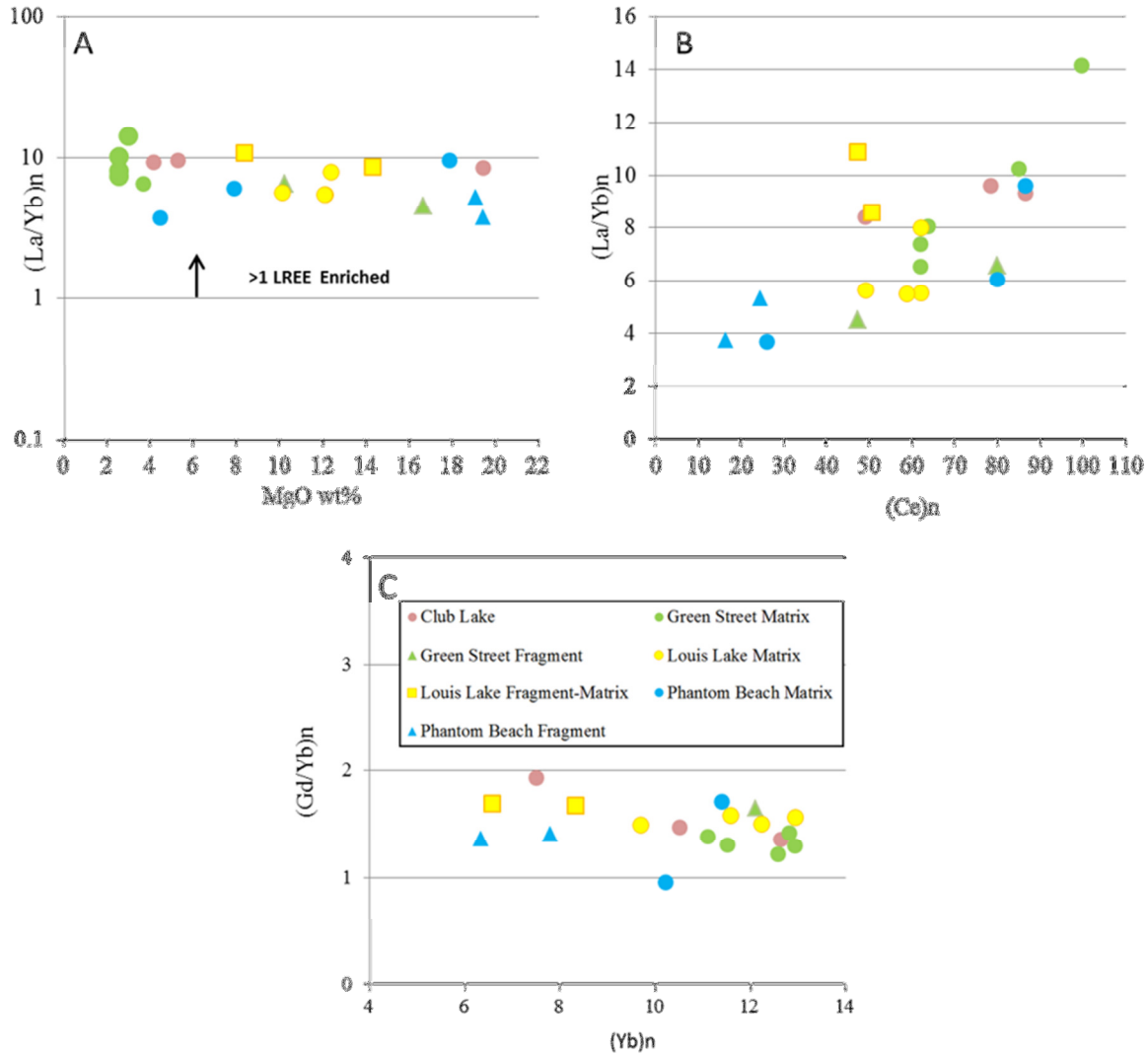

Figure 5-34. Bivariate plots showing relationships between chondrite normalized REE. A) $(La/Yb)_n$, vs MgO wt%. B): $(La/Yb)_n$ vs (Ce)n. C) $(Gd/Yb)_n$ vs $(Yb)_n$.

6.0 DISCUSSION

In order to help better understand the petrogenesis of the Boundary intrusions and add to the current limited database, this study focused on the intrusion breccia matrix and fragment characteristics and relationships. Detailed outcrop mapping, petrography and geochemical analyses were collected to help decipher the breccia associations and apply that information to develop ideas on their formation. This section will highlight relevant features of the results and use them to discuss matrix and fragment sources, breccia formation, transport and emplacement.

6.1 Petrogenesis of the Boundary Intrusion Breccias

High field strength elements such as Nb, Ta, Zr, Hf, Th, Ce, Ti and Y, as opposed to the low field strength elements (mobile cations Ka, Ca, Na…etc.) and mobile oxyanions (P, S, U…etc.), have been used in this study to assess the petrogenetic nature of the Boundary intrusions. The high field strength elements (HFSE) are ions of intermediate ionic potential and have a relative tendency to remain immobile during weathering and metamorphism up to and including the lower to mid-Amphibolite facies grades (Pearce, 1996). The Boundary intrusions have been determined to be affected by greenschist grade metamorphism which peaked ca. 1815 Ma (Gordon *et al*., 1990).

Boundary intrusion samples are calc-alkaline to alkaline in nature (Figures 5-28 and 5-29) and most closely resemble examples of transitional volcanic arc basalt variations shown by Pearce (1982) (Figure 6-1E). Geochemical patterns show an overall typical island arc signature where incompatible elements are enriched relative to MORB with a sharp decrease in normalized abundance of Nb and Ta relative to Ba and Th (or increase in the normalized ratio of Th or Ba to Nb or Ta) (Figure 6-1A to D), but do not show the same depletion of increasingly compatible elements (Nb to Ti, and Cr) relative to MORB as seen in island arc examples provided by Pearce (1982). Differences with typical island arc signatures arise where moderately incompatible elements for Boundary intrusion samples (for elements less compatible than Sm) are slightly enriched compared to MORB. Explanations for transitional volcanic arc basalt signatures offered by Pearce (1996) include more than one episode of enrichment of the mantle source with one related to subduction, or that magma mixing (and contamination) is a factor. Fragment samples from Phantom Beach are less enriched or depleted in nearly all selected elements for discussion (Th, Nb, Ce, Zr, Ti and Y) relative to MORB, suggesting basalt more tholeiitic in nature.

Syme (1975) suggested that consistently high and increasing oxygen and water fugacities (f_{O2} and f_{H2O}) during differentiation created the calc-alkaline trend. This was likely driven by the formation and fractionation of dominant Fe-affinity minerals such as magnetite (± pyroxene/olivine) in early differentiates, thus producing Mg-rich melt for the formation of Mg-rich amphiboles (and pyroxenes). This was later reiterated in a study by O'Hanley and Kyser (1994) where the authors concluded that a distinctive vertical trend on an FeO/MgO vs SiO_2 diagram (Figure 6-2) is attributed to the co-precipitation of augite with hornblende (perhaps olivine) which resulted in the suppression of the typical Fe-enrichment in fractionated magmas. Boundary intrusions from this study are largely Mg dominant, and comparatively more fractionated than samples from the 1994 study (Figure 6-2). A broadly linear trend exists over the suite of samples suggesting a line of successive differentiates is not unreasonable.

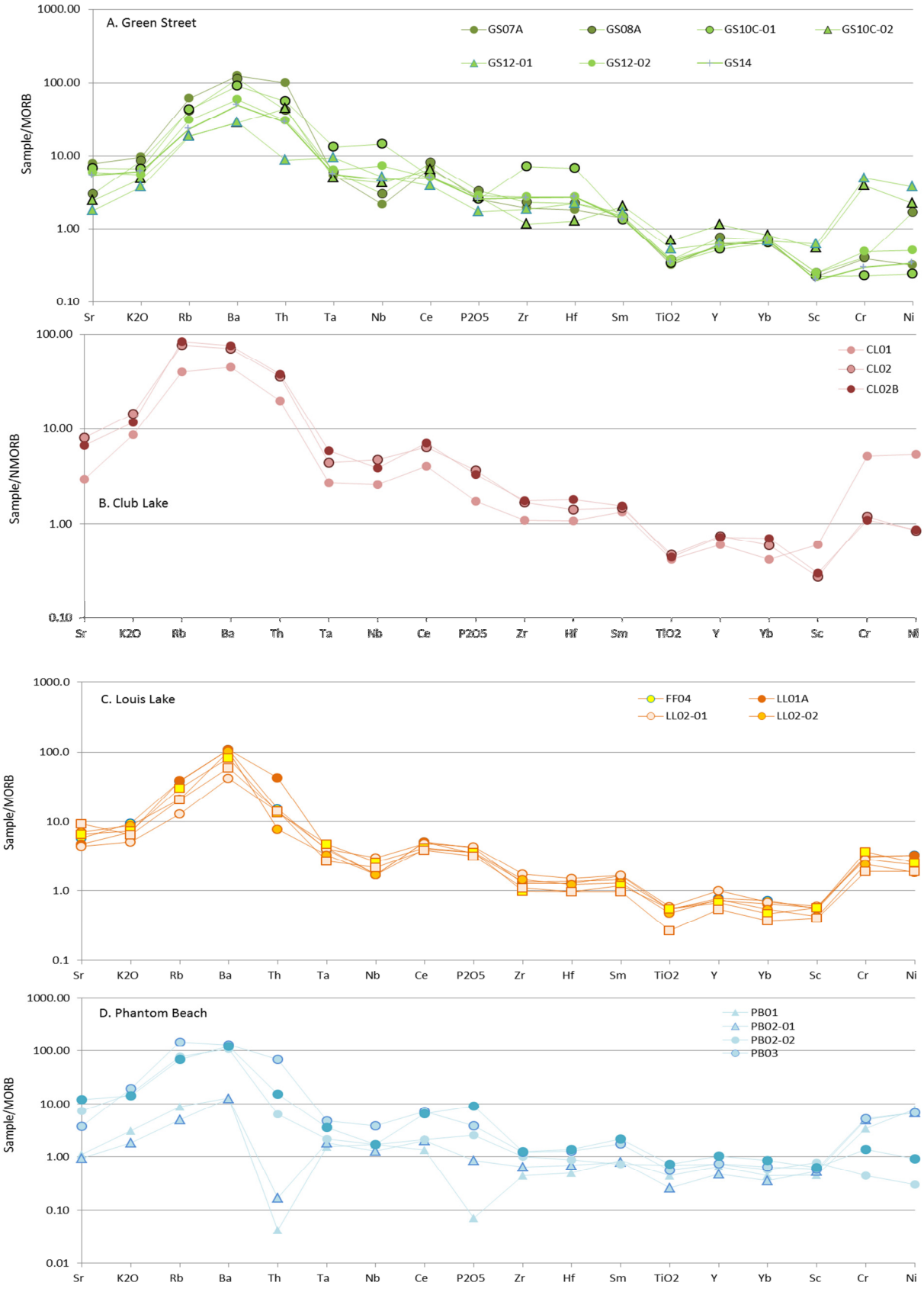
A. Green Street
GS07A
GS08A
GS10C-01
GS10C-02
GS12-01
GS12-02
GS14
Sample/MORB
1000.00
100.00
10.00
1.00
0.10
Sr K2O Rb Ba Th Ta Nb Ce P2O5 Zr Hf Sm TiO2 Y Yb Sc Cr Ni
B. Club Lake
CL01
CL02
CL02B
Sample/NMORB
100.00
10.00
1.00
0.10
Sr K2O Rb Ba Th Ta Nb Ce P2O5 Zr Hf Sm TiO2 Y Yb Sc Cr Ni
C. Louis Lake
FF04
LL01A
LL02-01
LL02-02
Sample/MORB
1000.0
100.0
10.0
1.0
0.1
Sr K2O Rb Ba Th Ta Nb Ce P2O5 Zr Hf Sm TiO2 Y Yb Sc Cr Ni
D. Phantom Beach
PB01
PB02-01
PB02-02
PB03
Sample/MORB
1000.00
100.00
10.00
1.00
0.10
0.01
Sr K2O Rb Ba Th Ta Nb Ce P2O5 Zr Hf Sm TiO2 Y Yb Sc Cr Ni

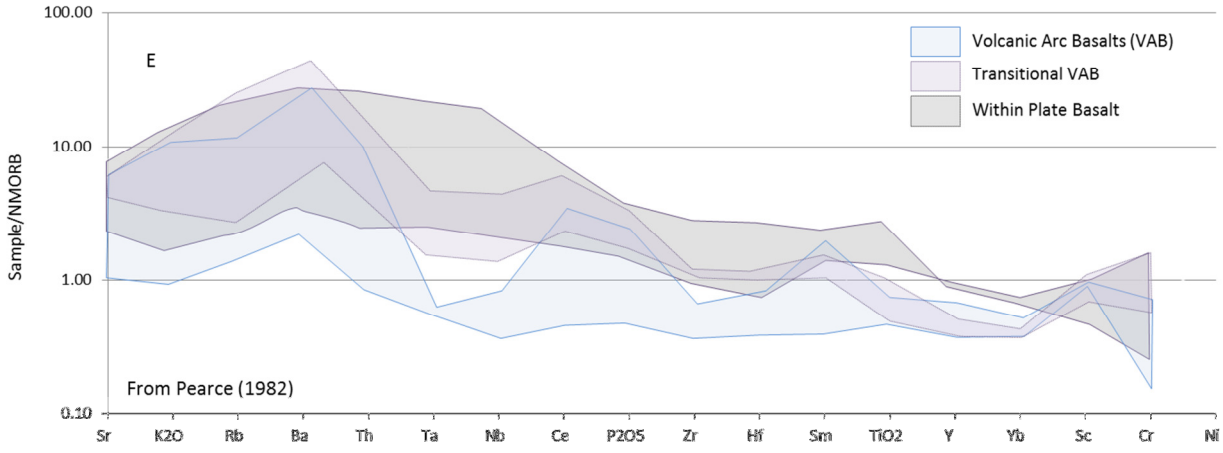

Figure 6-1. MORB-normalized trace element diagrams of Boundary intrusion samples. Refer to Figures 5-2, 5-6, 5-8, 5-16, and 5-23 for sample locations in images A - D. Examples of within plate basalts, volcanic arc basalts, and transitional volcanic arc basalt variation from Pearce, (1982) shown in diagram E. Values for MORB from Sun and McDonough (1989).

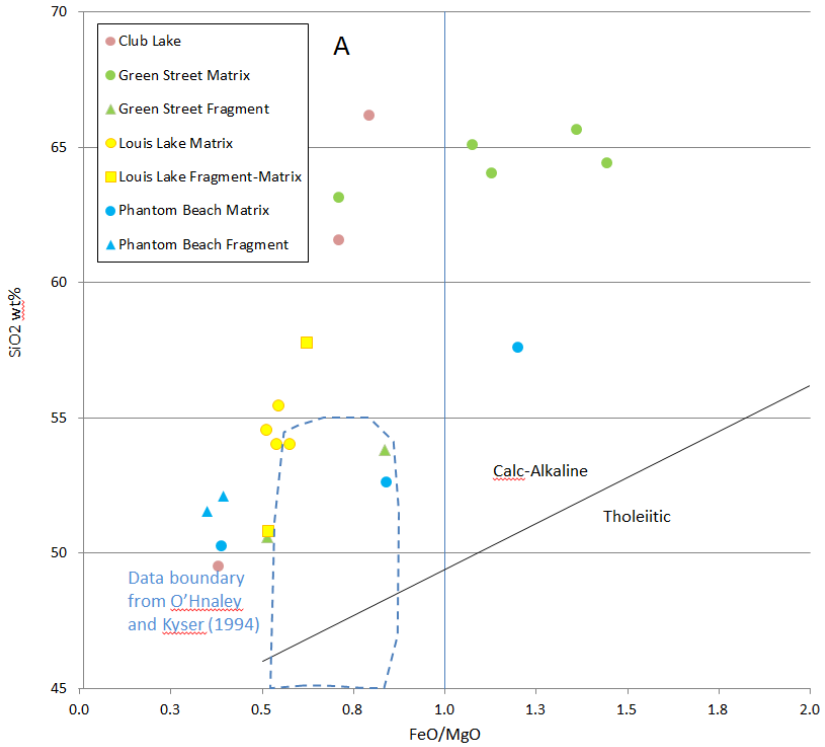

Figure 6-2. Iron (total) and magnesium in Boundary intrusion samples plotted against silica content (Modified from Gill (1981).

In order to determine if a mantle- or slab-derived component is a more likely source, Pearce and Parkinson (1993) used an extended MORB-normalized plot with a range of elements ordered by relative incompatibility with a fertile spinel-lherzolite mantle (Figure 5-32 and Figure 6-1). The assumption is made that Nb, Zr, Ti, Y and Yb are dominantly mantle-derived (Pearce and Parkinson, 1993) and are not added to the magma source through subduction processes (i.e., these elements are conservative) (Pearce, 1996). Though useful for most arc basalts as an indicator of melt and mantle composition, use of these elements is applied with caution as other complex volcanic arc geochemical patterns have shown unexpected enrichment patterns (e.g. boninite from Mariana trench, Pearce *et al*., 1992). Boundary intrusions show an enrichment of normalized Ta and Nb relative to Zr and Hf relative to MORB, a feature attributed to an enriched mantle source or by small degrees of melting with residual garnet (Pearce and Parkinson, 1993 and references therein). Boundary intrusion samples show similarities to the pattern of basalt from the Lesser Antilles (Brown *et al*., 1977; White *et al*., 2017) used to represent melting product patterns for more complex mantle sources such as magma mixing or magma which has undergone several enrichment or depletion events (Pearce, 1982). All Boundary intrusion matrix samples and most fragment samples (with the exception of PB01 and PB02-01) have negative Nb anomalies with respect to Th and Ce, suggesting that the mantle source has been affected to some degree by dehydration of a subducting slab.

Three mafic to ultramafic fragment samples more closely resemble the pattern of WPB or IAT (Figure 6-1A, D and E). All fragment samples exhibit a gentler slope from Ba to Ta, a feature more similar to the pattern of within-plate-basalts. Fragments from both Green Street and Phantom Beach are also less enriched in the more incompatible elements than the matrices, the largest differences best seen in the Phantom Beach suite. This feature more closely resembles the more tholeiitic patterns of the within-plate basalt and island arc varieties of Pearce (1982). Phantom Beach rocks also have significant depletion of elements relative to MORB (Zr to Sc), anomalously low absolute Th and P concentrations, each a feature typical of island arc tholeiites (lower boundary of VAB shaded area of Figure 6-1E). It should be noted that no repeat samples have been completed for the Phantom Beach fragments, and future observations and interpretations should be made with inclusion of a repeat sample. Though Green Street fragment samples are less enriched in incompatible elements than the intrusion matrix, they are still

relatively enriched overall. The enrichment of incompatible elements for Green Street fragments (GC_GS10C-02) coupled with a less pronounced negative Nb anomaly (Table 5-3), may suggest an enriched source, such as MORB melting or mantle wedge-MORB mixing, less affected by dehydration or partial melting due to a subducting slab. Phantom Beach fragment trace element patterns may suggest a relatively less enriched to slightly depleted mantle source, and also not affected by dehydration of a subducting slab (GC_PB01 and GC_PB02-01, Table 5-3), unlike the remaining Boundary intrusion samples in this study.

High normalized Zr to Ti ratios are indicative of Ti-bearing oxides crystallizing with major phases such as plagioclase, olivine and augite, which results in depletion of Ti relative to Zr in the remaining melt, a process that coincides with rock compositions becoming more SiO_2-rich or more alkaline. Rock compositions also trend towards increased Zr relative to Ti and Y with assimilation of the upper crust during ascent (Pearce, 1996). For most Boundary Intrusion samples, zirconium is near N-MORB concentration and Ti and Y are consistently depleted or near N-MORB (Figure 6-1). The highest Zr to Ti ratio occurs in leucocratic Green Street samples and this, along with comparatively more enriched Th (Figure 6-3A and B) (as well as Nb and Ce concentrations, relative to other samples), may suggest Green Street magmatism could be affected by crustal assimilation which has driven compositions towards a more upper crust composition (Pearce, 1996), as well as representing a more fractionated series.

Pearce (1996) indicated that crust-contaminated volcanic arc basalts will plot in the VAB field on the Th-Ta-Hf diagram, but outside of the VAB section on the Ti-V diagram by Shervais (1982). Most Boundary intrusion samples plot in the MORB field (Figure 6-3C), similar to the calc-alkaline series shown by Shervais (1982), with the general trend aligned with the MORB-ARC (labeled ‘20’) line suggesting contamination by assimilation from crustal sources for nearly all samples. Caution should be used when making observations from this plot, however, as samples subjected to either or both magnetite or hornblende fractionation will have anomalously high Ti/V ratios and Shervais warns this diagram should not be used to assign tectonic setting. It may be possible that magnetite or hornblende fractionation may have been a factor related to the genesis of the Boundary intrusion magmas, nevertheless, the samples of this study have been plotted for comparison’s sake.

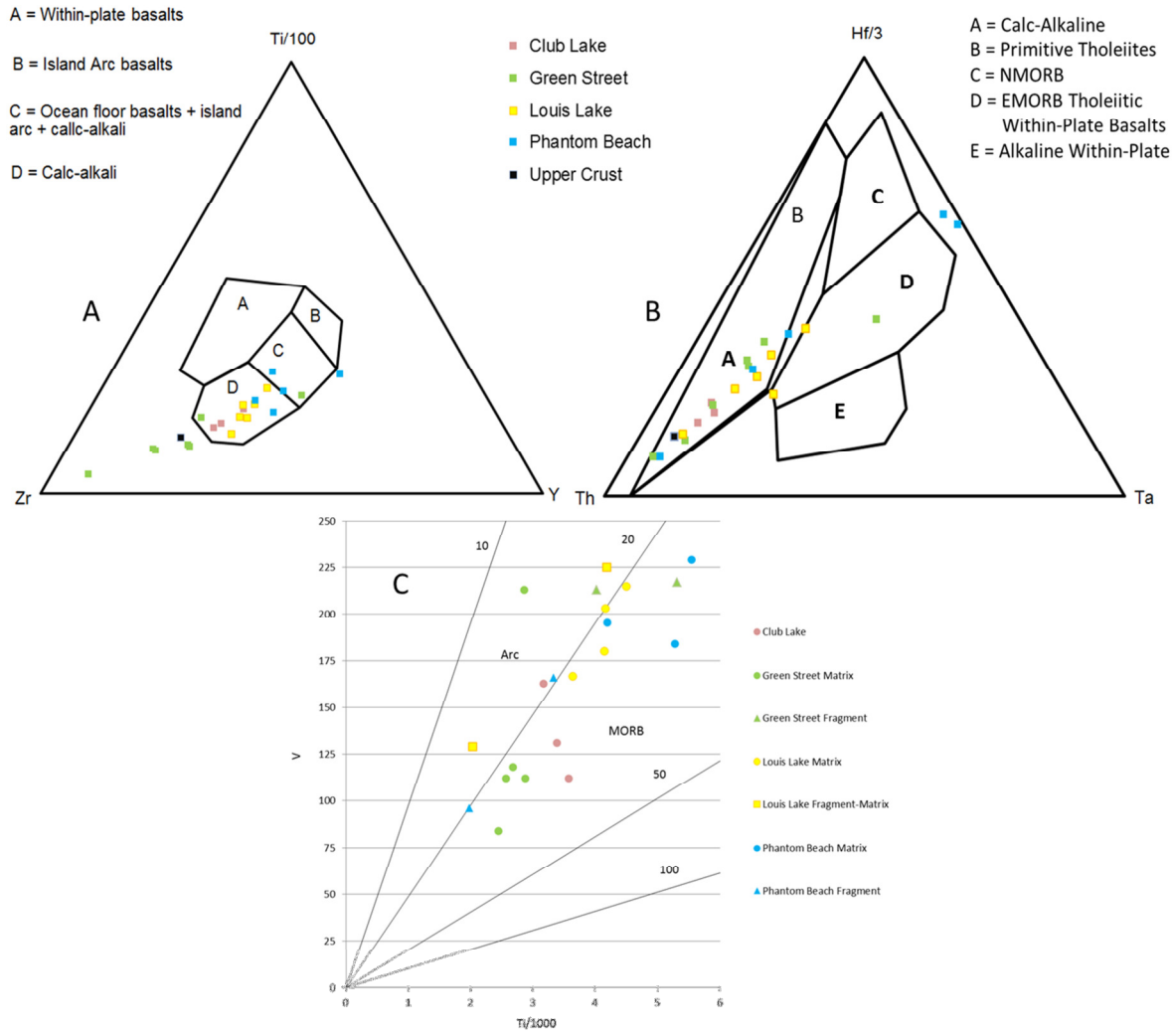

Figure 6-3. Green Street samples trend towards Zr and Th indication magma-upper crust interaction (Pearce, 1996). Image A from Pearce and Cann (1973) and Image B from Wood et al, 1979). Upper crust value from Rudnick and Gao, 2014. Diagram C: Ti/V plot for Boundary intrusion samples (from Shervais, 1982).

MORB normalized concentrations of Y values are consistently higher than normalized TiO_2 in all Boundary intrusion samples (Figure 6-1); the opposite is indicative of WPB, where a high normalized TiO_2/Y ratio is the result of deep melting (> 50 km) and Y is preferentially retained in garnet residua (Pearce, 1996). The TiO_2 and Y ratios may petrogenetically place the source at shallow depths (<50 km) with higher water contents where garnet is not a factor in retaining yttrium relative to titanium. Normalized TiO_2 and Y concentrations in Boundary intrusion

samples most likely reflect fractionation from non- garnet source (amphibolite?) at shallow depths. Boundary intrusion samples show similarities with the Schist Lake and Vick Lake samples concerning $(TiO_2/Y)_{MN}$ (Figure 6-4A) ratios having values less than one. This coupled with the LREE enrichment seen in the Boundary intrusion samples and select sample suites from Stern *et al*. (1995) may indicate a similar mantle source in their generation. Figure 6-4B also illustrates the distribution of measured Ti/Y values for the Boundary intrusions of this study compared with volcanic arc samples from Stern *et al*. (1995). There is a distinct increase in alkalinity (Nb/Y) in the Boundary intrusions with some overlap of samples from Schist Lake and Vick Lake samples (green polygon), while Ti/Y values remain relatively consistent.

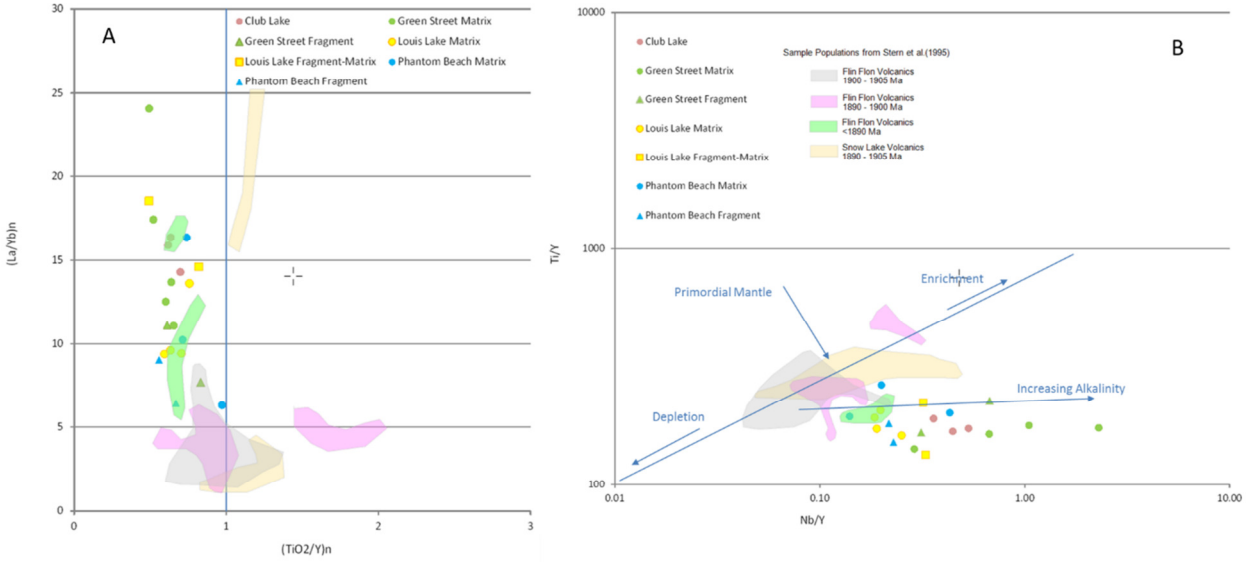

Figure 6-4. Comparisons to data from Stern *et al*. (1995) for select high field strength elements. A) Ti/Y vs Nb/Y plot for samples from this study and Stern *et al*. (1995). B: Normalized La/Yb vs normalized TiO_2/Y for Boundary intrusions of this study and samples from Stern *et al*. (1995). Green polygon includes Schist Lake and Vick Lake; pink polygon includes Bear Lake suite and the Bakers Narrows suite; grey polygon includes Hook Lake, Hidden-burley and the Beaver Road sample suites; orange polygon includes sample suites from Snow Lake, including Moore Lake, Snell basalts, and Welch boninites and tholeiites. Legend for Image B as in Image A.

Performing an assessment on geothermobarometry on the Boundary and the mafic intrusive fragments intrusions during crystallization would be based on mineral assemblages and therefore qualitative at best. Much original hornblende is present, but greenschist metamorphism has overprinted any other original pyroxene or olivine with actinolite. Overall, thin section textures

of the intrusion matrix and fragments reveals a system in disequilibrium due to occasional chemical zoning in both plagioclase and amphiboles, reaction rims around amphiboles (chlorite and finer-grained actinolite?) (Figures 6-5). Zoning is indicative of changing chemical composition during crystallization, but some (or most) reaction rims may be a product of metamorphic effects. Considering the presence of olivine, augite, magnetite and ilmenite in the Boundary intrusion samples collected by O'Hanley and Kyser (1994), analyses indicate equilibration temperatures between 600 – 700 degrees Celsius and crystallization at lower pressures of approximately 2 kilobars (kbars).

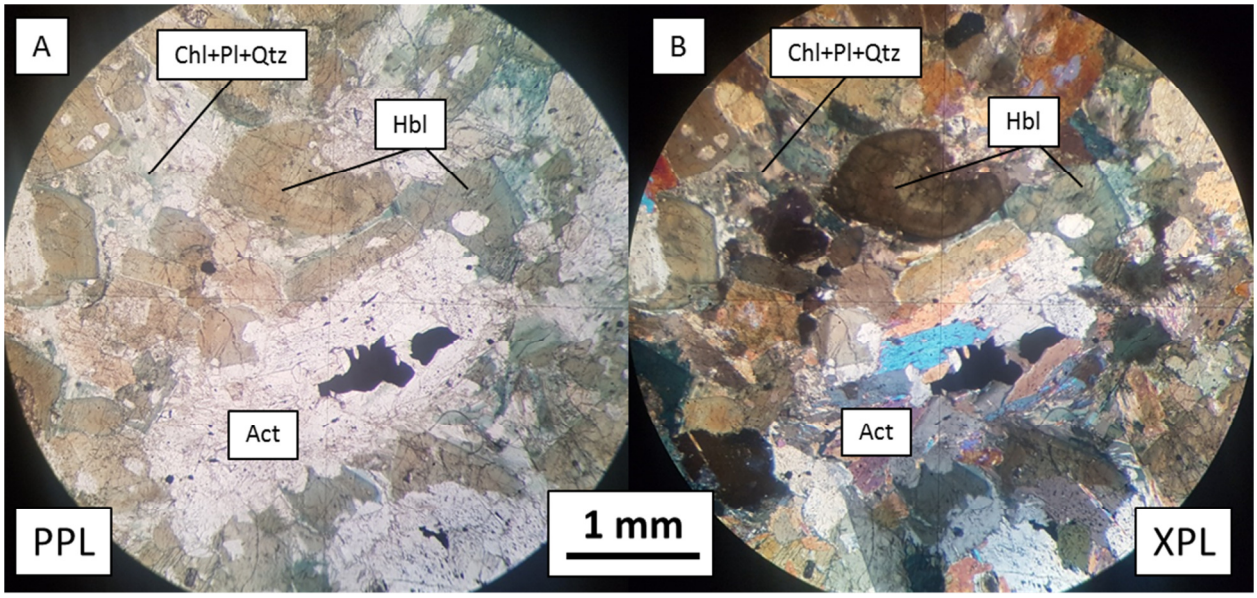

Figure 6-5. Petrographic image showing disequilibrium textures in Green Street mafic fragment of sample TS_GS01A-02B. Sample shows selective alteration of mafic mineral to actinolite within hornblende glomerocryst and zoning within hornblende. Image A in PPL; Image B in XPL. Act = Actinolite; Chl = Chlorite; Hbl = Hornblende; Pl = plagioclase; Qtz = Quartz.

6.2 Fractionation within Sample Suites

Similar patterns exist between all Boundary intrusion samples of this study for HFS elements Th, Nb, Ce, Zr, Ti and Y, with the exception of fragment samples mentioned in the previous section and matrix samples (GC_GS10C-02 and GC_GS10C-01, GC_GS12-01 and GC_GS12-02, GC_PB02-01 and GC_PB-01) (Figure 6-6). Club Lake and Louis Lake sample suites do not

contain fragment samples, but do consist of meso- to melanocratic rocks which can be compared to the more leucocratic samples (Figure 6-1B and C). Patterns of each sample area are overall consistent with each other (with some variations) suggesting they are fractionated from the same magma source and have undergone similar fractionation processes. Club Lake melanocratic sample GC_CL-01 has slightly lower abundances for most elements and similar normalized TiO_2 and Y concentrations to leucocratic samples.

MORB-normalized trace element patterns for O'Hanley and Kyser (1994) Boundary intrusions samples have consistent shapes but they conclude that the samples do not represent a single fractionated suite, but do show similar melt characteristics. This is similar to Boundary intrusions of this study when considering the entire group of samples. The majority of samples in this study do illustrate similar melt characteristics through Nb, Ta, Zr, Hf, Zr, Ti and Y features, but Zr/TiO_2 ratios do not indicate that all samples of this study are related by the same fractionation event. Within individual samples suites such as Green Street, however, Zr/TiO_2 ratios suggest these samples are a series of a fractionation event.

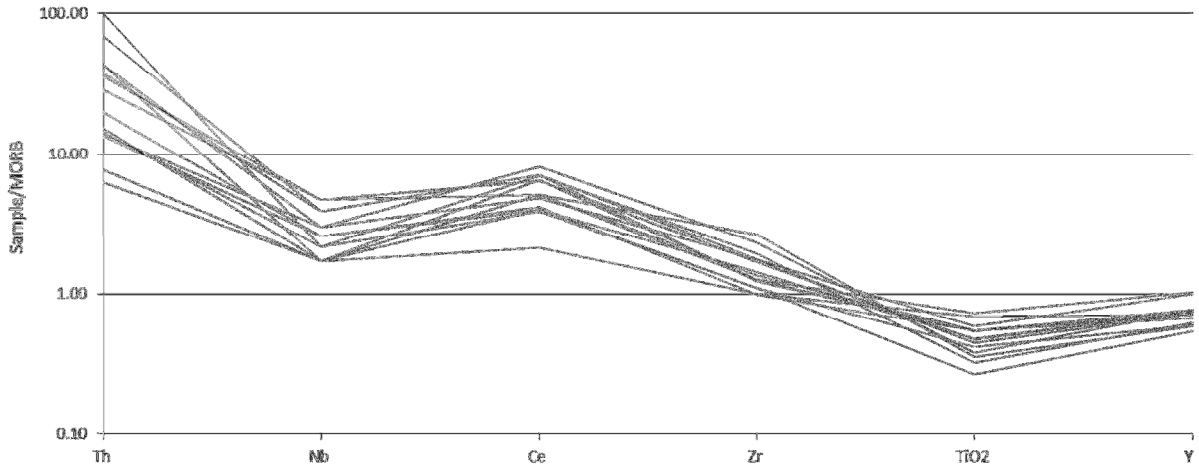

Figure 6-6. HFSE plotted against MORB (Sun and McDonough, 1989) for all Boundary intrusion samples except for GC_GS10C-01, GC_GS10C-02, GC_GS12-01, GC_GS12-02, GC_PB01, and GC_PB02-01.

During plagioclase, olivine, augite and magnetite crystallization, Zr is enriched relative to TiO_2 in the melt and coincides with the increasing silica trend (Pearce, 1996). Trace element patterns for Green Street (Figure 6-1A and Figure 6-7A) samples could conceivably represent a fractionated magma from the same source as the fragments, supported by the higher normalized Zr/TiO_2 ratios for the more fractionated matrix samples. The subhorizontal intrusion breccia at Louis Lake exhibits a slightly higher normalized Zr/TiO_2 ratio indicating a more fractionated subset of the host Louis Lake intrusion. However, in the case of Louis Lake, Phantom Beach samples and Club Lake (Figure 6-1 and Figure 6-7), more samples are needed to imply a Zr/TiO_2 fractionation trend if one exists.

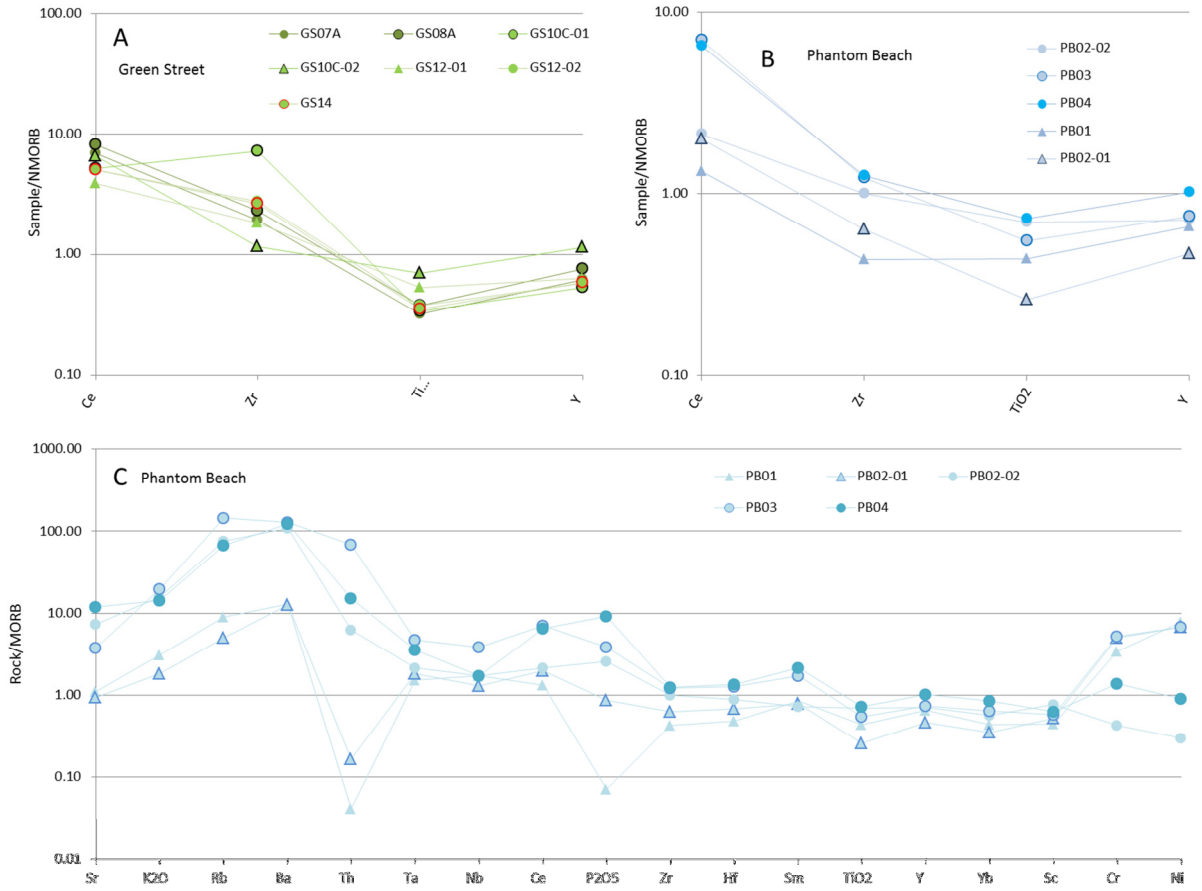

Figure 6-7. Trace element diagrams for Green Street and Phantom Beach samples illustrating normalized Zr/TiO_2 ratios (image A and B). Pattern comparisons (Image C) between sample PB03 (hornblendite), fragments and younger Phantom Beach Boundary intrusion phases. Circle symbols represent matrix samples; triangle symbols represent fragment samples. Normalizing values from Sun and McDonough (1989).

The negative correlation of SiO_2 with the oxides MgO, FeO, and CaO (Figure 5-30 and Figure 6-8) suggests fractionation of Fe-, Mg- and CaO-rich minerals such as amphiboles and (clino) pyroxenes from early differentiates. From the observations made from the trace element data and the limited datapoints available in the major oxide trends, meso- to melanocratic intrusion samples from Green Street and Louis Lake may be fractionated rocks of the same magma source as those more leucocratic (alkalic) samples from the same intrusion. The negative correlation of MgO with Na_2O, Al_2O_3 and SiO_2 shows that plagioclase was a minor fractionating component in the meso- to melanocratic samples, and this is supported by modal percentages of minerals obtained through petrographic analysis. Though trace element data is suggestive of a related suite of rocks for all matrix samples, and Harker diagrams for both MgO and SiO_2 show a linear trend, isotope data and age dating would be needed to confirm if the separate intrusions and their fragments are indeed cogenetic.

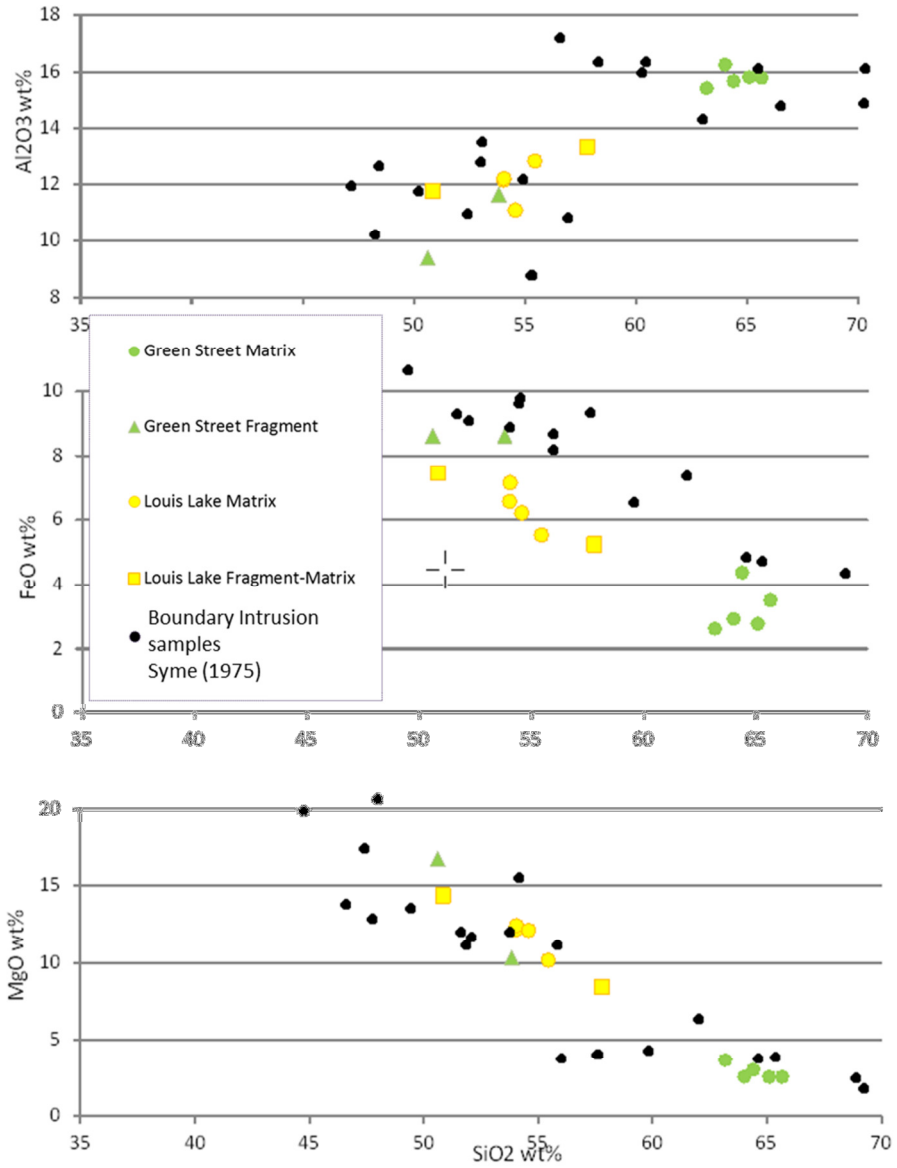

Figure 6-8. SiO_2 wt% plotted against Al_2O_3, FeO, MgO. Distribution of samples from this study is similar to distribution of Boundary intrusion samples of Syme (1975) (shown in black).

Syme (1975) obtained linear relationships between ultramafic, mafic, and felsic samples of the Boundary intrusion suite on Harker diagrams, but noted slope changes and gaps between sets of samples in several of the plots. The data used for this study is very similar in the distribution on the same diagrams (Figure 6-8), despite that the present dataset covers a slightly narrower range of SiO_2 values. The same change can be seen for MgO vs SiO_2 between ultramafic/mafic and felsic rocks at approximately 60 wt% SiO_2. The slope change may indicate the exhaustion of magnesium by mafic minerals, especially hornblende, during crystallization. Reasons for gaps in

the datasets of Syme (1975) and this study are uncertain, but can be caused by several factors during the rock suites genesis, such as magma mixing and contamination or by a lack of representative samples. The conclusion by Syme (1975) was that even though the patterns suggest a conceivable comagmatic relationship, it was unlikely the felsic rocks were an extreme differentiate from the mafic Boundary intrusions. However, later studies by O'Hanley and Kyser (1994) concluded through analysis of whole rock and isotope systematics that the Boundary intrusions were genetically related and trends are consistent with fractionation from a similar magma source.

6.3 Fragment Sources

Petrographic analysis of select, but locally representative fragments within the Green Street, Louis Lake, and Phantom Beach intrusions indicates that most mafic intrusive fragments are a variety of gabbro, ranging from hornblende gabbro to plagioclase-bearing hornblendite (Table 5-2). The fragments could also be considered gabbronorite to plagioclase-bearing pyroxenites, assuming the primary mineral before regional greenschist metamorphism was clinopyroxene, possibly (and most likely) augite. While no definitive pyroxene minerals were identified in thin section, relict textures found in actinolite grains (Figure 5-13) suggest it is a reasonable assumption.

Louis Lake leucocratic stoped blocks bear significant resemblance to the matrix of the matrix-supported Louis Lake breccia, as all thin sections samples contain dominant plagioclase (40 – 50%) with near equal, but lesser mafics of actinolite and hornblende. This is not unexpected as trace element data suggests they are differentiates of the same magma source, and the presence of stoped blocks indicates repeated pulses of magma encompassing already crystalized earlier fractionated magmas. The mafic fragment within the main intrusion (Table 5-2) is also mineralogically comparable to the darker layer of the stoped block, its modal range suggesting the rock-type melagabbro. Mafic intrusive fragments of the clast-supported intrusion breccia which cross-cuts the main Louis Lake intrusion (Figure 5-6, Figure 5-9B and B1) has similar plagioclase content as the main intrusion (breccia matrix), but lacks the presence of quartz.

Green Street fragments, mineralogically, are similar to the mafic intrusive fragments found in the matrix-supported Louis Lake intrusion breccia and in the cross-cutting sub-horizontal breccia. As plagioclase content is low in the Green Street fragments, they also bear resemblance to mafic-rich sections of the Louis Lake intrusion on the east side of Louis Lake (Figure 5-8). With the exception of the presence of biotite in the Club Lake melanocratic intrusion, the Green Street fragments are also similar in mineralogy. Geochemically, Green Street fragments commonly group near or overlapping Louis Lake samples (Figures 5-30, 6-2, and 6-3).

The Phantom Beach mafic intrusive fragments (Figure 5-19 and 5-21) within the tonalite intrusion are near identical in mineralogy to the neighbouring hornblendite intrusion. Though the similar mineralogy suggests that the source of the fragments is the hornblendite intrusion, trace element data (Figure 6-1 and Figure 6-7) suggests that the mafic fragments are from a different intrusion, and possibly are not genetically related to the intrusions of this study.

6.4 Disaggregation, Incorporation and Assimilation

Magmas are contaminated by magma-mixing or by the disaggregation, incorporation and dissolution of foreign material such as mantle rocks, or country rock from the upper or lower crust. The assimilation of another rock or melt contaminates the original magma and contributes to the overall diversity of magmas and igneous rocks. Magmas can contain xenoliths or xenocrysts, which are clear evidence of disaggregation and incorporation, and incomplete or in-progress assimilation and contamination of the country rock by the magma. Depending on the temperature, pressure and composition of the foreign material and magma, xenoliths may or may not equilibrate and homogenously mix into the main magma (to varying degrees) (Best and Christiansen, 2001). Details affecting the degree of contamination and the geochemical modeling of such features are outside the scope of this thesis, however some obvious evidence of assimilation will be presented.

Disaggregation and assimilation may be accomplished by mechanical methods, such as mechanical abrasion during transport in a fluid system, or by corrosion, resorption, or assimilation by a hydrothermal fluid or magma (Laznicka, 1988). Melt at grain boundaries in a

xenolith can be generated through exposure to the required physical and chemical conditions to generate melt, or by heating the existing interstitial material between crystal grains. This is done through exposure to heat from various sources, the addition of volatiles, changes in pressure or temperature through decompression (Yoder, 1976), or shearing (Holtzman and Kohlstedt, 2007). A study by Dungan and Davidson (2004) concluded that grain-boundary melting of xenoliths in a magma lead to xenolith disaggregation and partial assimilation which consequently affected the initial bulk magma chemistry.

Examples of assimilation textures in hand sample and thin section for this study are shown in Figure 6-9 below. Partial melting of a volcanic fragment in the Green Street area can be seen in Image A, and possible disaggregation of a gabbro fragment in Image B. The leucocratic material (quartz and plagioclase) interstitial to the gabbro crystal grains (Images B – G), in some cases, has the appearance of separating the grains from others in the fragment. It may be that assimilation into the matrix is taking place through preferential melting of the interstitial material thereby releasing the amphibole crystals into the magma matrix. Though no obvious disaggregation textures clearly defined for the outcrop, image C from Louis Lake may also represent assimilation as the fragment boundary appears more diffuse in the lower part of the fragment as compared to the sharper upper boundary. It is possible that for fragments *appearing* to undergo disaggregation some or all of the leucocratic interstitial material is part of the original fragment composition. If this is the case, it may be that some fragments have undergone much less or no assimilation. If, in the case of the Boundary intrusions, the interstitial material is original to the rock, then preferential melting of the interstitial matrix of the fragment is conceivable as the composition is similar to the matrix and therefore could melt from the heat present in the magma. It is more likely that the plagioclase-quartz dominant intrusion could melt the quartz-plagioclase interstitial material rather than the higher temperature-forming minerals such as hornblendes and pyroxenes (+possible olivine). This process may also create floating xenocrysts in the matrix. Image F1 to F3 schematically demonstrates the disaggregation of a Boundary intrusion fragment by the process of possible grain boundary melting and melting of interstitial material. Image G shows a fragment from an unknown location (Mueller, 2013) that has not undergone any obvious assimilation into the magma matrix that can be identified with the naked eye. It is compared to Image H, which shows a fragment that has been identified

as frozen in the process of disaggregation and assimilation into the matrix. These textures are comparable to fragment textures in the Boundary intrusion breccias.

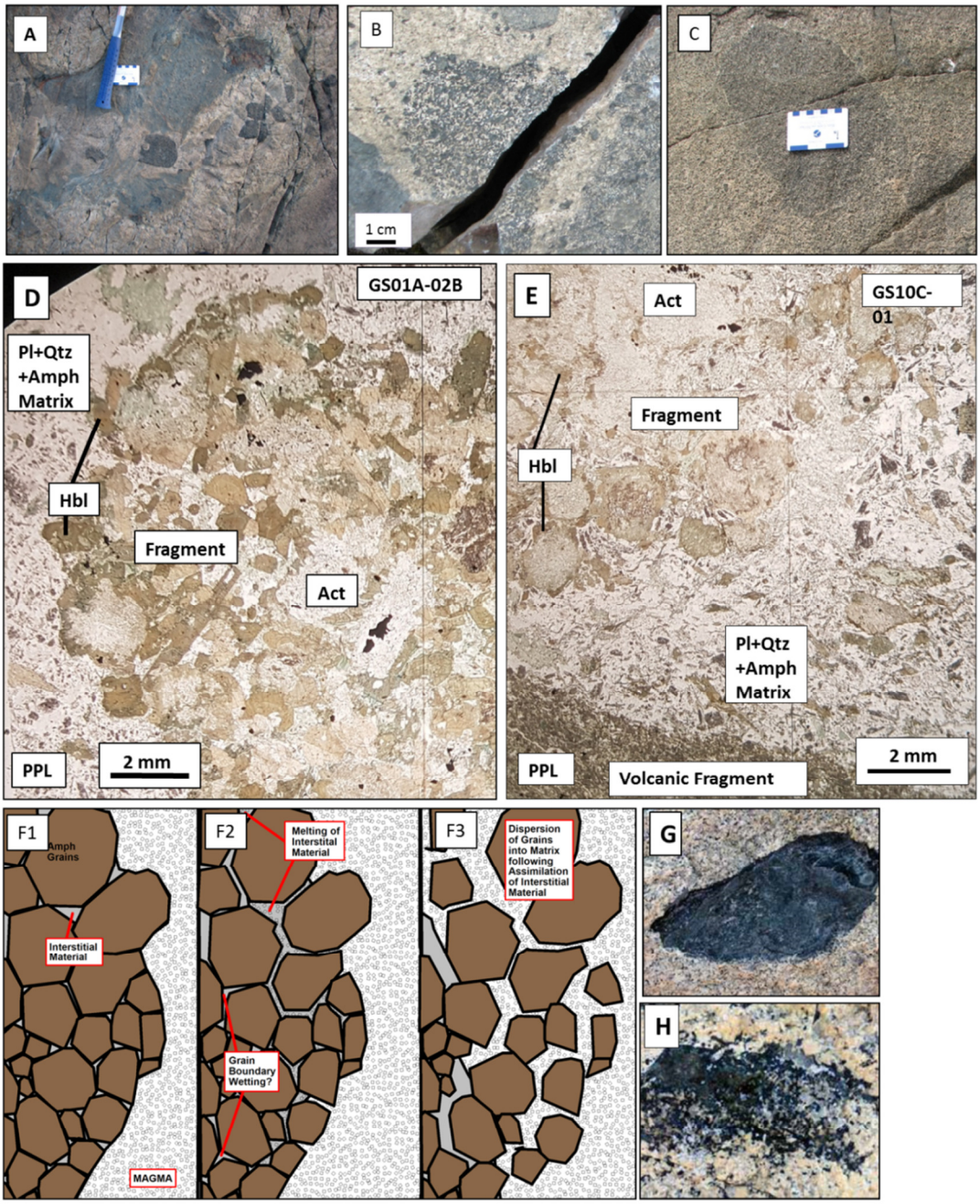

Figure 6-9. Examples of disaggregation and assimilation textures in outcrop and thin section. Examples from this study from Green Street in A) partial melting of volcanic fragments in the Boundary intrusion matrix (near GS02), and B) GS10C and C) east side of Louis Lake outcrop, both partial assimilation of gabbro fragments. Petrographic samples in plain light for Green Street for in Image D, TS_GS01A-02B shows intact fragment in sharp contact with Green Street matrix; Image E, TS_GS10C-01 for comparison, shows fragment with very irregular contact with Green Street matrix possibly undergoing disaggregation and assimilation into the matrix. Image F1-3 illustrates possible stages of disaggregation of fragment into magma matrix. G) Fragment with no assimilation, and H) partial assimilation. Examples H and I from Mueller, 2013.

The existence of multiple mineral populations can give insight to open-system behaviours such as incorporation and assimilation of xenoliths into magma (Streck, 2008). Streck (2008) noted examples from various studies which have used crystal size distribution (Marsh, 1988; Armienti, 2008), minerals of the same type but of different compositions (Boden, 1989), and minerals of the same composition with textural differences (Helz, 1987), to indicate whether open-system processes have resulted in the variety present in the magma of interest. All Boundary intrusions of this study consist of abundant euhedral, subhedral to rounded anhedral amphiboles in the matrix, and the difference in textures between the crystal grains may support inferences of their existence as xenocrysts or antecrysts in the intrusion matrix. The subhedral to euhedral amphiboles are dominantly hornblende (Figure 6-10A), while rounded anhedral grains may have an oxide core surrounded by dominant actinolite and rimmed by subhedral to euhedral grains of hornblende (Figure 6-10B). The actinolite grains resemble crystal grains seen in fragments (Figure 6-9D), and the presence of actinolite itself indicates the greenschist grade replacement of a former mineral, most likely pyroxene (and less likely olivine) in the case of the Boundary intrusions of this study. To further support the idea the rounded grains have not crystalized from the encompassing magma, a thin chilled margin next to a volcanic fragment shows the clear absence of rounded grains, and rare euhedral amphiboles (some may have altered to chlorite) (Figure 6-10C and D).

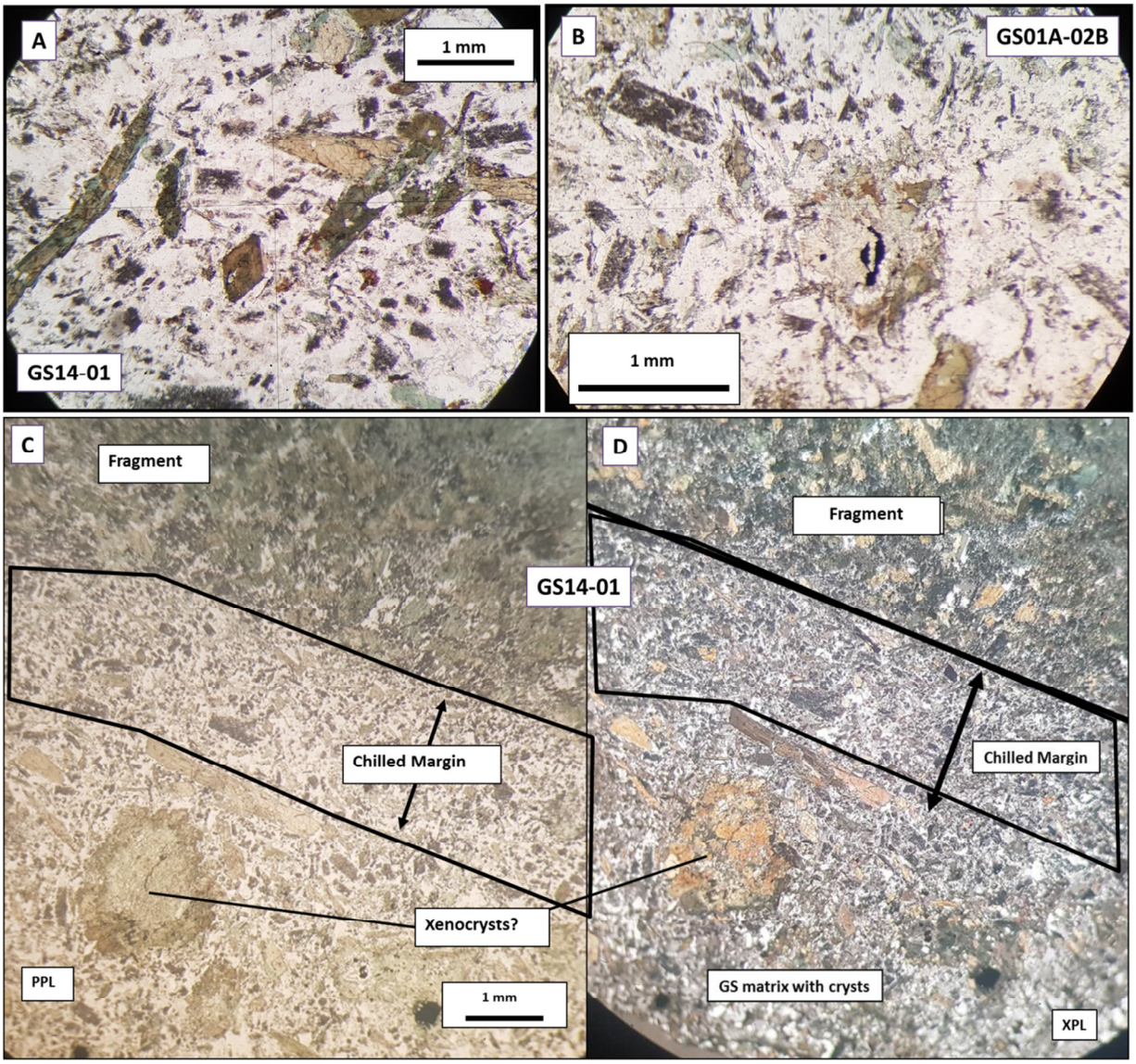

Figure 6-10. Examples of euhedral and anhedral amphiboles in the Boundary intrusion matrix. Image A from TS_GS14-01 shows euhedral hornblende in the plagioclase-quartz matrix. Image B is a rounded actinolite-hornblende crystal surrounded by a plagioclase-quartz matrix. Images C (PPL) and D (XPL) demonstrate the absence of rounded amphiboles within the area of a chilled margin.

6.5 Formation of the Boundary Intrusion Breccia Bodies

Features of an intrusion-hosted breccia body, including the fragments, matrix and relationships between the two components, can be used to help reconstruct the mechanisms of formation of the breccia and its history (Jébrak, 1997). Mechanisms of brecciation (fragmentation) have been summarized by Sillitoe (1985), Morin and Corriveau (1996) and Ferreira *et al*. (2014). Breccias of all types are common in the upper crustal levels where rocks are more brittle and therefore more susceptible to fracturing and faulting (Sibson, 1986), and therefore processes of fragmentation and incorporation are better constrained for these shallow crustal breccias. Fragmentation processes at any level include: remobilization of clasts in fault zones, magmatic-hydrothermal processes, degassing at mantle depth, magmatic stoping due to thermal stress, magma infill of pre-existing faults and fractures, and dyke propagation and emplacement (refer to section 3). This section will focus on the observable field aspects of the mapped Boundary intrusion breccias and offer suggestions for possibilities of fragmentation and breccia formation.

6.5.1 Fragmentation and Entrainment

Green Street

The Green Street matrix-supported breccia contains abundant mafic intrusive fragments and volcanic fragments, with the mafic intrusive fragments comprising approximately 20% of the total population (Figure 5-3). The northern section of the Green Street Boundary intrusion dyke is densely populated with up to 200 fragments per square meter. Fragments are typically less than 15 cm in diameter, but can be larger, infrequently up to 1.8 m in diameter. The arrangement of fragments is chaotic (chaotic breccia), except for *in-situ* volcanic fragments clearly delaminated from the country rock and close to its original position (mosaic or jigsaw breccia) (Figure 5-3B and F). Some volcanic fragments are captured in the magma close to the wallrock from which they were fractured, and are therefore clearly illustrate hydraulic fracturing and delamination at the deposition level. Hydraulic fracturing creates fractures and is also assisted by pre-existing fractures where a set of three intersecting planes of discontinuity create an aggregate to be incorporated into the magma (Laznicka, 1988). Figure 6-11 is a schematic

model of brecciation processes relevant to the Boundary intrusions and shows how hydraulic fracturing (B, C and D) and delamination (C and E), such as that seen in the Green Street area, can occur.

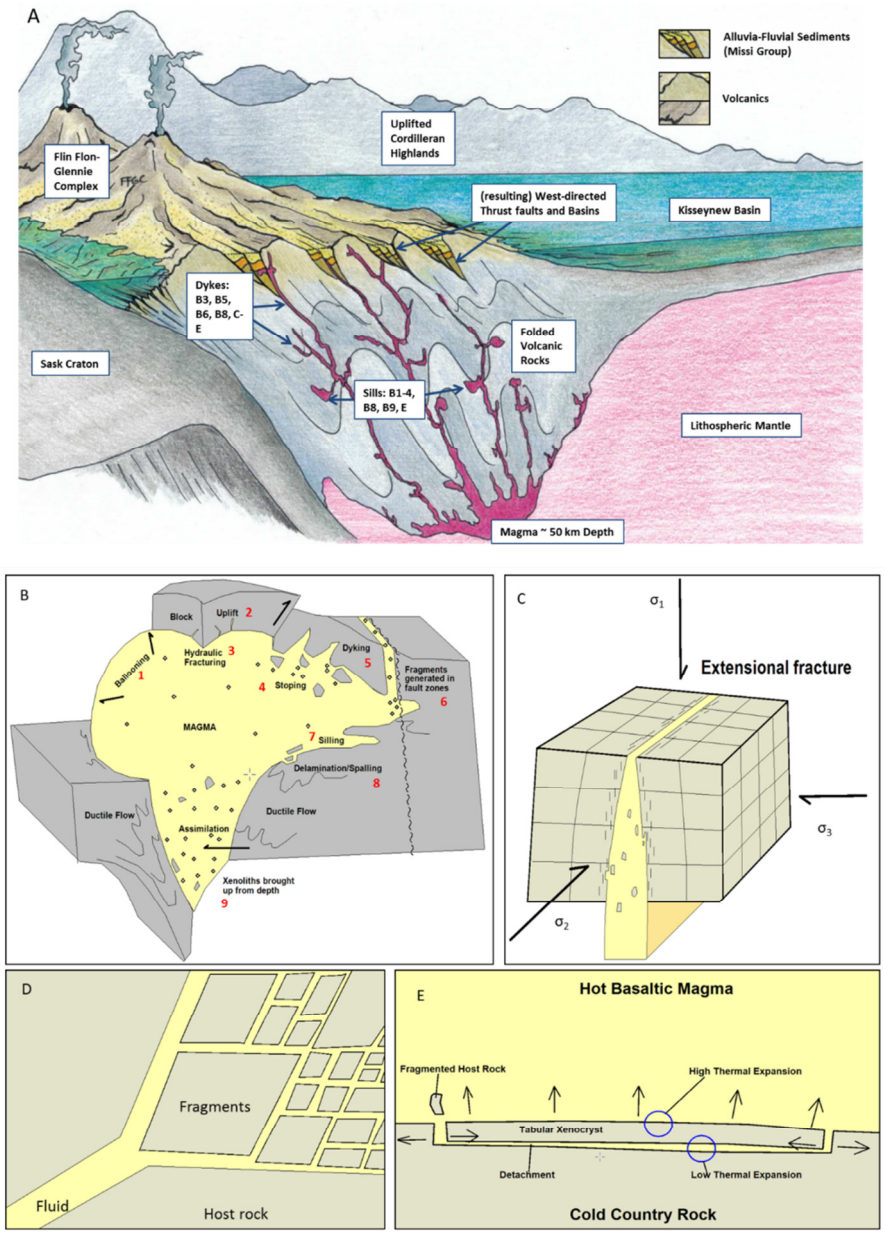

Figure 6-11. Schematic model of processes associated with emplacement of intrusion-related breccias in a volcanic environment applicable to the formation of the Boundary intrusions. A) Emplacement of the Boundary intrusions. Note that the diagram is not to scale and not meant to represent exact locations of Boundary intrusion occurrence relative to volcano structure. Scale of features are exaggerated or compressed for visual purposes. B) Methods of fragmentation/brecciation associated with general magma emplacement applicable to a variety of scales. Redrawn and modified from Best and Christiansen (2001) and Laznicka (1988). C) Fragmentation (delamination and spalling) during crack-tip propagation of a dyke. Redrawn from Best and Christiansen (2001) and modified after Morin and Corriveau (1996). D) Brecciation during tectonic comminution creating mosaic breccia. Fragments rounding can occur with continued fault movement. Redrawn from Jébrak (1997). E) Thermal delamination of tabular fragment. Redrawn from Motoki *et al*. (2009).

The abundance and types of xenoliths contained in the Green Street breccia is an indication that the host magma was efficient in facilitating fragmentation and/or incorporating existing fragments, as suggested by Morin and Corriveau (1996) in their study of intrusion breccias in the Grenville Province. The difference in the abundance of gabbro to volcanic rock fragments in the breccia, though, could indicate the progressive reduced ability of the magma to fragment, entrain and carry xenoliths during ascent (Ferreira *et al.*, 2014). However, considering the presence of gabbro fragments up to 1.8 m in diameter, this suggests that they were easily extracted by the magma at whatever depth they existed and carried to the exposed depth at a rate which allows large fragment transport. The smaller population of gabbro fragments may therefore be only an indication that the magma encountered more available loose volcanic rock during its travel. Mafic to ultramafic intrusions exist around the sample study areas of this study and it is likely the fragments sources are not far from the emplacement depth.

Most dykes at any level in the crust are probably created as magma rapidly stresses and fractures the rock (Shaw, 1980) and fills the propagating crack as it advances (crack-tip propagation, hydraulic fracturing) (Best and Christiansen, 2001). The Green Street dyke itself, as well as the smaller dykes off the main intrusion, and the presence of mosaic breccias (Figure 5-2 and 5-3A, B and F) indicate hydraulic fracturing was a major process in dyke propagation at that depth, consequently accounting for most, if not all country rock fragmentation. Intense fracturing, delamination and spalling (Figure 6-11C and E) of the country rock during ascent of the magma as part of the hydraulic process could explain the abundance of xenoliths in an intrusion breccia (Morin and Corriveau, 1996). Degassing from the exsolution of volatiles during magma ascent is another possibility as a fragmentation process. This is a process attributed to the abundant xenoliths present in kimberlite deposits (Ferreira *et al.*, 2014) (See Figure 3-4F). The Boundary intrusions do not contain the high content of volatiles that most kimberlite or similar magmas typically contain (greater than 5% LOI (Shee *et al.*, 1989)), but they are considered hydrous, as indicated largely by the amphibole content. Increased volatile content, exsolution and expansion of bubbles decrease the density of magma, thus adding to its effective buoyancy and ability to ascend faster (Best and Christiansen, 2001). Stress on the country rock is created through rapid ascent associated with the exsolution of exsolved volatiles (e.g., Ferreira *et al.*, 2014). Or the

degassing of volatiles itself (drilling by a gas-charged magma) can add pressure to the surrounding country rock, creating fractures and consequently fragments which can then be entrained in the magma (Best and Christiansen, 2001).

The chaotic texture, or lack of clustering of fragments of a similar rock type and lack of alignment of (larger) xenoliths of the breccia may also suggest the flow of the magma was turbulent or at least indicate a lack of laminar flow. It should be noted that in order to properly assess the likeliness of turbulent flow or laminar flow, a thorough mapping of the breccias would be carried out with focus on systematically recording quantitative and qualitative fragment features. This would include noting the alignment of fragments, placement of fragments of particular sizes and rocktypes, and a fragment-size distribution analysis. The mosaic breccias of Green Street, as well as breccias containing rounded and possibly disaggregated gabbro fragments, can be considered evidence to dismiss tectonic remobilization of fragments as a single method of fragmentation (Bryant, 1968). However, as noted by Syme (1975), the Boundary intrusions lie within what appears to be the hinge of a fold and their location likely controlled by the fold structures. Additionally, fractures within the volcanic country rock associated with the folding could be a source of fragments the ascending Green Street Boundary intrusion.

Louis Lake

The Louis Lake breccia is also matrix-supported and chaotic containing mafic intrusive fragments and volcanic fragments, with mafic intrusive fragments comprising between 15 - 50% of the total population. Fragment size ranges from 15 cm to 2 m (not including the stoped blocks), but local clusters of smaller fragments do occur (Figure 5-9A and A1). The Louis Lake intrusion breccia differs in a few significant observable features from the Green Street breccia: 1) it contains large (stoped?) blocks of earlier crystallized Boundary intrusions, 2) it does not contain the abundance of smaller fragments as seen in the Green Street breccia, and 3) no contacts with the country rock are exposed, and therefore no evidence of crack-tip propagation or hydraulic fracturing exists, or evidence to confirm a sill structure. However, the Louis Lake breccia does share similarities to the Green Street intrusion in terms of its hydrous nature and this suggests dyking via the crack-tip propagation method cannot be ruled out throughout some part

of the ascent history. In fact, LOI values are quite similar (all between 1.6 – 3.7% LOI), and the proportion of amphiboles in the Louis Lake host intrusion is notably 20 – 30% more than Green Street. Also, the abundance, variety and random orientation of fragments is similar to the Green Street breccia suggesting the magma was as efficient in incorporating xenoliths at various depths and magma flow was turbulent.

The presence of possible stoped blocks in the Louis Lake Breccia is an indication that magma inflation occurred in dykes and produced a variety of acting local principle stresses (Parsons *et al.*, 1992) which allowed the emplacement of magma in horizontal sills, or allowed vertical dykes to intersect a stronger barrier causing the fluid to accumulate and balloon (Best and Christiansen, 2001) (Figure 6-11B). Blocks are formed as the magma applies thermal and hydraulic stress to the chamber walls and roof, thereby fracturing the rock and creating blocks to fall into the magma pool (Philpotts, 1990; Best, 2003). Ferreira *et al*. (2014) points out that in order for stoping to be an effective process, the country rock must be more dense than the intruding magma, and also be capable of being fractured (i.e., brittle).

The sub-horizontal breccia that intrudes the Louis Lake intrusion breccia is largely clast-supported (Figures 5-9B and B1). The same reasoning as the Green Street and Louis Lake Breccias can apply to theorize the fragmentation and entrainment processes. Both volcanic and mafic intrusive fragments are present in a plagioclase and amphibole-rich matrix, and this matrix could be a later younger (more fractionated) version of the Louis Lake magma which has sampled the same type of country rock during its ascent, though the volume of magma is much less and fragment sizes are much smaller. The intrusion of the clast-supported breccia into the Louis lake breccia is sharp, and though no termination point is observable, it is reasonable to attribute the emplacement to hydraulic fracturing during dyke propagation.

Phantom Beach

The Phantom Beach Breccia contains both clast-supported and matrix-supported chaotic breccias within the same intrusion, and fragments comprise volcanic and mafic intrusive fragments. Depending on the location within the intrusion, mafic intrusive fragments make up

approximately 50 – 100% of the population. The abundance, variety and chaotic organization of fragments is an indication, as seen with Green Street and Louis Lake, that the host magma had efficiently sampled the country rock during its ascent and the magma flow was turbulent in nature. It is unclear from the trace element data if the Phantom Beach mafic intrusive fragments could be from a similar magma source as the hornblendite, to which the Phantom Beach leucocratic intrusion intrudes. Though this intrusion was not mapped in detail, the mineralogical and geochemical data (the presence of hydrous minerals and similar values for LOI) could suggest that similar processes to Green Street and Louis Lake (crack-tip dyke propagation, delamination, spalling, and exsolution of volatiles) were involved in the process of fragmentation and advancement of the magma as a dyke.

6.5.2 Fragment Transport

Magma-transported fragments likely undergo rounding and size reduction due to physical attrition, assimilation and resorption into the melt (Laznicka, 1988); and smaller and more assimilated fragments are possibly a consequence of size reduction during more extended travel than larger, more cohesive fragments (Morin and Corriveau, 1996). However, it should be noted that the presence and condition (shape, dimensions, state of assimilation…etc.) of the xenoliths due to length of time spent traveling or intensity of turbulence within an intrusion breccia cannot be used to consistently assess the textural maturity or overall breccia genesis. This is due to several other factors (temperature and composition) and processes (milling in a vent or conduit, accretion of crystals, or resorption, as a few examples) which affect the ability of the magma to corrode, disaggregate, or round fragments during incorporation and ascent. Fragments therefore may not show a gradation of shape and size features which indicate relative time spent in transport (Laznicka, 1988).

Fragment shapes and sizes for volcanic fragments and mafic intrusive fragments are similar for all intrusions. All fragment types in all intrusion breccias range up to several tens of centimeters in diameter with occasional 1.8 – 2.0 m diameter fragments. Mafic intrusive fragments tend to be subrounded to well rounded, while volcanic fragments range from subrounded to angular. These fragment shape differences may imply that that distance and time travelled from the

fragment source increases the roundness of a fragment, and therefore the gabbroic fragments are more texturally mature. Relatively greater time and distance travelled for mafic intrusive fragments in the magma could also aid in the disaggregation and assimilation of those fragments. Disaggregated gabbro fragments could represent longer travel times or more distally fragmented sources than others of the same composition that are intact. More time in the magma chamber may have allowed enough heat transfer to effectively melt around and separate mineral grains at their shared boundaries, resulting in assimilation textures as those seen in the Green Street breccia (Figure 6-9).

The above interpretations are applied in a general nature for the all intrusions of this study. However, as mentioned, when considering other intrusion and fragment specific factors, such as temperature and composition, time and distance are not the only contributing properties on fragment shape and size. Temperatures can vary within an intrusive body due to more rapid cooling in its outer edges as a result of heat loss to the country rocks, and therefore the center of the intrusion may be hotter and retain more of its ability to assimilate fragments over the course of its ascent. However, the Boundary intrusions are relatively small (tens of meters for the intrusions of this study) and therefore temperature differences within the dyke and sill may not have been enough to cause differences in assimilation textures. A cooled margin (or chilled margin) at the intrusion-wallrock contact of a dyke, however, can prevent the further fragmentation and incorporation of country rock fragments into an intrusion; and chilled margins around fragments can inhibit the magma's ability to melt and assimilate the fragment. Volcanic fragments with chilled margins therefore retain their angular shape and original size after separation from the wallrock. Thin chilled margins can be seen in thin section adjacent to volcanic fragments in the Green Street intrusion and therefore could be a (partial) controlling factor on shape and size of these fragments. The composition of fragments in relation to the host intrusion can also affect the intrusion's ability to melt and assimilate. If fragments contain minerals which require higher temperatures to reach their liquidus than those of the intrusion, the fragments will not melt (Best and Christiansen, 2001). The Phantom Beach intrusion has a higher quartz content (and lower plagioclase content) than the Green Street or Louis Lake intrusion, and this may significantly affect the intrusion's capability to disaggregate the mafic

intrusive fragments. No obvious assimilation textures were noted in the field in the Phantom Beach intrusion.

6.5.3 Intrusion Breccia Rate of Ascent

Magmas containing xenoliths are indicated as having a high transport velocity through the crust in order to bring fragments to the point of deposition in the solidified magma (Sparks *et al*., 1977; Caricchi *et al*., 2007; Ferreira *et al.*, 2014). Ferreira *et al*. (2014) points out that most authors attribute a high ascent velocity to a magma which contains xenoliths, typically between 10 - 1000 meters per second. In order for magma to ascend, it must be buoyant. A sufficient difference in magma density and country rock density must exist in order for buoyancy to persist, and the ability to ascend buoyantly depends on the relative amount of resistive forces that is dictated by these interdependent factors: viscosity, temperature, pressure and the composition of both mediums. Buoyant (or gravity-driven) ascent can be stopped as the magma loses heat to the country rock, increases in viscosity, or has encountered resistive forces counteracting the buoyancy force. In the case where resistive forces are enough to stall the ascent, sills may form or dykes may cease and crystallize. Alternatively, magma can reach the surface and erupt (Best and Christiansen, 2001).

Viscosity, in particular, is an important physical property of a magma which largely controls the magma transport through the lithosphere, as well as some aspects of chemical evolution (Clemens and Petford, 1999). Viscosity can be increased by the presence of a solid fraction in the melt, whether it is crystals growing in the matrix, or xenoliths encompassed enroute to the melt's final deposition. A melt containing a critical portion of solids (crystals, suspended xenoliths…etc.) promotes an increase in the apparent magma viscosity and yield strength. As a result of increased viscosity and yield strength, the intrusion breccia may behave rheologically like a Bingham body (Ferreira *et al.*, 2014). In the case of a Bingham fluid, a threshold exists by which shear stress does not affect the fluid, as opposed to a Newtonian Fluid where strain rate and shear stress are linearly proportional. Calculations to approximate the settling velocity of a solid in a magma are typically used to estimate a minimum ascent rate for a rising magma body (Morin and Corriveau, 1996). Stoke's Law can be used to calculate the minimum ascent velocity

for a Newtonian fluid, however it is more appropriate to consider the intrusion breccia as a Bingham fluid due to the presence of suspended fragments using calculations by Shaw (1969). This method of ascent estimation will be applied to this study following examples completed by Ferreira *et al.* (2014) and Morin and Corriveau (1996).

Settling velocity (V) of a smooth isolated sphere in a Newtonian fluid, moving without any outside friction, is given by Stoke's Law:

$$V = 2r^2g\Delta p/90u, \quad (6.1)$$

where r is the fragment radius (cm), g is the acceleration due to gravity (981 cm/s^2), Δp is the difference in density between the xenolith and the magma (g/cm^3), and *u* is the viscosity of the magma (g/cm/s, or Pascal second (Pa s)). Assumptions are made in order to simplify the calculation of magma ascent: the fragment is considered a perfect sphere with homogenous density, and there is no other forces others than those considered in the calculation acting upon the fragment and magma (Best and Christiansen, 2001). Density estimations for Boundary intrusions of this study are taken from ranges provided by (in house, see section 4.0, *Methodology*) density tests on hand samples for the Boundary intrusions and from literature (Best and Christiansen, 2001). Viscosity values are taken from other similar rock compositions' estimates provided by various viscosity studies.

Mafic intrusive fragments within the Boundary intrusions are labelled as gabbro, melagabbro and hornblende-rich or hornblendite. According to a diagram illustrated in Best and Christiansen (2001), which provides a range of densities for common magma types (redrawn from Murase and McBirney, 1973), densities for the mafic intrusive fragment magma equivalent can range from 3.0 – 3.5 g/cm^3. The breccia matrix consists of varying amounts of plagioclase, quartz and mafics and equivalent magma density values could range between 2.6 -2.9 g/cm^3 (or more). Basaltic magma occupies a density range from approximately 2.7 – 3.1 g/cm^3. Measurements of density on Boundary intrusion hand samples fall within these ranges and reveal the following values: 3.3 – 3.4 g/cm^3 for mafic intrusive fragments (average 3.35 g/cm^3), ~2.5 g/cm^3 for Green Street intrusion, and 2.8 – 2.9 g/cm^3 (2.85 g/cm^3 average) for the Louis Lake intrusion. The

average fragment diameter for Green Street is 15 cm (r = 7.5 cm), 30 cm (r = 15 cm) for the Louis Lake breccia, and 10 cm (r = 5 cm) for the Louis Lake clast-supported breccia. The maximum fragment diameter present in the Green Street and Louis Lake intrusion breccia is 1.8 – 2.0 meters, and so the value 2.0 m (r = 1.0 m) will be used in both Green Street and Louis Lake calculations.

The intrusion breccia is most likely to have acted as a Bingham fluid and therefore a solid fraction must be considered for the intrusion breccia. Using the solid fraction, the recalculated velocity (V_f) considering a solid fraction is:

$$V_f = V(1-F)^{4.65}, \quad (6.2)$$

where V is from equation 6.1. In estimating the solid fraction, Morin and Corriveau (1996) assumed that all xenoliths have been reduced in size to a limited extent from initial incorporation to emplacement. The current volume occupied by the ultramafic xenoliths (interpreted to be from deeper depths) was used to represent the solid fraction during the early stages of ascent. However, it should be noted that from the magma chamber to the current location, fragment content (by volume) can range from 0% to greater than volume content visible today, the variation depending on the settling of fragments after emplacement and before solidification. Morin and Corriveau (1996) measured the portion of ultramafic xenoliths to be 15% of the total breccia volume of the exposed dyke of study and therefore used this number (F = 0.15) to represent the maximum solid fraction of the intrusion. Other xenoliths were not included in the volume measurement as they were not derived from the same source and therefore not present during initial ascent. The same approach will be applied in this study, though it is possible the mafic intrusive fragments and volcanic fragments have been incorporated at similar depths. The mafic intrusive fragments of the Green Street breccia comprise 20% of the fragment population, and fragment size for both volcanic and mafic intrusive fragments are similar (Figure 5-3A and E). Within the breccia, the fragment surface area is approximately 60%, therefore mafic intrusive content (by area) is estimated to be 12% (F = 0.12). For the Louis Lake breccia, the estimated mafic intrusive content ranges from 0 – 49%, the surface area of the fragments is estimated to range from 0 – 49%, and therefore the solid fraction is estimated to be 16% (F =

0.16). The solid fraction estimated for the clast-supported breccia is 44% (F = 0.44), using the values 80% and 55% for total fragment surface area and the mafic intrusive portion, respectively.

Ascent velocities for the Green Street and Louis Lake Boundary intrusion breccias vary widely depending on the value for viscosity used (Table 6-1). The geochemistry and mineralogy of the Green Street intrusion indicates that the magma was similar to andesite-trachyandesite-trachyte, and the Louis Lake intrusion within the andesite-basalt to andesite field (Figure 5-28). The viscosities for similar rock types at intrusion temperatures could range from approximately 3,550,000 Pa s to as low as 2000 Pa s, or lower, depending on the magma temperature, which vary from 700 degrees Celsius (equilibrium temperature of Boundary intrusions as determined by O'Hanley and Kyser (1994)) to approximately 1100 degrees Celsius. Table 6-1 shows the ascent values obtained for each Green Street and Louis Lake using the range of magma viscosity obtained from other examples in literature, including values lower much than 2000 Pa s for the sake of comparison.

The viscosity values which most likely can be applied to the Boundary intrusion samples range from ~2000.0 Pa to ~3,550,000 Pa s (Table 6-1). Resulting ascent velocities for a 15 cm diameter fragment in the Green Street intrusion range from 0.01 m/hr to 10.35 m/hr, and between 1.04 m/hr to 1.84 km/hr for a 200 cm fragment. Green Street magmas are slightly more alkaline (Figure 5-28) and therefore can conceivably have lower viscosities for similar temperatures resulting in higher ascent rates than the range indicated. Louis Lake ascent rates for a 30 cm and 200 cm diameter fragment range from 0.01 – 19.62 m/hr and 0.49 m/hr to 872.16 m/hr, respectively. The clast-supported breccia (CSB) is estimated to range from 1.63 m/yr to 0.33 m/hr for a fragment of 10 cm diameter. Parameters and calculation results are shown in Tables B1 – B4 of Appendix B. Phantom Beach ascent rates have not been estimated as this area has not been mapped in detail and therefore required information such as fragment size and percent gabbro fragments is unknown. Xenolith-rich silicate magmas are estimated to have a range of 1.1 km/hr (hornblende andesites, Blatter *et al*., 1998) to 10 km/yr (for MORB and plume-derived basalts, McKenzie, 2000), and the xenolith-bearing Deccan Alkali basalts from 5.9 – 30.2 km/hr (Kokandakar *et al*., 2018). Ascent rates proposed for kimberlite magmas are as high as 144 km/hr (Peslier and Luhr, 2006; Peslier *et al*., 2008), and it is unlikely that the ascent velocities

for the Boundary intrusions themselves reach similar speeds. The values calculated for this study are within the ranges proposed by both Kokandakar *et al*. (2018) and Blatter *et al*. (1998).

Similar studies carried out by Ferreira *et al*. (2014) and Morin and Corriveau (1996) show results similar to the rocks of this study. Ferreira *et al*. (2014) estimated the minimum ascent rate for a set of syenite dykes in the Borborema Province in northeastern Brazil. Using the same method applied here, minimum ascent velocity ranged from 72 m/hr to 1.08 km/hr for a 30 cm long diorite xenolith and viscosity values of 680 – 4600 Pa s for temperatures from 900 – 1000 degrees Celsius. The dykes contained a large amount of ultramafic and mafic xenoliths distributed in a chaotic fashion, similar to Green Street (Figure 5-3A and E). The dykes of this study, however, are much smaller, only up to 1.5 m in width, whereas the Green Street dyke is approximately 20 m at its widest. The presence of the dykes and their breccias was postulated a result of high ascent rates due to initial low viscosity and an increased ability to fracture the conduit. Morin and Corriveau (1996) showed similar (to this study) initial minimum ascent velocities (1.8 km/hr) for a xenolith laden Proterozoic minette dyke in the Grenville Province, Québec, though breccia patterns indicate laminar flow during emplacement as opposed to turbulent flow. The minette dyke is up to 1.7 m in width and xenolith-rich, comprising up to 50% of the total dyke volume. The fragment population is polymictic, containing approximately 60% of mafic and ultramafic composition, and the solid fraction is estimated at 15%. Viscosity (Newtonian) and temperature were estimated to be 40 Pa s at 1050 degrees Celsius. Ascent velocities during emplacement were estimated using a higher viscosity value (10^3 Pa s) due to increased solid fraction in the magma, which resulted in preferential xenolith distribution along the center of the dyke.

Table 6-1. Ascent velocity at various temperatures and viscosities for the Boundary intrusions of this study.

Parameters obtained from literature		Green Street (~65% SiO_2)		Louis Lake (~57% SiO_2)		Clast-supported breccia (~57% SiO_2)
Comments	Viscosity (g/cms^{-1})	Ascent Velocity (V_f) for 15 cm fragment (m/hr)	Ascent Velocity (V_f) for 200 cm fragment (km/hr)	Ascent Velocity (V_f) for 30 cm fragment (m/hr)	Ascent Velocity (V_f) for 200 cm fragment (km/hr)	Ascent Velocity (V_f) for 10 cm fragment (m/hr)
Viscosity values for alkaline magmas at 1000°C; ~46% SiO_2[1]	803.53	25.77	4.58	48.84	2.17	0.82
Viscosity values for Fuji basalt; 1230°C; ~53% SiO_2[2]	52	398.24	70.80	754.76	33.55	12.73
Viscosity values for andesite (Mount Hood, Washington); 1200°C; ~60% SiO_2[4]	1,000	20.71	3.68	39.25	1.74	0.66
Viscosity values for Fuji basalt with 23% crystallinity; 1130°C; ~53% SiO_2[2]	1,950	10.62	1.89	20.13	0.9	0.34
Viscosity values for andesite (Mount Hood, Washington); 1150-1200°C; ~60% SiO_2[4]	100,000	0.21	0.04	0.39	0.02	0.01
Viscosity values for tonalite at 950°C; ~65% SiO_2[4]; range from Log 3.19 – 6.55 Pa s[5]	1,548.82 3,548,133.89	13.37 0.01	2.38 1.04 m/hr	25.35 0.01	1.1 0.49 m/hr	0.43 1.63/yr

1, Kokandakar et al., 2018; 2, Sato, 2005; 3, Ryan and Blevins, 1987 (1 Bar/10^5 Pascals); 4, Murase and McBirney, 1973; 5, Clemens and Petford, 1999.

7.0 SUMMARY

The Boundary intrusions of Creighton, Saskatchewan and Flin Flon, Manitoba are a set of felsic to ultramafic breccia-laden intrusions in the upper crust emplaced at approximately 1842 Ma during the Trans-Hudson Orogeny. This study aimed to add new data and insights to the Boundary intrusions by considering the breccia components of the intrusions.

Trace element geochemistry has revealed patterns which bare resemblances to the transitional varieties described by Pearce (1982) where magma sources were postulated to have a complex and mixed parentage. Magma sources may have underwent magma mixing, several depletion and enrichment events, as well as being affected by crustal assimilation during magma ascent. This agrees with previous authors (O'Hanley *et al*., 1993; O'Hanley and Kyser, 1994) which have described the Boundary intrusions as complex and showed through the use of isotope and trace element data that the intrusions have a mixed parentage of mixed depleted mantle with contamination from rocks of the Flin Flon Belt. Based on normalized Zr/TiO_2 ratios and trace element patterns, fractionation within sample suites including breccia fragments, is likely for the Green Street and possibly the Louis Lake areas, but not clearly supported between fragments and matrix of the Phantom Beach area. More sampling would be required to demonstrate a clear relationship through fractionation, if one exists.

Ascent rates of an intrusion, or the settling velocity of a sphere in that intrusion, have been calculated for the Green Street and Louis Lake areas. Considering the magmas as Bingham fluids, the range of rate of ascent for Green Street varies from 0.01 – 10.35 m/hr for a magma carrying a 15 cm diameter fragment, and 1.04 m/hr – 1.84 km/hr for a 200 cm diameter fragment. The Louis Lake intrusion ascent velocities range from 0.01 – 19.62 m/hr and 0.49 m/hr to 872.16 m/hr for a 30 cm and 200 cm diameter fragment, respectively. The clast-supported breccia (CSB) is estimated to range from 1.63 m/yr to 0.33 m/hr for a fragment of 10 cm diameter.

The breccia morphology offers insight into the fragmentation processes in operation to create the breccia. Chaotic breccias of the Green Street, Louis Lake and Phantom Beach sample sites

indicate that the host magma had efficiently sampled the country rock during part of the ascent and the magma flow was possibly turbulent in nature. Hydraulic or mosaic breccias are seen at the margins of intrusions where contacts can be observed (Green Street) or where possible stoped blocks exist (Louis Lake), evidence of the magma advancing and fragmenting through dyke crack-tip propagation. Other relevant fragmentation processes include spalling, mechanical delamination, thermal delamination, stoping, or increased pressure or ascent rate from the release of volatiles during ascent. Fragment roundness and angularity of volcanic and gabbro fragments, and degree of assimilation of (in particular) the gabbro fragments into the magma matrix suggests that gabbro fragments may have traveled longer distances within the magma or have been incorporated into the magma for longer periods of time.

8.0 RECOMMENDATIONS FOR FUTURE STUDY

There still remain a number of questions concerning the petrogenesis of the Boundary intrusions. While this list of suggested future work is not comprehensive, it will address some of the main questions that could direct the future studies on the Boundary intrusions.

- Is there any genetic relationship to other known volcanic or intrusive suites in the Flin Flon-Glennie Complex? Similarities are also noted between major and trace element patterns between the metavolcanics of Wekusko Lake, Manitoba and the Boundary intrusions by O'Hanley and Kyser (1994), and these authors stated that the similar ages, petrology and geochemistry permitted to two to be genetically related. It is suggested that more detailed studies be carried out which focus on relating the Boundary intrusions to other volcanic/intrusive rocks within a reasonable geological timeframe (for the relation to be possible). This can be done comparing isotope systematics coupled with geochemical major and trace element patterns. Stern *et al*. (1995) presented geochemical and isotope data for arc volcanism dated from 1.90 – 1.86 Ga in the Flin Flon Belt. While a comparison is made in this study (Figure 6-4), a more in depth analysis of the similarities and differences between rocks of this period could be included in the pursuit of other arc rocks genetically related to the Boundary intrusions, specifically younger rocks of that period from the Schist Lake suite or the Vick Lake tuff.
- Are there any past or currently active island arc examples to which the Boundary intrusions can be compared? O'Hanley and Kyser (1994) had noted similar features, such as intrusion shape, composition and compositional zoning, between the Boundary intrusions and the Alaskan-type ultramafic intrusions (e.g., Irvine, 1974; Saleeby, 1992) and Appinite intrusions of Scotland (Hall, 1967; Platten, 1991) and in northern Michigan (Wilkin and Bornhorst, 1993). A more in-depth search for intrusions and volcanic rocks that show similarities (geochemically, petrographically, and mineralogically) may help better explain the petrogenesis of the Boundary intrusions.

- Are all Boundary intrusions and the mafic intrusive fragments included in their breccias from the same mantle source or even cogenetic? From what depth are the fragments sourced? What level of contamination has the Boundary intrusions encountered? What can the xenoliths and antecrysts tell us about the AFC processes which have operated on the Boundary intrusions? Geochemical studies (ICP-MS, EPMA) combined with sampling methods such as electron microprobe analysis may offer insight into the AFC processes in operation which helped form the Boundary intrusions.
- This study offered a qualitative overview and the most detailed mapping to date of two examples of the Boundary intrusion breccias. In order to facilitate studies on the AFC processes involved in the petrogenesis of the intrusions, more detailed and quantitative breccias studies are recommended. This could be done on a larger scale which would include all Boundary intrusion breccias and allow for comparisons between sample sites. While this study did attempt to qualify the ascent rate for the Green Street and Louis Lake Boundary intrusion breccias, the values for rock density and viscosity were obtained from literature. It is suggested that density and viscosity measurements be obtained from lab analysis and methods such as those used by Ferreira *et al*. (2014). Ferreira *et al*. (2014) calculated magma viscosity following the method outlined by Giordano *et al*. (2008) which used chemical analysis for the rocks of interest. Examples of quantitative characterization of (hydrothermal) breccias have been carried out by Cas *et al*. (2011), where dimensions, shape and orientation of breccia clasts have been measured and plotted in order to best classify processes that may result in definable characteristics (for example, the amount of fragment rotation in a jigsaw breccia vs an autobreccia). Studies by Jébrak (1997) have also used particle size distribution of fragments within a breccia to determine the fractal dimension (see Blenkinsop, 1991 for more details), for which high values relate to energetic processes of fragmentation.

9.0 REFERENCES

AGI, 2005. Glossary of Geology, 5th Edition. American Geological Institute. Alexandria, Virgina: United Book Press, 2005.

Ansdell, K.M., 2005. Tectonic evolution of the Manitoba-Saskatchewan segment of the Paleoproterozoic Trans-Hudson Orogen, Canada. Canadian Journal of Earth Sciences. Vol. 42, 741-759.

Ansdell, K.M. and Kyser, K.T., 1991. Plutonism, deformation, and metamorphism in the Proterozoic Flin Flon greenstone belt, Canada: Limits on timing provided by the single-zircon Pb-evaporation technique. Geology, 1991, Vol. 19 (5), 518–521.

Ansdell, K.M., Lucas, S.B., Connors, K., Stern, R.A., 1995. Kisseynew metasedimentary gneiss belt, Trans-Hudson orogen (Canada): Back-arc origin and collisional inversion. Geology, November 1995. Vol. 23(11), 1039-1043.

Armienti, P., 2008. Decryption of igneous rock textures: crystal size distribution tools. Rev Mineral Geochem. Vol 69, 623-649.

Ashton, K.E., 1999. A proposed lithotectonic domainal re-classification of the southeastern Reindeer Zone in Saskatchewan. In Summary of Investigations 1999. Vol. 1. Saskatchewan Geological Survey, Saskatchewan Energy and Mines, Miscellaneous Report 99-4, 92-100.

Ashton, K.E., Lewry, J.F., Heaman, L.M., Hartlaub, R.P., Stauffer, M.R., and Tran, H.T., 2005. The Pelican Thrust Zone: basal detachment between the Archean Sask Craton and Paleoproterozoic Flin Flon – Glennie Complex, western Trans-Hudson Orogen. Canadian Journal of Earth Sciences. Vol. 42, 685–706.

Bailes, A.H. and Galley, A.G., 1999. Evolution of the Paleo-proterozoic Snow Lake arc assemblage and geodynamic setting for associated volcanic-hosted massive sulphide deposits, Flin Flon Belt, Manitoba, Canada. Canadian Journal of Earth Sciences, Vol. 36, 1789–1805.

Bailes, A.H. and Syme, E.C., 1989. Geology of the Flin Flon–White Lake area. Manitoba Energy and Mines, Geological Services, Geological Report GR87-1, 313 p.

Bailey, K.A., 2006. Emplacement, petrogenesis and volcanic reconstruction of the intrusive and extrusive Myo rhyolite complex, Flin Flon and Creighton, Saskatchewan. M.Sc. thesis, Laurentian University, Sudbury, 123 p.

Best, M. G., 2003. Igneous and Metamorphic Petrology. Turin, Blackwell Publishing, 729 p.

Best, M.B and Christiansen, E.H., 2001. Igneous Petrology. Massachusetts, USA: Blackwell Science, 2001, 458 p.

Blatter, D. L., and Carmichael, I. S. E., 1998. Hornblende peridotite xenoliths from central Mexico reveal the highly oxidized nature of subarc upper mantle. Geology. Vol. 26, 1035 – 1038.

Blenkinsop, T.G., 1991. Cataclasis and processes of particle size reduction. Pure and Applied Geophysics. Vol. 136, 59 – 86.

Boden, D.R., 1989. Evidence for step-function zoning of magma and eruptive dynamics, Toquima caldera complex, Nevada. J. Volcanol Geotherm. Res 37, 39-57.

Brown, G.M., Holland, J.G., Sigurdsson, H., Tomblin, J.F., and Arculus, R.J., 1977. Geochemistry of the Lesser Antilles volcanic island arc: Geochimica et Cosmochimica Acta, V. 41, No. 6, 785 – 801.

Byers, A.R., Kirkland, S.J.T. and Pearson, W.J. (1965): Geology and mineral deposits of the Flin Flon area, Saskatchewan. Sask. Dep. Miner. Resour., Rep. 62, 95p.

Bryant, D. G., 1968. Intrusive breccias associated with ore. Warren (Bisbee) mining district, Arizona. Economic Geology, Vol. 63, 1 – 12.

Cann, J.R., 1970. Rb, Sr, Y, Zr AND Nb in some ocean floor basaltic rocks. Earth and Planetary Science Letters. Vol. 10, 7-11.

Caricchi, L., Burlini, L., Ulmer, P., Gerya, T., Vassali, M., Papale, P., 2007. Non-Newtonian rheology of crystal-bearing magmas and implications for magma ascent dynamics. Earth and Planetary Science Letters. Vol. 264, 402 – 419.

Cas, R., Giordano, G., Balsamo, F., Esposito, A., and Mastro, S.L., 2011. Hydrothermal Breccia Textures and Processes: Lisca Bianca Islet, Panarea Volcano, Aeolian Islands, Italy. Economic Geology, Vol. 106, 437 – 450.

Clemens, J. D., and Petford, N., 1999. Granitic melt viscosity and silicic magma dynamics in contrasting tectonic settings. Journal of the Geological Society, London. Vol. 156, 1057-1060.

Corrigan, D., Z. Hajnal, B. Nemeth, and S. Lucas., 2005. Tectonic Framework of a Paleoproterozoic Arc-continent to Continent-continent Collisional Zone, Trans-Hudson Orogen, from Geological and Seismic Reflection Studies1, 2, 3. Canadian Journal of Earth Sciences/Revue Canadienne Des Sciences De La Terre 42.4 (2005): 421-34A. Web.

Corrigan, D., Pehrsson, S., Wodicka, N., and De Kamp, E., 2009. The Paleoproterozoic Trans-Hudson Orogen: a prototype of modern accretionary processes. Geological Society, London, Special Publications, 327, 457-479.

Devine, C.A., 2003. Origin and emplacement of volcanogenic massive sulphide–hosting, Paleoproterozoic volcaniclastic and effusive rocks within the Flin Flon subsidence structure, Manitoba and Saskatchewan, Canada. M.Sc. thesis, Laurentian University, Sudbury, Ontario, 279 p.

Devine, C.A., Gibson, H.L., Bailes, A.H., MacLachlan, K., Gilmore, K. and Galley, A.G., 2002. Stratigraphy of volcanogenic massive sulphide-hosting volcanic and volcaniclastic rocks of the Flin Flon formation, Flin Flon (NTS 63K12 and 13), Manitoba and Saskatchewan; in Report of Activities 2002, Manitoba Industry Trade and Mines, Manitoba Geological Survey, 9-19.

DeWolfe, Y.M., 2008. Physical volcanology, petrology and tectonic setting of intermediate and mafic volcanic and intrusive rocks in the Flin Flon volcanogenic massive sulphide (VMS) district, Manitoba, Canada: growth of a Paleoproterozoic juvenile arc; Ph.D. thesis, Laurentian University, Sudbury, 269 p.

DeWolfe, Y.M. and Gibson, H.L. 2006. Stratigraphic subdivision of the Hidden and Louis formations, Flin Flon, Manitoba (NTS 63K16SW); in Report of Activities 2006, Manitoba Science, Technology, Energy and Mines, Manitoba Geological Survey, 22–34.

Dungan, M.A., and Davidson, J., 2004. Partial assimilative recycling of the mafic plutonic roots of arc volcanoes: An example from the Chilean Andes. Geology, September 2004, Vol. 32, No. 9, 773 – 776.

Earle, S. (2019). Physical Geology – 2nd Edition. Victoria, B.C.: BC campus. Retrieved from https://opentextbc.ca/physicalgeology2ed/.

Emmons, W. H., 1938. Diatremes and certain ore-bearing pipes: Am. Inst. Mining Metall. Engineers Tech. Pub. 891, 1-15.

Ferreira V.P., Sial, A.N., Weinberg, R. F., and Pimental, M. M., 2014. Deep-seated fragmentation, transport of breccia dykes and emplacement: An example from the Borborema province, northeastern Brazil. Journal of South American Earth Sciences. Vol 58, Issue C, 300-308.

Fisher, R.V.,1960. Classification of volcanic breccias. Bulletin of the Geological Society of America, v. 71(7), 973-982.

Floyd, P., & Winchester, J. (1978). Identification and discrimination of altered and metamorphosed volcanic rocks using immobile elements. Chemical Geology, 21(3), 291-306.

Geological Survey of Finland (GSF), 2019. Forum of the European Geological Surveys, R. Salminen. Accessed April 3, 2019. < http://weppi.gtk.fi/publ/foregsatlas/text/
Gill, J.B., 1981. Orogenic Andesites and Plate Tectonics. Berlin: Springer.

Giordano, D., Russell, J.K., Dingwell, D.B., 2008. Viscosity of magmatic liquids: a model. Earth Planet. Sci. Lett. 271, 123 -134.

Gordon, T., Hunt, P., Bailes, A., Syme, E., Lewry, John F., & Stauffer, Mel R. (1990). U-Pb ages from the Flin Flon and Kisseynew belts, Manitoba; chronology of crust formation at an early Proterozoic accretionary margin. Special Paper - Geological Association of Canada, 37, 177-199.

Hall, A., 1967. The chemistry of appinitc rocks associated with the Ardara pluton, Donegal, Ireland. Contributions to Mineralogy and Petrology. Vol. 16, 156 – 171.

Heaman *et al*., 1992. U-Pb geochronological investigations in the Trans-Hudson Origen, Saskatchewan. Summary of Investigations, Saskatchewan Energy and Mines, Miscellaneous Report 92-4, 120-123.

Helz, R.T., 1987. Diverse olivine types in lavas of the 1959 eruption of Kilauea volcano and their bearing on eruption dynamics. In: Volcanism in Hawaii. Decker RW, Wright TL, Stauffer PH (eds) US Prof Paper. 1350, 691-722.

Holtzman, B. K., and D. I. Kohlstedt (2007), Stress-driven melt segregation and strain partitioning in partially molten rocks: Effects of stress and strain, Journal of Petrology, 48(12), 2379-2406.

Howard, Ned, ????. Genetic classification of Breccias. Retrieved from https://www.academia.edu/9593848/GENETIC_CLASSIFICATION_OF_BRECCIAS.

Hulin, C. D., 1948, Factors in the localization of mineralized districts: Am. Inst. Mining Metall. Petroleum Engineers Trans., V.178, 36-52.

Irvine, T.N., 1974. Petrology of the Duke Island ultramafic complex, southeastern Alaska. Geological Society of America. Mem. 138

Jébrak, M., 1997. Hydrothermal breccias in vein-type ore deposits: A review of mechanisms, morphology and size distribution. Ore Geology Reviews, V. 12(3), 111-134.

Jensen, L. S., 1976. Ontario Geological Survey Miscellaneous Paper 66. Ontario Geological Survey Miscellaneous Paper, 1976, Issue 66. Web.

Kidd, J., 1815. A geological essay on the imperfect evidence in support of a theory of the earth, deducible either from its general structure or from the changes produced on its surface by the operation of existing causes.

Kokandakar, G.J., Ghodke, S.S., Rathna, K., More, L.B., Nagaraju, B., Bhosle, M. V., and Kumar, K. V., 2018. Density, viscosity and velocity (ascent rate) of alkaline magmas. Journal Geological Society of India. Vol. 91, 135 – 146.

Lafrance, B., Gibson, H.L., Pehrsson, S., Schetselaar, E., DeWolfe, Y. M., and Lewis, D., 2016. Structural reconstruction of the Flin Flon volcanogenic massive sulfide mining district, Saskatchewan and Manitoba, Canada, In press. Economic Geology. Vol. 111 (4), 849-875.

Lawless, J.V., and White, P.J., 1990. Ore-related breccias: A revised genetic classification, with particular reference to epithermal deposits. Proceedings of the 12th New Zealand Geothermal Workshop 1990, Harvey, C.C. (ed.), Freeston, D.H. (ed.), Scott, G.L. (ed.), 197-202.

Laznicka, P., 1988. Breccias and coarse fragmentites: petrology, environments, associations, ores. Amsterdam; New York: Elsevier, 832 p.

Lazzarotto, M., Gagné, S. and Pattison, D.R.M., 2016. Tectonometamorphic investigations in the Athapapuskow Lake area, west-central Manitoba (part of NTS 63K12); in Report of Activities 2016, Manitoba Growth, Enterprise and Trade, Manitoba Geological Survey, 87–98

Lazzarotto, M., Pattison, D.R.M., and Gagné, S., 2017. Prehnite-pumpellyite– to amphibolite-facies metamorphism in the Athapapuskow Lake area, west-central Manitoba (parts of NTS 63K12, 13). Report of Activities 2017, Manitoba Growth, Enterprise and Trade, Manitoba Geological Survey, 104–116.

Le Maitre, R. W., 1976. The chemical variability of some common igneous rocks. Journal of Petrology, V. 17, 589 – 637.

Locke, A., 1926, The formation of certain ore bodies by mineralization stoping: ECON. GEOL., V. 21, 431-453.

Lorenz, V., and Kurszlaukis, S., 2007. Root zone processes in the phreatomagmatic pipe emplacement model and consequences for the evolution of maar–diatreme volcanoes. Journal of Volcanology and Geothermal Research, 159, 4–32.

Lucas, S.B., Stern, R.A., Syme, E.C., Reilly, B.A. and Thomas, D.J., 1996. Intraoceanic tectonics and the development of continental crust: 1.92-1.84 Ga evolution of the Flin Flon Belt, Canada. GSA Bulletin. May 1996, Volume 108 (5), 602-629.

Lucas, S.B., Syme, E.C., and Ashton, K.E., 1999. New perspectives on the Flin Flon Belt, Trans-Hudson Orogen, Manitoba and Saskatchewan: an introduction to the special issue on the NATMAP Shield Margin Project, Part 1. Canadian Journal of Earth Sciences, Vol. 36, 135-140

Macculloch, J., 1821. A geological classification of rocks. London: Longman, Hurst, Rees, Orme and Brown.

Marsh, B.D., 1988. Crystal size distribution (CSD) in rocks and the kinetics and dynamics of crystallization I. Theory. Contrib Mineral Petrol., Vol. 99, 277-291.

Maxeiner, R., Sibbald, T., Slimmon, W., Heaman, L., & Watters, B., 1999. Lithogeochemistry of volcano-plutonic assemblages of the southern Hanson Lake Block and southeastern Glennie Domain, Trans-Hudson Orogen: Evidence for a single island arc. Canadian Journal of Earth Sciences/Revue Canadienne Des Sciences De La Terre, 36(2), 209-225.

McKenzie, D., 2000. Constrains on the melt generation and transport from U-series activity ratios. Chemical Geology, Vol. 162, 337 – 357.

McPhie, J., Doyle, M., and Allen, R., 1993. Volcanic Textures: A guide to the interpretation of textures in volcanic rocks. CODES Key Centre, University of Tasmania, Hobart, 198 p.

Mendez da Costa, E., 1757. A natural history of fossils. London, Royal Society, 299 p.

Morin, D. and Corriveau, L, 1996. Fragmentation processes and xenolith transport in a Proterozoic minette dyke, Grenville Province, Quebec. Contributions to Mineralogy and Petrology. Vol. 125, 319-331.

Motoki, A., Sichel, S.E., and Petrakis, G.H., 2009. Genesis of the tabular xenoliths along contact plane of the mafic dykes of Cabo Frio area, State of Rio de Janeiro, Brazil: Thermal delamination or hydraulic shear fracturing? Geosciências, Vol. 28, 15-26.

Mueller, K., 2013. Chapter 4, Igneous Rocks. Department of Earth & Climate, San Francisco State University. http://funnel.sfsu.edu/students/luyilin/Lu_Yilin/yl/physical%20geology%20prof%20karl%20mueller%20u%20of%20colorado%20/Ch04%20Igneous%20rocks.pdf

Murase, T. and McBirney, A.R., 1973. Properties of some common igneous rocks and their melts at high temperatures. Geol. Soc. Am. Bull. 84, 3563 – 3592.

Norton, D. L., and Cathies, L. M., 1973. Breccia pipes—products of exsolved vapor from magmas. E: CON. GEOL., V. 68, 540-546.

O'Hanley, D.S., Kyser, K.T. and Stauffer, M., 1993. Provenance, deformation and alteration history of mafic-ultramafic rocks east of Amisk Lake, and the provenance of the mafic and ultramafic Boundary intrusions, in the Flin Flon Domain, Trans-Hudson Orogen. Lithoprobe Report (unpublished), Trans-Hudson Orogen Transect, University of Saskatchewan, Report No. 34, 190-205.

O'Hanley, D.S. and Kyser, K.T., 1994. The Petrogenesis of the Alaskan-type mafic and ultramafic boundary intrusions, Flin Flon Domain, Trans-Hudson Orogen. Lithoprobe Report (unpublished), Trans-Hudson Orogen Transect, University of Saskatchewan, Report No. 38, 80-99.

Olianti, C.A.E., and Harris, C., 2018. A low-δ O intrusive breccia from Koegel Fontein, South Africa: Remobilisation of basement that was hydrothermally altered during global glaciation? Lithos, 300–301 (2018), 33–50.

Parsons, T., N. H. Sleep, and G. A. Thompson, 1992. Host rock rheology controls on emplacement of tabular intrusions: Implications for underplating of extending crust, Tectonics, 11(6), 1348– 1356.

Pearce, T.,1968. A contribution to the theory of variation diagrams. Contributions to Mineralogy and Petrology, 19(2), 142-157.

Pearce J.A., 1976. Statistical analysis of major element patterns in basalts. J. Petrol., 17, 15-43.

Pearce, J.A., 1982. Trace element characteristics of lavas from destructive plate boundaries. In: R.S. Thorpe (Editor), Andesites: Orogenic Andesites and Related Rocks. Wiley, Chichester, 525-547.

Pearce, J.A., 1996. A user' s guide to basalt discrimination diagrams; in Wyman, D.A. (ed.), Trace Element Geochemistry of Volcanic Rocks: Applications for Massive Sulphide Exploration. Geol. Assoc. Can., Short Course Notes. Vol. 12., 79- 114.

Pearce JA. and Cann JR., 1973, Tectonic setting of basic volcanic rocks determined using trace element analyses. Earth Planet. Sci. Lett., 19, 290-300.

Pearce, Julian A., Sieger R. Van Der Laan, Richard J. Arculus, Bramley J. Murton, Teruaki Ishii, David W. Peate, Ian J. Parkinson, Fryer, Patricia, Stokking, Laura B., Ali, Jason Richard, Ballotti, Dean L., Burke, Margaret M., Ciampo, Giuliano, Haggerty, Janet A., Haston, Roger B., Heling, Dietrich, Hobart, Michael A., Johnson, Lynn E., Lagabrielle, Yves, McCoy, Floyd W., Maekawa, Hirokazu, Marlow, Michael S., Milner, Greg J., Mottl, Michael J., Phipps, Stephen P., Rigsby, Catherine A., Saboda, Kristine L., Stabell, Bjorg, Xu, Yulin, Dearmont, Lona H., Mazzullo, Elsa K., Stewart, Norman J., and Winkler, William R., 1992. Boninite and Harzburgite from Leg 125 (Bonin-Mariana Forearc); a Case Study of Magma Genesis during the Initial Stages of Subduction. Proceedings of the Ocean Drilling Program, Scientific Results 125 (1992): 623-59. Web.

Pearce, J.A. and Parkinson, I.J., 1993. Trace element models for mantle melting: application to volcanic arc petrogenesis. In: Prichard, H. M., Alabaster, T., Harris, N. B. W. & Neary, C. R. (eds) Magmatic Processes and Plate Tectonics. Geological Society, London, Special Publications 76, 373 – 403.

Perry, V. D., 1961. The significance of mineralized breccia pipes: Mining Eng., V. 13, 367-376.

Peslier, A. H. and Lhur, J. F., 2006. Hydrogen loss from olivines in mantle xenoliths from Simcoe (USA) and Mexico: mafic alkaline magma ascent rates and water budget of the sub-continental lithosphere. Earth and Planetary Science Letters. Vol. 242, 302- 319.

Peslier, A. H., Woodland, A. B., and Wolff, J. A., 2008. Fast kimberlite ascent rates estimated from hydrogen diffusion profiles in xenolithic mantle olivines from southern Africa. Geochimica et Cosmochimica Acta. Vol. 72, 2711 – 2722.

Philpotts, A.R., 1990. Principles of Igneous and Metamorphic Petrology. Prentice Hall, Englewood Cliffs, NJ, 498 pp.

Platten, L.M., 1991. Zoning and layering in diorites of the Scottish Caledonian Appinite suite. Geological Journal. Vol. 26, 329 – 348.

Ross, P. S. & Bédard, L. P., 2009. Magmatic affinity of modern and ancient subalkaline volcanic rocks determined from trace-element discriminant diagrams. Canadian Journal of Earth Sciences. 46, 823–839.

Ryan, M. P., and Blevins, J. Y. K., 1987. The viscosity of synthetic and natural silicate melts and glasses at high temperatures and 1 Bar (105 Pascals) pressure and at higher pressures. U.S. Geological Survey Bulletin; 1764.

Saleeby, J.B., 1992. Age and tectonic setting of the Duke Island ultramafic intrusion, southeast Alaska. Canadian Journal of Earth Sciences. Vol. 29, 506 – 522.

Sato, H., 2005. Viscosity measurement of subliquidus magmas: 1707 basalt of Fuji volcano. Journal of Mineralogical and Petrological Sciences, Volume 100, 133 – 142.

Saussure, Horace-Bénédict, 1796. Agenda, Ou tableau général des observations et des recherches dont les résultats doivent servir de base à la théorie de la terre. Journal des mines, no. 20. Paris, an. 4 (1796), 1–70.

Shao, Y.J., Zhang, Y.Z., Zhang, J.D., Ding, Z.W., Chen, X.L., and Liu, Z.F., 2008. Formation mechanism of breccia pipe type in Yixingzhai gold deposit. Journal of Central South University of Technology (English Edition), V. 15(1), 89-94.

Shaw, H.R., 1969. Rheology of basalt in the melting range. J. Petrol., 10: 510-535.

Shaw, H.R., 1980. The fracture mechanisms of magma transport from the mantle to the surface. In: R.B. Hargraves (Editor), Physics of Magmatic Processes. Princeton University Press, Princeton, N.J., 201-264.

Shee, S.R., Bristow J.W., Bell, D.R., Smith, C.B., Allsopp, H.L., Shee, P.B., 1989. The petrology of kimberlites, related rocks and associated mantle xenoliths from the Kuruman province, South Africa. N. Ross (Ed.), Kimberlites and Related Rocks. Geol. Soc. Aust. Spec. Publ. (1989), 60-82.

Shervais, J., 1982. Ti-V plots and the petrogenesis of modern and ophiolitic lavas. Earth and Planetary Science Letters, 59(1), 101-118.

Sibson, R.H.,1986. Brecciation processes in fault zones: Inferences from earthquake rupturing. Pure and Applied Geophysics. Vol. 124, 159–174.

Sillitoe, R.H., 1985. Ore-related breccias in volcanoplutonic arcs. Economic Geology, Vol. 80(6), 1467-1514.

Simard, R-L. and Creaser, R.A., 2007. Implications of new geo-logical mapping, geochemistry and Sm-Nd isotope data, Flin Flon area, Manitoba (part of NTS 63K12); in Report of Activities 2007, Manitoba Sciences, Technology, Energy and Mines, Manitoba Geological Survey, 7–20

Simard, R.L., Maclachlan, K., Gibson, H.L., DeWolfe, Y.M., Devine, C.A., Kremer, P.D., Lafrance, B., Ames, D., Syme, E.C., Bailes, A.H., Bailey, K., Price, D., Pehrsson, S., Lewis, E.M., Lewis, D. and Gailey, A.G., 2010. Geology of the Flin Flon area, Manitoba and Saskatchewan (part of NTS 63K12, 13). Manitoba Innovation, Energy and Mines, Manitoba Geological Survey, Geoscientific Map MAP2010-1 and Saskatchewan Ministry of Energy and Resources, Geoscience Map 2010-2, 1 colour map, scale 1:10000.

Simard, R.L., Maclachlan, K., Gibson, H.L., DeWolfe, Y.M., Devine, C.A., Kremer, P.D., Lafrance, B., Ames, D., Syme, E.C., Bailes, A.H., Bailey, K., Price, D., Pehrsson, S., Lewis, E.M., Lewis, D. and Gailey, A.G., 2012. Geology of the Flin Flon area, Manitoba and Saskatchewan (parts of NTS 63K12, 13). Manitoba Energy and Mines, Geological Report GR2012-2.

Sparks, R.S.J., Pinkerton, H., MadDonald, R., 1977. The transport of xenoliths in magmas. Earth and Planetary Science Letters. Vol. 35, 234 – 238.

Stauffer, M.R., 1984. Manikwean: an early Proterozoic ocean in Central Canada: its igneous history and orogenic closure. Precambrian Research. Vol 25, 257-281.

Stauffer, M.R., 1990. The Missi formation: an Aphebian molasse deposit in the Reindeer Zone of the Trans-Hudson orogen, Canada: in Lewry, J.F. and Stauffer, M.R., eds.: The Early Proterozoic Trans-Hudson Orogen of North America: Geological Association of Canada, Special Paper 37, 121-141.

Stern, R.A., Syme, E.C., Bailes, A.H. and Lucas, S.B. 1995. Paleoproterozoic (1.90–1.86 Ga) arc volcanism in the Flin Flon belt, Trans-Hudson Orogen, Canada; Contributions to Mineralogy and Petrology, V. 119, 117–141.

Stern, R. A., Machado, N., Syme, E. C., Lucas, S. B. and David, J., 1999. Chronology of crustal growth and recycling in the Paleo-proterozoic Amisk collage (Flin Flon Belt), Trans-Hudson Orogen, Canada, Canadian Journal of Earth Sciences, V. 36, 1827-1807.

Stockwell, C.H., 1946. Flin Flon – Mandy Area, Manitoba and Saskatchewan. Geological Survey of Canada. Paper 46-14, 8p.

Stockwell, C.H., 1960. Flin Flon – Mandy Area , Manitoba and Saskatchewan. Geological Survey of Canada. Paper 46-14, 5p.

Streck, M.J., 2008. Mineral Textures and Zoning as Evidence for Open System Processes. Reviews in Mineralogy and Geochemistry, Vol. 69, 595 – 622.

Sun, S., & Mcdonough, W., 1989. Chemical and isotopic systematics of oceanic basalts: Implications for mantle composition and processes. Geological Society, London, Special Publications, 42(1), 313-345.

Syme, E.C., 1975. Petrogenesis of the Boundary intrusions, Flin Flon area, Saskatchewan-Manitoba. Masters thesis, University of Saskatchewan, Department of Geological Sciences, 1975.

Syme, E.C., 1988. Athapapuskow Lake Project. In Manitoba Energy and Mines, Minerals Division, Report of Field Activities, 20-34.

Syme, E.C. and Bailes, A.H. 1993. Stratigraphy and tectonic set- ting of Early Proterozoic volcanogenic massive sulphide deposits, Flin Flon, Manitoba; Economic Geology, V. 88, 566–589.

Syme, E.C., Lucas, S.B., Bailes, A.H. and Stern, R.A., 1999b. Contrasting arc and MORB-like assemblages in the Paleo-proterozoic Flin Flon Belt, Manitoba, and the role of intra-arc extension in localizing volcanic-hosted massive sulphide deposits; Canadian Journal of Earth Sciences, v. 36, 1767–1788.

Syme, E.C. and Forester, R.W., 1977. Petrogenesis of the Boundary intrusions in the Flin Flon area of Saskatchewan and Manitoba. Canadian Journal of Earth Sciences 14: 444-455.

Valentine, G., & White, J., 2012. Revised conceptual model for maar-diatremes; subsurface processes, energetics, and eruptive products. Geology (Boulder), 40(12), 1111-1114.

Vry, V.H., Wilkinson, J.J., Seguel, J., and Millan, J., 2010. Multistage Intrusion, Brecciation, and Veining at El Teniente, Evolution of a Nested Porphyry System. Econ. Geol., V. 105(1), 119-153.

Walker, R. T., 1928. Mineralized volcanic explosion pipes: Eng. Mining Jour., V. 126, 895-898, 939-942, 976-984.

Whalen, J.B., 1992. Elbow Lake project Part B: granitoid plutons. In Manitoba Energy and Mines, Minerals Division, Report of Activities, 47-51.

White, W., Copeland, P., Gravatt, D.R., and Devine, J.D., 2017. Geochemistry and geochronology of Grenada and Union islands Lesser Antilles: The case for mixing between two magma series generated from distinct sources. Geosphere, V. 13, No. 5, 1359 – 1391, doi:10.1130/GES01414.1.

Wilcox, R. E., 1979. The liquid line of descent and variation diagrams. Yoder HS (ed) The evolution of igneous rocks: Fiftieth anniversary perspectives. Princeton Univ Press, 205–232.

Wilkin, R.T., and Bornhorst, T.J., 1993. Archean Appinites from the northern complex, Michigan. Journal of Geology. Vol. 101, 107 – 114.

Winchester, J., & Floyd, P. (1977). Geochemical discrimination of different magma series and their differentiation products using immobile elements. Chemical Geology, 20(C), 325-343.

Wood, D. A., 1980, The application of a Th-Hf-Ta diagram to problems of tectonomagmatic classification and to establishing the nature of crustal contamination of basaltic lavas of the British Tertiary volcanic province: Earth and Planetary Science Letters, V. 50, no. 1, 11-30.

Wood. D.A., Joron, J.-L., and Treuik M., 1979. A re-appraisal of the use of trace elements to classify and dis- criminate between magma series erupted in different tectonic settings. Earth Planet. Sci. Lett., 45: 326-336.

Wright, A.E., and Bowes, D.R., 1963. Classification of volcanic breccias: A discussion. Bulletin of the Geological Society of America, V. 74(1), 79-86.

Yoder, H. S. (1976), Generation of Basaltic Magma, 265.

APPENDIX A

TABLE A1: LIST OF ROCK, THIN SECTION AND GEOCHEMICAL SAMPLES

Rock Sample ID	Area	Primary Sample Rock Type	Secondary Sample Rock Type	NOTES	UTM_E*	UTM_N*	ELEV	Thin Section ID	Thin Section Description	Geochemical Analysis ID	SRC ID	Description
GS01	Green Street	Hornblende-bearing quartz leucodiorite - tonalite		Xenolith free Boundary intrusion	313,659.0	6,071,090.0	341.4					
GS01A		Hornblende-bearing quartz leucodiorite - tonalite		Boundary intrusion with fragments	313,659.0	6,071,090.0	341.4	TS_GS01A-02B	Encompasses mafic fragment, entire samples looks like there is a lot of mixing and the fragments are being absorbed/melted			
GS02		Hornblende-bearing quartz leucodiorite - tonalite	Gabbro fragments	Boundary intrusion with fragments	313,648.0	6,071,068.0	350.5	TS_GS02-01	Encompasses mafic fragment			
		Hornblende-bearing quartz leucodiorite - tonalite	Gabbro fragments				350.5	TS_GS02-02A	Encompasses mafic fragment			
GS03		Volcanic rhyolite			313,644.0	6,071,113.0	345.0					
GS04		Hornblende-bearing quartz leucodiorite - tonalite		Homogenous and leucocratic, rare to no fragments or crysts	313,629.0	6,071,056.1	346.9	TS_GS04-01	Includes crosscutting felsic dyke in Boundary intrusion matrix			
GS05		Volcanic rhyolite	Hornblende-bearing quartz leucodiorite - tonalite	Volcanic rock-Boundary intrusion contact	313,619.6	6,071,046.6	339.0	TS_GS05-01	Contact between Boundary intrusion and volcanic rock (rhyolite)			

*NAD83, UTM zone 14, NTS 63K12, 13

Rock Sample ID	Area	Primary Sample Rock Type	Secondary Sample Rock Type	NOTES	UTM_E*	UTM_N*	ELEV	Thin Section ID	Thin Section Description	Geochemical Analysis ID	SRC ID	Description
GS06	Green Street	Volcanic rhyolite	Hornblende-bearing quartz leucodiorite - tonalite	Volcanic rock-Boundary intrusion contact	313,641.6	6,071,064.8	339.7					
GS07A		Hornblende-bearing quartz leucodiorite - tonalite		Homogenous and leucratic, rare to no fragments or crysts	313,628.2	6,071,048.4	336.8	TS_GS07A-01	Homogenous Boundary intrusion,porphyritic, thin section includes possible xenocryst	GC_GS07A-01	5	
GS07B		Hornblende-bearing quartz leucodiorite - tonalite		Homogenous and leucratic, rare to no fragments or crysts	313,628.0	6,071,048.8	343.8	TS_GS07B-01	Homogenous, porphryitic, thin section is across an asicular crystal			
GS08A		Hornblende-bearing quartz leucodiorite - tonalite	Undefined mafic intrusive fragments + volcanic fragments	Volcanic fragment and mafic intrusive fragment diffuse in Boundary intrusion matrix	313,654.7	6,071,076.8	350.5			GC_GS08A-01	6	Diffuse and small fragments (volcanics)
GS08B		Hornblende-bearing quartz leucodiorite - tonalite	Undefined mafic intrusive fragments + volcanic fragments	Volcanic fragment and mafic intrusive fragment diffuse in Boundary intrusion matrix	313,654.7	6,071,076.8	350.5	TS_GS08B-01	Diffuse and small fragments (volcanics), thin section includes volcanic fragment			
GS09A		Hornblende-bearing quartz leucodiorite - tonalite	Gabbro fragments	Leucocratic dyke with mafic fragment being incorporated; 9A = leucocratic	313,642.9	6,071,088.5	343.8					
GS09B		Hornblende-bearing quartz leucodiorite - tonalite	Gabbro fragments	Leucratic dyke with mafic fragment being incorporated;9B = meso- to melanocratic	313,642.9	6,071,088.5	343.8					

Rock Sample ID	Area	Primary Sample Rock Type	Secondary Sample Rock Type	NOTES	UTM_E*	UTM_N*	ELEV	Thin Section ID	Thin Section Description	Geochemical Analysis ID	SRC ID	Description
GS10A	Green Street	Hornblende-bearing quartz leucodiorite - tonalite	Gabbro fragments; volcanic host rock fragments	Boundary intrusion with fragments at varying degrees of disaggregation	313,665.3	6,071,090.4	341.4					
GS10B		Hornblende-bearing quartz leucodiorite - tonalite	Gabbro fragments; volcanic host rock fragments	Contains mafic intrusive fragments	313,665.3	6,071,090.4	341.4	TS_GS10B-01	Fragment-rich sample, includes volcanic and intrusive fragments, thin section includes mafic fragment			
GS10C		Hornblende-bearing quartz leucodiorite - tonalite	Gabbro fragments; volcanic host rock fragments	Mafic intrusive + volcanic fragments	313,665.3	6,071,090.4	341.4	TS_GS10C-01	Fragment-rich sample, includes VF and MIF + possible xenocrysts or antecrysts, possible disaggregation of fragment	GC_GS10C-01	11	Matrix
		Hornblende-bearing quartz leucodiorite - tonalite	Gabbro fragments; volcanic host rock fragments					TS_GS10C-02	Fragment-rich sample, includes VF and MIF + possible xenocrysts or antecrysts, possible disaggregation of fragment	GC_GS10C-02	15	Fragment; partially disaggregated
GS11A		Hornblende-bearing quartz leucodiorite - tonalite	Gabbro fragment	Mafic intrusive fragment- Boundary intrusion contact in area of fracturing/jointing	313,668.0	6,071,090.0	340.0					
GS11B		Hornblende-bearing quartz leucodiorite - tonalite	Gabbro fragment		313,668.0	6,071,090.0	340.0					

Rock Sample ID	Area	Primary Sample Rock Type	Secondary Sample Rock Type	NOTES	UTM_E*	UTM_N*	ELEV	Thin Section ID	Thin Section Description	Geochemical Analysis ID	SRC ID	Description
GS11C	Green Street	Hornblende-bearing quartz leucodiorite - tonalite	Gabbro fragment		313,668.0	6,071,090.0	340.0					
GS12		Gabbro	Hornblende-bearing quartz leucodiorite - tonalite	Boundary intrusion-mafic fragment contact; large fragment	313,664.0	6,071,081.3	338.7	TS_GS12-01B	Includes mafic and volcanic fragment	GC_GS12-01	12	Large fragment of Boundary intrusion (mafic intrusion), little to no disaggregation
GS12		Gabbro	Hornblende-bearing quartz leucodiorite - tonalite					TS_GS12-02	Includes mafic and volcanic fragment	GC_GS12-02	13	Matrix
GS13		Hornblende-bearing quartz leucodiorite - tonalite	Undefined volcanic fragments	Leucocratic breccia with volcanic fragments	313,658.0	6,071,097.1	336.1	TS_GS13-01	Includes mafic and volcanic fragment			
GS14		Hornblende-bearing quartz leucodiorite - tonalite		dyklet	313,648.0	6,071,087.0	340.0	TS_GS14-01	Dyke, thin section includes contact with volcanics	GC_GS14-01	14	Dyke
FF18A		Pillowed plagioclase-phyric basalt flow			313,711.0	6,071,141.0	335.0	TS_FF18A-01	Shows contact between volcanic and intrusive rock	GC_FF18A-01	18	Porphyritic intrusive (in contact with volcanic rock)
FF18B		Pillowed plagioclase-phyric basalt flow			313,711.0	6,071,141.0	335.0					

Rock Sample ID	Area	Primary Sample Rock Type	Secondary Sample Rock Type	NOTES	UTM_E*	UTM_N*	ELEV	Thin Section ID	Thin Section Description	Geochemical Analysis ID	SRC ID	Description
LL01A	Louis Lake	Gabbro		East side of central part of Louis Lake; mafic, gabbro, with xenocrysts?	315,703.9	6,071,415.2	333.2	TS_LL01A-02	Coarse-grained Boundary intrusion with possible xenocrysts	GC_LL01A-01	1	Homogenous sample, coarse-grainec, SE of Louis Lake
		Gabbro										
LL01B		Gabbro		East side of central part of Louis Lake; with felsic vein/dyke	315,703.9	6,071,415.2	333.2	TS_LL01B-01	Boundary intrusion with felsic vein, thin section includes felsic vein			
LL02		Augite hornblende leuco- to meladiorite		Layering	315,615.2	6,071,574.8	340.9	TS_LL02-01	Shows layering within Boundary intrusion	GC_LL02-01	19	Mesocratic layer
		Augite hornblende leuco- to meladiorite								GC_LL02-02	25	Leucocratic layer
LL03A		Augite hornblende melagabbro	Gabbro and undefined volcanic fragments	Fragment in Boundary intrusion	315,609.5	6,071,576.7	333.5	TS_LL03A-01	Leucratic-volcanic contact	GC_LL03A	20	Fragment
LL04A		Augite hornblende leucodiorite	Gabbro and undefined volcanic fragments	Breccia, more leucocratic	315,611.2	6,071,574.5	336.1	TS_LL04A-02		GC_LL04A-01	21	Subhorizontal breccia with mafic intrusive and volcanic fragments
		Augite hornblende leucodiorite	Gabbro and undefined volcanic fragments	Breccia, more leucocratic	315,611.2	6,071,574.5	336.1	TS_LL04A-03				
LL04B		Augite hornblende leucodiorite	Gabbro and undefined volcanic fragments	Breccia, more leucocratic	315,611.2	6,071,574.5	336.1					

Rock Sample ID	Area	Primary Sample Rock Type	Secondary Sample Rock Type	NOTES	UTM_E*	UTM_N*	ELEV	Thin Section ID	Thin Section Description	Geochemical Analysis ID	SRC ID	Description
FF01A	Louis Lake	Biotite-augite meladiorite			315,574.0	6,071,576.0	338.0					
FF01B		Biotite-augite meladiorite			315,574.0	6,071,576.0	338.0					
FF04		Hornblende meladiorite			315,968.0	6,071,119.0	333.0	TS_FF04-01	Boundary intrusion, thin section represents entire rock	GC_FF04-01	7	SE end of Louis Lake
PB01	Phantom Beach	Hornblendite		Polymict breccia, high fragment to matrix ratio, randomly oriented, leucocratic matrix	314,848.9	6,069,575.4	340.4	TS_PB01-02	Breccia, mafic fragments, felsic matrix	GC_PB01-01	22	Mafic fragment
PB02		Tonalite - melatonalite	Hornblendite fragment	Fragments are more rounded and less diffuse compared to intrusion breciias	314,863.1	6,069,579.3	344.0	TS_PB02-01	Large thin section, breccia, mafic fragments, felsic matrix	GC_PB02-01	23	Mafic fragment
		Tonalite - melatonalite						TS_PB02-02	Matrix with possible older (?) more assimilated (?) fragments than large mafic fragments in same rock	GC_PB02-02	24	Late intrusion
PB03		Hornblendite		Boundary intrusion here is darker green, more melanocratic	314,862.5	6,069,590.8	343.3	TS_PB03-01	Homogenous coarse-grained gabbro	GC_PB03-01	2	Mesocratic intrusion, homogeous.

Rock Sample ID	Area	Primary Sample Rock Type	Secondary Sample Rock Type	NOTES	UTM_E*	UTM_N*	ELEV	Thin Section ID	Thin Section Description	Geochemical Analysis ID	SRC ID	Description
PB04	Phantom Beach	Tonalite - melatonalite		More leucocratic intrusion	314,869.1	6,069,589.1	338.5	TS_PB04-01	Leucocratic intrusion, mixing?	GC_PB04-01	3	Leucocratic intrusion
PB05		Tonalite - melatonalite	Undefined mafic intrusive fragments + volcanic fragments	Breccia in more leucocratic part, mafic volcanic + felsics + possibly coarse-grained mafics fragments; higher fragment-matrix ratio compared to further south in outcrop	314,873.7	6,069,594.1	339.7					
BI HB01	777 Mine	Biotite-augite meladiorite		Underground sample				TS_HB01-01	Includes felsic intrusion			
BI HB02		Biotite-augite meladiorite		Underground sample								
CL01	Club Lake	Plagioclase-bearing gabbro		Mafic, coarse grained, homogenous with weak fabric dipping easterly; moderate-strong altered dark green, some orange-red staining	312,513.0	6,075,650.0	340.0	TS_CL01-01	Coarse-grained Boundary intrusion gabbro	GC_CL01-01	17	Very coarse-grained homogenous gabbro
CL01A		Plagioclase-bearing gabbro			312,513.0	6,075,650.0	340.0	TS_CL01A-01	Fine- to coarse-grained gabbro, thin section represents entire rock			

Rock Sample ID	Area	Primary Sample Rock Type	Secondary Sample Rock Type	NOTES	UTM_E*	UTM_N*	ELEV	Thin Section ID	Thin Section Description	Geochemical Analysis ID	SRC ID	Description
CL02	Club Lake	Tonalite - melatonalite		Missi-Boundary intrusion dyke contact; coarse grained, altered pale-pink-green, fabric parallel to contact with Missi; contains xenoliths/fragments	312,631.0	6,075,511.0	340.0	TS_CL02-02	Overall homogenous, some possible xenocrysts	GC_CL02-01	16	Homogenous samples with possible xenocrysts
CL02A		Tonalite - melatonalite		Missi-Boundary intrusion dyke contact; coarse grained, altered pale-pink-green, fabric parallel to contact with Missi Group; contains xenoliths/fragments	312,631.0	6,075,511.0	340.0	TS_CL02A-01	Felsic-Boundary intrusion contact			
CL02B		Tonalite - melatonalite		Missi-Boundary intrusion dyke contact	312,631.0	6,075,511.0	340.0	TS_CL02B-02	Medium- to coarse-grained gabbro/diorite, possible phenocrysts	GC_CL02B-01	4	Medium- to coarse-grained gabbro/diorite, Missi-Boundary intrusion contact
CL02C		Tonalite - melatonalite		Boundary intrusion chilled margin	312,631.0	6,075,511.0		TS_CL02C-01	Dyke, fabric			
FF13	Myo lake	Flin Flon formation, massive and pillowed			313,843.0	6,070,071.0	348.0			GC_FF13_01	8	
FF17		Felsic dyke/sill, quartz-plagioclase-phyric, intrusive			313,657.0	6,069,826.0	342.0			GC_FF17-01	9	Mafic section
										GC_FF17-02	10	Felsic section

TABLE A2: GEOCHEMICAL RESULTS

Analyte		SiO2	TiO2	Al2O3	Fe2O3	FeOtotal	MnO	MgO
Units		wt %	wt %	wt %	wt %	wt %	wt %	wt %
Detection Limit		0.1	0.01	0.01	0.01	0.03	0.01	0.01
Description	Sample Type							
GC_LL01A-01	Basement	52.2	0.67	11.8	9.13	7.15	0.14	12
GC_PB03-01	Basement	48.8	0.68	9.63	10.2	7	0.15	17.4
GC_PB04-01	Basement	51.2	0.9	14.2	10.5	6.71	0.12	7.74
GC_CL02B-01	Basement	64.4	0.55	14.2	6.16	3.35	0.06	4.1
GC_GS07A-01	Basement	64.4	0.4	15.5	4.79	3.5	0.05	2.52
GC_GS08A-01	Basement	62	0.46	15.1	5.52	4.38	0.07	2.92
GC_FF04-01	Basement	52.4	0.67	11.8	9.68	6.57	0.14	11.8
GC_FF13-01	Basement	53.8	0.47	12.6	8.73	5.84	0.13	10.8
GC_FF17-01	Basement	43.9	0.34	20	11.1	7	0.15	8.12
GC_FF17-02	Basement	45.2	0.43	19.7	8.87		0.12	5.34
GC_GS10C-01	Basement	63.8	0.42	15.5	5.3	2.77	0.07	2.52
GC_GS12-01	Basement	49	0.65	9.09	12.2	8.61	0.23	16.2
GC_GS12-02	Basement	61.8	0.47	15.1	5.87	2.62	0.09	3.6
GC_GS14-01	Basement	63	0.44	16	5.44	2.92	0.08	2.54
GC_GS10C-02	Basement	52.2	0.86	11.3	12.1	8.61	0.19	9.99
GC_CL02-01	Basement	58.9	0.57	14.3	6.08	3.79	0.09	5.09
GC_CL01-01	Basement	47.8	0.51	8.53	10.1	7.44	0.16	18.8
GC_FF18A-01	Basement	48.4	0.45	17.7	8.87	3.65	0.12	3.21
GC_LL02-01	Basement	53.1	0.73	10.8	9.7	6.21	0.17	11.8
GC_LL03A	Basement	48.8	0.67	11.3	10.2	7.44	0.16	13.8
GC_LL04A-01	Basement	56.3	0.33	13	7.38	5.25	0.13	8.19
GC_PB01-01	Basement	50	0.54	6.1	10.2	6.86	0.19	18.9
GC_PB02-01	Basement	50.4	0.32	5.94	10.7	7.59	0.27	18.5
GC_PB02-02	Basement	56.2	0.86	14.1	11.3	5.4	0.1	4.39
GC_LL02-02	Basement	54	0.59	12.5	8.36	5.54	0.15	9.88
GC_FF17-02R	Repeat	45.5	0.42	19.7	9.01		0.12	5.4
GC_GS12-01 R	Repeat	49	0.64	9.02	12.1	8.9	0.23	16.1
GC_LL02-02 R	Repeat	54.2	0.59	12.6	8.3	5.54	0.15	9.82
GC_FF17-01 R	Repeat	43.9	0.35	20	11.7	7.15	0.15	8.06
SY3	Standard	59.6	0.14	11.8	6.44		0.3	2.62
SY3/CG51509	Standard	59.3	0.14	11.6	6.49	3.73	0.3	2.6
SY3/CG51509	Standard	59.4	0.14	12	6.44	3.73	0.3	2.65
SY3/OKA2/CG51509	Standard	59.3	0.14	11.7	6.41	3.79	0.31	2.7

Analyte		CaO	Na2O	K2O	P2O5	LOI	SUM	Be
Units		wt %	wt %	wt %	wt %	wt %	wt %	ppm
Detection Limit		0.01	0.01	0.01	0.01	0.1		0.1
Description	Sample Type							
GC_LL01A-01	Basement	6.08	3.13	0.89	0.24	3.4	99.68	1
GC_PB03-01	Basement	6.2	1.44	2.47	0.27	2.9	100.14	1.4
GC_PB04-01	Basement	6.82	3.58	1.8	0.64	2.7	100.2	1.1
GC_CL02B-01	Basement	2.87	3.51	1.48	0.23	2.7	100.26	1.6
GC_GS07A-01	Basement	4.19	4.42	1.22	0.18	1.9	99.57	1.8
GC_GS08A-01	Basement	3.44	5.06	1.07	0.23	3.7	99.57	2.4
GC_FF04-01	Basement	5.97	2.75	1.19	0.29	3	99.69	1
GC_FF13-01	Basement	5.61	3.47	1.12	0.28	2.7	99.71	1
GC_FF17-01	Basement	9.25	1.88	0.69	<0.01	3.8	99.23	0.4
GC_FF17-02	Basement	14.7	0.9	1.16	0.02	3	99.44	0.3
GC_GS10C-01	Basement	4.88	5.02	0.85	0.18	2	100.54	1.9
GC_GS12-01	Basement	8.68	1.11	0.47	0.12	3.2	100.95	1.4
GC_GS12-02	Basement	6.16	4.9	0.7	0.2	2.2	101.09	1.6
GC_GS14-01	Basement	5.17	5.29	0.79	0.18	1.6	100.53	1.9
GC_GS10C-02	Basement	7.5	2.32	0.61	0.19	3	100.26	1.8
GC_CL02-01	Basement	4.35	3.61	1.8	0.25	4.3	99.34	1.2
GC_CL01-01	Basement	8.36	1.18	1.08	0.12	3.5	100.14	0.9
GC_FF18A-01	Basement	17.9	0.16	0.16	<0.01	3	99.97	0.2
GC_LL02-01	Basement	7.37	2.79	0.64	0.3	2.7	100.1	1
GC_LL03A	Basement	8.12	2.07	0.91	0.25	4	100.28	0.9
GC_LL04A-01	Basement	6.69	4.43	0.82	0.22	2.6	100.09	0.8
GC_PB01-01	Basement	10.2	0.7	0.39	<0.01	3	100.22	0.6
GC_PB02-01	Basement	10	0.55	0.23	0.06	3.3	100.27	0.6
GC_PB02-02	Basement	4.63	3.84	2	0.18	2.4	100	0.6
GC_LL02-02	Basement	6.73	3.9	1.12	0.25	2.6	100.08	0.9
GC_FF17-02R	Repeat	14.9	0.89	1.16	0.01	3	100.11	0.3
GC_GS12-01 R	Repeat	8.67	1.1	0.47	0.18	3.3	100.81	1.5
GC_LL02-02 R	Repeat	6.68	3.93	1.12	0.26	2.6	100.25	1
GC_FF17-01 R	Repeat	9.26	1.88	0.68	<0.01	3.8	99.78	0.3
SY3	Standard	8.21	4.14	4.22	0.53		98	21.1
SY3/CG51509	Standard	8.27	4.05	4.23	0.51		97.49	21.2
SY3/CG51509	Standard	8.18	4.1	4.18	0.52		97.91	19.4
SY3/OKA2/CG51509	Standard	8.13	4.13	4.28	0.52		97.62	21.3

Analyte		Sc	V	Cr	Co	Ni	Cu	Zn
Units		ppm	ppm	ppm	ppm	ppm	ppm	ppm
Detection Limit		2	2	2	0.1	1	0.1	1
Description	**Sample Type**							
GC_LL01A-01	Basement	23	203	877	43.4	324	31.9	120
GC_PB03-01	Basement	23	195	1440	79.4	678	23.5	219
GC_PB04-01	Basement	25	229	380	40.1	91	45.7	70
GC_CL02B-01	Basement	12	131	301	20	87	6.5	54
GC_GS07A-01	Basement	9	84	108	13.2	32	75.6	64
GC_GS08A-01	Basement	10	213	111	27.1	169	9.5	70
GC_FF04-01	Basement	22	180	840	46	326	13	167
GC_FF13-01	Basement	20	154	719	38.7	237	11.9	113
GC_FF17-01	Basement	43	337	27	46.1	41	21.1	79
GC_FF17-02	Basement	38	379	18	38.1	31	34.2	67
GC_GS10C-01	Basement	9	112	63	15.4	24	14.8	45
GC_GS12-01	Basement	25	213	1370	55.7	373	26.4	225
GC_GS12-02	Basement	10	112	134	19.6	51	9.5	45
GC_GS14-01	Basement	8	118	82	12.1	34	14.4	36
GC_GS10C-02	Basement	22	217	1060	38.4	223	28.4	163
GC_CL02-01	Basement	11	112	327	17.6	84	3.6	44
GC_CL01-01	Basement	24	163	1420	55.4	540	39.8	192
GC_FF18A-01	Basement	35	300	115	26.7	31	69.6	55
GC_LL02-01	Basement	24	215	775	36.7	237	5.8	133
GC_LL03A	Basement	23	225	1010	42.7	254	24.6	529
GC_LL04A-01	Basement	16	129	525	25.7	191	4	73
GC_PB01-01	Basement	18	166	935	39.8	780	7.9	124
GC_PB02-01	Basement	21	96	1370	44.1	677	8.9	298
GC_PB02-02	Basement	31	184	119	19.1	30	93.4	52
GC_LL02-02	Basement	17	167	657	29	184	4.2	77
GC_FF17-02R	Repeat	39	371	17	37.7	29	33.6	66
GC_GS12-01 R	Repeat	24	211	1330	57.2	368	27.6	241
GC_LL02-02 R	Repeat	17	176	666	28.6	191	4.2	90
GC_FF17-01 R	Repeat	43	345	25	45.1	37	19.6	76
SY3	Standard	10	52	9	7.5	11	17	231
SY3/CG51509	Standard	11	51	10	7.6	10	16.7	230
SY3/CG51509	Standard	10	52	9	7.6	8	16.4	218
SY3/OKA2/CG51509	Standard	8	51	9	7.4	10	16.8	234

Analyte		Ga	Ge	As	Se	Rb	Sr	Y
Units		ppm	ppm	ppm	ppm	ppm	ppm	ppm
Detection Limit		0.1	0.1	0.1	1	0.1	1	0.01
Description	Sample Type							
GC_LL01A-01	Basement	11	0.2	2.3	<1	21.9	425	20.2
GC_PB03-01	Basement	11.3	0.1	2.5	<1	82	337	20.9
GC_PB04-01	Basement	13.7	0.1	2.5	<1	38.1	1080	28.6
GC_CL02B-01	Basement	15.5	0.2	2	<1	47.3	597	20.2
GC_GS07A-01	Basement	14.5	0.1	3.2	<1	34.5	709	17.3
GC_GS08A-01	Basement	16	0.2	11	<1	23.3	269	21.4
GC_FF04-01	Basement	12.7	0.2	2.4	<1	21.7	516	21.6
GC_FF13-01	Basement	12	0.1	4	<1	25.3	926	14.1
GC_FF17-01	Basement	10.1	0.2	6.7	<1	21	253	7.3
GC_FF17-02	Basement	12.8	0.1	4.5	<1	34.2	389	7.37
GC_GS10C-01	Basement	15.2	1.5	5.4	<1	24.1	610	14.8
GC_GS12-01	Basement	11.5	1.4	3.3	<1	10.4	160	17.8
GC_GS12-02	Basement	15.3	1.2	16	<1	17.2	531	16.2
GC_GS14-01	Basement	15.7	1	8.8	<1	13.1	490	16.4
GC_GS10C-02	Basement	12.5	2.6	3.7	<1	10.5	219	32
GC_CL02-01	Basement	13	1.5	1	<1	43.3	722	20.7
GC_CL01-01	Basement	8.5	1.6	1.9	<1	22.5	266	16.7
GC_FF18A-01	Basement	13.2	2.1	11.8	<1	3.4	123	15.9
GC_LL02-01	Basement	11	1.8	2.7	<1	7.2	392	27.9
GC_LL03A	Basement	10.7	1.4	2.9	<1	17.1	592	18.8
GC_LL04A-01	Basement	12.1	1.6	35.5	<1	11.6	840	15.2
GC_PB01-01	Basement	6.8	1.8	1.9	<1	5	100	18.4
GC_PB02-01	Basement	7.1	1.8	2.3	<1	2.8	85	13.1
GC_PB02-02	Basement	13.4	1.4	2.2	<1	43	663	20
GC_LL02-02	Basement	11.9	1.7	1.6	<1	11.8	639	21.1
GC_FF17-02R	Repeat	12.7	0.1	4.3	<1	32.9	392	6.69
GC_GS12-01 R	Repeat	11.8	1.6	3.2	<1	10.7	155	18.5
GC_LL02-02 R	Repeat	12	1.7	1.8	<1	11.6	611	21
GC_FF17-01 R	Repeat	10.4	0.1	7.2	<1	20.3	251	7.43
SY3	Standard	24.4	0.2	10.1	11	211	293	723
SY3/CG51509	Standard	25.7	0.1	10.1	10	209	294	721
SY3/CG51509	Standard	24.7	<0.1	12.8	13	217	304	708
SY3/OKA2/CG51509	Standard	27.6	<0.1	12.1	11	208	299	733

Analyte		Zr	Nb	Mo	Ag	Cd	Sn	Sb	Te
Units		ppm	ppm	ppm	ppm	ppm	ppm	ppm	ppm
Detection Limit		1	1	0.1	0.1	0.1	0.1	1	0.1
Description	Sample Type								
GC_LL01A-01	Basement	100	4	<0.1	<0.1	0.4	0.2	<1	<0.1
GC_PB03-01	Basement	91	9	<0.1	<0.1	0.8	0.1	1	<0.1
GC_PB04-01	Basement	93	4	<0.1	<0.1	0.1	0.1	<1	<0.1
GC_CL02B-01	Basement	130	9	<0.1	<0.1	0.1	0.2	<1	<0.1
GC_GS07A-01	Basement	142	5	<0.1	<0.1	0.2	1.6	1	<0.1
GC_GS08A-01	Basement	171	7	0.6	<0.1	0.1	<0.1	1	0.1
GC_FF04-01	Basement	94	4	<0.1	<0.1	0.1	0.1	1	<0.1
GC_FF13-01	Basement	58	3	<0.1	<0.1	0.3	<0.1	1	<0.1
GC_FF17-01	Basement	21	<1	4.1	<0.1	<0.1	<0.1	2	<0.1
GC_FF17-02	Basement	36	<1	0.5	<0.1	0.2	<0.1	3	<0.1
GC_GS10C-01	Basement	531	34	3	<0.1	0.2	0.8	3	<0.1
GC_GS12-01	Basement	136	12	3	0.1	0.6	1	3	<0.1
GC_GS12-02	Basement	203	17	5	<0.1	0.1	0.2	2	<0.1
GC_GS14-01	Basement	196	11	4	<0.1	0.1	0.3	2	<0.1
GC_GS10C-02	Basement	86	10	<0.1	0.3	0.5	0.4	<1	<0.1
GC_CL02-01	Basement	124	11	<0.1	0.3	0.1	0.3	<1	<0.1
GC_CL01-01	Basement	81	6	<0.1	0.2	1	0.2	<1	<0.1
GC_FF18A-01	Basement	29	5	<0.1	0.2	0.4	<0.1	<1	<0.1
GC_LL02-01	Basement	129	7	<0.1	0.2	0.3	0.4	<1	<0.1
GC_LL03A	Basement	73	6	<0.1	0.2	0.5	0.4	29	<0.1
GC_LL04A-01	Basement	81	5	<0.1	0.2	0.1	<0.1	<1	<0.1
GC_PB01-01	Basement	32	4	<0.1	0.2	0.2	0.3	<1	<0.1
GC_PB02-01	Basement	47	3	<0.1	0.1	0.8	<0.1	<1	<0.1
GC_PB02-02	Basement	74	4	<0.1	0.2	0.3	<0.1	<1	<0.1
GC_LL02-02	Basement	106	4	<0.1	0.2	0.2	0.4	<1	<0.1
GC_FF17-02R	Repeat	35	<1	0.6	<0.1	<0.1	<0.1	3	0.1
GC_GS12-01 R	Repeat	134	10	5	<0.1	0.3	0.5	3	<0.1
GC_LL02-02 R	Repeat	102	5	<0.1	0.2	0.2	0.6	<1	<0.1
GC_FF17-01 R	Repeat	23	1	3.8	0.2	<0.1	<0.1	2	0.1
SY3	Standard	322	142	0.6	2.6	0.4	5.6	1	<0.1
SY3/CG51509	Standard	316	140	<0.1	2.5	0.3	5.6	<1	<0.1
SY3/CG51509	Standard	340	120	<0.1	2.6	0.2	6.1	2	<0.1
SY3/OKA2/CG51509	Standard	317	147	<0.1	3	0.4	5.9	<1	<0.1

Analyte		Cs	Ba	La	Ce	Pr	Nd	Sm	Eu
Units		ppm	ppm	ppm	ppm	ppm	ppm	ppm	ppm
Detection Limit		0.1	1	1	1	0.01	0.1	0.01	0.01
Description	Sample Type								
GC_LL01A-01	Basement	0.4	689	22	38	4.81	20	3.79	1.29
GC_PB03-01	Basement	2.1	815	26	53	6.27	26.1	4.55	1.4
GC_PB04-01	Basement	0.9	775	22	49	6.65	30.4	5.7	1.99
GC_CL02B-01	Basement	0.7	480	28	53	6.37	24.8	4.08	1.52
GC_GS07A-01	Basement	0.8	785	27	52	5.54	20.5	3.71	1.24
GC_GS08A-01	Basement	0.6	715	43	61	6.66	24.4	3.9	1.31
GC_FF04-01	Basement	0.2	688	17	38	5	22	4.28	1.5
GC_FF13-01	Basement	0.4	602	14	28	3.71	15.2	2.93	1.21
GC_FF17-01	Basement	0.1	108	3	6	0.88	4	0.83	0.41
GC_FF17-02	Basement	0.1	106	8	7	0.95	4	0.78	0.4
GC_GS10C-01	Basement	0.9	567	22	39	5.52	18	3.46	0.96
GC_GS12-01	Basement	0.4	181	13	29	4.87	18.9	4.32	0.99
GC_GS12-02	Basement	0.4	370	20	38	5.57	19.5	3.76	1.08
GC_GS14-01	Basement	0.2	315	22	38	5.46	18.7	3.53	1.04
GC_GS10C-02	Basement	0.6	178	23	49	6.44	25.2	5.37	1.4
GC_CL02-01	Basement	0.8	449	24	48	5.77	21.2	3.87	1.26
GC_CL01-01	Basement	0.6	281	15	30	4.07	16.4	3.53	1.08
GC_FF18A-01	Basement	0.1	25	7	10	1.33	5.8	1.43	0.5
GC_LL02-01	Basement	0.1	268	16	36	4.93	19.7	4.36	1.16
GC_LL03A	Basement	0.2	517	17	31	3.92	15.4	3.12	1.14
GC_LL04A-01	Basement	0.2	379	17	29	3.45	12.7	2.54	1.01
GC_PB01-01	Basement	0.1	81	7	10	1.59	9.5	2.26	0.66
GC_PB02-01	Basement	<0.1	80	8	15	2.14	9.3	2.07	0.57
GC_PB02-02	Basement	1	688	9	16	1.98	7.7	1.9	0.9
GC_LL02-02	Basement	<0.1	651	13	30	3.97	15.7	3.43	1.15
GC_FF17-02R	Repeat	0.1	107	7	6	0.93	4.4	0.81	0.38
GC_GS12-01 R	Repeat	0.4	186	15	31	5.08	19.6	4.34	1.02
GC_LL02-02 R	Repeat	<0.1	665	14	32	4.16	16.7	3.43	1.14
GC_FF17-01 R	Repeat	0.1	107	4	7	0.9	4.3	0.84	0.37
SY3	Standard	1.4	440	1320	2240	218	662	105	16.5
SY3/CG51509	Standard	1.2	441	1330	2220	213	651	104	16.9
SY3/CG51509	Standard	1.9	421	1300	2130	214	642	112	15.5
SY3/OKA2/CG51509	Standard	1.3	452	1330	2270	215	645	107	17.1

Analyte		Gd	Tb	Dy	Ho	Er	Tm	Yb	Lu
Units		ppm	ppm	ppm	ppm	ppm	ppm	ppm	ppm
Detection Limit		0.1	0.01	0.01	0.01	0.01	0.01	0.01	0.01
Description	**Sample Type**								
GC_LL01A-01	Basement	3.78	0.62	3.59	0.9	1.78	0.31	1.97	0.3
GC_PB03-01	Basement	4.01	0.67	3.87	0.99	1.98	0.32	1.94	0.3
GC_PB04-01	Basement	5.54	0.84	5.05	1.26	2.53	0.42	2.62	0.4
GC_CL02B-01	Basement	3.54	0.59	3.44	0.85	1.93	0.3	2.15	0.3
GC_GS07A-01	Basement	3.17	0.48	2.79	0.71	1.6	0.27	1.89	0.3
GC_GS08A-01	Basement	3.76	0.59	3.45	0.87	1.95	0.31	2.18	0.3
GC_FF04-01	Basement	4.19	0.66	3.7	0.91	2	0.33	2.2	0.3
GC_FF13-01	Basement	2.87	0.44	2.54	0.61	1.25	0.21	1.34	0.2
GC_FF17-01	Basement	1.06	0.19	1.23	0.33	0.69	0.11	0.73	0.1
GC_FF17-02	Basement	1	0.19	1.23	0.32	0.69	0.12	0.73	0.1
GC_GS10C-01	Basement	3.11	0.5	2.69	0.67	1.5	0.3	1.96	0.3
GC_GS12-01	Basement	4.12	0.66	3.53	0.84	1.77	0.33	2.06	0.3
GC_GS12-02	Basement	3.47	0.55	2.92	0.73	1.61	0.32	2.2	0.3
GC_GS14-01	Basement	3.17	0.53	2.89	0.72	1.56	0.29	2.14	0.3
GC_GS10C-02	Basement	4.77	0.74	4.66	1.08	2.33	0.37	2.52	0.4
GC_CL02-01	Basement	3.2	0.48	2.96	0.67	1.51	0.25	1.79	0.3
GC_CL01-01	Basement	2.99	0.43	2.5	0.55	1.22	0.18	1.28	0.2
GC_FF18A-01	Basement	1.68	0.29	2.01	0.51	1.18	0.19	1.31	0.2
GC_LL02-01	Basement	3.8	0.61	3.76	0.87	1.86	0.3	2.08	0.3
GC_LL03A	Basement	2.88	0.45	2.81	0.63	1.33	0.2	1.42	0.2
GC_LL04A-01	Basement	2.3	0.34	2	0.47	1.02	0.16	1.12	0.2
GC_PB01-01	Basement	2.27	0.39	2.55	0.6	1.3	0.21	1.33	0.2
GC_PB02-01	Basement	1.79	0.3	1.87	0.43	0.96	0.14	1.08	0.2
GC_PB02-02	Basement	2.02	0.36	2.6	0.65	1.46	0.24	1.74	0.3
GC_LL02-02	Basement	3	0.48	2.83	0.67	1.43	0.23	1.65	0.2
GC_FF17-02R	Repeat	0.97	0.17	1.18	0.3	0.67	0.11	0.74	0.1
GC_GS12-01 R	Repeat	4.09	0.65	3.61	0.87	1.84	0.32	2.11	0.3
GC_LL02-02 R	Repeat	3.11	0.49	2.97	0.68	1.48	0.24	1.68	0.2
GC_FF17-01 R	Repeat	1.1	0.2	1.32	0.32	0.74	0.11	0.71	0.1
SY3	Standard	103	17.7	117	30.5	67.7	10.8	59.5	7.4
SY3/CG51509	Standard	102	18.2	120	30.8	67.8	10.9	59.7	7.7
SY3/CG51509	Standard	108	19	116	30.4	64.5	11.5	63.5	7.5
SY3/OKA2/CG51509	Standard	106	17.7	118	29.2	65.9	11.1	61	7.5

Analyte		Hf	Ta	W	Hg	Tl	Pb204	Pb206	Pb207
Units		ppm	ppm	ppm	ppm	ppm	ppm	ppm	ppm
Detection Limit		0.1	0.01	1	0.1	0.01	0.001	0.001	0.001
Description	**Sample Type**								
GC_LL01A-01	Basement	2.8	0.54	1	0.1	0.09	0.092	3.15	2.29
GC_PB03-01	Basement	2.6	0.61	9	0.4	0.31	0.045	2.36	1.41
GC_PB04-01	Basement	2.8	0.46	1	0.1	0.1	0.019	0.752	0.5
GC_CL02B-01	Basement	3.7	0.76	4	0.2	0.17	0.021	1.17	0.708
GC_GS07A-01	Basement	3.7	0.7	1	0.1	0.14	0.063	2.84	1.71
GC_GS08A-01	Basement	4.6	0.79	2	0.1	0.1	0.017	1.18	0.577
GC_FF04-01	Basement	2.6	0.51	1	0.1	0.08	0.02	0.707	0.521
GC_FF13-01	Basement	1.8	0.34	1	0.1	0.09	0.049	1.48	1.3
GC_FF17-01	Basement	0.5	0.06	<1	0.1	0.13	0.015	0.738	0.454
GC_FF17-02	Basement	0.7	0.06	1	0.2	0.12	0.048	2.35	1.33
GC_GS10C-01	Basement	13.8	1.73	<1	0.1	0.08	0.036	1.75	1.06
GC_GS12-01	Basement	4.6	1.23	<1	0.5	0.04	0.043	3.02	1.28
GC_GS12-02	Basement	5.6	0.83	<1	0.3	0.06	0.031	1.51	0.962
GC_GS14-01	Basement	5.6	0.73	<1	<0.1	0.02	0.027	1.53	0.851
GC_GS10C-02	Basement	2.6	0.64	1	<0.1	0.07	0.226	4.58	5.28
GC_CL02-01	Basement	2.9	0.57	<1	<0.1	0.18	0.063	1.46	1.49
GC_CL01-01	Basement	2.2	0.35	<1	<0.1	0.09	0.082	1.66	1.89
GC_FF18A-01	Basement	0.7	0.14	<1	<0.1	0.02	0.033	0.761	0.808
GC_LL02-01	Basement	3.1	0.52	<1	<0.1	0.03	0.021	0.596	0.489
GC_LL03A	Basement	2	0.61	<1	<0.1	0.06	0.035	2.27	0.926
GC_LL04A-01	Basement	2	0.35	<1	<0.1	0.03	0.037	0.956	0.905
GC_PB01-01	Basement	1	0.2	<1	<0.1	0.02	0.009	0.266	0.227
GC_PB02-01	Basement	1.4	0.24	<1	<0.1	0.01	0.008	0.227	0.221
GC_PB02-02	Basement	1.8	0.28	2	0.1	0.11	0.026	0.942	0.664
GC_LL02-02	Basement	2.5	0.43	1	<0.1	0.03	0.025	0.61	0.637
GC_FF17-02R	Repeat	0.5	0.06	<1	0.2	0.15	0.04	2.29	1.3
GC_GS12-01 R	Repeat	4.1	0.64	<1	0.2	0.02	0.051	2.06	1.44
GC_LL02-02 R	Repeat	2.5	0.45	2	0.1	0.02	0.022	0.628	0.577
GC_FF17-01 R	Repeat	0.5	0.06	1	0.1	0.11	0.016	0.745	0.454
SY3	Standard	9.7	29.2	1	0.1	0.66	0.091	79.9	8.62
SY3/CG51509	Standard	9.7	29.4	1	0.1	0.57	0.087	77.4	8.57
SY3/CG51509	Standard	11.2	24	4	<0.1	0.44	0.094	77.6	8.18
SY3/OKA2/CG51509	Standard	9.5	27.8	1	0.1	0.81	0.096	77.7	8.92

	Analyte	Pb208	PbSUM	Bi	Th	U
	Units	ppm	ppm	ppm	ppm	ppm
	Detection Limit	0.001	0.001	0.1	0.01	0.01
Description	Sample Type					
GC_LL01A-01	Basement	5.14	10.7	0.1	5.15	6.7
GC_PB03-01	Basement	3.29	7.1	0.1	8.23	6.33
GC_PB04-01	Basement	1.15	2.43	<0.1	1.83	2.93
GC_CL02B-01	Basement	1.66	3.56	<0.1	4.5	5.37
GC_GS07A-01	Basement	3.69	8.3	<0.1	11.9	3.74
GC_GS08A-01	Basement	1.31	3.08	<0.1	5.14	4.5
GC_FF04-01	Basement	1.09	2.34	<0.1	1.82	2.26
GC_FF13-01	Basement	3.27	6.1	<0.1	2.23	1.88
GC_FF17-01	Basement	0.966	2.17	0.1	0.57	2.25
GC_FF17-02	Basement	2.86	6.6	0.2	1.69	6.37
GC_GS10C-01	Basement	2.61	5.46	0.2	6.76	13.7
GC_GS12-01	Basement	2.9	7.24	0.1	1.05	14.8
GC_GS12-02	Basement	2.41	4.91	<0.1	3.63	5.09
GC_GS14-01	Basement	1.98	4.39	0.1	3.44	11
GC_GS10C-02	Basement	11.2	21.3	<0.1	5.34	1.91
GC_CL02-01	Basement	3.23	6.24	<0.1	4.27	2.14
GC_CL01-01	Basement	3.98	7.61	<0.1	2.36	1.27
GC_FF18A-01	Basement	1.69	3.29	<0.1	0.65	0.6
GC_LL02-01	Basement	1.07	2.18	<0.1	1.66	1.68
GC_LL03A	Basement	1.84	5.07	0.2	1.61	12.8
GC_LL04A-01	Basement	1.95	3.85	<0.1	1.7	7.2
GC_PB01-01	Basement	0.476	0.978	<0.1	<0.01	1.26
GC_PB02-01	Basement	0.412	0.868	<0.1	0.02	1.3
GC_PB02-02	Basement	1.39	3.02	<0.1	0.75	1.66
GC_LL02-02	Basement	1.14	2.46	<0.1	0.92	2.01
GC_FF17-02R	Repeat	2.78	6.41	0.2	1.77	6.3
GC_GS12-01 R	Repeat	3.29	6.84	<0.1	1.05	12.3
GC_LL02-02 R	Repeat	1.16	2.39	<0.1	0.91	1.97
GC_FF17-01 R	Repeat	1	2.21	0.1	0.62	2.18
SY3	Standard	46.1	134	0.3	990	652
SY3/CG51509	Standard	43.3	129	0.3	1010	656
SY3/CG51509	Standard	43.5	129	0.2	1050	646
SY3/OKA2/CG51509	Standard	43.7	130	0.2	1020	660

A3: Magnesium Numbers for Select Boundary intrusion Samples:

Sample ID	Matrix (M) / Fragment (F)	Mg Number
GC_GS08A	MF	55.2
GC_GS07A	M	56.7
GC_PB02-02	M	59.7
GC_GS14	M	61.2
GC_GS10C-01	M	62.3
GC_PB04	M	67.9
GC_GS10C-02	F	68.1
GC_CL02B	M	69.2
GC_CL02	M	71.5
GC_GS12-02	M	71.5
GC_LL04A	MF	74.1
GC_LL01A	M	76
GC_LL02-02	M	76.6
GC_FF04	M	76.8
GC_LL03A	MF	77.5
GC_GS12-01	F	77.6
GC_LL02-01	M	77.7
GC_PB02-01	F	81.8
GC_PB03	M	82.0
GC_CL01	M	82.4
GC_PB01	F	83.5

A4: ICP-MS AND ICP-OES WHOLE ROCK AND TRACE ELEMENT ANALYSIS

SASKATCHEWAN RESEARCH COUNCIL

Method: Whole Rock and Trace Elements Analysis of Geological Samples by ICP-OES and MS

Method Reference: WR/TR

Method Summary:

Sample Preparation:

Depending on the sample type (non-mineralized, mineralized, etc.) each preparation step was performed in the designated sample preparation area. Rock samples were dried in their original plastic bags, and then jaw crushed. A subsample was split out using a riffler. The subsample was pulverized using a grinding mill. An agate mill is used, unless the sample is radioactive and then they are ground by puck and ring mill. The grinding mills were, at minimum, cleaned between samples, silica sand cleaning was employed in between groups. The pulp was transferred to a barcode labeled plastic snap top vial.

Sample Fusion:

An aliquot of sample was combined with flux and fused in the Ox automated fusion instrument. After the fusion, the molten material was poured into solution. The solution was then vigorously stirred until the bead was dissolved. The solution was then topped up and analyzed by ICP-OES and ICP-MS.

Sample Analysis:

Instruments were calibrated using certified commercial solutions. The instruments used were for ICP-MS Nexion 300S and for ICP-OES PerkinElmer Optima 5300DV or Optima 8300DV.

Geoanalytical Laboratories
Saskatchewan Research Council | 125 – 15 Innovation Blvd | Saskatoon SK
306-933-8118 | Fax 306-933-5656 | geolab@src.sk.ca | www.src.sk.ca

SASKATCHEWAN RESEARCH COUNCIL

Method: The Multi-Element Determination of Basement Samples by ICP-MS

Method Reference: ICP-MS2 (Basement)

Method Summary:

Sample Preparation:

Rock samples were dried in their original plastic bags, and then jaw crushed. A subsample was split out using a sample riffler. The subsample was pulverized using a puck and ring grinding mill. The pulp was transferred to a barcode labeled plastic snap top vial.

Total Digestion:

An aliquot of pulp was digested to dryness in a hot block digestion system using a mixture of ultra-pure concentrated acids HF:HNO_3:HClO4. The residue was dissolved and made to volume using deionized water prior to analysis.

Partial Digestion:
An aliquot of pulp in a digestion tube, was digested in a mixture of ultra-pure concentrated nitric and hydrochloric acids (HNO3:HCl) in a hot water bath, and then diluted using deionized water prior to analysis.

Quality Control:

Geochemical Analysis ICP-OES: Multi-Element Total Digestion:

Total digestion and analysis was performed on samples to determine the dilution required prior to ICP-MS analysis. The ICP-MS detection limits for total analysis included all elements except for the following: Al2O3, CaO, Fe2O3, K2O, MgO, MnO, Na2O, P2O5, TiO2, Ba, Ce, Cr, La, Li, Sr and Zr. These elements were analyzed ONLY by ICP for total digestion leaching. Instruments were calibrated using certified commercial solutions. The instruments used were PerkinElmer Optima 4300DV or Optima 5300DV.

Partial digestions by ICP-MS:

As, Ge, Hg, Sb, Se and Te were done on the partial digestion only, these elements are not suited to total digestion analysis. The ICP-MS instruments used were Perkin Elmer Elan DRC II or Perkin Elmer NEXION.

Geoanalytical Laboratories
Saskatchewan Research Council | 125 – 15 Innovation Blvd | Saskatoon SK
306-933-8118 | Fax 306-933-5656 | geolab@src.sk.ca | www.src.sk.ca

A6: LOSS ON IGNITION

SASKATCHEWAN RESEARCH COUNCIL

Method: Loss on Ignition Determination

Method Reference: LOI

Method Summary:

Rock samples were dried in their original plastic bags and then jaw crushed. A subsample was split out using a riffler. The subsample was pulverized using a puck and ring grinding mill. The grinding mills were cleaned between samples using steel wool and compressed air or silica sand. The pulp was transferred to a labeled plastic snap top vial.

Sample Preparation:

A crucible was weighed and the weight was recorded. An aliquot of sample was weighed into the crucible and the total initial weight was recorded. The sample was placed in a muffle oven. The samples were removed from the oven and allowed to cool. The sample was then re-weighed.

The following calculation was performed for LOI %:

$$\frac{\boldsymbol{Inital\ Weight} - [(\boldsymbol{crucible} + \boldsymbol{sample\ dry}) - (\boldsymbol{crucible\ weight})]}{\boldsymbol{Initial\ Weight}}\ \boldsymbol{X\ 100}$$

Detection Limit:

The detection limit for the LOI method is 0.1%.

Quality Control:

One in every 40 samples is analyzed in duplicate. All quality control results must be within specified limits otherwise corrective action is taken.

Geoanalytical Laboratories
Saskatchewan Research Council | 125 – 15 Innovation Blvd | Saskatoon SK
306-933-8118 | Fax 306-933-5656 | geolab@src.sk.ca | www.src.sk.ca

A7: FEO TOTAL

Method: The Determination of Ferrous Iron in Solution

Method Reference: FEO

Method Summary:

Sample Preparation:

The samples were crushed, split and agate ground prior to digestion using the following procedure: Rock samples were jaw crushed and a subsample was split out using a riffler. The subsample was pulverized using an agate grinding mill. The grinding mills were cleaned between samples with silica sand. The pulp was transferred to a barcode labeled plastic snap top vial.

Sample analysis:

An aliquot of sample was dissolved in a crucible with 1:2 H_2SO_4 and concentrated HF acid. The sample was heated until the solution was clear. The sample was transferred to a flask and H_3BO_3 (Boric acid), H_2SO_4 (Sulphuric acid), and H_3PO_4 (Phosphoric acid) was added. The sample was titrated immediately with N/10 $KMnO_4$. The percentage of ferrous iron in solution (FEO) in the sample was calculated from the end point titration.

Detection Limit: 0.03%

Quality Control:

A replicate sample was included with every 40 samples.

Geoanalytical Laboratories
Saskatchewan Research Council | 125 – 15 Innovation Blvd | Saskatoon SK
306-933-8118 | Fax 306-933-5656 | geolab@src.sk.ca | www.src.sk.ca

A8: ICP-OES AND ICP-MS DETECTION LIMITS

SASKATCHEWAN RESEARCH COUNCIL

Detection Limits:

Lithium Metaborate Fusion by ICP-OES

Element	Symbol	Detection Limit
Aluminium	Al_2O_3	0.01%
Calcium	CaO	0.01%
Chromium	Cr	2 ppm
Iron	Fe_2O_3	0.01%
Magnesium	MgO	0.01%
Manganese	MnO	0.01%
Phosphorous	P_2O_5	0.01%

Element	Symbol	Detection Limit
Potassium	K_2O	0.01%
Scandium	Sc	2 ppm
Sodium	Na2O	0.01%
Silica	SiO_2	0.1%
Titanium	TiO2	0.01%
Vanadium	V	2 ppm
Loss on Ignition	LOI	0.1%

Trace Elements by ICP-MS

Element	Symbol	Detection Limit
Antimony	Sb	1 ppm
Arsenic	As	0.1 ppm
Barium	Ba	1 ppm
Beryllium	Be	0.1 ppm
Bismuth	Bi	0.1 ppm
Cadmium	Cd	0.1 ppm
Cerium	Ce	1 ppm
Cesium	Cs	0.1 ppm
Cobalt	Co	0.1 ppm
Copper	Cu	0.1 ppm
Dysprosium	Dy	0.01 ppm
Erbium	Er	0.01 ppm
Europium	Eu	0.01 ppm
Gadolinium	Gd	0.1 ppm
Gallium	Ga	0.1 ppm
Germanium	Ge	0.01 ppm
Hafnium	Hf	0.1 ppm
Holmium	Ho	0.01 ppm
Lanthanum	La	1 ppm
Lead204	Pb204	0.001 ppm
Lead206	Pb206	0.001 ppm
Lead207	Pb207	0.001 ppm
Lead208	Pb208	0.001 ppm
Lead SUM	PbSUM	0.001 ppm
Lutetium	Lu	0.01 ppm

Element	Symbol	Detection Limit
Mercury	Hg	0.1 ppm
Molybdenum	Mo	0.1 ppm
Niobium	Nb	1 ppm
Neodymium	Nd	0.1 ppm
Nickel	Ni	1 ppm
Praseodymium	Pr	0.01 ppm
Rubidium	Rb	0.1 ppm
Selenium	Se	1 ppm
Samarium	Sm	0.01 ppm
Silver	Ag	0.1 ppm
Strontium	Sr	1 ppm
Tantalum	Ta	0.01 ppm
Terbium	Tb	0.01 ppm
Tellurium	Te	0.1 ppm
Tin	Sn	0.1 ppm
Thorium	Th	0.01 ppm
Thallium	Tl	0.01 ppm
Thulium	Tm	0.01 ppm
Tungsten	W	1 ppm
Uranium	U	0.01 ppm
Ytterbium	Yb	0.01 ppm
Yttrium	Y	0.01 ppm
Zinc	Zn	1 ppm
Zirconium	Zr	1 ppm

Quality Control:

A control sample is prepared and analyzed with each batch of samples. One in every 40 samples was analyzed in replicate. All quality control results must be within specified limits (3 standard deviations) otherwise an investigation will proceed and appropriate corrective action taken. QC measures and data verification procedures applied also include the preparation and analysis of 3 standards and 1 blank. The blank is flux only.

Geoanalytical Laboratories
Saskatchewan Research Council | 125 – 15 Innovation Blvd | Saskatoon SK
306-933-8118 | Fax 306-933-5656 | geolab@src.sk.ca | www.src.sk.ca

APPENDIX B

PROOF OF CALCULATIONS

Stoke's Law:

(1) $V = 2r^2g\Delta p/90u$

V	=	Settling velocity (cm/s)
r	=	Radius of spherical particle (cm)
g	=	Acceleration due to gravity (cm/s^2)
p_s	=	Density of solid (spherical) particle (g/cm^3)
P_l	=	Density of liquid (g/cm^3)
n	=	Viscosity of liquid (g/cms^{-1}) (Pascal-second (Pa s))

Other:

d	=	Diameter of spherical particle (cm)

Shaw's (1969) recalculation of settling velocity with fluid containing solid fraction:

(2) $V_f = V\ (1\text{-}F)^{4.65}$

V_f	=	Settling velocity within fluid containing solid fraction (cm/s)
F	=	Solid fraction of the liquid (e.g., 25% = 0.25 for F)

*NOTE: Viscosity is expressed as Pascal second (Pa s). 1 Pa s = 10 Poise

TABLES B1-B4: RESULTS FOR SETTLING VELOCITY FOR THE GREEN STREET INTRUSION

B1: GREEN STREET PARAMETERS:

Calculation Number	**d**	**r**	**r^2**	**g**	**p_s**	**p_l**	**n**	**F**
GS 1	15	7.5	56.25	981	3.35	2.5	2000	0.12
GS 2	15	7.5	56.25	981	3.35	2.5	3550000	0.12
GS 3	200	100	10000	981	3.35	2.5	2000	0.12
GS 4	200	100	10000	981	3.35	2.5	3550000	0.12
GS 5	15	7.5	56.25	981	3.35	2.5	803.52	0.12
GS 6	15	7.5	56.25	981	3.35	2.5	52	0.12
GS 7	15	7.5	56.25	981	3.35	2.5	1000	0.12
GS 8	15	7.5	56.25	981	3.35	2.5	1950	0.12
GS 9	15	7.5	56.25	981	3.35	2.5	100000	0.12
GS 10	15	7.5	56.25	981	3.35	2.5	1548.52	0.12
GS 11	15	7.5	56.25	981	3.35	2.5	3548133.89	0.12
GS 12	200	100	10000	981	3.35	2.5	803.52	0.12
GS 13	200	100	10000	981	3.35	2.5	52	0.12
GS 14	200	100	10000	981	3.35	2.5	1000	0.12
GS 15	200	100	10000	981	3.35	2.5	1950	0.12
GS 16	200	100	10000	981	3.35	2.5	100000	0.12
GS 17	200	100	10000	981	3.35	2.5	1548.52	0.12
GS 18	200	100	10000	981	3.35	2.5	3548133.89	0.12

B2: GREEN STREET RESULTS:

Calculation Number	V cm/s	V_f cm/s	V_f m/s	V_f m/hr	V_f km/hr	V_f km/day
GS 1	1	0	0.00	10.35	0.01035	0.24850
GS 2	0	0	0.00	0.01	0.00001	0.00014
GS 3	93	51	0.51	1840.74	1.84074	44.17775
GS 4	0	0	0.00	1.04	0.00104	0.02489
GS 5	1	1	0.01	25.77	0.02577	0.61853
GS 6	20	11	0.11	398.24	0.39824	9.55769
GS 7	1	1	0.01	20.71	0.02071	0.49700
GS 8	1	0	0.00	10.62	0.01062	0.25487
GS 9	0	0	0.00	0.21	0.00021	0.00497
GS 10	1	0	0.00	13.37	0.01337	0.32095
GS 11	0	0	0.00	0.01	0.00001	0.00014
GS 12	231	127	1.27	4581.69	4.58169	109.96055
GS 13	3563	1967	19.67	70797.68	70.79768	1699.14422
GS 14	185	102	1.02	3681.48	3.68148	88.35550
GS 15	95	52	0.52	1887.94	1.88794	45.31051
GS 16	2	1	0.01	36.81	0.03681	0.88355
GS 17	120	66	0.66	2377.42	2.37742	57.05803
GS 18	0	0	0.00	1.04	0.00104	0.02490

B3: LOUIS LAKE PARAMETERS:

Calculation Number	d	r	r^2	g	p_s	p_l	n	F
LL1	30	15	225	981	3.35	2.85	2000	0.16
LL2	30	15	225	981	3.35	2.85	3550000	0.16
LL3	200	100	10000	981	3.35	2.85	2000	0.16
LL4	200	100	10000	981	3.35	2.85	3550000	0.16
LL5	30	15	225	981	3.35	2.85	803.52	0.16
LL6	30	15	225	981	3.35	2.85	52	0.16
LL7	30	15	225	981	3.35	2.85	1000	0.16
LL8	30	15	225	981	3.35	2.85	1950	0.16
LL9	30	15	225	981	3.35	2.85	100000	0.16
LL10	30	15	225	981	3.35	2.85	1548.52	0.16
LL11	30	15	225	981	3.35	2.85	3548133.89	0.16
LL12	200	100	10000	981	3.35	2.85	803.52	0.16
LL13	200	100	10000	981	3.35	2.85	52	0.16
LL14	200	100	10000	981	3.35	2.85	1000	0.16
LL15	200	100	10000	981	3.35	2.85	1950	0.16
LL16	200	100	10000	981	3.35	2.85	100000	0.16
LL17	200	100	10000	981	3.35	2.85	1548.52	0.16
LL18	200	100	10000	981	3.35	2.85	3548133.89	0.16
CSB1	10	5	25	981	3.35	2.85	2000	0.44
CSB2	10	5	25	981	3.35	2.85	3550000	0.44
CSB3	10	5	25	981	3.35	2.85	803.52	0.44
CSB4	10	5	25	981	3.35	2.85	52	0.44
CSB5	10	5	25	981	3.35	2.85	1000	0.44
CSB6	10	5	25	981	3.35	2.85	1950	0.44
CSB7	10	5	25	981	3.35	2.85	100000	0.44
CSB8	10	5	25	981	3.35	2.85	1548.52	0.44
CSB9	10	5	25	981	3.35	2.85	3548133.89	0.44

B4: LOUIS LAKE RESULTS

Calculation Number	V cm/s	V_f cm/s	V_f m/s	V_f m/hr	V_f km/hr	V_f km/day
LL1	1	1	0.01	19.62	0.01962	0.47097
LL2	0	0	0.00	0.01	0.00001	0.00027
LL3	55	24	0.24	872.16	0.87216	20.93191
LL4	0	0	0.00	0.49	0.00049	0.01179
LL5	3	1	0.01	48.84	0.04884	1.17226
LL6	47	21	0.21	754.76	0.75476	18.11416
LL7	2	1	0.01	39.25	0.03925	0.94194
LL8	1	1	0.01	20.13	0.02013	0.48304
LL9	0	0	0.00	0.39	0.00039	0.00942
LL10	2	1	0.01	25.35	0.02535	0.60828
LL11	0	0	0.00	0.01	0.00001	0.00027
LL12	136	60	0.60	2170.86	2.17086	52.10054
LL13	2096	932	9.32	33544.73	33.54473	805.07358
LL14	109	48	0.48	1744.33	1.74433	41.86383
LL15	56	25	0.25	894.53	0.89453	21.46863
LL16	1	0	0.00	17.44	0.01744	0.41864
LL17	70	31	0.31	1126.45	1.12645	27.03473
LL18	0	0	0.00	0.49	0.00049	0.01180
CSB1	0	0	0.00	0.33	0.00033	0.00794
CSB2	0	0	0.00	0.00	0.00000	0.00000
CSB3	0	0	0.00	0.82	0.00082	0.01977
CSB4	5	0	0.00	12.73	0.01273	0.30546
CSB5	0	0	0.00	0.66	0.00066	0.01588
CSB6	0	0	0.00	0.34	0.00034	0.00815
CSB7	0	0	0.00	0.01	0.00001	0.00016
CSB8	0	0	0.00	0.43	0.00043	0.01026
CSB9	0	0	0.00	0.00	0.00000	0.00000